Mechanisms of neurodegeneration in the Transmissible Spongiform Encephalopathies

Gary James Clarke

A thesis submitted in partial fulfilment of the requirements of the University of Edinburgh for the degree of Doctor of Philosophy

The programme of research was carried out at the Institute for Animal Health, Neuropathogenisis Unit, Edinburgh

December 2005

Declaration

I declare that the work presented in this thesis is my own, except where otherwise stated. All experiments were designed by myself, in collaboration with my supervisors Professor James Ironside and Dr. Jan Fraser. No part of this work has been, or will be submitted for any other degree, diploma, or qualification.

Gary Clarke

December 2005

Acknowledgements

I would initially like to thank my supervisors Professor James Ironside and Dr. Jan Fraser who have continually supported me during my PhD research. Thank you for giving me the opportunity to study at the Institute for Animal Health under your guidance-your assessment of my work has always been invaluable. I also thank Dr. Andy Gill and Dr. Matt Hicks-half of this project wouldn't have been possible without your help. I would also like to thank the staff of the animal unit whose excellent work has made this research possible! I am grateful to the Medical Research Council (MRC) and the Biotechnology and Biological Sciences Research Council (BBSRC) for funding this research.

I would also like to thank all of the staff of NPU for their continual support, training, and patience! Initial thanks to the other members of the Neuropathogenesis group: Debbie, Janice, Karen B, Aileen and WingGee who have looked after me from the start! I'll miss you all. Special thanks to Dave Parnham for the support, the laughs and of course the endless abuse!! Thanks also to my good friends Sam Eaton, Diana Best, Katie Appleby, Gillian Morrow & Jayne Blanshard.

I look forward to my stress levels lowering and being a normal person again! Final thanks to my family for their continued support and encouragement, especially my mum who always puts others before herself. You are the bravest and kindest person I know; these recent months have made us all appreciate you more than ever-thank you!!!

Table of Contents

Abbreviations

AIF	Apoptosis-inducing factor
ABC	Avidin biotin complex
Apaf-1	Apoptotic protease activating factor 1
ATP	Adenosine triphosphate
BCA	Bicinchoninic acid
BSA	Bovine serum albumin
BSE	Bovine spongiform encephalopathy
CAD	Caspase-activated deoxyribonuclease
CNS	Central nervous system
CWD	Chronic Wasting disease
CJD	Creutzfeldt-Jakob disease
Cyt c	Cytochrome C
D.p.i.	Days post injection
DISC	Death-inducing signalling complex
DNA	Deoxyribonucleic acid
Diablo	Direct IAP-binding protein of low isoelectric point
DAB	Diaminobenzidine
DMSO	Dimethyl sulphoxide
dH_20	Distilled water
Dpl	Doppel protein (PrP homologue)
DMEM	Dulbecco's modified Eagle's medium
Endo G	Endonuclease G
ER	Endoplasmic reticulum
ELISA	Enzyme linked immunosorbent assay

fCJD	Familial Creutzfeldt-Jakob disease
FFI	Fatal Familial insomnia
FSE	Feline spongiform encephalopathy
FAD	Flavin adenine dinucleotide
FACS	Fluorescence activated cell sorting
FDCs	Follicular dendritic cells
FTIR	Fourier transform infra-red spectroscopy
GFAP	Glial fibrillary acidic protein
GPI	Glycosyl phosphatidylinositol
GSS	Gerstmann-Straussler-Scheinker syndrome
HBSS	Hank's balanced salt solution
Hsp70	Heat shock protein (molecular weight 70kDa)
HMW	High molecular weight
HPLC	High pressure liquid chromatography
iCJD	Iatrogenic Creutzfeldt-Jakob disease
ICAD	Inhibitor of caspase-activated deoxyribonuclease
I.C.	Intra-cerebral
ICC	Immunocytochemistry
IMS	Industrial methylated spirits
IMM	Inner mitochondrial membrane space
I.P.	Intra-peritoneal
kDa	Kilo Dalton's
LRS	Lymphoreticular system
MBM	Meat and bone meal
MES	2-(N-morpholino) ethane sulphonic acid

mtDNA	Mitochondrial deoxyribonucleic acid
MLS	Mitochondrial localisation sequence
MTT	3-(4,5-Dimethylthiazol-2-yl)-2,5-Diphenyltetrazolium Bromide
NB	Normal brain
NEM	N-ethylmaleimide
NGF	Nerve growth factor
N2a	Neuroblastoma cell line (mouse origin)
NAD	Nicotinamide adenine dinucleotide
PNS	Peripheral nervous system
PMT	Permeability transition pore
PMSF	Phenylmethanesulfonyl fluoride
PC12	Pheochromocytoma cell culture (rat origin)
PARP	Poly (ADP-ribose) polymerase
PVDF	Polyvinylidene difluoride
PMCA	Protein misfolding cyclic amplification
Prion	Proteinaceous infectious particle (PrP)
PrP^{27-30}	Proteinase-K resistant core of PrP^{sc}
PrP^{c}	Normal cellular isoform of PrP
PrP^{res}	Proteinase-K resistant core of PrP
PrP^{sc}	Abnormal disease-specific isoform of PrP
Prnd	Doppel protein gene
PRNP	Human prion protein gene
Prnp	Murine prion protein gene
$Prnp^{0/0}$	PrP null
$Prnp^{+/-}$	PrP heterozygote

ROS	Reactive oxygen species
RecPrP	Recombinant PrP
RNA	Ribonucleic acid
SAF	Scrapie associated fibrils
ScN2a	Scrapie-infected neuroblastoma cell line (mouse origin)
Sinc	Scrapie incubation period gene
SMB	Scrapie mouse brain
Smac	Secondary mitochondrial activator of caspases
SCID	Severe combined immunodeficiency
sCJD	Sporadic Creutzfeldt-Jakob disease
TUNEL	Terminal deoxynucleotidyl transferase mediated dUTP nick end labelling
TFA	Trifluoroacetic acid
TME	Transmissible mink encephalopathy
TMT	Trimethyltin
TSE	Transmissible spongiform encephalopathy
TVBs	Tubulovesicular bodies
vCJD	Variant Creutzfeldt-Jakob disease
VDAC	Voltage-dependent anion channel

Abstract

The transmissible spongiform encephalopathies (TSEs) are fatal neurodegenerative diseases of the CNS in humans and animals, characterised by long incubation periods and transmissibility within and between different species. The primary aims of this thesis were firstly to analyse the possible role of caspase-independent apoptotic cell death pathways in TSEs, and secondly to develop an *in vitro* model of neuronal loss in order to assess the relationship between amyloid fibril structure and neurotoxicity.

Caspase-independent pathways were analysed in two well characterised murine scrapie models (ME7/CV and 87V/VM). Whole or micro-dissected brain areas from terminal stage infected mice were separated into cytosolic and mitochondrial fractions, and their protein contents compared by Western blot to normal brain injected age-matched control animals. Micro-dissection proved to be a much more sensitive technique for the detection of apoptosis-related proteins *in vivo*. Caspase-independent apoptosis inducing factor (AIF) was found to translocate from the inner mitochondrial membrane space (IMM) to the cytosol in ME7/CV animals, but not in 87V/VM or in normal brain-injected control cohorts. The release of AIF into the cytosol is therefore specific to infection with the ME7 murine scrapie strain. Furthermore, cytochrome c (cyt c) was released from the IMM in all animals at the terminal stage of disease. However, cyt c was not released from the IMM in younger animals, indicating that dysfunction of the mitochondria is related to age and not to disease.

A neuronal PC12 cell system was established to model TSE neurodegeneration *in vitro*. Murine PrP105-125, homologous to the neurotoxic human PrP106-126 synthetic peptide, was developed specifically for this research. Mature amyloid fibrils were created containing β–sheet structures, but different tertiary structures as revealed

by electron microscopy, Thioflavin T binding assays and FT-IR techniques. The primary structure of the MoPrP105-125 peptide is critical for conferring the neurotoxicity, as a scrambled sequence is not toxic to neurons. Furthermore, the research within this thesis shows that the morphology of mature amyloid fibrils does not have a significant effect on toxicity, suggesting that the intermediate soluble protofibrillar structures may prove to be the more toxic species.

In conclusion, this research shows that the mechanisms of neuronal loss in two tested TSE models can follow different biochemical pathways, which might explain differences in the selective targeting of these TSE agents to different CNS neuronal populations. These studies also revealed that mitochondrial dysfunction occurred within the lifespan of the animals tested in this research, which may contribute to neuronal death in the ME7/CV model. In addition, an *in vitro* model demonstrated that PrP fibril toxicity was principally related to the primary sequence of the fibrils, and not to the secondary or tertiary structures of mature fibrils. These results are all relevant to the future development of potential therapeutic strategies for TSEs, and may also have wider implications for the treatment of other CNS amyloidogenic diseases.

Chapter 1: Introduction to Transmissible Spongiform Encephalopathies (TSEs)

1.1.1. General TSE background

The transmissible spongiform encephalopathies (TSEs), or prion diseases, are fatal, infectious, non-inflammatory neurodegenerative diseases of the central nervous system (CNS) in humans and animals. These conditions have also previously been described as sub-acute spongiform encephalopathies, slow viral diseases and transmissible dementias. TSEs in humans include Creutzfeldt-Jakob disease (CJD); with etiological subtypes of sporadic (sCJD), iatrogenic (iCJD), familial (fCJD) and variant (vCJD); Kuru, Fatal Familial Insomnia (FFI) and Gerstmann-Straussler Scheinker syndrome (GSS). In animals, TSE diseases include scrapie of sheep and goats, Chronic Wasting disease of elk and mule deer (CWD); Transmissible mink encephalopathy (TME) and Bovine spongiform encephalopathy (BSE). These diseases are unique in that they can present as a result of sporadic, infectious and genetic mechanisms; and all are transmissible by natural or experimental means. TSEs in humans and animals are differentiated by differences in clinical symptoms, incubation period and pathological changes in the brain (Sections 1.1.2. and 1.4.).

In recent years, new TSEs have emerged following the discovery of BSE in cattle in 1987 (Wells *et al.* 1987); a new form of CJD in humans termed vCJD (Will *et al.* 1996), and a novel TSE in domestic cats termed feline spongiform encephalopathy (FSE) (Wyatt *et al.* 1990). FSE has also been identified in captive wild cats including cheetas and pumas (Peet & Curran 1992; Willoughby *et al.* 1992). Other novel BSE-related TSEs have been identified in a range of ungulates including captive nyala and gemsbok (Jeffrey & Wells 1988; Wilesmith *et al.* 1988), in elands (Fleetwood &

Furley 1990), arabian oryx and greater kudu (Kirkwood *et al.* 1990) and American bison (Kirkwood & Cunningham 1999) (Table 1.1). The origin of the BSE agent is unknown but it is hypothesised that the practice of rendering cattle and sheep carcasses for cattle feed led to the spread of the disease by the consumption of contaminated meat and bone meal (MBM) (Wilesmith *et al.* 1988). In May 1990, FSE was identified in domestic cats, generating widespread concern that the BSE agent might be transmissible to other species. In 1990, a National Surveillance Unit was established in Edinburgh to enhance the surveillance for all forms of CJD. In March 1996, this National CJD Surveillance Unit announced the identification of a new form of CJD, now termed vCJD (Will *et al.* 1996). The link between BSE and vCJD was first proposed on the basis of epidemiological evidence (Will *et al.* 1996) and subsequently reinforced by the biochemical similarities between PrP^{res} (Section 1.3.2.) in the brains of BSE and vCJD infected hosts (Hill *et al.* 1997). Experimental murine transmission studies confirmed that the infectious agent in BSE had identical incubation periods and indisputable similarities between the distribution and extent of vacuolation in the brains of mice inoculated with the vCJD infectious agent (Bruce *et al.* 1997). Similar findings were subsequently reported following the experimental transmission of BSE and vCJD in transgenic mice expressing bovine PrP (Scott *et al.* 1997; Scott *et al.* 1999).

Disease	Host	Mechanisms of Pathogenesis
sCJD	Humans	Unknown, possibly due to somatic mutations or spontaneous conversion of PrP^{c} to PrP^{sc}
fCJD	Humans	Germ-line mutations in *PRNP* gene
iCJD	Humans	Accidental infection (e.g. from human growth hormone, corneal transplant, dura matter grafts)
vCJD	Humans	Infection from bovine tissues (possibly by oral ingestion)
Kuru	Humans (Fore tribe, Papua New Guinea)	Infection probably due to cannibalistic rituals
GSS	Humans	Germ-line mutations in *PRNP* gene
FFI	Humans	Germ-line mutations in *PRNP* gene
Scrapie	Sheep and goats	Unknown, disease appears to be spread by maternal and/or horizontal transmission
BSE	Cattle	Ingestion of infected MBM in animal feed
CWD	Mule deer and elk	Unknown, disease appears to be spread by horizontal transmission
TME	Mink	Unknown, probable infection from animal feed containing material from infected sheep/cattle
FSE	Domestic and wild cats	Ingestion of infected MBM in animal feed
Exotic Ungulate Encephalopathy	Greater kudu, Nyala, Oryx, Eland, Gemsbok, American Bison	Ingestion of infected MBM in animal feed

Table 1.1 **Spectrum of TSE disease in humans and animals**

1.1.2. Natural and experimental scrapie

Scrapie, which naturally affects sheep and goats has long been recognised, with the first definite record in the UK reported in 1732. By 1755, the volume of documented cases led the government to ban the mixing of healthy animals with those suspected of carrying the infection, as a means to limit the spread of disease. It is now understood that the disease was widespread throughout Europe at this time; known as la tremblante in France, Traberkrankheit in Germany and rida in Iceland. Scrapie is widespread in many sheep-producing regions worldwide including Great Britain and many other European Union countries (where it is a notifiable disease), the United States of America and Canada. Australia and New Zealand are generally accepted as being scrapie-free but flocks are not resistant to infection, as sheep imported into the US from New Zealand have succumbed to disease (Hourigan *et al.* 1979). The lack

of scrapie in New Zealand and Australia therefore appears to be due to the lack of agent in these countries, reasons for which remain unclear.

Clinical symptoms of the scrapie appear to vary between outbreaks of infection. The clinical course can last from as little as two weeks to six months, with incubation periods typically ranging from two to five years. Clinical symptoms begin with the social withdrawal of the animal from the flock, nervousness, apprehension, trembling, and uncoordinated movements. Throughout the clinical course other symptoms may include pruritis (as a result of intensive scratching against inanimate objects), emaciation and hyperaesthesia. Fertility appears to be unaffected, as lambs can be born to ewes which have entered the clinical phase of disease. Later in the clinical course, motor symptoms appear which include head trembling and ataxia.

Mechanisms of natural scrapie transmission are not fully understood, but it is known that infectivity can be passed from an infected ewe to her lambs both pre- and post-natally. However, it is also possible for infected ewes to give birth to uninfected, healthy offspring. Infectivity can be passed experimentally through both oral and skin scarification routes, and it is believed that natural scrapie may be transmitted by these mechanisms (Dickinson *et al.* 1974; Hourigan *et al.* 1979). Natural scrapie was first shown to be transmissible by intraocular inoculations between sheep following prolonged incubation periods (Cuille & Chelle 1936). These long incubation periods led researchers to propose that the infectious agent was a slow progressive virus.

In 1959, (Hadlow 1959) proposed similarities between TSE diseases in animals and humans, based upon the neuropathological similarities of scrapie and Kuru, a recently identified emerged endemic human TSE in the Fore tribe of Papua New Guinea (Gajdusek & Zigas 1957). Subsequently, Klatzo (Klatzo *et al.* 1959) noted neuropathological similarities between Kuru and CJD. Subsequent intracerebral (i.c.) inoculation of primates with Kuru brain material resulted in a spongiform encephalopathy remarkably similar to Kuru in humans (Gajdusek *et al.* 1966). Further successful inoculations of primates with sCJD and GSS verified the transmissibility of these diseases between humans and animals (Gibbs *et al.* 1969; Masters *et al.* 1981), suggesting common infectious mechanisms.

Many subsequent experimental transmission studies ensued; Pattison and Millson (Pattison & Milson 1961) were the first to recognise the existence of different strains of the transmissible agent from a single source of scrapie, resulting in the isolation of the clinically distinct isolates termed "drowsy" and "scratching" syndromes in goats. These characteristics remained highly consistent on subsequent goat-to-goat passage. The successful transmission of scrapie from these experimentally inoculated goats to mice (Chandler 1961; Zlotnik & Rennie 1963) and direct transmissions of sheep scrapie to mice (Chandler 1961; Zlotnik & Rennie 1962); was a major advance for TSE research. Many other models for scrapie research have been described, but the murine scrapie models have persisted due to their high reproducibility, relatively shorter incubation periods, and basic economical considerations. Approximately 20 phenotypically distinct experimental strains of the scrapie agent have been identified in mice following sub-passages of the infectious agent (Bruce *et al.* 1991; Bruce *et al.* 1992), although the precise number of strains existing naturally in sheep is unknown.

The development of these highly reproducible models of murine scrapie infection have resulted in numerous advances in the understanding of the pathology and biochemistry of scrapie as well as many of the other human and animal TSE diseases.

1.2. Host-encoded sialoglycoprotein, PrP^c

1.2.1. The prion protein and the prion protein gene

Prion diseases are characterised by the conformational conversion of a normal cell-surface protein (PrP^c) into a protease-resistant, β-rich form (PrP^{sc}) (Bolton *et al.* 1982). Expression of PrP^c is essential for the development of TSE disease, as highlighted by the lack of disease in PrP^c-deficient mice ($Prnp^{0/0}$) during experimental scrapie challenges (Bueler *et al.* 1992; Manson *et al.* 1992; Bueler *et al.* 1993). Evidence suggests that the primary sequence of PrP is a major determinant of the species-specificity, incubation period, and neuropathological characteristics observed in the different prion diseases (Westaway *et al.* 1987). Following translation, PrP^c is cleaved at the N terminus to leave a protein containing five octapeptide repeats (spanning residues 51-91) with two potential glycosylation sites in mice at residues 181 and 197 (Figure 1.1.). The molecular weight of the mature PrP^c protein *in vivo* ranges from 33-35 kDa (Oesch *et al.* 1985), depending on wheither the protein is di-, mono-, or un-glycosylated.

PrP^c is encoded by a single copy gene, *PRNP* in humans and *Prnp* in mice, the structure of which is known to be highly conserved amongst various mammals, usually consisting of 2 or 3 exons, a single open reading frame within a single exon and a guanine/cytidine-rich promoter sequence. In humans the gene is located on the short arm of chromosome 20, whilst in mice is located on chromosome 2 (Liao *et al.*

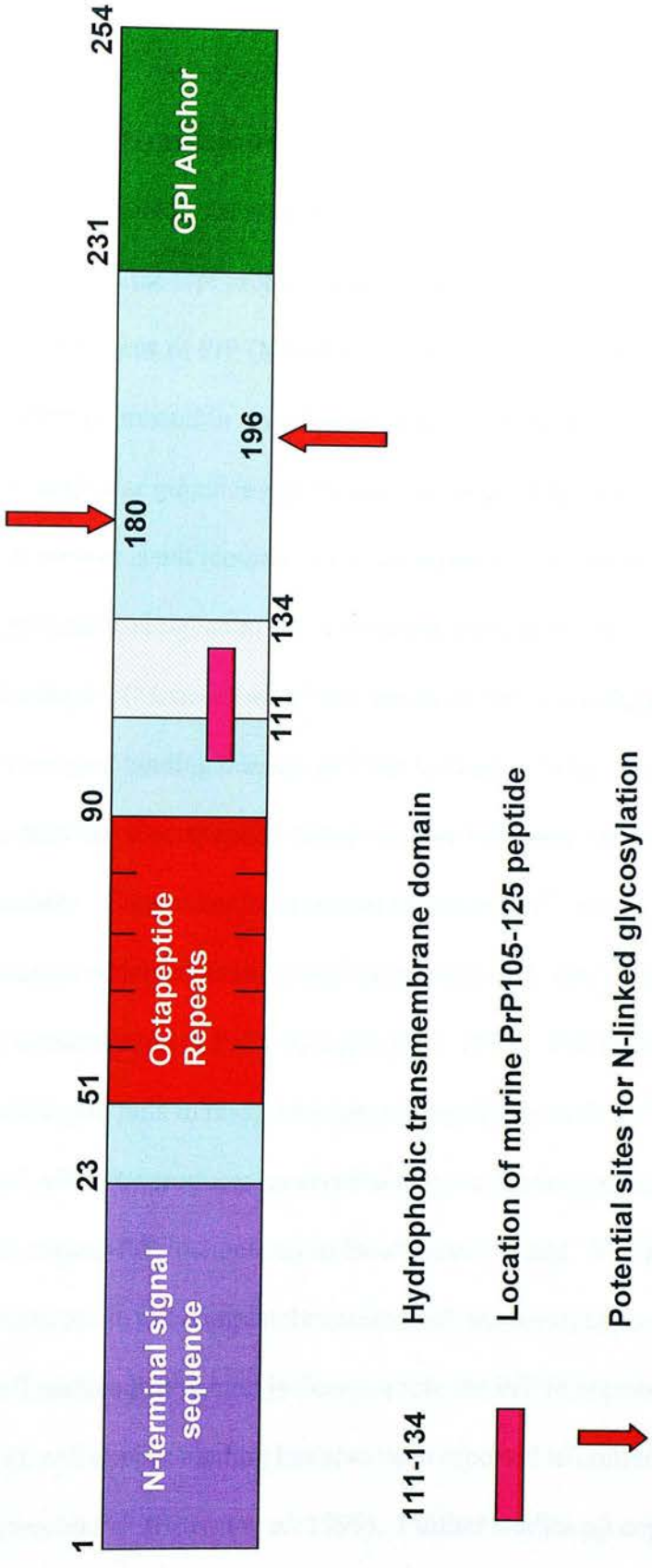

Figure 1.1 **Bar diagram of murine PrP**
Murine PrP consisting of 254 amino acids with attached glycosyl-phosphatidylinositol (GPI) anchor. The octapeptide repeat region and two potential glycosylation sites are also indicated. The synthetic MoPrP105-125 peptide used in the research described in Chapter 4 is based upon the hydrophobic region indicated between residues 111-134

1986; Sparkes *et al.* 1986). A PrP homologue, termed Doppel (Dpl), was discovered in 1999 (Moore *et al.* 1999) and may help us to understand the as yet unknown natural function(s) of the PrP^c protein (discussed in Section 1.2.3). The Dpl gene (*Prnd*) lies downstream of *Prnp*, and the Dpl protein exhibits approximately 25% homology to two-thirds of the C-terminus of PrP (Moore *et al.* 1999). Dpl expression is highest in the testes, and is over-expressed in some PrP-null mice resulting in late stage ataxia due to the loss of cerebellar granules and Purkinje neurons (Moore *et al.* 1999). However, the Dpl protein is not required for prion replication (Tuzi *et al.* 2002) and lacks certain sequences homolgous to the N-terminal domain of PrP containing the octapeptide repeat region (Moore *et al.* 1999), which in PrP is implicated in binding copper ions. This copper binding domain of *Prnp* is thought to be important as alterations to the number of octapeptide repeat regions influence the development of familial prion diseases. Copper has been shown to induce PrP^c into a protease-resistant conformation which contains a large proportion of β–sheet, and which is distinct from the conformation of PrP^{sc} (Quaglio *et al.* 1999). PrP lacking the octapeptide repeat region fails to restore scrapie susceptibility to $Prnp^{0/0}$ null mice (Supattapone *et al.* 1999) or produces an atypical disease phenotype, indicating an important role for copper-PrP interactions in the disease process. The functions of copper-PrP interactions are not completely understood; however, copper induces endocytosis of cell surface PrP^c which indicates a role for PrP in copper metabolism (Pauly *et al.* 1998), and copper binding has also been reported to confer superoxide dismutase properties on PrP (Brown *et al.* 1999). Further studies on copper-PrP interactions will hopefully contribute to understanding the true biochemical functions of PrP^c, these are further discussed in Section 1.2.3.

Dickinson named a gene governing scrapie incubation periods in inbred mice as the *Sinc* gene, derived from the term scrapie incubation period, and the two alleles of the gene were termed s7 and p7, which shorten and lengthen incubation periods respectively with neither allele showing dominance (Dickinson *et al.* 1968). *Sinc* and *Prn-i*, which encodes alleles N and I which also confer short and long incubation periods (Carlson *et al.* 1986; Carlson *et al.* 1988), were subsequently found to be linked to the *Prnp* mouse gene, and are now believed to be the same gene. The s7 and p7 allotypes in mice result from *Prnp* codon 108L/F and 189T/V dimorphisms, where $Prnp^{a}$ (previously termed s7) encodes 108L189T and $Prnp^{b}$ (previously termed p7) encodes 108F189V (Westaway *et al.* 1987). In 1998, Moore et al (Moore *et al.* 1998) introduced the polymorphisms for $Prnp^{b}$ (108F189V) into the $Prnp^{a}$ allele of 129/Ola mice, and inoculated these co-isogenic mice with infectivity, confirming the congruence of *Sinc*/*Prn-i* and *Prnp* and their control over incubation periods.

Inoculations of natural scrapie isolates into mice homozygous for $Prnp^{a}$ and $Prnp^{b}$ and the F1 cross populations have formed the basis of scrapie strain typing experiments. The majority of such experiments have concentrated on the C57BL ($Prnp^{a}$) and VM ($Prnp^{b}$) genotypes and the resulting heterozygote F1 cross, CV ($Prnp^{ab}$). Inoculations of natural scrapie into these mice have revealed two broad groups of murine scrapie strains, the ME7 and 22A groups. The ME7 group has relatively short incubation periods in $Prnp^{a}$ mice, but incubation periods are much longer when inoculated into $Prnp^{b}$ mice. The 22A group showed the reverse of this observation. ME7 group strains inoculated into CVF1 heterozygotes had incubation periods typically between those expected for the parental genotypes, but the incubation periods for the 22A group are longer. Further complicating genetic influences on incubation periods, a

third *Prnp* allele was reported ($Prnp^c$) with polymorphisms of 108F189T which in co-isogenic mice had incubation period increases greater than 100 days when challenged with the Chandler scrapie strain (Lloyd *et al.* 2004). The two murine scrapie models, defined by the combination of host and infecting scrapie strain, examined in this work are the 87V strain with the VM mice combination ($Prnp^b$) and the ME7 strain with the CVF1 cross (C57xVM) combination ($Prnp^{ab}$).

1.2.2. Biosynthesis and expression of PrP^c from *Prnp*

Basler *et al* (1986) first demonstrated that the *Prnp* gene in mice encoded for the expression of PrP^c. Subsequent investigations revealed PrP^c expression from $Prnp^a$ and $Prnp^b$ allotypes appear to be similar in brain tissue, (Westaway *et al.* 1987; Manson *et al.* 1992), therefore differences in incubation periods are less likely to be due to differing levels of PrP^c, but more likely the ability of different TSE agents to interact with the host PrP^c. PrP^c expression is essential for the development of TSE disease, as shown by the lack of disease in PrP^c -deficient mice ($Prnp^{0/0}$) during experimental scrapie challenges (Bueler *et al.* 1992; Manson *et al.* 1992; Bueler *et al.* 1993). Transgenic mice over-expressing PrP^c have reduced incubation periods, and heterozygosity ($Prnp^{+/-}$) appears to confer partial resistance to infection as observed by prolonged incubation periods. These observations further establish the central role of PrP^c in influencing susceptibility to TSE infectivity. Further transgenic and cell culture models have hinted at the normal physiological function(s) of PrP^c, these are discussed further in the next section.

Transcription of *Prnp* has been detected from day 12 of embryogenesis in the developing central and peripheral nervous systems (Westaway *et al.* 1987), and is

expressed constitutively in adult mice in a number of organs. Highest PrP^c expression is found in neuronal cells of the brain (particularly in pyramidal neurons of the hippocampus, cerebellar Purkinje cells and neurons within the thalamus and neocortex) and spinal cord (Manson *et al.* 1992), but is also expressed by non-neuronal cells including oligodendrocytes and astrocytes (Moser *et al.* 1995). PrP^c is also found in lower levels in heart, lung, kidney, spleen, liver, and lymphocytes (Caughey *et al.* 1988; Cashman *et al.* 1990; Mabbott *et al.* 1997). Nascent PrP^c is synthesised as a polypeptide chain of 256 amino acids (aa), which undergoes a number of post-translational modifications during translocation from the endoplasmic reticulum (ER) to the cell surface. The 22 aa N-terminal signal sequence directs the polypeptide to the ER, with subsequent cleavage of the signal sequence and removal of the 23 aa C-terminal hydrophobic signal sequence. In mice, the formation of a disulphide bond between cysteine residues 179 and 214 and glycosylation at asparginine residues 181 and 197, permits attachment of the glycosyl phosphatidylinositol (GPI) anchor at serine 231 which is essential for correct orientation of the protein at the plasma membrane (Stahl *et al.* 1987; Turk *et al.* 1988; Haraguchi *et al.* 1989; Zahn *et al.* 2000). Mature PrP^c are 33-35 kDa proteins (Bolton *et al.* 1982) which have a secondary structure composed primarily of α-helices, and are sensitive to digestion by proteinase-K (Pan *et al.* 1993). The abnormal isoform PrP^{sc} has a primary structure identical to PrP^c, but with an altered secondary structure and differing biochemical properties (Table 1.2) which may contribute to the pathogenic process.

PrP^c	PrP^{sc}
Located on the surface of cultured neuronal cells, via a GPI-anchor [1]	Can be located within the extracellular space in the neuropil [2] or surrounding neurons (e.g. 87V scrapie infections) [3] in mice, and intraneuronally in different species [4]
β-sheet content 3 %, α-helix content 42 % [5, 6]	β-sheet content 43 %, α-helix content 30 % [5, 6]
Size of protein, 33-35 kDa [7]	N-terminal truncation, by proteinase-K digestion, results in a molecular weight of 27-30 kDa [8]
Proteinase-K sensitive [9]	Proteinase-K resistant [9]
Soluble in non-denaturing detergents [10]	Insoluble in non-denaturing detergents [10]

Table 1.2 **Differences between the normal prion protein (PrP^c) and the proposed infectious isoform (PrP^{sc})**

[1](Stahl *et al.* 1987); [2](Jeffrey *et al.* 1994); [3](Jeffrey *et al.* 1994); [4](Jeffrey & Fraser 2001);[5](Caughey *et al.* 1991); [6](Safar *et al.* 1993); [7](Bolton *et al.* 1982) ; [8](McKinley *et al.* 1983; Oesch *et al.* 1985); [9](Pan *et al.* 1993); [10](Meyer *et al.* 1986).

1.2.3. PrP^c function

The normal physiological function of PrP^c has yet to be determined, however, a vast literature exists documenting various properties of the protein. The understanding of the normal function of this protein is essential in order to grasp its role in TSE infections. Transgenic and cell culture models are responsible for furthering our understanding, or confusion, of PrP^c function. Initial observations that $Prnp^{0/0}$ mice were clinically and pathologically normal suggested the function of PrP^c may have become evolutionary obsolete. However, the protein is highly conserved between mammals, has a short half-life and is highly expressed in numerous tissues (particularly neurons). Subsequent observations in $Prnp^{0/0}$ mice revealed altered sleep patterns, circadian rhythms and reduced long term potentiation in CA1 hippocampal neurons in comparison to wild type animals (Collinge *et al.* 1994; Tobler *et al.* 1996; Tobler *et al.* 1997). Other suggested functions include the long-term survival of

Purkinje neurons (Sakaguchi *et al.* 1996), synaptic functions (Collinge *et al.* 1994), and binding of endogenous metal ions to the octapeptide repeat region of the N-terminal segment with possible superoxide dismutase activity (SOD) as an anti-oxidant (Brown *et al.* 1997; Brown *et al.* 1997; Brown & Besinger 1998). Further to this, it is believed that PrP^{c} is endocytosed through clathrin-coated pits, cycling between the site of endocytosis and the plasma membrane (Shyng *et al.* 1993; Shyng *et al.* 1994). The function of this rapid recycling is unknown, but may indicate a cell signalling function. Some of the suggested PrP^{c} binding partners include metal ions such as Cu^{2+} Mn^{2+} and Zn^{2+} (Pan *et al.* 1992; Brown *et al.* 1997), laminin (Graner *et al.* 2000), and the laminin receptor precursor protein (Rieger *et al.* 1997).

Whatever the physiological function of PrP^{c}, its expression and location determine the susceptibility of a host to TSE infection. This is most likely by influencing interactions with endogenous/exogenous PrP^{sc} molecules. Animals without PrP^{c} expression are resistant to infection, and do not form PrP^{sc} following experimental challenge with TSE agents. The hypothesised interactions resulting in the accumulation of aggregated PrP^{sc} molecules will be discussed.

1.3. The nature of the infectious agent

1.3.1. Viruses, viroids, virinos and SAF

The identity of the infectious agent of TSE disease remains highly controversial, ranging from the suggestion that it is a novel sub-species of a virus or virino, to the idea that it is an entirely novel infectious species termed the prion. Early observations revealed that the scrapie agent was resistant to extremes of temperature (Stamp *et al.* 1959; Hunter & Millson 1964; Pattison 1965) and is inactivated in highly alkaline environments which may be attributed to (if present) hydrolysis of RNA, denaturation of dsDNA or protein denaturation. Ionisation studies revealed that the agent was resistant to levels of radiation known to inactivate known viruses (Alper *et al.* 1966) and infectivity is relatively resistant to formalin fixation and high levels of U.V. radiation (Pattison 1965; Alper *et al.* 1967; Latarjet & Muel 1970; Millson *et al.* 1976). However, it is now known that viruses with small genomes have similar profiles of resistance to ionising radiation. The observed resistance of the scrapie agent to nucleases, psoralens, proteases (eg proteinase-K, trypsin) although not typical of conventional viruses, have been observed in other viral species, and the failure to identify a nucleic acid component of the scrapie agent is not evidence for its absence. The discovery of viroids in 1971 (naked nucleic acids lacking polypeptide components) (Diener 1971) revealed the existence of new infectious agents smaller than known conventional viruses, further affirming the probability that new infectious sub-species have yet to be discovered and classified. Although U.V. radiation resistance profiles of viroids are similar to the scrapie agent, the concept that the scrapie agent was a viroid was discredited due to requirements for a host protein for infectivity (now known to be PrP^c), and a number of diverse physiochemical

properties including the resistance of the scrapie agent to nucleases and its sensitivity to phenol.

The emergence of new infectious agents justified a hypothesis that the scrapie infectious agent was a novel infectious species, with a small nucleic acid (encoding strain specific information) permitting interactions with the hosts' replication machinery and protected by a host-encoded protein coat. This virino hypothesis encompasses a number of the characteristics of these agents, including the lack of immune response in infected hosts, the concept of different scrapie strains, species barrier effects upon transmission to new hosts, the requirement for interactions with host protein(s), difficulties in separation of infectivity from host material, and resistance of nucleic acids to ionising radiation. Difficulties in extracting the infectious agent have restricted biochemical studies to the investigation of crude preparations. It is therefore virtually impossible to clarify if treatments are destroying/inactivating possible nucleic acid or protein components of the infectious agent. It is also possible that the adhesive nature of the agent to cellular components restricts the ability of these treatments to reach, if present, nucleic acid or protein components. It is therefore imperative to develop techniques which isolate the infectious agent to a high degree of purity, as a means to properly classify the infectious agent.

Electron microscopy had been used successfully to identify viral and viroid structures, the proposed similar size of viroids to the scrapie agent led researchers to use this technique to search for the scrapie agent. Scrapie associated fibrils (SAF) were subsequently identified in negatively stained detergent-treated membrane fractions,

which were not isolated in preparations from uninfected control samples (Merz *et al.* 1981). SAF were identified as paired or quadrupled fibrillar structures (4 to 6 nm), resembling but not identical to amyloid in some TSE strains and amyloidoses. Co-isolation of SAF and infectivity from the spleens of scrapie and CJD-infected mice led the researchers to propose a close association with infectivity. Prusiner reported fibrillar "prion rods" which are morphologically indistinguishable from SAF, varying only in length, a difference attributed to preparation procedures (Prusiner *et al.* 1982; Prusiner *et al.* 1983). Although amyloid plaque deposition is not characteristic of all TSE pathology, the extraction of SAF from all tested scrapie isolates has been reported (Merz *et al.* 1983). The relationship linking SAF and infectivity is unclear, thus the isolation of infectivity is again essential.

1.3.2. Prions

The prion, derived from the term proteinaceous infectious particle (Prusiner 1982; Prusiner *et al.* 1982), is based on a self-replicating kinetic model of protein folding. The prion hypothesis postulates the infectious agent to be either a small oligonucleotide closely associated with host protein(s), or a novel self-replicating protein devoid of a nucleic acid component (Prusiner 1982; Prusiner 1998). The principal support for the prion hypothesis stems from the work of Bolton who co-purified infectivity in scrapie-infected hamster brain with an abnormal protease-resistant protein, with a molecular mass of 27-30 kDa not detected in uninfected control animals (Bolton *et al.* 1982). This protein represents the protease-resistant core of a larger molecule, termed PrP^{sc}, which has an apparent molecular mass of 33-35 kDa (Prusiner *et al.* 1984). PrP^{sc} is used to describe the pathogenic isoform, whilst

digestion of PrP^{sc} by proteinase-K (at approximately aa 90) results in the N-terminally truncated fragment termed $PrP^{27\text{-}30}$ (McKinley *et al.* 1983; Oesch *et al.* 1985).

PrP^{sc} is now known to be an abnormal isoform of a normal host-encoded glycoprotein, PrP^{c} (Bolton *et al.* 1985). PrP^{sc} has a secondary structure comprised predominantly of β–sheets, has a tendency to form large insoluble aggregates and is partially resistant to proteinase-K digestion (Bolton *et al.* 1982; McKinley *et al.* 1983; Bolton *et al.* 1985; Oesch *et al.* 1985; Pan *et al.* 1993) (Table 1.2). Biochemical analysis has further highlighted differences in size of the isoform, which can plausibly be attributed to differences in conformation, and altered glycosylation patterns (Kascsak *et al.* 1986; Somerville & Ritchie 1990; Somerville *et al.* 1997). It is believed that the conformational differences are due to post-translational events, as scrapie infection does not alter the quantity or sequence of PrP mRNA (Oesch *et al.* 1985; Basler *et al.* 1986). The prion hypothesis suggests that different strains of TSE agent could be attributed to different conformations of PrP^{sc}, and that each conformation would interact differently with PrP^{c} to determine strain characteristics (Bessen *et al.* 1995). Another theory suggests that modifications to PrP^{sc}, such as altered glycosylation, may be sufficient for transmitting strain-specific information (Hecker *et al.* 1992; Weissmann *et al.* 1993). PrP^{sc} in cell cultures and in the brain is proteolytically cleaved at the N-terminus in the region akin to proteinase-K cleavage (approximately aa 90) leaving a molecular weight of 27-30 kDa (termed $PrP^{27\text{-}30}$) (McKinley *et al.* 1983; Oesch *et al.* 1985), whereas PrP^{c} is cleaved (approximately aa 110) in a portion of the protein known to be amyloidogenic and neurotoxic (Caughey *et al.* 1991; Chen *et al.* 1995). It is hypothesised that as the neurotoxic portion

remains intact in PrP^{sc}, but not in PrP^{c}, that this may be important in determining the pathogenicity of PrP.

The postulated conversion sequence of PrP^{c} to PrP^{sc} is poorly understood, but is hypothesised to proceed slowly from PrP^{c} molecules interacting with endogenous point mutation-containing PrP^{c} or with exogenous PrP^{sc}. The site of conversion is undetermined, but cell culture studies suggest that conversion may occur on the extracellular surface of the cell membrane or within calveolae following endocytosis (Caughey & Raymond 1991; Vey *et al.* 1996), correlating with the cellular location of PrP^{c}. The GPI anchor does not appear to be required for the generation of infectivity (Legname *et al.* 2004), however, deletion of the GPI-anchor *in vivo* reduces infectivity replication by up to ten fold, demonstrating the importance of cell surface PrP^{c} for the transmission of infectivity (Chesebro *et al.* 2005). The homology between PrP^{c} and PrP^{sc} has been shown to determine the efficiency of the conversion process, as a mutational difference of even one amino acid can, but will not always, prevent the production of PrP^{sc} and transmission of disease (Priola & Chesebro 1995; Manson *et al.* 1999). The re-folding hypothesis suggests that the spontaneous conversion of PrP^{c} to PrP^{sc} would be energetically unfavourable. However, the seeding hypothesis suggests that the formation of an aggregated "seed" of PrP^{sc}, would be capable of autocatalysing the conversion of further PrP^{sc} molecules from endogenous PrP^{c} molecules. Another theory suggests that conversion may be directed by binding to as yet unidentified protein(s), termed protein X, which would act as a molecular chaperone (Kaneko *et al.* 1997).

Efforts to better understand the spontaneous conversion of PrP^{c} to PrP^{sc}, have resulted in the development of numerous *de novo* cell culture and transgenic murine models. The requirement of PrP^{c} expression for the development of TSE infection (Bueler *et al.* 1992; Manson *et al.* 1992; Bueler *et al.* 1993), and the effects of PrP gene mutations on the development of disease suggest that spontaneous conversion of PrP^{c} to PrP^{sc} may be facilitated by some PrP gene mutations. Initial attempts to produce *de novo* PrP^{sc} in cell culture systems were unsuccessful (Taraboulos *et al.* 1992); however, murine neuroblastoma N2a cells and the yeast *Saccharomyces cerevisiae* have now been shown to generate PrP^{sc}-like molecules *in vitro* (Ma & Lindquist 1999). These PrP^{sc}-like molecules (Sup35) are biochemically similar to PrP^{sc} (Table 1.2), and *de novo* yeast PrP^{sc} molecules have recently been demonstrated to successfully transmit strain-specific TSE disease (Tanaka *et al.* 2004). The murine transgenic approach has revealed that the over-expression of PrP^{c} can lead to TSE-like neurodegeneration (Westaway *et al.* 1994), and also that a single amino acid mutation from proline to leucine (representative of some GSS cases) can result in the development of spontaneous TSE disease which is transmissible upon sub-passage to uninfected mice (Hsiao *et al.* 1990; Hsiao *et al.* 1994; Manson *et al.* 1999). Additional transgenic models further confirm that spontaneous mutations within the PrP gene can result in the generation of *de novo* PrP^{Sc} molecules (Telling *et al.* 1995; Telling *et al.* 1996). However, confirmation that PrP^{sc} constitutes the infectious agent, and is not just a pathological by-product of the disease process has yet to be proven. Although other proteins have been identified as potential biomarkers for TSE infection in humans such as 14-3-3 and neuron specific enolase proteins (Hsich *et al.* 1996; Beaudry *et al.* 1999), PrP^{sc} remains the most reliable biomarker in confirming TSE infection. However, natural and experimental cases of human and animal

disease exist where there are apparently no detectible levels of PrP^{sc} but where infectivity levels (as determined by mouse bioassay) are high (Telling *et al.* 1995; Dorandeu *et al.* 1998; Foster *et al.* 2001). The ratio of infectious units to PrP is known to be in the domain of $1:10^5$ (Bolton *et al.* 1991), suggesting that only a small portion of PrP is infectious or it is possible that the infectious agent has an altered conformation to PrP^{sc}, which may be isolated with PrP^{sc} using the methods used for its extraction. The infectious agent may be an as yet identified component, such as another protein or nucleic acid in association with or separate from PrP^{sc}. Confirmation that PrP^{sc} is infectious would require its generation *in vitro*, from recombinant or highly purified PrP^{c} molecules. PrP^{sc} would then have to be infectious on transmission to a susceptible host. In contrast, confirmation that PrP^{sc} is not the infectious agent would require the complete separation of PrP^{sc} from infectivity.

The generation of PrP^{res} *in vitro* has been achieved by two main techniques; the cell-free conversion assay and the protein misfolding cyclic amplification (PMCA) reaction. The cell-free conversion assay involves the incubation of excesses of PrP^{sc} with ^{35}S-labelled PrP^{c} (Kocisko *et al.* 1994). This reaction produced a small proportion of protease resistant molecules with a mobility profile similar to PrP^{res}. The generation of infectivity using this technique could not be proven, due to pre-existing levels of infectivity in the original reaction mixture. Additional studies incubating truncated recombinant murine PrP^{res} (PrP90-231) with excesses of PrP^{c} have generated molecules biochemically similar to PrP^{res}. In the absence of conversion techniques using full length $recPrP^{res}$, truncated recPrP (PrP90-231) is sufficient for the synthesis of PrP^{res}. Conversion appears possible as the cleaved N-

terminal portion appears to have a role in normal PrP^c function but not in the conversion process.

The PMCA reaction involves the incubation of PrP^c with scrapie-infected hamster brain homogenates, subjected to repeated sonication cycles (Saborio *et al.* 2001). The result is much higher quantities of PrP^{res}, in comparison to samples exempt from repeated sonication. Sonicating a polymeric aggregate or "seed" would break monomeric PrP^{res} molecules which may then autocatalytically convert further PrP^c to the abnormal conformation. PrP^{res} produced by PMCA also appears to be biochemically indistinguishable from PrP^{sc} in its mobility and resistance to proteinase-K. PMCA of purified proteins and cell lysates yield relatively low quantities of PrP^{res}, however the reaction is much more efficient using brain homogenates suggesting a requirement of cellular factors other than PrP to achieve optimal conversion. The addition of host encoded RNA molecules significantly enhances PrP^{res} production in a dose-dependent manner (Deleault *et al.* 2003), although amplification was inhibited by RNase molecules specific to single stranded RNA, whereas molecules specific to double stranded RNA and DNA had no effect. Other molecules such as thiols and glycosaminoglycans have also been reported to substantially enhance PrP^{res} generation by PMCA (Wong *et al.* 2001). The use of PMCA as a diagnostic tool has recently been reported. PCMA treated homogenates of scrapie infected hamsters and experimental BSE-infected cattle detected PrP^{res} prior to the detection of clinical symptoms. Sensitivity was such that PrP^{res} was detected by Western blot, in samples from pre-clinical animals which would otherwise appear negative (Soto *et al.* 2005). Future applications of PMCA would

have to be optimised for specific disease models, however, PMCA represents an attractive pre-clinical test for TSE diseases such as BSE and CWD.

Very recent reports document the successful development of TSE-like disease in transgenic mice over-expressing PrP^c which have been inoculated with abnormally-folded synthetic murine PrP^c molecules (MoPrP89-230). This disease was transmissible to transgenic, and on subsequent passage, wild-type mice (Legname *et al.* 2004; Legname *et al.* 2005). This research fails to definitively prove the prion hypothesis, as it is well documented that the high expression of PrP^c can result in the development of spontaneous TSE disease (Westaway *et al.* 1994). However, PrP^{res} molecules synthesised by the described *in vitro* PMCA technique have been reported to successfully transmit TSE disease to wild-type hamsters (Castilla *et al.* 2005). The *in vitro* conversion of PrP^c to PrP^{res} molecules, catalysed by interactions with other host cellular factors, is in correlation with the prion hypothesis. Future studies will need to determine whether newly generated PrP^{res} constitutes the sole infectious agent, before this hypothesis can be completely substantiated.

1.4. Murine scrapie strains

The prion donor is the last host in which the prion was passaged and its PrP sequence represents the "species or strain" of the prion. The prion hypothesis (Section 1.3.2) suggests that the presence of TSE strains could be attributed to different conformations of PrP^{sc}, and that each conformation would interact differently with PrP^c to determine specific strain characteristics (Bessen *et al.* 1995). These TSE strains are thought to confer the three-dimensional information to nascent PrP^{sc} molecules. Murine scrapie strains are distinguished by their distinct neuropathology,

lesion profiling (vacuolation scores) (Fraser & Dickinson 1968; Fraser & Dickinson 1973), incubation periods (Dickinson *et al.* 1968), but also by differences in clinical manifestations, ease of transmission to new species, agent susceptibility to thermal inactivation (Dickinson & Taylor 1978) and the immunological and biochemical detection of PrP^{sc}.

1.4.1. Lesion Profiles

Vacuolation of the neuropil is a neuropathological trait of all TSE diseases; however, the distribution of neuronal vacuolation targeted to specific brain areas differs between TSE strains. The quantitative analysis of the degree of vacuolation of the neuropil in nine specific grey and three specific white matter brain areas is termed the lesion profile (Fraser & Dickinson 1968). The extent and localisation of vacuolation is highly repeatable and dependent on the host-strain combination (Fraser & Dickinson 1973), resulting in specifically targeted vacuolation profiles. Vacuolation can depend on the route of inoculation, but as a way of classifying strains is advantageous over incubation period strain analysis in that lesion profiles are unaffected by altering doses of infectivity (Bruce *et al.* 1991). The mechanisms for the strain-targeted vacuolation have yet to be determined, but the targeting of vacuolation suggests specific interactions with neuronal subsets. The degree of vacuolation can vary from focal areas of small vacuoles to large areas of coalescing spongy lesions. CNS vacuolation within cells occurs mainly within dendrites with a low frequency in the early stages of infection which increase towards the terminal stages of disease. Vacuolation is also observed in axons, axon terminals and the neuronal perikaryon.

1.4.2. Incubation periods and species barrier effects

The incubation period is defined as the duration of time from the initial exposure of a host to an infectious agent to the development of specific clinical signs of infection. Murine scrapie models provide a highly reproducible means of monitoring incubation periods when inoculated i.c. into a cohort of highly inbred mice (Dickinson *et al.* 1968). Experimental transmission studies confirmed a "species barrier" effect when inoculating a scrapie strain into a new host of another species, where incubation periods of a characterised strain are initially longer when inoculated into a new host, but shorten and stabilise on subsequent passages in the second host. Not all inoculated animals succumb to disease in the primary transmission, but subsequent passages will result in transmission if the species barrier is overcome (Pattison 1965). Incubation periods are now known to be influenced by the host genotype, the infecting strain, age and sex of the host, the route of inoculation, and titre of infectivity (Dickinson & Meikle 1971; Dickinson 1975).

1.4.3. Experimental routes of transmission

1.4.3.1. LRS replication

The route of experimental transmission determines whether the infectious agent replicates directly in the CNS or peripheral nervous system (PNS), or if it replicates in the lymphoreticular system (LRS) prior to neuroinvasion and replication. Peripheral routes of inoculation usually result in a period of replication in LRS tissues prior to neuroinvasion and therefore prolonged incubation periods. Peripheral challenges may model certain natural routes of infection such as the oral ingestion of infected material and skin scarification. Peripheral challenges permit replication of infectivity in the spleen (Eckland *et al.* 1967), and splenectomised mice can have extended incubation

periods (Fraser & Dickinson 1970; Kimberlin & Walker 1989). Following replication in the spleen, infectivity spreads first to the thoracic and spinal cords, and brain (Kimberlin & Walker 1979; Kimberlin & Walker 1980). Splenectomising mice has no further effect on the duration of the incubation period once infectivity has reached the spinal cord, i.e. once neuroinvasion has been established. LRS cells involved in the replication and neuroinvasion of infectivity are not entirely clear, but ionising radiation exposure studies at different times prior and post-scrapie challenge do not affect replication in the spleen (Fraser & Farquhar 1987). Follicular dendritic cells (FDCs) are non-mitotic long-lived cells with resistance to ionising radiation, and their expression of PrP^{c} and location outside the CNS could provide a site for the replication of infectivity within the LRS system (Fraser & Farquhar 1987; Fraser *et al.* 1992; McBride *et al.* 1992). The generation of SCID (severe combined immunodeficiency) mice (Bosma *et al.* 1983) has been invaluable in identifying key cells involved in peripheral pathogenesis of TSEs. SCID mice (deficient in B-, T-cells and FDCs) do not accumulate PrP^{sc} in the spleen and are resistant to i.p. but not i.c. ME7 scrapie and CJD inoculations, suggesting a requirement for extraneuronal replication prior to neuroinvasion for these strains via peripheral routes of infection. Susceptibility of SCID mice to scrapie infection is restored through bone marrow grafts or inoculations of normal spleen cells (Brown *et al.* 1996; Fraser *et al.* 1996; Lasmezas *et al.* 1996) signifying the primary route of peripheral infection does involve LRS replication. However, SCID mice can be infected i.p. with inoculations containing high titres of infectivity (Brown *et al.* 1996; Fraser *et al.* 1996), suggesting peripheral nerve connections to the CNS (Section 1.4.3.2.) in addition to a pre-replication phase in the LRS. Immunologically-reconstituted SCID mice have functional FDCs, and their developmental inhibition with lymphotoxin-β receptor

fusion protein has been shown to inhibit PrP^{sc} accumulation in the spleen and to prolong the incubation period of infected animals (Klein *et al.* 1997). Further studies using skin scarification in mice, which is as efficient as i.p. inoculation (Taylor *et al.* 1996), have demonstrated a requirement for FDCs for the accumulation of infectivity and neuroinvasion following challenge with ME7 scrapie (Mohan *et al.* 2004; Mohan *et al.* 2005). The precise cellular interactions have yet to be uncovered but again once neuroinvasion has occurred, inhibition of FDC function has no effect on incubation period of peripheral challenged animals (Mabbott & Bruce 2002).

1.4.3.2. Neuronal transport

As previously stated infectivity has been demonstrated to travel rostrally from the spleen to the thoracic cord, spinal cord, and brain (Kimberlin & Walker 1979; Kimberlin & Walker 1980). Early evidence for the spread of infectivity within neurons was demonstrated by injecting ME7 directly into the mouse retinal vitreous body (intraocular) and also 139A scrapie directly into sciatic nerves (Fraser 1982; Kimberlin *et al.* 1983). Infectivity injected directly into PNS or CNS neurons avoids a pre-replication phase in the LRS, and the infectious agent travels to the brain. Peripheral inoculations into splenectomised or genetically asplenic mice indicate additional mechanisms for the spread of infectivity not requiring a pre-replication phase in the LRS. More recently, oral inoculation studies of hamsters with 263K scrapie have revealed the direct spread of infectivity via the splanchnic nerve to the mid-thoracic spinal cord and via the vagus nerve to the dorsal motor nucleus of the vagus nerve and solitary tract nucleus of the brainstem (Beekes *et al.* 1998; McBride *et al.* 2001). These findings correlate well with the primary detection of infectivity and PrP^{sc} in the spinal cord and medulla obloganta following peripheral inoculations.

It appears that both the parasympathetic and sympathetic nerve circuitry is involved in the transport of infectivity and neuroinvasion (Beekes *et al.* 1998; McBride & Beekes 1999; Glatzel *et al.* 2001), and that neuroinvasion is enhanced by overexpression of PrP^{c} (Glatzel & Aguzzi 2000).

The shortest incubation periods, when using comparable doses of infectivity to peripheral challenges, follow inoculations directly into the spinal cord or brain (i.c.) avoiding the pre-replication phase in the LRS. However, post-inoculation a large proportion of inoculum is cleared from the injection site and infectivity is detected in organs of the LRS such as the spleen (Millson *et al.* 1979). Infectivity remaining at the site of inoculation will replicate to critical levels in the CNS prior to the development of clinical disease. The delivery of infectivity directly to the CNS via i.c. inoculations represents an efficient means for establishing agent replication within the CNS.

1.4.4. Neuropathology

1.4.4.1. Accumulation of PrP^{sc}

Various immunological and biochemical techniques have been used to detect PrP^{c} and PrP^{sc}, although antibodies which apparently discriminate between the two conformations have yet to be made widely available. The sensitivity of PrP^{c} to proteinase-K (but resistance of PrP^{sc}) allows for the discrimination of the isoforms using Western and paraffin-embedded tissue blot techniques. In murine scrapie models, PrP^{sc} deposition can be numerous or sparse, and the site of deposition, form, and structure is again dependent upon host/agent interactions (Fraser & Bruce 1983; Bruce *et al.* 1993). PrP^{sc} deposition correlates with vacuolation and targeting can be

extensive or restricted to distinct neuronal populations depending upon the infecting strain and host. Digestion of PrP^{sc} by proteinase-K results in a protease-resistant core of 27-30 kDa (PrP^{27-30}) when analysed by western blot. PrP^{sc} glycosylation has been used as a further means to differentiate between strains as the glycosylation of PrP in mice at asparginine residues 181 and 197 results in three distinct bands representing the diglycosylated, monoglycosylated, and unglycosylated forms. Differences in PrP^{sc} glycosylation have been described in human TSEs, with a specific pattern found for vCJD (Hill *et al.* 1999; Parchi *et al.* 2000). PrP^{sc} glycosylation can also vary between brain regions in scrapie-infected mice and human sCJD (Somerville 1999; Head *et al.* 2001). Futhermore, different PrP isotypes have been detected within a single sCJD brain, raising the possibility of more than one sCJD strain within a host (Head *et al.* 2004) or these findings reinforce the need for the analysis of a combination of pathological characteristics when discriminating between murine scrapie strains.

1.4.4.2. Amyloid plaques

Amyloid plaques consist of extracellular aggregated PrP^{sc} molecules in a β–sheet conformation, and are characteristic of some but not all TSE infections. Plaque deposition occurs in consistent, predictable and distinct patterns *in vivo* (Bruce *et al.* 1989), and is thought that plaque formation originates at focal points along the length of dendrites and possibly along axons at nodes of Ranvier (Jeffrey *et al.* 1994). Primitive plaques initially lack a dense amyloid core and have few or no recognisable fibrillar components, but are thought to mature into classical fibrillar plaques upon the deposition of extracellular PrP^{sc} (Jeffrey *et al.* 1994). Mature plaques are composed of a dense core of amyloid fibrils, containing mainly disease-specific PrP, surrounded

by reactive astrocytes with abundant intermediate filament bundles and activated microglia (Doerr-Schott *et al.* 1990; Jeffrey *et al.* 1994). This aggregated PrP^{sc} is capable of binding extracellular compounds, including highly sulphated glycosaminoglycans (McBride *et al.* 1998). These observations suggest that aggregated and fibrillar forms of PrP are associated with damage to the neuropil. However, in defined areas pre-amyloid forms of PrP are also associated with selective damage to axon terminals and dendritic spines (Jeffrey *et al.* 1997). This axonal damage appears to be a highly specific process, at least in the initial stages of infection, therefore specific mechanisms or receptors confined to particular cells or neurites may be responsible for the selective neuronal damage corresponding to PrP^{sc} accumulation. Initial characterisations of GSS amyloid proteins identified 7 and 11 kDa PrP degradation products, indicating that GSS amyloid is formed as a result of the proteolytic cleavage of PrP (Tagliavini *et al.* 1991). The synthesis of peptides based on these GSS amyloid peptides identified the PrP106-126 sequence as the most neurotoxic region and also revealed similarities to the biochemical properties of PrP^{sc} (Forloni *et al.* 1993; Tagliavini *et al.* 1993; Forloni *et al.* 1994). The characterisation of amyloid peptides and the studies involving the human PrP106-126 peptide sequence will be reviewed in Section 4 to introduce the work of this thesis involving the homologous murine PrP105-125 synthetic peptide.

1.4.4.3. Neuronal loss, gliosis and tubulovesicular bodies

Spongiform change is often accompanied by a number of other neuropathological features including neuronal loss, astrogliosis and microglial activation. Neuronal loss is not due solely to differences in the susceptibility of different subsets of neurons to the disease process, but is also influenced by the host/strain combination (Bruce *et al.* 1976). Neuronal loss in murine scrapie models is thought to occur concurrently with vacuolation, but the mechanisms of neurodegeneration in relation to accumulating PrP^{sc} have yet to be determined. Clear detection of neuronal loss in murine scrapie models is found in CA1 sector of hippocampal neurons in mice infected with ME7 scrapie and in the photoreceptor retinal cells following infection with 79A scrapie (Scott & Fraser, 1984; Foster 1986). CA1 hippocampal neuronal loss in ME7 scrapie infections is extensive by the terminal stages of disease but such loss has been poorly described in other strains, presumably due to a rapid clearance of dead or dying cells from the neuropil. The rapid clearance of cells with abnormal neuronal functions, estimated between 200-300 cells per day, is indicative of apoptosis. Apoptosis has been suggested as a mechanism of cell death in TSE infections, and evidence for apoptosis in TSE infected hosts has been documented. These mechanisms are described in further detail in Section 3. Astrocytosis and activated microglia are non-specific neuropathological characteristics of TSE infection, and again their precise functions are unclear. Astrocytosis appears to be closely associated with neuronal loss, and astrocytosis and microglial stimulation can be prominent in the hippocampus and thalamus (Fraser 1979). Glial cells express PrP^{c}, and astrocytes have been demonstrated to support replication of PrP^{sc} and therefore contribute to disease susceptibility (Raeber *et al.* 1997). Co-localisation of glial cells with amyloid plaques

and PrP^{sc} deposition has been reported, and it is probable that the stimulation of these cells is a consequence of the deposition of PrP^{sc}.

Tubulovesicular bodies (TVBs) are spherical, particulate structures which are 23-45mm in diameter (David-Ferreira *et al.* 1968). TVBs are consistently detected in the brains of naturally and experimentally infected animals. TVBs have been recorded in many murine scrapie isolates, in natural scrapie, CJD, GSS, FSE and in BSE (Liberski *et al.* 1993). The origins of TVBs are unknown, but are detected prior to the described pathological hallmarks and increase in quantity with progression of the incubation period (Narang *et al.* 1987). Increasing quantities of TVBs correlate with increasing titres of infectivity, however TVBs appear devoid of and do not associate with PrP (Liberski *et al.* 1997; Jeffrey & Fraser 2000; Jeffrey & Fraser 2001). The roles of TVBs and gliosis in TSE pathogenesis remain unclear, but are important not only in strain discrimination but in understanding the neuropathology of TSE infectious agents.

1.4.5. The ME7/CV and 87V/VM models

The ME7 murine scrapie strain was isolated from a naturally infected Suffolk sheep (Zlotnik & Rennie 1963) and isolated in C57BL mice (Section 1.2.1.), whereas the 87V strain was isolated by from a naturally infected Scottish Blackface Cheviot cross following passage in VM mice (Bruce 1985; Bruce & Dickinson 1987). The ME7/CV and 87V/VM combinations are two distinct murine scrapie models; differing in incubation periods, sequence of pathological hallmarks and targeting of neuronal populations when inoculated by i.c. inoculation. PrP^{sc} in both models is located within neuronal cell membranes and surrounding neuropil in association with the

extracellular space. However, the intensity and targeting of PrP^{sc} to neuronal populations differs. These murine scrapie models target many different brain areas but due to the well characterised nature of the neuronal connections of the hippocampus, a large quantity of research has concentrated on the effects of these strains on this area.

The CVF1 cross (*Prnp*^{ab}) inoculated i.c. with ME7 results in consistently severe hippocampal vacuolation and an incubation period of approximately 250 days (Scott & Fraser 1984). Vacuolation, gliosis and diffuse granular deposits of PrP^{sc} are widespread in all brain areas in animals infected with ME7, although differing in severity between regions (Figures 1.2. and 1.4.A.). PrP^{sc} deposition is widespread within the hippocampus, whereas vacuolation and neuronal loss are specifically targeted to the CA1 hippocampal subfield. PrP^{sc} is first detected at ~70 days post inoculation (dpi) in the hippocampus by immunocytochemistry (ICC) (Jeffrey *et al.* 2001), whereas infectivity is detected ~50dpi. This observation suggests a lack of correlation between infectivity and PrP^{sc} in this model. At approximately 100dpi; astrogliosis, vacuolation and a decrease in long-term potentiation are evident within the hippocampus (Johnston *et al.* 1997). Abnormalities such as the loss of neuronal axon terminals and synapses are also found following detection of PrP^{sc} (Jeffrey *et al.* 2000). Dendritic abnormalities are detectable from 100dpi but by terminal stages of disease there may be complete or partial loss of dendritic spines and spherical distensions of the dendrites (Belichenko *et al.* 2000; Brown *et al.* 2001). Amyloid plaque deposition is rare in this model but aggregated fibrillar PrP can be observed in the hippocampus at ~154dpi by electron microscopy (Jeffrey *et al.* 2000). Clinical signs of disease appear at ~188 dpi, and death is within weeks.

VM mice (*Prnp*^{b}) inoculated with the 87V agent develop a disease with an incubation period of approximately 320dpi and a series of neuropathological changes differing in sequence to that of the ME7/CV model. Vacuolation and deposition of PrP^{sc} appear to be targeted to specific neuronal populations; including neurons of the CA2 region of the hippocampus, the dorsal lateral geniculate nucleus, and the thalamus. In contrast to the ME7/CV model PrP^{sc} is first detected in the hippocampus at approximately 200dpi. This deposition is preceded by dendritic dysfunction, astrogliosis, vacuolation and neuronal damage (Belichenko *et al.* 2000; Jeffrey *et al.* 2000) (Figures 1.3. and 1.4.B.); therefore pathological features do not appear to be as a direct consequence of PrP^{sc} deposition in this model. Dendritic dysfunction (~70dpi) is a further pathological feature localised to the CA2 pyramidal neurons. Amyloid plaques are common, particularly in the hippocampus and cerebral cortex where the plaques appear as mature dense plaques containing amyloid fibrils and surrounded by activated microglia (Bruce & Fraser 1975). The primary target for the initiation of neurodegeneration in TSE infections remains unknown, however evidence for apoptosis in the CA2 hippocampal subfield *in vivo* has been documented by the detection of the up-regulation of Fas and active Caspase 3 100dpi in the 87V/VM model (Jamieson *et al.* 2001a; Jamieson *et al.* 2001b). No such evidence for a similar mechanism has yet been detected in the ME7/CV model, although the difficulties in detecting apoptosis *in vivo* will be discussed in Chapter 3.

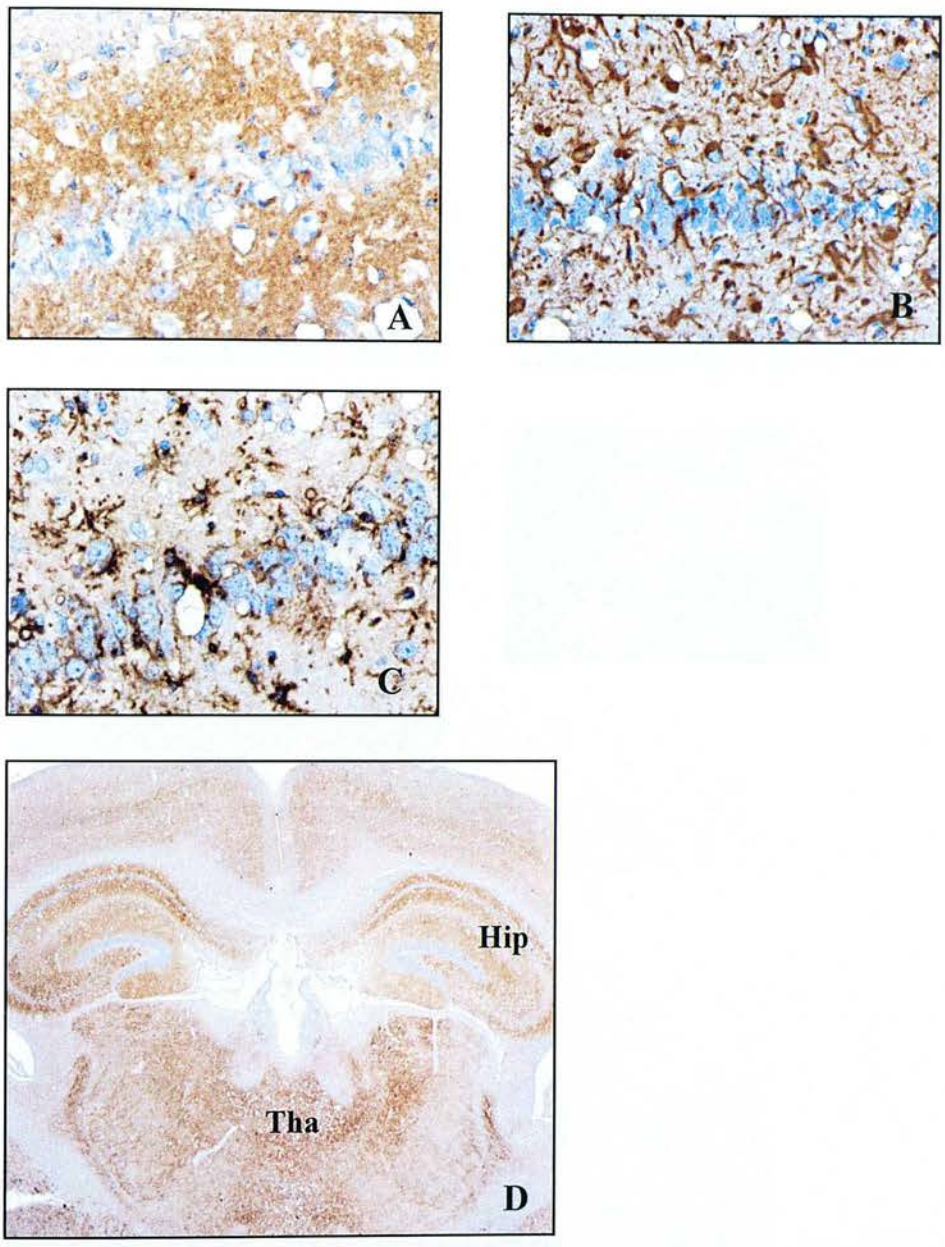

Figure 1.2 **Immunohistochemical staining of coronal brain sections of animals from the ME7/CV murine scrapie model**

ICC (Section 2.2.3) analysis of serial sections of paraffin-embedded terminal ME7/CV murine brain sections. Primary and secondary antibodies used in the analysis are described in Tables 2.1 & 2.2. Bound antibodies were detected with the ABC kit and diaminobenzidine, resulting in the brown precipitate, and neurons were "blued" for contrast using Scott's Tap water (Section 2.2.3). Analysis of apoptotic cell death was concentrated in the Hippocampus (Hip) and Thalamus (Tha), described in Chapter 3.

(A) Accumulation of PrP^{sc} (anti-PrP 6H4 antibody), neuronal loss, and vacuolation within the CA1hippocampal subfield

(B) Glial fibrillary acidic protein ICC analysis shows numerous reactive astrocytes

(C) Biotinylated tomato-lectin ICC analysis shows activatation of microglia

(D) Wide-spread accumulation of PrP^{sc} (including the cerebral cortex, hippocampus and thalamus) using the anti-PrP 6H4 antibody.

All magnifications were at x40, except **D** which was at x2

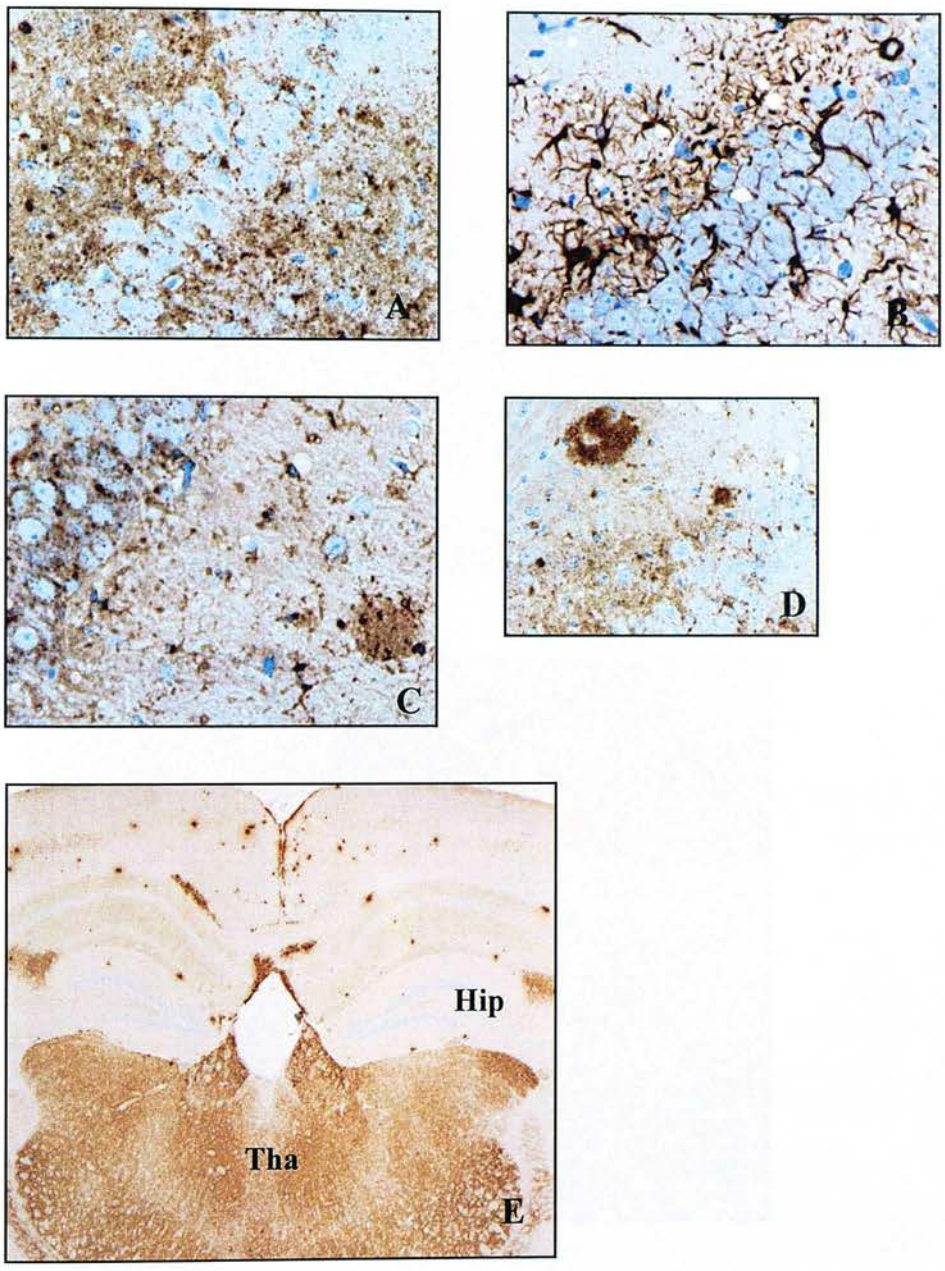

Figure 1.3 **Immunohistochemical staining of coronal brain sections of animals from the 87V/VM murine scrapie model**

ICC (Section 2.2.3) analysis of serial sections of paraffin-embedded terminal 87V/VM murine brain sections. Primary and secondary antibodies used in the analysis are described in Tables 2.1 & 2.2. Bound antibodies were detected with the ABC kit and diaminobenzidine, resulting in the brown precipitate, and neurons were "blued" for contrast using Scott's Tap water (Section 2.2.3). Analysis of apoptotic cell death was concentrated in the Hippocampus (Hip) and Thalamus (Tha), described in Chapter 3.

(A) Accumulation of PrP^{sc} (anti-PrP 6H4 antibody), disruption to, and vacuolation within the CA2 hippocampal subfield

(B) Glial fibrillary acidic protein ICC analysis shows numerous reactive astrocytes

(C) Biotinylated tomato-lectin ICC analysis shows activatation of microglia

(D) Amyloid plaques (typical of the 87V/VM model) immunoreactive with the 6H4 anti-PrP antibody.

(E) Wide-spread accumulation of PrP^{sc} (including the hippocampus and thalamus) using the anti-PrP 6H4 antibody.

All magnifications were at x40, except **E** which was at x2.

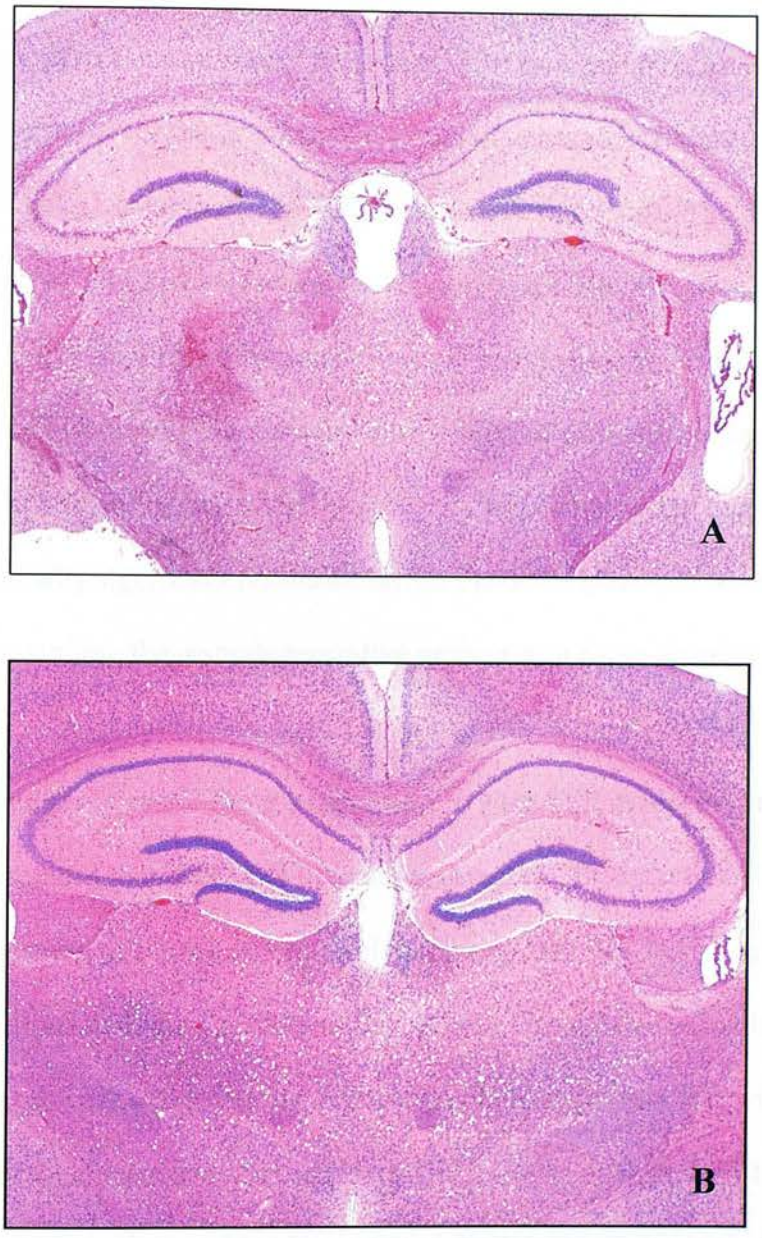

Figure 1.4 **Haematoxylin and eosin (H&E) stained coronal sections (Section 2.2.2), demonstrating the vacuolation of coronal brain sections of representative animals from the (A) ME7/CV and the (B) 87V/VM murine scrapie models**

Haematoxylin & Eosin staining of paraffin-embedded tissue sections of murine brain samples at the terminal stages of the (A) ME7/CV and (B) 87V/VM murine scrapie models (sections were parallel to those analysed for the ICC analysis in Figures 1.2 and 1.3). H&E was performed as described in Section 2.2.2. and sections show widespread degeneration of the neuropil.

1.5. *In Vitro* TSE models

Murine scrapie models have been crucial for increasing our knowledge of TSE disease, however the development of cell culture models for more detailed biochemical analysis of TSE infections is also important. The generation of *in vitro* models of TSE disease have reported various mechanisms for cell death, something which is often difficult to detect *in vivo* if apoptosis is involved. The long incubation periods of naturally and experimentally infected animals, economic considerations of animal husbandry, and often the relatively large numbers of animals required for statistically significant results all favour the development of an *in vitro* model for understanding the neurodegenerative processes of these diseases.

Difficulties in establishing a successful *in vitro* TSE model began with the observations that many cell lines are resistant to TSE infection. The first successful propagation of scrapie within a cell culture system was from a mouse brain challenged with the Chandler murine scrapie strain, which maintained infectivity upon sub-pass indicating that replication of the agent was occurring and maintained within dividing cells (Clarke & Haig 1970; Clarke & Haig 1970). The cell line is of mesodermal origin and has been termed the scrapie mouse brain (SMB) culture. Infection of a cell line can only be confirmed by taking cells from different sub-passages and performing a mouse bioassay to confirm the presence of infectivity, and also for analysis of protease-resistant PrP^{sc}. The Chandler strain can be eradicated by treatment with pentosan sulphate and SMB cultures remain susceptible to challenge with other scrapie strains, successfully maintaining infectivity and strain-specific characteristics as confirmed by bioassay (Birkett *et al.* 2001). Further attempts to establish cell culture models for TSEs include the mouse L cell fibroblasts (Clarke &

Millson 1976), PC12 cells (Rubenstein *et al.* 1984), spontaneously immortalised hamster brain cells (HaB) (Taraboulos *et al.* 1990), mouse neuroblastoma N2a cells (Butler *et al.* 1988; Race *et al.* 1988), and mouse-derived T-antigen-immortalised hypothalamic neurons (GT1 cells) (Mellon *et al.* 1990; Schätzl *et al.* 1997). In more recent years attempts have been made to establish *in vitro* models for familial TSE diseases using a human neuroblastoma cells line (M17) (Petersen *et al.* 1996), transformed mouse fibroblasts (3T3) (Priola & Chesebro 1998), and the Chinese hamster ovary cells (CHO) (Daude *et al.* 1997). It has now been reported that clones of CHO cells expressing mutant PrP have been created as models for GSS, FFI and sCJD (Harris 1999). However in attempts to replicate the neuronal effects observed *in vivo*, many researchers have concentrated on the neuronal PC12 and N2a cell cultures.

1.5.1. Hippocampal organotypic slice cultures

The ideal *in vitro* model for studying neurodegeneration would be to establish an organotypic slice culture system, a novel concept for application to TSE research. Organotypic slice cultures (derived from embryonic or neonatal animal tissues) are advantageous to dissociated cell cultures in that they retain the original cytoarchitecture of the tissue of origin, synaptic connections, differentiation of neurons, and almost normal physiological and morphological characteristics of cells *in vivo* (Gahwiler 1984; Gahwiler 1988; Gahwiler *et al.* 1997). This project was initially designed to investigate the feasibility of such a system using murine hippocampal slices as a means to maintain *in vivo* properties *in vitro*. Organotypic cultures would therefore allow the development and execution of more detailed research into the effects of various controlled conditions on neuronal tissues. The

effects of scrapie infection or treatment with toxic prion peptides (Forloni *et al.* 1993; Tagliavini *et al.* 1993) would allow more detailed studies on neuronal loss and cell death in these diseases. Unfortunately, technical difficulties prevented the successful development of such a model for this thesis, and this research has concentrated on the well characterised PC12 culture systems as a means to study neuronal cell death when exposed to toxic prion peptide sequences.

1.5.2. N2a Cells

Murine neuroblastoma cells (N2a) cells (Klebe & Ruddle 1969) were established as a model for TSE infection following their successful infection with murine scrapie and CJD, resulting in the production of abnormal PrP (Butler *et al.* 1988). Scrapie infected N2a cells (ScN2a) produce abnormal PrP^{sc} with the biochemical and physical properties already described in Table 1.2 however, these cells are only capable of propagating low levels of infectivity (Race *et al.* 1987; Race *et al.* 1988). ScN2a cells containing PrP^{sc} and the highest levels of infectivity have been selected and sub-cloned. It is estimated that 80-90% of ScN2a cells will be infected and contain a titre of infectivity of 10^5 $ID_{50}/10^7$ cells (Butler *et al.* 1988; Race *et al.* 1988; Bosque & Prusiner 2000). These cloned N2a and ScN2a cells have been used extensively for the analysis of PrP^{sc} formation and localisation. However, the highly cloned nature of these cells raises the possibility of clonal artefacts between cultures and may alter the comparability of data between researchers using these cells. The highly characterised neuronal PC12 cell line has been used for the research of neurodegenerative mechanisms in this thesis.

1.5.3. PC12 cells

The PC12 cells are derived from a transplantable rat adrenal pheochromocytoma, and are of neural cleft origin (Greene & Tischler 1976). PC12 cells differentiate into a neuronal phenotype when cultured with nerve-growth factor (NGF), when mitosis is reduced and the cells acquire the morphological, biochemical and physiological properties of differentiated sympathetic neurons. Differentiation with NGF results in neurite extension (500-1000μm), electrophysiological responsiveness and the synthesis of neurotransmitters. This differentiation is reversible, and within 72 hours of NGF withdrawal, cells de-differentiate and mitosis resumes (Greene & Tischler 1976). It is thought that NGF causes the neuronal differentiation *in vivo* of stem cells migrating from the neural cleft (Bjerre & Bjorklund 1973). It is therefore believed that PC12 cells are equivalent to such early progenitor cells, differentiating to the neuronal phenotype *in vitro* in the presence of NGF. It is also now known that NGF-differentiation increases PrP^c expression (Wion *et al.* 1988; Lazarini *et al.* 1994), which may contribute to the susceptibility of cells to infection with TSE agents.

Undifferentiated (naive) cell cultures are unable to maintain infectivity when treated with the 139A (Chandler) scrapie strain, whereas differentiated cultures are susceptible to infection and successfully propagate infectivity for several sub-passages (Rubenstein *et al.* 1984; Rubenstein *et al.* 1990). Differentiated PC12 cell cultures are also susceptible to infection with the ME7 scrapie strain, but infectivity titres are at much lower levels than with 139A. Differentiated PC12 cells are resistant to infection with the hamster scrapie strain 263K and surprisingly do not permit replication of the rat-passaged 139R scrapie strain (Rubenstein *et al.* 1992). Scrapie infections do not result in obvious altered morphology of PC12 cells. The relative

lack of cytopathological features is a common feature of scrapie-infected cell cultures and has been commonly reported for the other cell lines already mentioned. However, scrapie infection can alter a number of biochemical properties of infected PC12 cells. Infection of differentiated PC12 cells with either 139A and ME7 scrapie interferes in a dose-dependent manner with excitatory neurotransmittors of the cholinergic signalling pathway (acetylcholinesterase and choline acetyltransferase) and the inhibitory neurotransmitter γ-aminobutyric acid, but not with adrenergic signalling mechanisms (tyrosine hydroxylase) (Rubenstein *et al.* 1994). These disruptions to cholinergic pathway enzymes have also been confirmed in N2a cells infected with 139A (Race *et al.* 1987).

PC12 cell culture systems have been used extensively for modelling the neurotoxic effects of PrP^{sc} *in vivo* using the synthetic human peptide PrP106-126 (HuPrP106-126). In addition to HuPrP106-126, PC12 cells have been used for modelling other amyloidogenic diseases such as Alzheimer's disease using the β–amyloid peptide (Shearman *et al.* 1994). The studies of the HuPrP106-126 peptide will be detailed in Section 4 in relation to the work of this thesis in the analysis of the mouse synthetic peptide PrP105-125 (MoPrP105-125). The PC12 cell culture system therefore represents a good model for the *in vitro* modelling of the neurotoxic and neurodegenerative processes of TSE diseases. The investigation of such processes has led to the development of two main types of *in vitro* PrP conversion reaction (as discussed in Section 1.3.2), which may prove to be even more effective in understanding the progression of these diseases. The cell free conversion (Kocisko *et al.* 1994) has shown us that direct interactions between PrP^{c} and PrP^{sc} can account for the observed species barrier effects when new strains are introduced into a new host

(Kocisko *et al.* 1995). The PMCA reaction (Saborio *et al.* 2001) has proved to be more efficient for converting PrP^{c} to PrP^{res} molecules. Future research using this technique may prove to be an invaluable tool for; (1) the pre-clinical identification of TSE diseases, (2) the identification of PrP interacting proteins, and (3) the testing of therapeutic agents to break disease-specific PrP aggregates or even better prevent their formation. Increased understandings of the neurodegenerative mechanisms of these diseases could allow intervention strategies to be developed in an effort to inhibit the neurodegenerative processes.

As mentioned above, the research of this thesis concentrated on the *in vitro* use of a synthetic PrP peptide corresponding to the most conserved region of the PrP protein. These shorter synthetic peptides are based on the 7 and 11 kDa peptides found in amyloid from individuals diagnosed with GSS (Forloni *et al.* 1993; Tagliavini *et al.* 1993). These synthetic peptides harbouring fibrillogenic and neurotoxic properties, are fully discussed in Chapter 4, and have been used in this thesis to better understand the peptide conformations which might *in vivo* represent neurotoxic PrP conformations. Understanding the mechanisms resulting in the formation of neurotoxic PrP conformations may therefore allow strategies to be developed which prevent the initiation of neuronal cell death in these diseases. However, the mechansisms resulting in this neuronal loss are also poorly understood. Apoptosis, or programmed cell death (discussed in Chapter 3), has been identified as a mechanism of neuronal cell death following treatment with neurotoxic PrP peptides *in vitro* and *in vivo* (Forloni *et al.* 1993; Tagliavini *et al.* 1993; Ettaiche *et al.* 2000); and also in human TSE diseases and in murine scrapie disease models (Giese *et al.* 1995; Lucassen *et al.* 1995; Fraser *et al.* 1996; Jesionek-Kupnicka *et al.* 1997; Dorandeu *et*

al. 1998; Gray *et al.* 1999; Jamieson *et al.* 2001a; Puig & Ferrer 2001). Evidence for apoptosis in the TSEs will be described in depth in Chapter 3. The precise apoptotic pathways involved in executing the neuronal cell death process in the TSEs are not clear, but understanding these pathways represents an opportunity to interrupt the cellular mechanisms of neurodegeneration. This research has included the analysis of caspase-independent mechanisms of apoptotic cell death in two well described murine scrapie models, the ME7/CV and 87V/VM models described in Section 1.4.5. The involvement of caspase-independent proteins in models of other neurodegenerative diseases (Chapter 3) had been reported at the time of the conception of the work described in this thesis, therefore representing a novel and highly relevant potential pathway of neuronal cell death in the TSEs. The inclusion of this research was felt to be important as the identification of the precise mechanisms of cell death in these diseases may lead to future techniques which prevent the cell death processes in these and other neurodegenerative diseases.

1.6. Thesis aims

The aims of this thesis were therefore to:

- Establish a reproducible *in vitro* model suitable for analysing the mechanisms of neurodegeneration associated with the TSE diseases
- Use the established *in vitro* model to analyse the relationship of fibril structure to neurotoxicity
- Assess the role of caspase-independent mechanisms of neuronal cell death *in vivo* using the ME7/CV and 87V/VM murine scrapie models and *in vitro* using the above model of neurodegeneration

Chapter 2: Materials and Methods

2.1 Experimental animal procedures

2.1.1 Experimental animal groups and murine scrapie strain combinations

Animals were taken from the specified pathogen free colony maintained at the Institute for Animal Health, Neuropathogenesis Unit in Edinburgh. Animal-related procedures comply with the Animals (Scientific) Act of 1986 in accordance with Home Office regulations. The two inbred mouse strains inoculated in these experiments were the VM/Dk (VM, *Prnp*^{b} genotype) inoculated with the 87V murine scrapie strain, and the F1 cross between C57Bl/Dk and VM/Dk (CV, *Prnp*^{ab} genotype) inoculated with the ME7 murine scrapie strain. The incubation period and neuropathological details of these mouse and scrapie strain combinations have been detailed in Section 1.4.5.

2.1.2 Animal husbandry

Experimental animals were maintained in a tightly controlled environment and checked twice weekly at cleaning. Animals were kept in cages of up to six animals at a constant temperature between 19-23°C, with a 12 hour light/dark cycle to minimise animal stresses. Infected and uninfected controls were maintained in separate cages to prevent possible transmission through cannibalism. The specified pathogen-free status of the colony was sustained by a number of measures including autoclaving the animal bedding, irradiating solid food pellets and maintaining the water at an acidified pH of 2.3-3.0. Scoring for clinical signs of disease (by the staff of the animal unit) begins in the weeks prior to their expected development, and was continued on a weekly basis until the terminal stages of disease. Clinical signs are dependent upon the murine scrapie/host combination but include lethargy, hyperactivity, altered gait,

weight loss/gain, "startle" reflex and scratching behaviour. Animals were culled at the clinical end-point as it would be inhumane to prolong the suffering of infected animals. The clinical end points for the 87V/VM (and NB/VM control) and the ME7/CV (and NB/CV control) animals were approximately 320 dpi and 250 dpi respectively.

2.1.3 Scrapie inoculation and tissue collection procedures

2.1.3.1 Inoculum preparation

Inoculum for injection was prepared from the brains of animals which had reached the terminal stages of disease. Brains were removed using aseptic techniques and stored at -20°C, or below, until required. Brains were thawed, weighed, and homogenised in 0.9% sterile saline. Microbial contamination was minimised through the use of sterile single-use instruments and by screening inoculum for microbial content.

2.1.3.2 Intracerebral inoculation

Mice under halothane anaesthesia were injected by intracerebral inoculation into the right frontal cortex with a 25 gauge needle fitted with a 2mm needle guard to prevent penetration of the needle beyond the outer cortical layers. Mice were inoculated with 20µl of 1% brain homogenates prepared from scrapie-infected animals at the terminal stages of disease. Cohorts of control animals were inoculated with equivalent volumes of normal brain homogenates. Mice in these experiments were inoculated by the trained staff of the animal facility.

2.1.3.3 Mouse brain collection

All experimental animals were culled by cervical dislocation at the terminal stages of disease by the experienced staff of the animal handling facility. The skin was carefully cut from the hind- to fore-brain, the skull was cut open and the whole brain carefully removed. Brains for histopathological analysis were fixed and processed (Section 2.2.), whereas brains for biochemical analysis were snap-frozen in liquid nitrogen and samples homogenised or micro-dissected (Section 2.3.) immediately and proteins extracted (Section 2.3.1. or 2.3.2.2.). The ages of the animals for the 87V/VM experiment were sacrificed at 322, 322 and 319 dpi, an aged-matched NB/VM control was also taken for each time point. The three animals for the ME7/CV experiment were sacrificed at 248 dpi, aged-matched NB/CV controls were also taken at the same time point.

2.1.4 Antibodies

2.1.4.1 Primary antibodies

Antibody	Monoclonal/ Polyclonal	Western Blot dilution	ICC dilution	FACS dilution
Anti-PrP 8H4 [1]	Mouse Monoclonal	1/30,000	1/1000	1/200
Anti-PrP 6H4 [2]	Mouse Monoclonal	1/30,000	1/1000	1/400
Glial Fibrillar acidic protein (GFAP) [3]	Rabbit Polyclonal	n/a	1/400	n/a
Tomato lectin (biotinylated) [4]	n/a	n/a	1/50	n/a
Neurofilament protein (68kDa) [5]	Rabbit Polyclonal	n/a	n/a	1/600
Apoptosis-inducing factor (AIF) [6]	Rabbit Polyclonal	0.4 µg/ml	n/a	n/a
Endonuclease G (Endo G) [7]	Rabbit Polyclonal	0.5 µg/ml	n/a	n/a
Heat-shock protein 70 (Hsp70) [8]	Mouse Monoclonal	1/15,000	n/a	n/a
VDAC/Porin-1 [9]	Rabbit Polyclonal	1/2000	n/a	n/a
Cytochrome c [10]	Mouse Monoclonal	0.2 µg/ml	n/a	n/a
Active caspase-3 (alexa 488 conjugated) [11]	n/a	n/a	n/a	1/10
Anti-PrP 1B3 [12]	Rabbit Polyclonal	n/a	1/1000	1/400

Table 2.1 **Primary antibodies used in TSE research for Western blot, immunocytochemistry (ICC) and fluorescence activated cell sorting (FACS) analysis**

[1](Li *et al.* 2000); [2](Korth *et al.* 1997); [3] Supplied by DAKO; [4] Supplied by Sigma, 1mg/ml stock solution; [5-9] Supplied by Abcam Ltd; [10] Supplied by Chemicon Incorporated, 0.2 mg/ml stock solution. This antibody recognises residue 64 which is exposed only by the conformation adopted by holocytochrome c; [11] Supplied by Cell Signalling Technologies. This antibody recognizes only active caspase-3 which is cleaved at Asp175 (17/19 kDa); [12] Farquhar *et al.* 1989

2.1.4.2 Secondary antibodies

Antibody	HRP/fluorochrome/ Biotinylated	Western Blot dilution	ICC dilution	FACS dilution
Goat anti-mouse Alexa-488 [1]	Fluorochrome conjugated	n/a	n/a	1/1000
Goat anti-mouse [2]	HRP conjugated	1/30000	n/a	n/a
Goat anti-rabbit [3]	HRP conjugated	1/30000	n/a	n/a
Rabbit anti-mouse [4]	Biotinylated	n/a	1/400	n/a
Goat anti-rabbit [5]	Biotinylated	n/a	1/500	n/a
Streptavidin-Alexa594 [6]	Fluorochrome conjugated	n/a	0.2µg/ml	n/a
Goat anti-rabbit FITC [7]	Fluorochrome conjugated	n/a	n/a	1/200

Table 2.2 **Secondary antibodies used in TSE research for Western blot, immunocytochemistry (ICC) and fluorescence activated cell sorting (FACS) analysis**

[1,6] Supplied by Molecular Probes Ltd, 1mg/ml and 0.5mg/ml stock solutions respectively; [2-3] Supplied by Upstate Ltd, 1mg/ml stock solutions; [4-5] Supplied by Jackson Laboratories (USA), 1mg/ml and 0.9mg/ml stock solutions respectively; [7] Supplied by Sigma Immunochemicals

2.2 Processing of tissues for pathological analysis

2.2.1. Brain fixation, processing and cutting procedures for paraffin-embedded tissues

Brains removed for histopathological analysis were fixed overnight in 10% formol saline, decontaminated in 98% formic acid for 60 minutes, and returned to 10% formol saline prior to embedding in paraffin wax. Brains were transferred to an automated tissue-embedding processor (Jung TP, Leica) and processed for embedding in wax following a routine dehydration protocol (Table 2.3).

Solution	Duration in solution
70% alcohol	40 minutes
80% alcohol	40 minutes
95% alcohol	40 minutes
99% alcohol	40 minutes
99% alcohol	40 minutes
99% alcohol/Xylene (equal parts)	30 minutes
99% alcohol/Xylene (equal parts)	30 minutes
Xylene	30 minutes
Xylene	30 minutes
Paraffin wax	25 minutes
Paraffin wax	25 minutes
Paraffin wax	25 minutes

Table 2.3 **Automated tissue processing procedure for 10% formol saline fixed (formic acid treated) mouse brains for embedding in paraffin wax**

Tissues were removed from the automated processor, trimmed coronally at four standard cutting levels (Figure 2.1) and orientated within a cassette for embedding in hot paraffin wax (Figure 2.2). Prior to cutting sections for routine histopathological and immunocytochemical analysis, blocks were trimmed of excess wax and cooled on ice for 2 hours. Cooled blocks were then cut at 6μm using a microtome, serial sections floated in a water bath at 37°C, and sections transferred to Superfrost-Plus

slides. Sections were air dried overnight at room temperature, oven dried for 2 days at 37°C, and stored at room temperature until required.

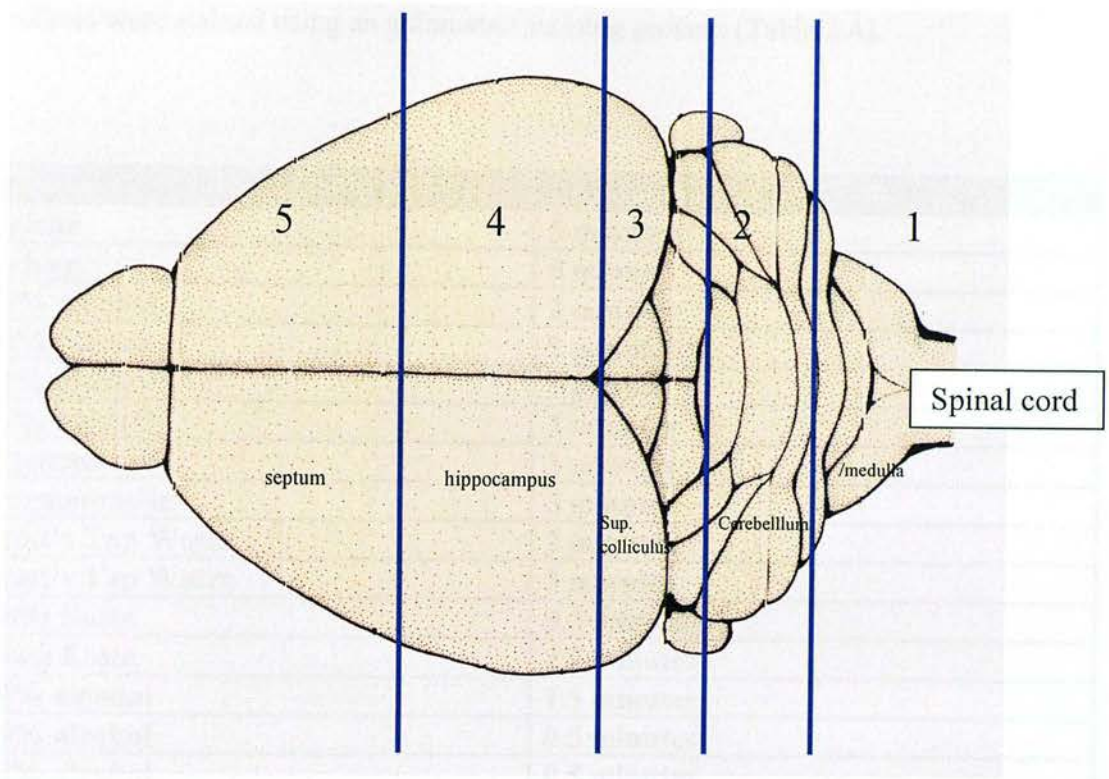

Figure 2.1 **Mouse brain sectioning levels for immunocytochemical and Haematoxylin & Eosin staining**
Blue lines indicate the brain sectioning levels used routinely for histopathological analysis. Brains are cut coronally (from fore to hind brain) at the septum, hippocampus, superior colliculus, and cerebellum & medulla (Fraser & Dickinson 1968)

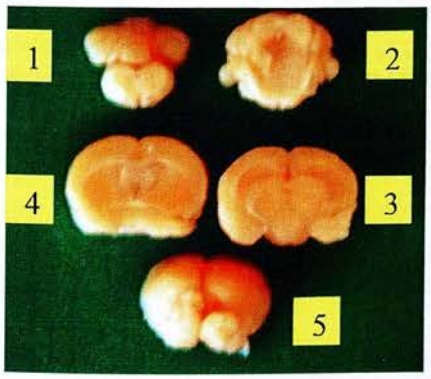

Figure 2.2 **Alignment of coronal mouse brain sections in paraffin wax embedded blocks**
Mouse brains are cut at the coronal levels described in Figure 2.1.

2.2.2 Haematoxylin and Eosin staining

Paraffin-embedded 6μm tissue sections (Section 2.2.1.) were stained with haematoxylin and eosin for histopathological analysis, including vacuolation scoring. Sections were stained using an automated staining process (Table 2.4).

Solution	Duration in solution
Xylene	5 minutes
Xylene	5 minutes
90% alcohol	2 minutes
90% alcohol	2 minutes
95% alcohol	1 minute
99% alcohol	3 minutes
Haematoxylin	3 minutes
Haematoxylin	3 minutes
Scott's Tap Water	2 minutes
Scott's Tap Water	3 minutes
Putts Eosin	0.5 minutes
Putts Eosin	2.5 minutes
70% alcohol	1.5 minutes
95% alcohol	0.5 minutes
95% alcohol	0.5 minutes
99% alcohol	0.5 minutes
99% alcohol	0.5 minutes
99% alcohol /Xylene (equal parts)	1 minute
Xylene	1 minute
Xylene	1 minute
Xylene	1 minute

Table 2.4 **Automated process for Haematoxylin & Eosin staining**
Standard protocol for the analysis of tissue sections by Haematoxylin & Eosin in the analysis of the pathology related to infection with TSE disease (as described in Figure 1.4)

2.2.3 Immunocytochemical analysis of paraffin-embedded samples

Paraffin-embedded 6μm tissue sections (Section 2.2.1.) were hydrated by passage through alcohols (Table 2.5) to water prior to immunocytochemical (ICC) analysis.

Solution	Duration in solution
Xylene	5 minutes
Xylene	5 minutes
99% alcohol	3 minutes
94% alcohol	3 minutes
70% alcohol	3 minutes

Table 2.5 **Hydration procedure of paraffin-embedded tissue sections for ICC analysis**
Standard protocol for the hydration of paraffin-embedded tissue sections prior to analysis by ICC

If samples were to be labelled for PrP using 6H4 (Table 2.1), antigen unmasking was achieved by autoclaving hydrated sections at 121°C for 15 minutes in dH_20 followed by immersion in 98% formic acid for 5 minutes. If labelling sections for astrocytes (glial fibrillary acidic protein (GFAP)) or microglia (tomato lectin) (Table 2.1), these pre-treatments were not required. Endogenous peroxidases were blocked by incubation for 10 minutes in 1% hydrogen peroxide in methanol, followed by thorough washes in dH_20. If labelling for GFAP or PrP, non-specific antibody labelling was prevented by incubation of samples with 100μl of 1/20 normal serum for 20 minutes at room temperature (The normal serum chosen to block was from the same species used to raise the secondary antibody). Normal serum was gently removed, without washing sections, and 100μl of the primary antibody incubated overnight (if 6H4 or tomato lectin) or for 1 hour (if GFAP) at room temperature. Primary antibodies were removed by 3 washes each for 5 minutes in 250ml wash buffer; PBS/BSA (for GFAP and PrP) or TBS pH 7.6/1% Triton x-100 (for tomato lectin). If labelling for PrP or GFAP, 100μl of biotinylated secondary antibody (Table

2.2) was added to each slide and incubated for 60 minutes at room temperature. Secondary antibodies were removed by 3 washes each for 5 minutes in 250ml appropriate wash buffer. Avidin-Biotin complex (ABC)-solutions were prepared by adding 10µl reagent A and 10µl reagent B to 1000µl antibody diluent (for GFAP or PrP) or to 1000µl TBS (for tomato lectin). 100µl of ABC Elite was added to each slide and incubated at room temperature for 30 minutes; followed by 3 washes each for 5 minutes in 250ml appropriate wash buffer. ABC bound to specific epitopes was visualised by immersing slides into 0.05% diaminobenzidine (DAB) in 1x PBS activated with 0.025% hydrogen peroxide. DAB staining was performed for 3-5 minutes and slides washed thoroughly in dH_20 then counterstained and dehydrated (Table 2.6) prior to cover-slipping sections with DPX mountant (BDH). To determine the specificity of labelling, duplicate sections were incubated with 1/1000 normal serum and processed as detailed above (The normal serum chosen was from the same species used to raise the primary antibody). Staining was analysed by light microscopy (E800, Nikon) and images were captured with the digital camera (Micropublisher 5.0 RTV) and images captured using the Image Pro Plus software.

Solution	Duration in solution
Haematoxylin	**1 minute**
Scott's Tap Water	**0.5 minutes**
Distilled Water	**5 minutes**
70% alcohol	**3 minutes**
94% alcohol	**3 minutes**
99% alcohol	**3 minutes**
99% alcohol	**0.5 minutes**
99% alcohol /Xylene (equal parts)	**0.5 minutes**
Xylene	**1 minute**
Xylene	**1 minute**
Xylene	**1 minute**

Table 2.6 **Counterstaining and dehydration procedure for paraffin-embedded tissue sections following the ICC protocol**

2.3 Western blot analysis of murine brain samples

2.3.1 Sub-cellular fractionation of whole brain samples by sucrose gradients

Snap-frozen brain samples were partially thawed on ice and weighed in pre-cooled Dounce homogenisers. 10% brain homogenates were prepared by adding 9x volumes/weight of 0.32M sucrose solution to each sample, in a method adapted from a published protocol (Merz *et al.* 1981) in consultation with Robert Somerville (IAH, Edinburgh). Protease degradation was inhibited by adding phenylmethanesulfonyl fluoride (PMSF) and N-ethylmaleimide (NEM) at final concentrations of 1mM to each sample. All techniques were performed on ice, or where possible at 4°C. Brains were gently homogenised with 20-30 strokes of the pestle, transferred to 15ml centrifuge tubes (Corning) and centrifuged at 1000*g* (2250rpm) for 10 minutes (GS-GR centrifuge) (Figure 2.3). Supernatants were carefully removed and the nuclear pellet discarded. Centrifugation was repeated to enhance the purity of the fractions. Supernatants were aliquoted into 2ml centrifuge tubes (Corning) and centrifuged at 10,000*g* (9,500rpm) for 10 minutes (JA20 rotor, J2-21 centrifuge). The pellet represents the crude mitochondrial extract and the supernatant the crude cytosolic fraction. Crude mitochondrial extracts were re-suspended in 1ml 0.32M sucrose and layered on top of 3ml 2M sucrose solution in 4ml centrifuge tubes. Samples were centrifuged at 100,000*g* for 60 minutes and supernatants gently removed and discarded. Residue was carefully cleaned from the inside of each centrifuge tube and crude mitochondrial pellets re-suspended in 1ml 0.8M sucrose solution. Extracts were carefully layered onto 1.5ml of 1.0M sucrose solution layered onto 1.5ml of 1.2M sucrose solution in new 4ml centrifuge tubes. Samples were centrifuged at 100,000*g* for 60 minutes and supernatants gently removed and discarded. Residue was carefully cleaned from the inside of each centrifuge tube and pellets re-suspended

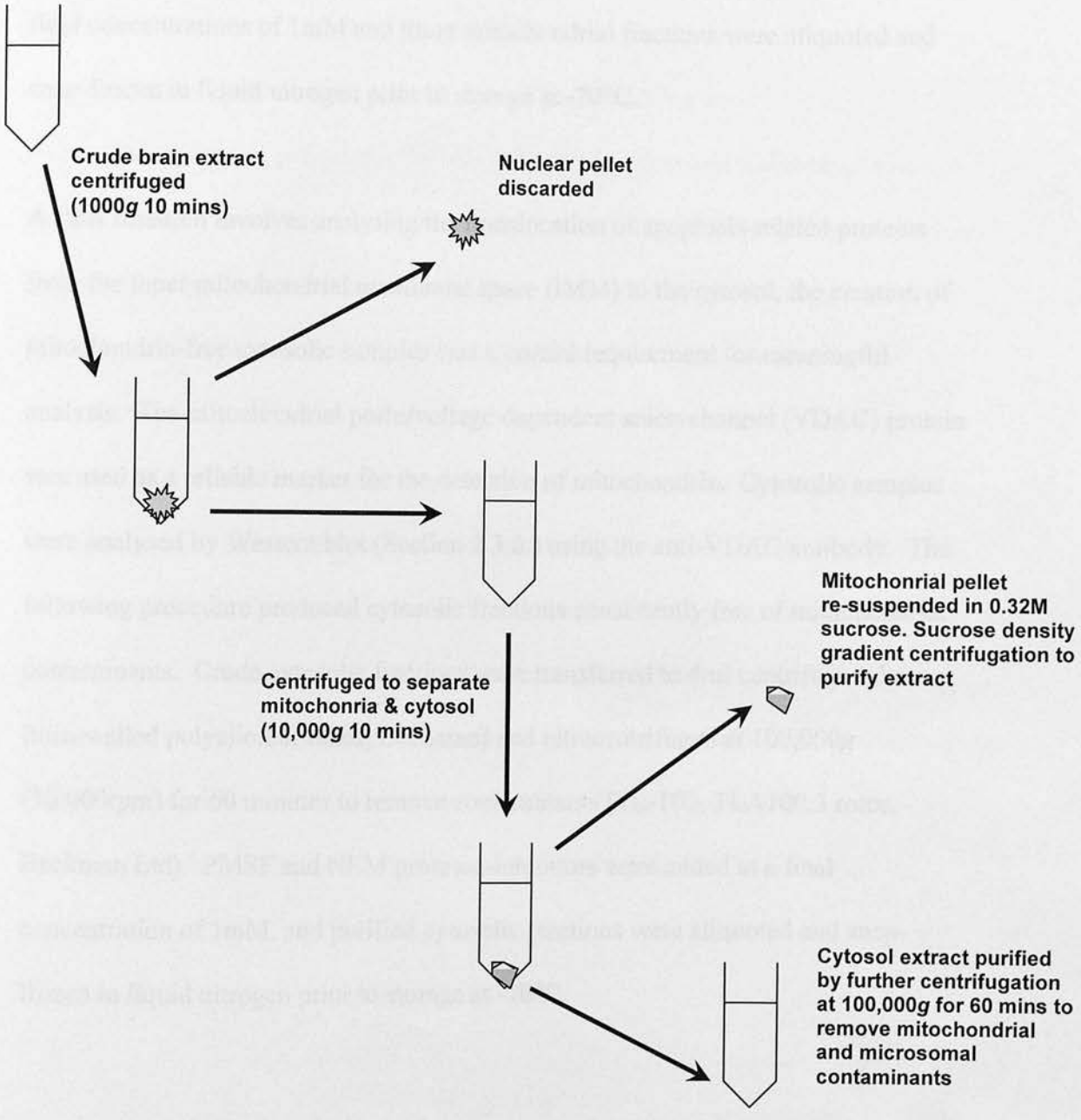

Figure 2.3 **Centrifugation protocol for the subcellular fractionation of crude brain extracts into mitochondrial and cytosolic fractions**

Frozen (-70°C) mouse brains were thawed and 10% homogenates prepared in 0.32M sucrose (Section 2.3.1.). Samples were centrifuged at 1000*g* for 10 mins at 4°C and nuclear deposits discarded. The supernatant was centrifuged at 10,000*g* for 10 mins at 4°C, and the supernatant (crude cytosol) carefully separated from the pellet (crude mitochondria). The cytosol was purified by ultracentrifugation at 100,000*g* 60 mins at 4°C. The pellet was resuspended in 1ml 0.32M sucrose and layered onto 3ml 2M sucrose and centrifuged at 100,000*g* for 60 mins. The pellet was then resuspended in 1ml 0.8M sucrose and layered onto 1.5ml 1M sucrose which was layered on 1.5ml 1.2M sucrose and centrifuged for 60 mins at 100,000*g*. The pellet represents the purified mitochondrial extract, which was resuspended in 1ml 0.32M sucrose. PMSF and NEM protease inhibitors were added at all stages at a final concentration of 1mM.

in 1ml 0.32M sucrose solution. PMSF and NEM protease-inhibitors were added at final concentrations of 1mM and these mitochondrial fractions were aliquoted and snap-frozen in liquid nitrogen prior to storage at -70°C.

As this research involves analysing the translocation of apoptosis-related proteins from the inner mitochondrial membrane space (IMM) to the cytosol, the creation of mitochondria-free cytosolic samples was a crucial requirement for meaningful analysis. The mitochondrial porin/voltage-dependent anion channel (VDAC) protein was used as a reliable marker for the detection of mitochondria. Cytosolic samples were analysed by Western blot (Section 2.3.6.) using the anti-VDAC antibody. The following procedure produced cytosolic fractions consistently free of mitochondrial contaminants. Crude cytosolic fractions were transferred to 4ml centrifuge tubes (thin-walled polyallomar tubes, Beckman) and ultracentrifuged at 100,000*g* (50,000rpm) for 60 minutes to remove contaminants (TL-100, TLA100.3 rotor, Beckman Ltd). PMSF and NEM protease-inhibitors were added at a final concentration of 1mM, and purified cytosolic fractions were aliquoted and snap-frozen in liquid nitrogen prior to storage at -70°C.

2.3.2 Sub-cellular fractionation from microdissected mouse hippocampus and thalamus

2.3.2.1 Micro-dissection of mouse hippocampus and thalamus

The micro-dissection procedures for obtaining the hippocampal and thalamus samples were performed following a published protocol (Barr *et al.* 2004), the details of which will be described. Brains were removed from -70°C storage and allowed to partially thaw on a -20°C cold plate. Each brain was cut using disposable scalpel blades (Swann Norton No. 11) at the level of the hippocampus (Figure 2.1). The thalamus was carefully dissected using the scalpel and curved forceps, and the hippocampus was excised using a punch technique involving the hollow cannula of a biopsy needle (Scottish Medical) (Figure 2.4). Several punches were required to remove each hippocampus, and tissue was expelled from the cannula using an empty 5ml syringe attached to one end. The pooled hippocampus and thalamus samples from each brain were then snap-frozen in liquid nitrogen and immediately processed to separate proteins according to their subcellular location (Section 2.3.2.2.).

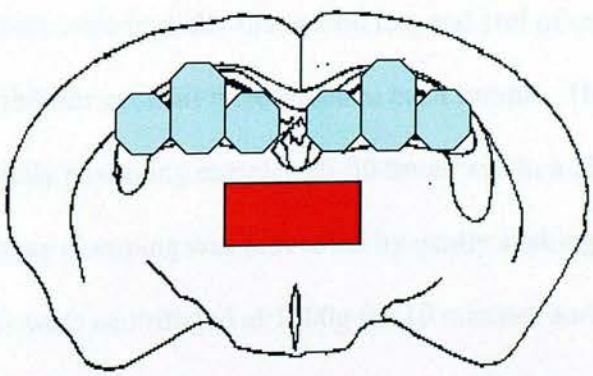

Figure 2.4 **Micro-dissection of hippocampus and thalamus for the sub-cellular fractionation procedure**
Frozen (-70°C) mouse brains are thawed on a -20°C cold plate and cut at the level of the hippocampus (Figure 2.4). A hollow bore of a biopsy needle was used to gently collect both hippocampi (blue hexagons). A disposable scalpel blade is then used to gently excise the thalamus (location indicated by a solid red box).

2.3.2.2 Sub-cellular fractionation technique for micro-dissected samples

In addition to analysing samples created from whole mouse brains, it was thought that micro-dissecting areas with TSE pathology, such as the hippocampus and thalamus, would enhance the likelihood of detecting apoptosis-related proteins. A scaled down version of the sucrose-gradient centrifugation procedure (Section 2.3.1.) was attempted several times however, the repeated centrifugation procedures resulted in unacceptable losses from these small samples. A commercial kit (Calbiochem) was purchased and proteins from micro-dissected brain areas were separated according to their solubility in different sub-cellular locations. The precise chemical compositions of the extraction buffers in this kit where not publicised by the manufacturer. The protocol used in these extractions was based on that for frozen-tissue samples. As before (Section 2.3.1.), cytosolic samples were analysed by Western blot (Section 2.3.6.) using the anti-VDAC antibody to ensure that samples were free of contaminating mitochondria. Optimisation of the kit to achieve the required purity required increasing the centrifugation steps and altering the homogenisation procedures. All techniques were performed on ice, or where possible at 4°C. Snap-frozen brain samples were partially thawed on ice, and 1ml of extraction buffer 1 and 5µl of protease-inhibitor cocktail were added to each sample. Homogenisation was performed by serially passaging samples 20-30 times within a 19 gauge needle using 1ml syringes. Tissue clumping was prevented by gently shaking the samples for 10 minutes. Samples were centrifuged at 1000*g* for 10 minutes and supernatants (cytosol) gently removed and purity enhanced by centrifuging two further times at 10,000*g* for 10 minutes to remove contaminating mitochondria-containing pellets. Cytosolic fractions were aliquoted and snap-frozen in liquid nitrogen prior to storage at -70°C. The original pellet was re-suspended in 1ml extraction buffer 2 and 5µl

protease-inhibitor cocktail and shaken for 30 minutes. Samples were centrifuged at 6000*g* for 10 minutes and the mitochondrial supernatants were aliquoted and snap-frozen in liquid nitrogen prior to storage at -70°C.

2.3.3 BCA total protein determination assay

Total protein estimation was determined using the microplate protocol of the bicinchoninic acid (BCA) assay (Pierce). This assay uses BCA to detect cuprous ions generated from cupric ions by reaction with protein in the samples under alkaline conditions. Bovine serum albumin (BSA) standards (Pierce) and samples to be analysed were diluted in (a) 0.32M sucrose if samples were prepared using those described in Section 2.3.1. or (b) in extraction buffers 1 or 2 if samples were prepared using techniques described in Section 2.3.2.2. BSA standards were prepared (1500µg/ml, 1000µg/ml, 750µg/ml, 500µg/ml, 250µg/ml, 100µg/ml and 50µg/ml) and samples to be analysed were diluted in the ratio of 1:5 and 1:10 to calculate the total protein content in each sample as derived from the standard curve. 25µl of each standard and diluted sample were added in duplicate to wells of a 96 well microplate. The BCA working reagent was prepared fresh for each assay by combining BCA reagents A and B in the ratio of 50:1. 200µl of this working reagent was added to standard and test samples, and was also used as a blank for the assay. The microplate was sealed and incubated at 37°C for 30 minutes, then allowed to cool to room temperature for 5 minutes. The absorbance values at 570nm were then read and analysed on a V-Max microplate reader (Molecular devices). Protein concentrations for each sample were derived from the BSA standard curve.

2.3.4 Preparation of samples for Western blot analysis

2.3.4.1 Brain sample preparation

Total protein from the samples to be analysed was assessed (Section 2.3.3.) and mitochondrial and cytosolic samples were taken so as to contain 30μg total protein per sample. The aim of this analysis was to detect the translocation of proteins from the mitochondria to the cytosol, therefore cytosolic samples containing 60 and 90μg of total protein were also prepared to maximise detection of translocated proteins. If required, samples were concentrated using a methanol precipitation technique. To methanol precipitate samples, a 4x volume of ice-cold methanol/2% acetic acid was added to each sample, the tube gently inverted twice and precipitated overnight at -20°C. Samples were centrifuged at 16,000*g* for 10 minutes, methanol/2% acetic acid supernatants were carefully removed and the protein pellet dried for up to 2 hours in a centrifugal vacuum concentrator (Thermo Savant Speed-Vac). Dried samples were each re-suspended in 20μl 1x Sample buffer, sample-reducing agent added at 1x, and samples gently vortexed. Samples were heated at 98°C for 5 minutes prior to SDS-PAGE (Section 2.3.5.).

2.3.4.2 Positive control preparation

Positive controls of 3T3 cell lysate for Endonuclease G (Endo G) and K-562 cell lysate for apoptosis-inducing factor (AIF) were purchased from Abcam. Both cell lysates reacted strongly with the anti-Hsp70 antibody but weakly with the anti-VDAC1 antibody. Depending upon the batch of positive control, the anti-cyt c antibody would recognize either of the cell lysates or both. Positive control samples were loaded at a concentration of 3μg/ml in 1x sample buffer. Sample reducing agent

was added (1x) and samples were heated at 98°C for 5 minutes prior to SDS-PAGE (Section 2.3.5.).

2.3.5 SDS-PAGE procedure

All biological reagents and experimental equipment were purchased from Invitrogen, unless otherwise stated, and analysed using procedures derived from published protocols (Laemmli 1970). Protein separation was performed using pre-cast 12 well Novex Bis-Tris-HCl (pH 6.4) 4-12% acrylamide gradient gels under reducing conditions. Running buffer (1x) (50mM MES, 50mM Tris Base, 3.47mM SDS, 0.125mM EDTA) was prepared fresh from a stock solution (x20) (Invitrogen) in ultrapure water for each procedure. Gel combs were carefully removed from the wells of the pre-cast gels and wells gently rinsed with 1xRunning buffer. Gels were assembled in the Novex gel tanks and 500µl NuPAGE antioxidant was added to 200ml 1x Running buffer and added to the upper chamber of the tank. The outer chamber of the gel tank consisted of 1xRunning buffer. 6µl of the SeeBlue Plus2 pre-stained standard and 20µl of each sample (Section 2.3.4.1), positive control (Section 2.3.4.2.) and blank (1x sample buffer) were electrophoresed using a BIORAD PowerPac at 200V for 55-60 minutes until the dye front reached the foot of the gel. Gels were carefully removed from the gel cassette and trimmed of excess acrylamide prior to the Western blot procedure (Section 2.3.6.)

2.3.6 Western blot procedure

All biological reagents and experimental equipment were purchased from Invitrogen, unless otherwise stated. Proteins were transferred from the 4-12% Bis-Tris gels to polyvinylidene difluoride (PVDF) membranes using the Novex Transblot module; 3MM filter paper and PVDF membranes were purchased pre-cut. Transfer buffer (1x) (25mM Bicine, 25mM Bis-Tris, 1.025mM EDTA, 0.05mM chlorobutanol, 10% methanol [v/v], 1ml NuPAGE antioxidant) was prepared fresh from a stock solution (x20) (Invitrogen) in ultrapure water for each procedure. For the transfer of proteins from each gel, a "transfer sandwich" (Figure 2.5) was constructed consisting of a single PVDF membrane, two pieces of 3MM filter paper and five blotting pads. PVDF membranes were pre-wet by immersion in 100% methanol (BDH) for 10 seconds followed by thorough washes in dH_20. PVDF membranes, 3MM filter paper and blotting pads were then pre-soaked in 1x Transfer Buffer for at least 10 minutes prior to transfer. The "transfer sandwich" was constructed within the Novex Blot module, and inserted into the Novex gel tank. The "transfer sandwich" was constantly kept wet with 1x Transfer buffer and the chamber of the Novex blot module was topped up with 1x Transfer buffer when assembled into the Novex gel tank. The outer chamber of the gel tank was filled with dH_20, and transfer was performed at 120mA per gel for 60 minutes at 30 volts using a BIORAD PowerPac 200. Following transfer, the proteins on the PVDF membrane were fixed by immersion in 100% methanol for 10 seconds followed by thorough dH_20 washes prior to Ponceau Red staining (Section 2.3.7.) or the immunoblotting procedure (Section 2.3.8.)

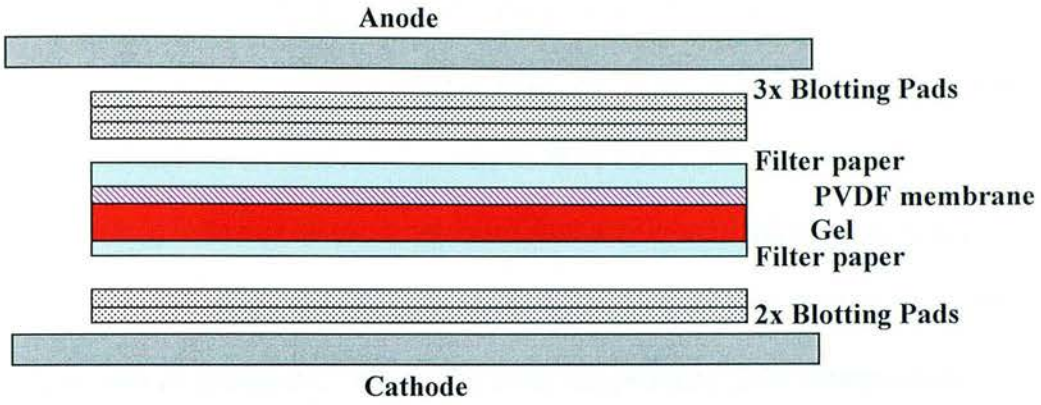

Figure 2.5 **Transfer "sandwich" for the transfer of SDS-PAGE separated proteins to the PVDF membrane**
Electrical current from the cathode to the anode transfers SDS-PAGE separated proteins to the PVDF membrane

2.3.7 Ponceau Red staining

The transfer of proteins to the PVDF membrane was confirmed by incubating the PVDF membrane with Ponceau Red (Sigma) on the shaker at room temperature for up to 5 minutes. Excess stain was removed and the membrane washed three times in dH_20 to visualize the protein bands. PVDF membranes were de-stained through several 20ml TBS/0.5% Tween 20 washes on the shaker at room temperature prior to the immunoblotting procedure (Section 2.3.8.).

2.3.8 Immunoblotting procedure and protein detection

All incubations were performed at room temperature on the shaker and using reagents purchased from Invitrogen, unless otherwise stated. PVDF membranes were blocked with 20ml 3% non-fat dried milk (Upstate) in TBS for 2 hours prior to incubation with the primary antibody of choice (Table 2.1.). PVDF membranes were then incubated overnight at 4°C in 20ml of antibody solution in freshly prepared 3% non-fat dried milk in TBS. Membranes were washed three times in 20ml TBS/0.5% Tween 20 for 5 minutes per wash, followed by a 15 minute block in 20ml 3% non-fat

dried milk in TBS. PVDF membranes were then incubated in 20ml of secondary antibody solution (Table 2.1.) in freshly prepared 3% non-fat dried milk in TBS for 40 minutes. Membranes were washed six times in 20ml TBS/0.5% Tween-20 for 10 minutes per wash, followed by two washes in 20ml dH_20 for 10 minutes per wash. Proteins were visualised by chemiluminescence by incubation with the Visualizer™ detection reagent (Upstate) for 3 minutes at room temperature. Membranes were sandwiched between acetate film pieces and placed within a light-proof cassette. Proteins were then detected by exposing the membranes to photographic Lumi-film (Roche) for up to 10 minutes. Exposed film pieces were developed as follows: 2x 30 seconds developer (AGFA; 100ml developer + 400ml dH_20), 2x 30 seconds stop solution (400ml dH_20 + 1ml 2% acetic acid), 2x 30 seconds fix solution (AGFA; 100ml fixer + 300ml dH_20), followed by thorough washes in water. Film pieces were allowed to dry and aligned with the membranes within the cassettes. Protein sizes were determined according to the pre-stained SeeBlue Plus2 standard, and membranes were discarded or re-probed for the detection of other proteins (Section 2.3.9.).

2.3.9 Antibody stripping and re-probing procedure

To re-probe a membrane for other proteins, membranes were removed from the light-proof cassette and washed twice in 20ml TBS/0.5% Tween-20 for 10 minutes per wash. Membranes were then incubated with the membrane strip and re-probe buffer (Pierce) for 40 minutes and washed twice in 20ml TBS/0.5% Tween-20 for 10 minutes per wash. Membranes were blocked with 20ml 3% non-fat dried milk in TBS for 2 hours and immunoblotting continued as described in Section 2.3.8.

2.4 Analysis of MoPrP105-125 peptide and MoScrambled105-125 peptide samples

2.4.1 Synthesis of MoPrP105-125 and MoScrambled105-125 peptides

Peptides of MoPrP105-125 (normal) and MoScrambledPrP105-125 (scrambled) (Figure 2.6.) were synthesised by Dr. Lawrence Hunt (IAH Compton) using conventional Fmoc chemistry on a Pioneer Peptide synthesis system (PerSeptive Biosystems). Fmoc amino acids and resins were purchased from Novabiochem, solvents were prepared in MilliQ water unless stated otherwise, and 10ml cleavage cocktails (1% v/v tri-isopropyl silane; 2.5% v/v ethanedithiol in Trifluoroacetic acid (TFA) were required per 0.1mM batch of peptide. Peptides containing the normal and scrambled sequences were separately dissolved in 10% acetonitrile containing 0.1% TFA. The hydrophobic nature of the normal peptide required a specialised synthesis involving the agitation of 10mg or less of this solution for 10 minutes at room temperature in 5ml acetonitrile. Following addition of 10µl TFA, samples were again agitated for 10 minutes. 2ml MilliQ water was added and samples agitated until peptides completely dissolved. Normal and scrambled peptide containing solutions were centrifuged to remove excess suspension and supernatants pumped onto a high pressure liquid chromatography (HPLC) column as 14% peptide (86% Solvent A). HPLC was performed using Xterra prep MS C18 columns (Waters) on a Biocad Sprint (PerSeptive Biosystems). HPLC solvents were solvent A (0.1% v/v TFA in MilliQ water) versus solvent B (0.1% TFA in acetonitrile) at a flow rate of 7ml/minute. Gradients were 10% solvent B for 1 minute, elution with 10-40% solvent B for 7.5 minutes, and 10% solvent B for 30 seconds. Mass spectrometry was performed on a Quattro II (Micromass) to identify correct peptide sequences, samples were pooled and freeze-dried for storage.

^{105}KTN LKHVAGAAAAGAVVGGLG^{125} mouse

^{106}KTNMKHMAGAAAAGAVVGGLG^{126} human

^{105}LATVKVGAGHGANVAAGKGAL^{125} mouse scrambled

***Figure 2.6* Primary amino acid sequence of synthetic PrP peptides used in this research**
Comparison of the primary amino acid sequence of the MoPrP105-125 sequence used for the research described in this thesis, in comparison to the well studied HuPrP106-126 peptide, discussed in Chapter 4. The mouse scrambled peptide was synthesised based on the human scrambled peptide used in all other peptide research, which was created from the same amino acids but in a random sequence.

2.4.2 Peptide sample preparations

MoPrP105-125 (normal) and MoScrambledPrP105-125 (scrambled) (Figure 2.6.) peptides were dissolved at final concentrations of 2mg/ml in a series of vehicle buffers including 10mM 2-(N-morpholino) ethane sulfonic acid (MES) (Melford), 200mM citrate (Sigma) and tissue culture tested distilled water (GibcoBRL). The findings of initial studies (Section 4.3) involving these buffers revealed that MES buffers would be more appropriate for the requirements of this research, and were therefore studied in more detail in the continuing studies. These buffers comprised; 10mM MES buffers containing either 0mM, 50mM or 200mM concentrations of NaCl (BDH) which were prepared at pH 5 and pH 7 in sterile tissue-culture tested water (GibcoBRL) and sterile-filtrated through a 0.2μM filter pore. Peptide solutions were incubated at 37°C in a water bath for periods up to 14 days. Aliquots were removed at various time-points, snap-frozen in liquid nitrogen and maintained at -20°C prior to analysis by Thioflavin-T assay (Section 2.4.3.) or fourier transform infra-red spectroscopy (Section 2.4.4.)

2.4.3 Thioflavin-T binding assay

Thioflavin-T (Sigma) binds rapidly to amyloid fibrils with altered excitation maxima and enhanced emission than unbound Thioflavin-T. Analysis of peptide amyloid fibril formation in peptide samples (Section 2.4.2.) involved incubating samples with a molar excess of Thioflavin-T (Sigma), using a procedure modified slightly from a published protocol (Heegaard *et al.* 2004). A 2mM stock solution of Thioflavin-T was prepared in sterile MilliQ water, diluted in the test peptide vehicle buffer to achieve 20μM Thioflavin-T. 250μl of the 20μM Thioflavin-T solutions were added to a thoroughly cleaned Quartz crystal cuvette (Starna) and fluorescent excitation performed at 437nm with a step size of 1nm/second between 450-550nm on a PerkinElmer LS-50 fluorimeter. The average of three readings was used to baseline correct samples. 5μl of an aliquot of each peptide sample (2mg/ml) was removed from storage at -20°C and mixed with 250μl 20μM Thioflavin-T sample in appropriate peptide vehicle buffer and analysed for altered excitation and therefore the presence of amyloid fibrils.

2.4.4 Secondary structure analysis of normal and scrambled MoPrP105-125 peptides by Fourier Transform Infra-red spectroscopy

Secondary structure analysis was performed using Fourier transform infra-red spectroscopy (FTIR) to analyse the peptide samples in the tested peptide vehicle buffers (Section 2.4.2). Analysis concentrated primarily on the amide I region (1600-1700cm^{-1}) which is most widely used for secondary structure analysis. The FTIR spectrometer (Vector 22, Bruker) was constantly purged with nitrogen to minimise interference from background water vapour and the mercury cadmium telluride detector was cooled with liquid nitrogen. Each spectrum represented the average of

256 scans, recorded with a $4cm^{-1}$ resolution in the range 1000-4000 cm^{-1}. The internal reflection element was a cleaned germanium crystal (50 x 20 x 2 mm), with an aperture angle of 45° yielding 25 internal reflections. The FTIR signal from a cleaned germanium crystal in the purged spectrometer was taken for background corrections. In addition, a background atmospheric water vapour signal was taken from the open spectrometer for additional background corrections. 10µl of an aliquot of each peptide sample (2mg/ml) was removed from storage at -20°C and gently spread onto a cleaned germanium crystal using a 20µl pipette tip and the sample dried under a gentle flow of nitrogen gas. The spectrometer was allowed to purge of water vapour for 10 minutes prior to reading each FTIR signal. To assess the quantities of α–helix and random structure from the amide I region, a Hydrogen-Deuterium ($^2H_20$) exchange was performed to separate their overlying FTIR spectra. Nitrogen gas coupled to a source of Deuterium was connected to the germanium crystal and complete Deuterium exchange was established after 20 minutes. FTIR spectra for deuterated samples were base-line corrected by subtracting the crystal and water vapour backgrounds. For comparisons between peaks of different samples, samples were baseline corrected at points prior to the amide I peak (1900nm), at the foot of the amide I peak and also after the amide III peak (1400nm). Specific secondary structure curve fittings were performed by Dr. Matthew Hicks (University of Warwick, U.K) using the Grams software analysis package (Thermo Corporation, California).

2.4.5 Electron microscopy sample preparation and analysis

Electron microscopy was used to analyse the morphology of fibrils formed in the peptide samples (Section 2.4.2). 5µl of an aliquot of each peptide sample (2mg/ml) was removed from storage at -20°C onto a sterile plastic sheet. A 3.05mm carbon/formvar 200 mesh grid (TAAB Laboratories Ltd) was gently floated on top of the peptide sample and incubated at room temperature for 5 minutes. Grids were carefully blotted onto filter paper, allowed to air dry for 5 minutes, and negatively stained by floating on top of 5µl 2% sodium phosphotungstate (pH 7.2) for 30 seconds. Grids were carefully blotted onto filter paper and allowed to air dry. Samples were analysed by electron microscopy by Gilian McGovern (Veterinary Laboratory Agency, Lasswade).

2.5 Culture of naive and NGF-differentiated PC12 cells

2.5.1 Source of PC12 cells

PC12 cells were derived from a male transplantable rat (*Rattus norvegicus*) adrenal pheochromocytoma, which respond reversibly to NGF-differentiation. PC12 cells adhere poorly to plastic and attachment is increased by growing the cells on Collagen IV-coated surfaces. Naive (undifferentiated) PC12 cells are round in shape and have a tendency to grow in small clumps; NGF-differentiated PC12 cells have enlarged cell bodies and extended neuritic processes. NGF-differentiation is dependent upon the presence of Collagen IV coated surfaces, the concentration of NGF and the density of cells exposed to NGF. The cells were obtained from LGC Promochem and cultured as described (Greene & Tischler 1976). All biological reagents used were obtained from GibcoBRL Life Technologies (Invitrogen) and all disposable plastic-ware from Corning Costar, unless stated otherwise.

2.5.2 Collagen IV coating procedure for glass coverslips

PC12 cells adhere poorly to plastic and glassware, however treatment with murine Collagen IV substantially increases their attachment and replication of these cells. Murine collagen IV was maintained at -70°C and dissolved at a concentration of 5µg in 0.05N HCl (BDH Ltd). Circular glass coverslips to be coated were cleansed and sterilised in 70% alcohol and dried by blotting onto sterile filter paper. Coverslips were transferred to 24-well plates and 300µl of dissolved collagen-IV was added and plates were placed on the cell shaker for 60 minutes at room temperature. The collagen suspension was then removed and used to treat further surfaces. Coated surfaces were washed a minimum of three times for 20 minutes each with 1ml sterile endotoxin-free tissue culture water (GibcoBRL). Surfaces were then dried in a sterile laminar fume hood, followed by overnight sterilisation using the U.V. light source. Coated surfaces were stored at 4°C for up to 4 weeks.

2.5.3 Media preparation

2.5.3.1 Media for naive PC12 cells

Cells were grown in Dulbecco's modified Eagle's medium (DMEM) supplemented with 10% heat-inactivated horse serum, 5% heat-inactivated newborn calf serum, 1% 200mM L-glutamine (Sigma) and 1% Penicillin/Streptomycin. Cells were maintained at 37°C, 5% CO_2 and cells had a two-thirds media change every two days. Cells were spilt in the ratio of 1:2 when cells reached 80-90% confluence. Freshly prepared and microbial free-media was maintained for no more than 4 weeks at 4°C.

2.5.3.2 Media for NGF-differentiated PC12 cells

Cells were grown in DMEM supplemented with 5% heat-inactivated horse serum, 1% 200mM L-glutamine, 1% Penicillin/Streptomycin and 100ng/ml 2.5S NGF. NGF was maintained in frozen aliquots and added to media aliquots immediately prior to adding to the cells. Cells were maintained at 37°C, 5% CO_2 and cells had a two-third media change every two days. Cells were cultured for 14 days prior to exposure to MoPrP105-125 and MoScrambledPrP105-125 (Section 2.5.12.).

2.5.4 Protocol for culture of PC12 cells from liquid nitrogen stock

25ml of media (as described in Section 2.5.3.1.) was heated to 37°C for a minimum of 20 minutes in a water bath to reduce media alkalinity. Frozen PC12 cell aliquots were removed from the liquid nitrogen stock (Section 2.5.7.) and thawed rapidly in the water bath for 2 minutes. Thawed cells were transferred to a 15ml centrifuge tube (Corning) containing 9ml of the heated media. Cells were washed of dimethyl sulphoxide (DMSO) (Sigma) by centrifugation at 250*g* for 5 minutes at 4°C. Without disturbing the cell pellet, the supernatant was discarded and the pellet washed again by re-suspension in 10ml heated media, followed by a further centrifugation step. The supernatant was again carefully discarded and the pellet re-suspended in 5ml media and transferred to a 25cm^2 Collagen IV-coated vented flask (BD Biosciences). Cells were incubated at 37°C, 5% CO_2 and a two-thirds media change was performed after 24 hours. Maintenance of the cell cultures was performed as described in Section 2.5.5.

2.5.5 Sub-culturing procedure

Cells were monitored daily to check cell growth and to check for evidence of microbial contamination. When cells reached 80-90% confluence, they were split in a ratio of 1:2 using the following technique. Media was removed from all flasks and cells in each flask were washed with 3ml Mg^{2+}- and Ca^{2+}- free Hanks balanced salt solution (HBSS) for 2 minutes on the cell shaker. HBSS was then discarded and 3ml enzyme-free cell dissociation buffer (Invitrogen) was added to each flask and incubated at 37°C, 5% CO_2 for 15 minutes. Cells were dislodged by gentle tapping of the flask and by washing the dissociation buffer over the surface of the flask several times using a 5ml strippete. Cell solutions were pooled and centrifuged at 250*g* for 5 minutes at 4°C. Supernatants were discarded and cells were re-suspended by adding 2ml heated media (Section 2.5.3.1.) for every flask to be split (1:2 split ratio). Cell clumps were dissociated by passaging cells several times through 1000µl and then 200µl pipette tips. 1ml volumes of this cell suspension were added to each of two $25cm^2$ flasks each containing 4ml of heated media and returned to the incubator, and cells again split when necessary.

For cells to be differentiated with NGF, a flask of confluent cells was harvested as described above. Complete differentiation media (Section 2.5.3.2.) was prepared and heated in the water bath for a minimum of 20 minutes at 37°C. Centrifuged cells were spit in the ratio 1:4 and therefore for every flask to be differentiated, pellets were re-suspended in 4ml differentiation media. 1ml of this suspension was added to each of four $25cm^2$ flasks, each containing 4ml of differentiation media, and returned to the incubator. A two-thirds media change was performed every two days with freshly-prepared differentiation media.

2.5.6 Protocol for counting adherent PC12 cells

Media was removed from the cells to be harvested and cells were washed with 3ml Mg^{2+}- and Ca^{2+}- free HBSS for 2 minutes on the cell shaker. HBSS was then discarded and 3ml cell dissociation buffer (Invitrogen) was added to each flask and incubated at 37°C, 5% CO_2 for 15 minutes. Cells were dislodged by gentle tapping of the surface and by washing the dissociation buffer over the adhered surface several times using a 5ml strippete. Pooled cell suspensions were centrifuged at 250*g* for 5 minutes at 4°C and re-suspended in 1ml heated media (Section 2.5.3.1.). Cell clumps were dissociated by passaging cells several times through 1000µl and then 200µl pipette tips. A 10µl aliquot of the cell suspension was removed and added to 90µl toluidin blue (Sigma). 10µl of this cell suspension was then added to a haemocytometer and cell counts were performed within a total of 25 squares, where viable cells (white) exclude the uptake of the toluidin blue dye. The number of viable cells per ml of media was approximately calculated and used to dilute cells to the desired concentration.

2.5.7 Protocol for the creation of frozen stocks of PC12 cells

Upon receiving the cell stock from LGC Promochem, cells were subcultured to obtain large quantities in order to obtain sufficient cells for the duration of the experiment and also to create stocks so that all cells to be used were from low sub-passage numbers. Cells to be frozen had a two-thirds media change 24 hours prior to the freezing down process. Freeze-media was prepared on the day of the process and consisted of 9ml media (as described in Section 2.5.3.1.) and 1ml DMSO which was maintained on ice for 30 minutes prior to freezing down the cells. Cells were maintained, harvested and counted (Sectionss 2.5.5.-2.5.6.) to estimate the number of

viable cells. Cells were centrifuged at 250*g* for 5 minutes at 4°C, and re-suspended in the appropriate volume of freeze media to obtain approximately 3 x 10^6cells/ml. Cell suspensions were aliquoted in 1ml volumes into 1.2ml cryovials and placed into the Cryo -1°C Freezing container (Nalgene) to gently freeze the cells for optimum viability. Cells were frozen at -70°C for 24 hours prior to transferring the cells to liquid nitrogen for storage.

2.5.8 Immunofluorescence procedure

Cells to be analysed by immunofluorescence were harvested using the technique described (Section 2.5.5.) and the cell pellet re-suspended in 1ml of either media for naive (Section 2.5.3.1.) or differentiated (Section 2.5.3.2.) cell cultures. Viable cells were counted (Section 2.5.6.) and re-suspended at a concentration of 50,000cells/ml in the appropriate media. Collagen IV-coated glass coverslips (Section 2.5.2.) were transferred to the base of 24-well plastic culture plates and 1ml of the cell suspension added to the number of wells required. Naive and NGF-differentiated cells were grown for periods of 7 and 14 days prior to immunofluorescence analysis.

Media was completely removed from the wells containing the cells to be analysed and cells fixed by gently adding 1ml of ice-cold methanol down the side of each cell-containing well. Cells were fixed for 20 minutes at -20°C, and methanol completely removed. Cells were then permeabilized for 10 minutes at room temperature with 1ml of TBS/0.2% Triton x-100. Permeabilization reagent was removed by three 5 minute washes with 1ml TBS/BSA, and cells were blocked for 60 minutes at room temperature with 400µl TBS/2%BSA. The blocking reagent was removed and 400µl 1/1000 anti-PrP 8H4 primary antibody (Table 2.1) was added and incubated overnight at room temperature. Primary antibody was removed and cells washed by three 5

minute washes with 1ml TBS/BSA. 400µl of 1/1000 goat anti-mouse biotinylated secondary antibody (Table 2.2) was incubated for 60 minutes at room temperature followed by three 5 minute washes with 1ml TBS/BSA. Cells were then incubated with streptavidin-conjugated Alexa 594 (Table 2.2) for 60 minutes at room temperature in the dark. Excess antibody was removed by three 5 minute washes with TBS/BSA. Immunofluorescence-labelled cells on coverslips were transferred to Superfrost-Plus slides and cover-slipped with fluorescent-mounting medium (DAKO). To determine the specificity of antibody labelling, duplicate cell samples were incubated with 1/1000 normal mouse serum (Jackson's, USA) and processed as detailed above. Staining was analysed by fluorescent confocal microscopy (Zeiss) and images captured using the Axioskop 2 camera.

2.5.9 Western blot analysis of PC12 cells for PrP^c expression

SDS-PAGE and Western blot protocols (previously described in Sections 2.3.5. and 2.3.6.) were used to analyse the PrP^c expression of naive and NGF-differentiated PC12 cells. Cells were dislodged from collagen IV-coated 25cm^2 flasks using techniques already described for harvesting cells (Section 2.5.5.). To maximise detection, all cells from a confluent 25cm^2 flask were dislodged and re-suspended in either 2 ml lysis buffer; (1) 40mM NaCl, 3mM KCl, 50mM $NaHCO_3$, 2g/litre glucose, 1% NP40, pH 7.5 (Brown *et al.* 1997), or (2) 150mM NaCl, 0.5% Triton x-100, 0.5% deoxycholic acid, 50mM EDTA, 2mM EDTA as described in (Wooten *et al.* 2000). Protease degradation was inhibited by adding PMSF and NEM at final concentrations of 1mM to each sample. Cell suspensions were maintained at 4°C and vortexed every 15 minutes for 1 hour. Cell lysates were prepared in 1X sample buffer using dilutions of 1:5, 1:10 and 1:20 and lysates analysed according to the described

protocols (Sections 2.3.5. and 2.3.6.) using the anti-PrP antibodies in Table 2.1. Unfortunately, attempts to detect PrP^c by Western blot were unsuccessful and are not discussed further in this thesis.

2.5.10 Flourescence-activated cell sorting (FACS) procedure

2.5.10.1 External Staining for PrP^c

Naive and NGF-differentiated PC12 cells to be analysed for FACS analysis were dislodged from collagen IV-coated T25cm^2 flasks using techniques already described for harvesting cells (Section 2.5.5.). Cells were counted (Section 2.5.6.) and re-suspended in 1xFACS buffer (100ml 10xFACS buffer + 1g sodium azide, 1g BSA, 1g EDTA + 900ml dH_20) (1 litre 10x FACS buffer: 25.6g Na_2PO_4, 74.8g NaCl, 3.88g KH_2PO_4, 2.01g KCl) at a concentration of 50,000cells/100µl, and 100µl volumes added to the wells of U-form 96 well plate in quadruplicate. All stages were performed on ice, or where possible at 4°C. In the absence of isotype controls for the primary antibodies, non-specific binding was determined by including cells incubated with secondary but no primary antibodies. Cells were incubated with 50µl of the anti-PrP 8H4 primary antibody (Table 2.1), or 50µl 1xFACS buffer for controls, for 40 minutes and centrifuged at 16,000*g* for 5 minutes. Pellets were washed three times by re-suspension in 200µl 1xFACS buffer and centrifugation at 16,000*g* for 5 minutes. Pellets were re-suspended in 100µl 1xFACS buffer and incubated with 50µl of the Goat anti-mouse Alexa 488 secondary antibody (Table 2.2) for 40 minutes. Pellets were again washed three times by re-suspension in 200µl 1xFACS buffer and centrifugation at 16,000*g* for 5 minutes. Cells were re-suspended in 400µl 1xFACS buffer in FACS tubes (Falcon), fixed with 1% paraformaldehyde for 15 minutes at 37°C, and analysed using a FACS Calibur (BD Biosciences). The 488nm line of the

argon laser was used to excite the fluorochrome-conjugated secondary antibodies, and G_0/G_1 doublet naive PC12 cells were gated out for comparison with mitotically-arrested NGF-differentiated cultures. Statistical analysis for FACS was derived from the analysis of 10,000 cells per sample.

2.5.10.2 Internal staining for neurofilament protein and active caspase-3

Naive and NGF-differentiated PC12 cells to be analysed for FACS analysis were harvested and prepared for FACS analysis as described in Section 2.5.10.1. Prior to incubating the cells with a primary antibody, cells were fixed with 1% paraformaldehyde for 15 minutes at 37°C, washed three times by re-suspension in 200µl 1xFACS buffer and centrifugation at 16,000*g* for 5 minutes. Cells were permeabilised with 0.2% Triton-x100 (in 1xFACS buffer) for 10 minutes and washed three times by re-suspension in 200µl 1xFACS buffer and centrifugation at 16,000*g* for 5 minutes. Cells were incubated with 50µl of the primary antibody of choice (Table 2.1), or 50µl 1xFACS buffer for controls, for 40 minutes and centrifuged at 16,000*g* for 5 minutes. Pellets were washed three times by re-suspension in 200µl 1xFACS buffer and centrifugation at 16,000*g* for 5 minutes. Pellets were re-suspended in 100µl 1xFACS buffer and incubated with 50µl of secondary antibody (Table 2.2) for 40 minutes. Pellets were again washed three times by re-suspension in 200µl 1xFACS buffer and centrifugation at 16,000*g* for 5 minutes. Cells were re-suspended in 400µl 1xFACS buffer in FACS tubes (Falcon) and analysed as before using a FACS Calibur (BD Biosciences).

2.5.10.3 Annexin V labelling

Naive and NGF-differentiated PC12 cells to be analysed for FACS analysis were harvested and prepared for FACS analysis as described in Section 2.5.10.1. Cells were counted (Section 2.5.6.) and re-suspended in 1xFACS buffer at a concentration of 50,000cells/100µl, and 100µl volumes added to the wells of U-form 96 well plate in quadruplicate. All stages were performed on ice, or where possible at 4°C. Annexin V binding was investigated using a commercially available kit (Vybrant Apoptosis detection kit, Molecular Probes). 100µl of the 1x Annexin-binding buffer was added to each well to block potential unspecific binding to Annexin V. Viability and Annexin V staining was then attempted by the addition of 5µl Alexa Fluor 488 Annexin V (Component A) and 1µl of propidium iodide (Component B). Unfortunately Annexin V was found to bind non-specifically in this assay, despite several attempts to improve the specificity of the binding. Potential reasons for this non-specificity are discussed in Section 4.3.9.

2.5.11 Cell proliferation and cytotoxicity assays

2.5.11.1 MTT assay

The MTT [3-(4,5-Dimethylthiazol-2-yl)-2,5-Diphenyltetrazolium Bromide] assay was investigated in order to measure PC12 cell proliferation, and cytotoxicity following exposure to neurotoxic PrP peptides (Section 4). The percentage reduction of the tetrazolium salt is therefore related to the viability of cell cultures in the test assay. PC12 cells were harvested and counted as described (Sections 2.5.5.-2.5.6.) and re-suspended at a concentration of 800cells/200µl in the appropriate media. 200µl of the cell suspension was added to each well of a Collagen IV-coated 96-well plate (BD Biosciences) until sufficient wells for the assay were obtained. Cells were incubated

for 24 hours at 37°C, 5% CO_2 and a 50% media change was performed prior to addition of the desired amount of test reagent to triplicate wells as described (Section 2.5.12.). Plates were incubated at 37°C, 5% CO_2 for the desired period of exposure to the peptide sequences. 25µl of 0.5mg/ml MTT (Sigma) solution in PBS was then added to each well and incubated at 37°C, 5% CO_2 for 4 hours. Converted formazans were released from PC12 cells by addition of 100µl of cell lysis buffer (20% (w/v) SDS in 50% *N,N*-dimethyl formamide, pH 4.7). Plates were agitated for 10 mins on the cell shaker, and colorimetric determination of MTT reduction was carried out by taking absorbance readings at 570nm on a V-Max microplate reader (Molecular Devices). Unfortunately, the MTT assay could not be successfully reproduced and eventually the alamarblue assay (Section 2.5.11.2.) was developed as a suitable assay for the purposes of the work described in this thesis.

2.5.11.2 Alamarblue assay

The alamarblue assay is a sensitive reduction-oxidation (REDOX) assay which has been developed to quantitatively measure the proliferation of cell lines and as cytotoxicity assay for the screening of various chemical compounds. The chemical reduction of the alamarblue compound by viable cells results in a specific fluorometric and colorimetric change, which can be used to measure the proliferation and viability of cell cultures. Inhibition of cell growth through the exposure to toxic compounds maintains the alamarblue reagent in the oxidised form. The percentage reduction of alamarblue in cell cultures exposed to a test agent can quantitatively measure the cytotoxicity of that test compound on exposed cells. The reduction of the alamarblue compound is thought to involve mitochondrial, cytosolic and microsomal enzymes.

PC12 cells were harvested and counted as described (Sections 2.5.5.-2.5.6.) and re-suspended at a concentration of 800cells/200µl in the appropriate media. 200µl of the cell suspension was added to each well of a Collagen IV-coated 96-well plate (BD Biosciences) until sufficient wells for the assay were obtained. Cells were incubated for 24 hours at 37°C, 5% CO_2 and a 50% media change was performed. 20µl of the alamarblue reagent (Serotec) was added to each well and the desired amount of test reagent added to wells in triplicate as described (Section 2.5.12.). Plates were incubated at 37°C, 5% CO_2 for the desired period of exposure to the peptide sequences. Plates were blanked by transferring 100µl of media alone to each of three wells in uncoated 96 well plates (Sigma). Readings for negative control (media + alamarblue) and test samples are obtained by again transferring 100µl of each sample to wells of the uncoated 96 well plate. The absorbances of the wells were read at both 570nm and 600nm on a V-Max microplate reader (Molecular Devices), and the percentage reduction calculated as per the protocol provided by the manufacturer.

2.5.12 Protocol for the exposure of cells to MoPrP105-125 and Trimethyltin (TMT)

Test wells were prepared as described in Section 2.5.11.2., containing naive or 14 day NGF-differentiated PC12 cells (800cells/200µl). Test wells were prepared in triplicate, incubated for 24 hours at 37°C, 5% CO_2 prior to a 50% media change and 20µl of the alamarblue reagent (Serotec) added to each well. Test wells were exposed to either the normal (MoPrP105-125) or scrambled peptide sequences at concentrations of 0µM, 50µM, 80µM, 100µM, or 150µM for periods of 24 hours, 48 hours, 72 hours, 5 days and 7 days. Peptide conformations were prepared as detailed in Section 2.4.2. Negative control samples, consisting only of equivalent volumes of

the buffers minus any peptide, were added in triplicate and analysed over the same duration for each experiment. A positive control for the alamarblue assay was obtained by incubating PC12 cells in triplicate with 400μM Trimethyltin (TMT) (Sigma-Aldrich), a neurotoxic compound which has been demonstrated to induce apoptosis and necrosis in PC12 and other cell culture systems. The cytotoxicity of the peptide conformations, scrambled peptide conformations, vehicle buffers minus peptides, and cells exposed to TMT were measured by alamarblue assay (Section 2.5.11.2.). The most toxic peptide conformation determined by this assay was then added to further cells and these cells were analysed for activated caspase-3 using the FACS protocols detailed in Section 2.5.10.3.

2.5.12. Statistical Analysis

Statistical analysis for the cytotoxicity and FACS data obtained in Section 4 was performed following consultations with Jill Sales from the Biological Statistic Service, Scotland (BioSS). This data was analysed in all cases using balanced two-way ANOVA (analysis of variance) on the minitab statistical package (Minitab, Version 14). Two-way ANOVA analysis was chosen to analyse the effects of independent variables and to analyse if there were interaction effects of these independent variables. Data from the alamarblue cytotoxicity analysis was transformed using the angular transformation to convert percentages prior to the balanced ANOVA analysis.

Chapter 3: Mechanisms of neuronal cell death in TSEs

3.1 Neuronal degeneration

Neuronal loss is not due solely to differences in the susceptibility of different subsets of neurons to the disease process, but is influenced by the infecting agent and the host genotype (Bruce *et al.* 1976). The mechanisms by which neuronal damage are related to accumulating PrP^{sc} are not fully understood; this research will investigate further the mechanisms of neurodegeneration in these diseases. Understanding the mechanisms of cell death in murine scrapie models may identify intervention strategies to inhibit, repair or delay the neurodegenerative brain damage caused by these fatal diseases.

3.1.1 Necrosis

Necrosis represents the localised death of a cell, tissue or organ in response to stresses beyond their homeostatic capabilities. Extreme stresses resulting in necrosis include the withdrawal of oxygen or essential nutrients, and also the exposure to toxic compounds or the presence of mutated genes. Necrotising cells have a number of distorted morphological hallmarks, including; extensively vacuolated cytoplasms, swollen mitochondria and dilated endoplasmic reticula (ER). Cells also swell and lyse, inducing inflammatory responses within the host. DNA damage specifically activates the DNA repair enzyme poly (ADP-ribose) polymerase (PARP), which has generally been considered to be a necrosis-specific event. PARP polymerises poly (ADP-ribose) from NAD monomers, resulting in the depletion of cellular ATP levels which would be required for the active process of programmed cell death (Apoptosis). Increasing knowledge of the mechanisms of cell death suggest that there may be

many crossovers than the presently accepted strict definitions of necrosis, apoptosis and autophagy. At present there is no evidence for necrotic cell death in the TSE diseases, but numerous publications detailing mechanisms of neuronal autophagy and apoptosis.

3.1.2 Neuronal autophagy

Autophagy is a tightly controlled process required for normal cellular turnover, where the target cell or protein is sequestered by autophagic vacuoles resulting in the degradation of the cellular constituents. As autophagy is a constitutive process, only excessive and misplaced autophagic vacuoles resulting in cell death are the hallmarks of a disease state. The characteristic hallmarks of autophagy are: the formation of autophagic vacuoles comprised of cytoplasm sequestered with single, double or multiple membranes; membranous whorls, residual bodies, multivesicular bodies and engulfed organelles. The full mechanisms of autophagy are poorly understood, particularly in neurons. Increasing numbers of biological markers are being identified, but morphological analysis by electron microscopy remains the major technique for identifying autophagy.

Neuronal autophagy has also been documented as a mechanism for neuronal cell loss in the TSE infections and to date has been reported in experimental CJD, scrapie and BSE (Boellaard *et al.* 1989; Boellaard *et al.* 1991; Jeffrey *et al.* 1992; Liberski *et al.* 1992). Neuronal autophagy has also been documented in other neurodegenerative diseases and their experimental models: in Huntington's disease (Roizon 1974, 1979; Kegel 2000; Petersen 2001), in Alzheimer's disease (Cataldo *et al.* 1994; Cataldo *et*

al. 1995; Cataldo *et al.* 1996; Stadelmann *et al.* 1999) and in Parkinson's disease (Anglade *et al.* 1997). Autophagy and apoptosis appear to have some common mechanisms and autophagic independence or inter-dependence with apoptosis needs to be further clarified. Both apoptosis and autophagy can be induced by the opening of the mitochondrial permeability transition pore (PTP) (Lemasters *et al.* 1998) and the presence of autophagy is associated with an increased tendency for cells to undergo apoptosis (Jia *et al.* 1997). Whether autophagy proceeds independently of apoptosis is uncertain, as reports using neuronal cell cultures indicate that autophagy induction is sensitive to apoptotic stimuli (Larsen & Sulzer 2002). It is therefore conceivable that as evidence for apoptosis and autophagy exists, and that their mechanisms appear to interconnect, that both processes could have distinct roles in contributing to neuronal cell loss in these diseases.

3.1.3 Neuronal apoptosis: Caspase-dependent

Apoptosis is a carefully co-ordinated series of events, and has long been the phenotype of programmed cell death (Kerr *et al.* 1972), and is essential for cell development, maturation, normal tissue turnover and regulation of immune systems. Apoptosis is co-ordinated by the Fas mediated pathway, the cysteine protease (caspase) and Bcl-2 protein families and can be triggered by toxic compounds, chemicals, the absence of growth factors, physical stresses including γ– and UV-irradiation, oxidative stress and heat shock. The activation and suppression of apoptotic processes are also mediated by various cell-surface receptors that detect physiological changes, where the binding of death ligands to specific receptors activates the respective apoptotic mechanism. Apoptosis is thought to be an important mechanism of neuronal cell death in TSE infections based upon the

detection of cellular and nuclear shrinkage, condensation and fragmentation of nuclear chromatin by electron microscopy and biochemically by endonuclease-mediated internucleosomal fragmentation of DNA into multiple oligosomal sub-units of 180 bp (Giese *et al.* 1995; Lucassen *et al.* 1995; Fraser *et al.* 1996; Jesionek-Kupnicka *et al.* 1997; Dorandeu *et al.* 1998; Gray *et al.* 1999; Puig & Ferrer 2001).

Transgenic mouse models over-expressing Bcl-2 in the nervous system are protected from cell death during development, highlighting the anti-apoptotic function of the protein (Martinou 1994). Fas is one of the key initiators in the apoptotic cascade; Fas ligand (FasL) binds to the Fas receptor (FasR), and this results in the formation of the death-inducing signaling complex (DISC). This leads to the activation of initiator and effector caspases, mediated through either a mitochondria-dependent or the mitochondria-independent pathway (Scaffidi *et al.* 1998). Upon activation of a death signal, a self-amplifying cascade amongst the caspase enzymes occurs, resulting in the activation of the relatively inactive caspase zymogens within the cytosol. This apoptotic mechanism is mediated by cytochrome c (cyt c). Cytochrome c is translated as apopcytochrome c in the cytosol, translocates to the mitochondria, and is converted to holocytochrome c following the addition of a haem group in the mitochondria. The research of this thesis concentrates on the holocytochrome c isoform, the only isoform capable of inducing apoptosis (Yang *et al.* 1997), and is referred to as cytochrome c within the text of this thesis. Cyt c is released from the mitochondria in response to oxidative stress, due to elevated levels of extra-mitochondrial Ca^{2+}. The redox state of cyt c (following cytosolic release) is independent of the apoptotic capabilities of the protein, although cyt c is thought to remain in the cytosol in the reduced form (Hampton *et al.* 1998).

Anti-apoptotic proteins (Bcl-2, Bcl-X_L) maintain the integrity of mitochondrial membranes and prevent cyt c release (Kluck *et al.* 1997; Yang *et al.* 1997), and pro-apoptotic proteins (e.g. Bax, Bak) result in membrane permeabilisation. The physical interactions of Bcl-2 and Bax with proteins of the PTP can result in opening of the PTP and translocation of soluble intermembrane proteins via the outer mitochondrial membrane. The PTP is thought to be involved in the translocation of Ca^{2+} into the mitochondrial matrix and release of cyt c, through a nitric oxide-independent mechanism. In Alzheimer's disease and cerebral ischemia, cytosolic Ca^{2+} concentrations are pathologically elevated resulting in the release of cyt c and the activation of neuronal apoptosis (Schild *et al.* 2001). However no evidence exists to confirm that this occurs in prion diseases. The release of cyt c into the cytosol results in the activation of a caspase cascade and apoptotic cell death (Liu *et al.* 1996). Cyt c interacts with Apaf-1 (apoptotic protease activating factor 1) to form the apoptosome (a complex consisting of cyt c, ATP, procaspase-9 and Apaf-1), resulting in the activation of caspase 9 and downstream effector caspases and therefore apoptotic cell death (Zou *et al.* 1999). Cyt c release is mediated through balanced interactions of pro- and anti-apoptotic members of the Bcl-2 family, which therefore have an important role in the mediation of apoptosis. The up-regulation of Fas and Caspases as markers for neurodegeneration in prion diseases have been documented for the first time in murine 87V scrapie infections (Jamieson *et al.* 2001a), highlighting the importance of these caspase-dependent apoptotic markers in the early detection of the neurodegenerative pathways associated with prion diseases.

3.1.4 Neuronal apoptosis: Caspase-independent

In addition to the role of caspases in apoptosis, Apoptotis Inducing Factor (AIF) and Endonuclease G (EndoG) have emerged as mediators of apoptosis in both the presence and absence of caspases (Li *et al.* 2001; Susin *et al.* 1999; van Loo *et al.* 2001). AIF and EndoG are IMM proteins released to the nucleus and cytosol upon permeabilisation of the mitochondrial membrane. Therefore these proteins are released from the mitochondria in addition to cyt c, although the sequence and apoptotic stimuli resulting in their release has yet to be fully clarified. These proteins are also regulated by the Bcl-2 protein family members and their release, or not, further determines the fate of the cell. The ability of these proteins to execute apoptosis in the absence of caspases represents a novel area of interest in TSEs, and their involvement in neurodegenerative models of ischemia and Parkinson's Disease has recently been documented (Cao *et al.* 2003; Wang *et al.* 2003; Zhu *et al.* 2003). Difficulties in the detection of neuronal loss *in vivo* have resulted in modest advances in the understanding of the neurodegenerative pathways associated with TSEs. The research on caspase-independent mechanisms will therefore highlight the roles, if any, of these proteins in murine models of TSE disease.

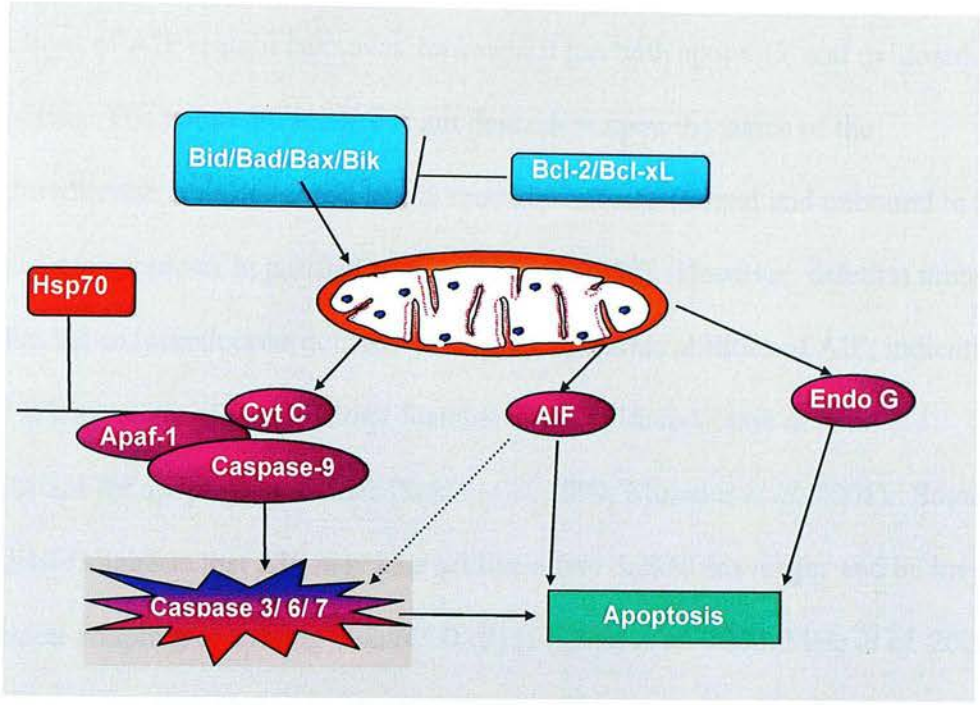

Figure 3.1 **Apoptotic functions of some of the inner mitochondrial membrane proteins**
Brief schematic highlighting apoptotic functions of the inner mitochondrial membrane (IMM) proteins analysed in this research. Endo G and AIF apoptotic mechanisms are not completely clear, however it is thought AIF can be apoptotic in both the presence and absence of caspases. Cyt c forms the apoptosome with Apaf-1 and caspase 9 to activate downstream effector caspases. Apoptosome formation and IMM protein release is influenced by Hsp70, and also by pro- and anti-apoptotic members of the Bcl-2 protein family

3.1.4.1 Apoptosis-inducing factor

AIF is a flavoprotein synthesised as a precursor (~67 kDa), directed by an N-terminal mitochondrial localisation sequence (MLS) of 100 amino acids for incorporation into the IMM. Proteolytic cleavage of the MLS results in mature AIF (~57 kDa) consisting of a nuclear localisation signal, a C-terminal region with high homology to eukaryotic and prokaryotic oxidoreductases (consisting of flavin adenine dinucleotide (FAD) and nicotinaminde adenine dinucleotide (NAD) binding sites), and a DNA binding domain. Mature AIF appears to be expressed ubiquitously from embryonic development to the adult stage, specifically localised to the IMM. The precise

functions of AIF remain unknown; however, it has both apoptotic and oxidoreductase activities. The apoptotic activity is not dependent upon the status of the oxidoreductase activity, as full length recombinant AIF (bound and unbound to FAD) stimulates apoptosis in purified nuclei (Ye *et al.* 2002). However, deletion mutants within the oxidoreductase domain remove the apoptotic abilities of AIF, indicating that at least some of the structural features of the oxidoreductase domain are important for apoptotic activities (Susin *et al.* 1999; Miramar *et al.* 2001). Some evidence suggests that AIF may also act like a free radical scavenger and be involved in redox coupling or cycling with NAD (P) H (Klein *et al.* 2002; Mate *et al.* 2002). AIF has a structure similar to glutathione peroxidase, important in the dismutation of hydrogen peroxide and therefore protection against oxidative stress (Mate *et al.* 2002). Cerebellar cells expressing low levels of AIF are extremely sensitive to peroxide mediated oxidative stress, whereas cells over-expressing AIF are resistant (Klein *et al.* 2002). AIF may therefore function as an antioxidant within the IMM under normal physiological conditions, but assuming pro-apoptotic functions following release from the IMM.

Upon the induction of apoptosis, AIF is released from the IMM and translocates to the nucleus and cytosol. In the nucleus AIF is thought to directly bind DNA (Ye *et al.* 2002) to induce partial chromatin condensation and DNA fragmentation to high molecular weighted (HMW) fragments (~50 kB) but without the oligonucleosomal 180-200 bp ladder characteristic of caspase-mediated apoptosis (Susin *et al.* 1999). Cytoplasmic microinjections of recombinant AIF results in the morphological and biochemical changes typical of apoptosis even when cells are cultured with the pan caspase inhibitor Z-VAD.fmk (Susin *et al.* 1999). Further evidence for a role of AIF

in enabling apoptosis is that AIF null mice die at an early stage of embryogenesis, due to the lack of cavitation of embryoid bodies that is essential for normal development directed by apoptosis (Joza *et al.* 2001). The release of AIF from the mitochondria is thought to affect the barrier function permeability of the mitochondrial membrane. Therefore, AIF released from the IMM will affect the membrane function of other mitochondria (Susin *et al.* 1997). Bcl-2 inhibits the release of AIF from the IMM, but if AIF has already been released from the IMM and is present in the nucleus and cytosol the cytoprotective effects are lost (Susin *et al.* 1999).

Purified nuclear heat-shock protein 70 (Hsp70), a cytoprotective factor, antagonises AIF to prevent AIF-induced chromatin condensation (Ravagnan *et al.* 2001). Hsp70 has previously been shown to inhibit apoptosis by preventing apoptosome formation by binding Apaf-1, therefore preventing caspase-9 activation (Beere *et al.* 2000; Saleh *et al.* 2000). In Apaf-1 knockout cells, Hsp70 continues to inhibit apoptosis indicating the ability to block apoptosis through further mechanisms (Ravagnan *et al.* 2001). Hsp70 and AIF interactions have so far been demonstrated in cell-free systems and in intact cells (Ravagnan *et al.* 2001), but a functional relationship has yet to be established *in vivo*. In addition to the release of AIF under apoptotic conditions, AIF release has also been demonstrated experimentally in conditions of ATP depletion, that lead to a characteristic necrotic phenotype of advanced DNA fragmentation and characteristic lack of chromatin condensation (Daugas *et al.* 2000). Therefore AIF appears to be a dual/multi function protein, with one function of that of a caspase-independent mitochondrial death effector active in conditions of either necrosis or apoptosis.

In addition to the existing *in vitro* studies, recent publications have documented the *in vivo* activities of AIF in neuronal apoptosis. High molecular weight DNA fragmentation and localisation of AIF to hippocampal and ipsilateral cortical nuclei has been demonstrated following traumatic brain injury in rats (Zhang *et al.* 2002). This HMW fragmentation and AIF translocation has also been found in a rat model of transient-global ischemia in CA1 hippocampal neurons (Cao *et al.* 2003) and also in a rat model of hypoxia-ischemia in neonatal animals (Zhu *et al.* 2003). AIF translocation has also been documented in the penumbra following middle cerebral artery occlusion in adult rats (Ferrer *et al.* 2003) and in a mouse model of sporadic Parkinson's disease (Wang *et al.* 2003).

3.1.4.2 Endonuclease G

Endo G is a non-specific mitochondrial nuclease (~30 kDa) that is highly conserved between eukaryotes. It is encoded by a nuclear gene and directed to the mitochondria by an N-terminal signal sequence which is subsequently cleaved for the incorporation of mature Endo G into the mitochondria, where it forms homodimers. Mammalian Endo G has been identified not only in the IMM, but also within the mitochondrial DNA (mtDNA) complex (Li *et al.* 2001; van Loo *et al.* 2001). The lack of a nuclear localisation sequence and its preference for GC-rich substrates (which resemble the DNA sequences in the mtDNA complex) had led researchers to believe that Endo G had a role in mtDNA replication (Cote & Ruiz-Carrillo 1993). However, more recent research has identified a role for Endo G in the mediation of caspase-independent apoptosis (Wang 2001). Caspase-activated deoxyribonuclease (CAD), also known as DNA fragmentation factor 40, is a nuclease which results in HMW DNA fragmentation and DNA laddering when cleaved from its inhibitor ICAD/DFF45 by

caspase 3. In the absence of caspases in mice lacking CAD/DFF40 and in mice with caspase-resistant ICAD/DFF45, HMW DNA fragmentation and DNA laddering still occurs, indicating the activity of a caspase-independent nuclease. This nuclease has been identified as Endo G (Li *et al.* 2001; van Loo *et al.* 2001).

The majority of Endo G is located in the IMM, remaining inactive until its release and translocation to the nucleus. The full mechanisms resulting Endo G activation are unknown, but are thought to be under the control of the Bcl-2 family members as Bcl-2 over-expression blocks the translocation of Endo G from the mitochondria to the nucleus (van Loo *et al.* 2001). Pro-apoptotic truncated Bid (tBid) has been shown to induce the release of Endo G and cyt c from mitochondria *in vitro* and *in vivo*, resulting in DNA fragmentation. Although Bid is cleaved to tBid (pro-apoptotic) by caspase 8 resulting in cyt c release and formation of the apoptosome (Li *et al.* 1998; Luo *et al.* 1998; Gross *et al.* 1999), Bid can also be cleaved independently of caspases by granzyme B and lysosomal proteases, further indicating that Endo G can be activated in a caspase-independent manner (Heibein *et al.* 1999; Stoka *et al.* 2001). Although partially purified Endo G results in DNA laddering in isolated nuclei, full DNA degradation is thought to require the activities of exonucleases and DNaseI (Widlak *et al.* 2001). No evidence yet suggests that AIF and Endo G work together in mammalian apoptosis, however homologues of these proteins in *Caenorhabditis elegans* (Wah-1 and csp-6 respectively) suggest that they work synergistically (Wang *et al.* 2002). Therefore, AIF and Endo G are both evolutionarily conserved. Whether or not they act synergistically in mammals, they appear to be important in the mediation of caspase-independent apoptosis in certain neurological disorders. The release of AIF and Endo G therefore represent interesting mechanisms of apoptosis

which deserve consideration in TSE diseases and which will be addressed by this research.

The aims of this thesis (Section 1.6) are to investigate the fundamental mechanisms of neurodegeneration in the TSEs. As described above, evidence exists for caspase-dependent mechanisms of cell death in several TSE diseases and TSE disease models. This thesis has concentrated on potential roles of AIF, Endo G and Cyt c in two well described murine scrapie models (ME7/CV and 87V/VM) at the terminal stages of disease (Section 1.4.5). As cyt c appears to be involved in both caspase-dependent and caspase-independent cell death pathways in other disease models, the translocation of Cyt c from the IMM to the cytosol in TSEs would represent a relatively upstream marker of neurodegeneration. The analysis of AIF and Endo G for similar translocation is a downstream event in the apoptosis cascade, and would confirm wheither caspase-independnet mechanisms are involved in the neurodegenerative process in the TSE diseases.

3.2 Results

3.2.1 Production of mitochondria-free cytosolic samples

The creation of mitochondria-free cytosolic samples was essential for the analysis of apoptosis-related protein translocation from the inner IMM to the cytosol. Cytosolic samples containing 60 and 90μg total protein were probed with the anti-voltage-dependent anion channel (VDAC1) primary antibody, to allow the detection of contaminating mitochondria. VDAC1 is an abundant protein of the outer mitochondrial membrane found in all eukaryotes. VDAC1 forms a large voltage-gated channel responsible for metabolism, mitochondrial homeostasis and apoptotic cell death through the mediation of cyt c release (Shimizu *et al.* 1999). Mitochondrial extracts from identical brain samples confirmed reactivity with VDAC1. 3T3 or K562 cell lysates varied with reactivity with VDAC1, depending on the batch, and were poorly reactive as these are cellular lysates.

Initially, samples created by the sucrose-gradient fractionation protocol (Section 2.3.1.) revealed the presence of mitochondrial contaminants in the cytosolic fractions. Increased centrifugation speeds of 100,000*g* (50,000rpm) for 60 minutes, and careful removal of cytosolic supernatants produced consistently mitochondria-free samples. In addition, samples created by the sub cellular fractionation (Calbiochem) protocol (Section 2.3.2.2.) were contaminated with mitochondria in the cytosolic fractions. Two further final centrifugation steps at 10,000g, each for 10 minutes, greatly increased the purity of the fractions. Cytosolic purity was maximised by homogenising dissected samples by serial passage through a 19 gauge metal needle using 1ml syringes, in comparison to the samples originally created by homogenisation with mini-dounce homogenisers. Cytosolic fractions created by these

protocols were consistently free of mitochondria and are ideal for the study of the translocation of IMM proteins to the cytosol.

3.2.2 Primary antibodies and positive controls for analysing IMM protein translocation

Sub-cellular fractionated cytosolic samples were analysed for VDAC1, AIF, Endo G and cyt c. Cytosolic samples created from these homogenates were free of mitochondria as confirmed by the lack of reactivity with the anti-VDAC1 antibody. Western blot analysis with Hsp70 was also performed for micro-dissected samples, but not for sucrose-gradient fractionated samples as this antibody was not available at the time of this research. Hsp70 was examined to confirm the presence of protein on the membranes as this protein is present in both the mitochondria and cytosol, and also because this protein can inhibit both caspase and caspase-independent apoptotic pathways (Beere *et al.* 2000; Ravagnan *et al.* 2001). The 3T3 cell lysate was purchased as a positive control for Endo G (and AIF), and the K562 cell lysate was purchased as a positive control for AIF. Both cell lysates cross-reacted strongly with the anti-Hsp70 antibody but weakly with the anti-VDAC1 antibody. Depending upon the batch of positive control, the anti-cyt c antibody would recognize either of the cell lysates or both.

3.2.3 AIF translocation to the cytosol is detected in micro-dissected ME7/CV but not 87V/VM samples, or in samples prepared from whole brain

To investigate caspase-independent mechanisms of neuronal cell death, mitochondria-free cytosolic samples were prepared from whole brain homogenates and also from micro-dissected pooled hippocampal and thalamic samples from the ME7/CV and 87V/VM murine scrapie models (Section 1.4.5.). Samples were separated into sub-cellular fractions by the whole brain sucrose gradient technique (Section 2.3.1.) and analysed by Western blot (Figures 3.2-3.9). Furthermore, the hippocampi and thalamus which are two of the areas presenting TSE pathology in the ME7/CV (Figure 1.2) and 87V/VM (Figure 1.3) models, were micro-dissected, pooled, sub-cellular fractionated using the Calbiochem kit (Section 2.3.2.2.) and analysed by Western blot (Figures 3.10-3.17). Apoptosis is notoriously difficult to detect *in vivo*, due to the rapid clearance of apoptotic cells. If neuronal apoptosis is occurring *in vivo* in these murine scrapie models then these micro-dissected areas, which show a marked neuronal loss (Jeffrey *et al.* 2000; Jamieson *et al.* 2001(a); Jamieson *et al.* 2001(b)), should contain a higher proportion of apoptotic to normal cells. Based on this evidence, the use of micro-dissected areas would maximise the likelihood of detecting apoptosis-related proteins.

Cytochrome c detection in the tested samples will be discussed in Section 3.2.4.

Samples containing 30μg of mitochondrial proteins from both the whole brain (Figures 3.2/ 3.4/ 3.6/ 3.8) and micro-dissected brain homogenates (Figures 3.10/ 3.12/ 3.14/ 3.16) always detected AIF, Endo G, VDAC and cyt c (and Hsp70 when analysed). Cytosolic samples containing 30μg of total protein from the whole brain fractionated samples from both the whole brain (Figures 3.2/ 3.4/ 3.6/ 3.8) and micro-

dissected brain homogenates (Figures 3.10/ 3.12/ 3.14/ 3.16) never contained detectable AIF, Endo G or VDAC proteins. Hsp70, where tested, was always detected and cyt c was occasionally detected in these samples. Cytosolic samples containing 60 and 90μg total protein from the whole brain fractionated samples from both the whole brain (Figures 3.3/ 3.5/ 3.7/ 3.9) and micro-dissected brain homogenates (Figures 3.11/ 3.13/ 3.15/ 3.17) were always free of mitochondrial contaminants as determined by the lack of VDAC1 proteins. Endo G was never detected in either the 60 or 90μg total protein samples indicating that this endonuclease protein is either not detected or not involved in mediating neuronal cell death in murine scrapie disease. AIF was not detected in the 87V/VM or NB/VM cytosolic samples containing 60 or 90μg total protein from samples prepared by the whole brain (Figures 3.7 and 3.9) or micro-dissection fractionation techniques (Figures 3.15 and 3.17). However, AIF was detected in the ME7/CV (but not NB/CV) cytosolic samples containing 60 or 90μg total protein from samples prepared by the micro-dissection fractionation technique (Figures 3.13 and 3.17). Furthermore, AIF was not detected in equivalent ME7/CV and NB/CV 60 or 90μg total protein-containing cytosolic samples created by the whole brain fractionation protocol (Figures 3.3 and 3.5). These results further highlight the differences noted in Section 1 between the mechanisms of neuronal cell death in the ME7/CV and 87V/VM murine scrapie models. In addition, these results indicate that the micro-dissection protocol reduces the dilution effect of non-apoptosing cells to cells potentially undergoing apoptosis, and may therefore be a much more suitable technique for the *in vivo* detection of apoptosis.

3.2.4 Cytochrome c is detected in the cytosol in terminal stage murine scrapie and aged-matched normal brain injected control animals in micro-dissected and whole brain homogenates

Cytosolic samples created from whole mouse brain homogenates (Figures 3.2-3.9) and micro-dissected brain areas (Figures 3.10-3.17) were also analysed for the presence of cyt c. Cytochrome c is an important mediator of intrinsic apoptosis, whose presence in the cytosol can initiate the caspase cascade by formation of the apoptosome (Liu *et al.* 1996; Zou *et al.* 1999). Mitochondrial samples (30µg protein) from both the whole brain (Figures 3.2/ 3.4/ 3.6/ 3.8) and micro-dissected brain homogenates (Figures 3.10/ 3.12/ 3.14/ 3.16) always contained cyt c protein. It was expected that if cyt c were to be detected in the cytosolic fractions it would detected only in those brain homogenates prepared from murine scrapie infected mice, if neuronal cell death was occurring through apoptotic pathways. However, cytochrome c was present in low amounts in almost all of the cytosolic samples (30µg protein) prepared by the micro-dissection fractionation procedure (Figures 3.10/ 3.12/ 3.14/ 3.16), but not in the cytosol of whole brain fractionated samples except for extremely weak bands in samples prepared from NB/VM mice (Figure 3.6). Cytosolic samples containing 60 and 90µg total protein from both the whole brain (Figures 3.3/ 3.5/ 3.7/ 3.9) and micro-dissected brain homogenates (Figures 3.11/ 3.13/ 3.15/ 3.17) all contained larger quantities of the cyt c protein. Visually, cyt c levels in the cytosol of normal and scrapie-infected brain homogenates were similar. It was therefore impossible to verify if cyt c levels were higher in murine scrapie infected samples (as would be expected if intrinsic neuronal apoptosis was occurring), in comparison to normal brain injected control samples. The unexpected presence of cyt c in all cytosolic samples (60 and 90µg protein) led to the hypothesis that cyt c may be

present in these samples due to the sample preparation procedure or that age-related mechanisms may be involved. Samples from younger mice (NB/CV and NB/VM) were prepared by both extraction procedures and analysed for the presence of cyt c (Section 3.2.5).

3.2.5 Cytochrome c is not detected in the cytosol of normal brain injected animals at 70dpi in micro-dissected nor in whole brain fractionated brain homogenates

Cyt c had been detected in some of the cytosolic samples containing 30µg protein, and in all samples containing 60 and 90µg protein from the ME7/CV, 87V/VM and NB control animals (Section 3.2.4.). To analyse whether cyt c was being detected as a consequence of age-related functions (such as mitochondria malfunction) or due to the protocols used for fractionating the samples, normal brain injected CV and VM mice were analysed at approximately 70 dpi (Figure 3.19). Cytosolic samples were created using both the micro-dissected and whole brain fractionation protocols, and samples containing 60µg (Figure 3.19A) and 90µg (Figure 3.19B) protein were analysed by Western blot with the anti-cyt c antibody. Cyt c was present both in the 3T3 and K562 positive controls (Figure 3.19) but absent from wells containing 60 and 90µg protein for both the micro-dissected and whole brain fractionation techniques. Stripping and re-probing the membrane with Hsp70 revealed that protein was definitely present in all of the tested samples. Therefore, the presence of cyt c in the cytosol is not due to the procedure used to fractionate the samples but appears to be due to age-related mechanisms.

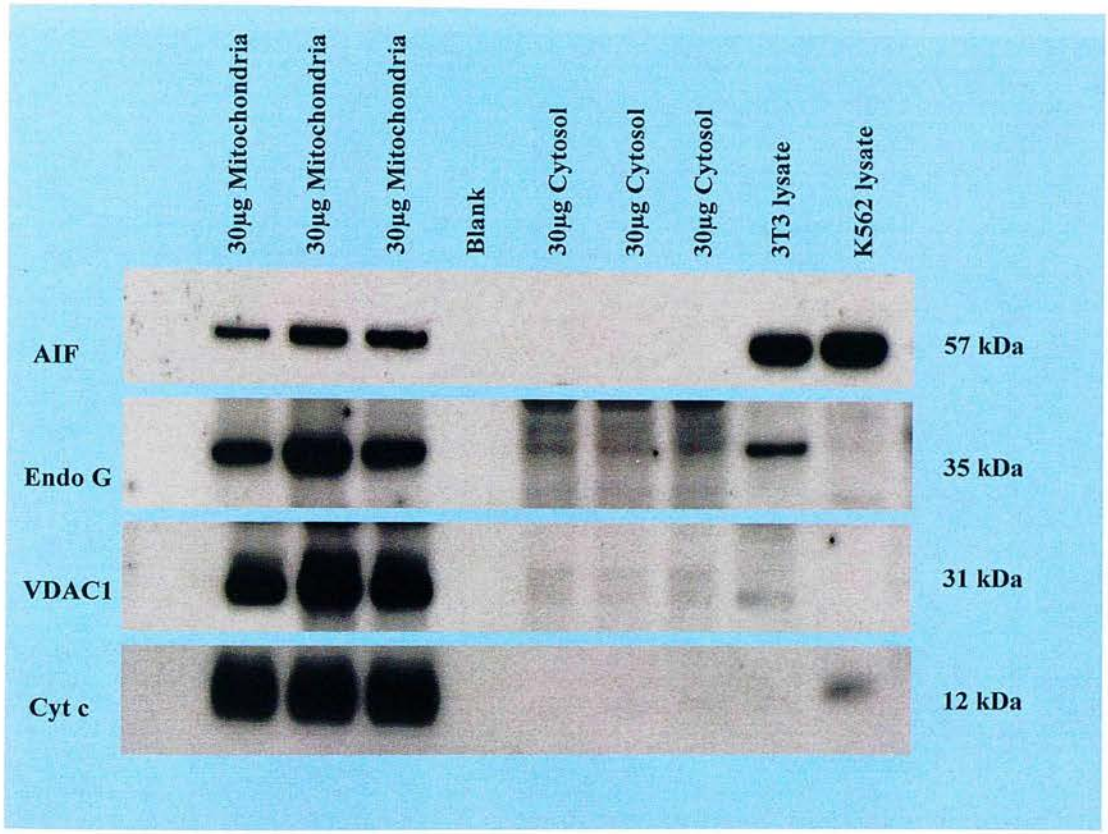

Figure 3.2 **Sub-cellular location of apoptosis-related proteins isolated from whole brain homogenates from normal brain injected terminal stage age-matched CV mice**

AIF, Endo G, VDAC1 and cyt c localize to the mitochondria, but are not detected in cytosolic fractions. 30µg of each mitochondrial and cytosolic fraction from normal CV brains (n=3), and 3µg of K562 and 3T3 positive control cell lysates (Abcam), were loaded to each gel. Samples were prepared and analyzed for VDAC1 as described (Sections 2.3.5., 2.3.6. and 2.3.8.). One blot was used for this analysis, which was stripped and re-probed (Section 2.3.9.) for AIF, Endo G and cyt c respectively. Western blots were exposed for periods of 1, 5 and 10 mins. Blots shown here were obtained following 5mins exposure.

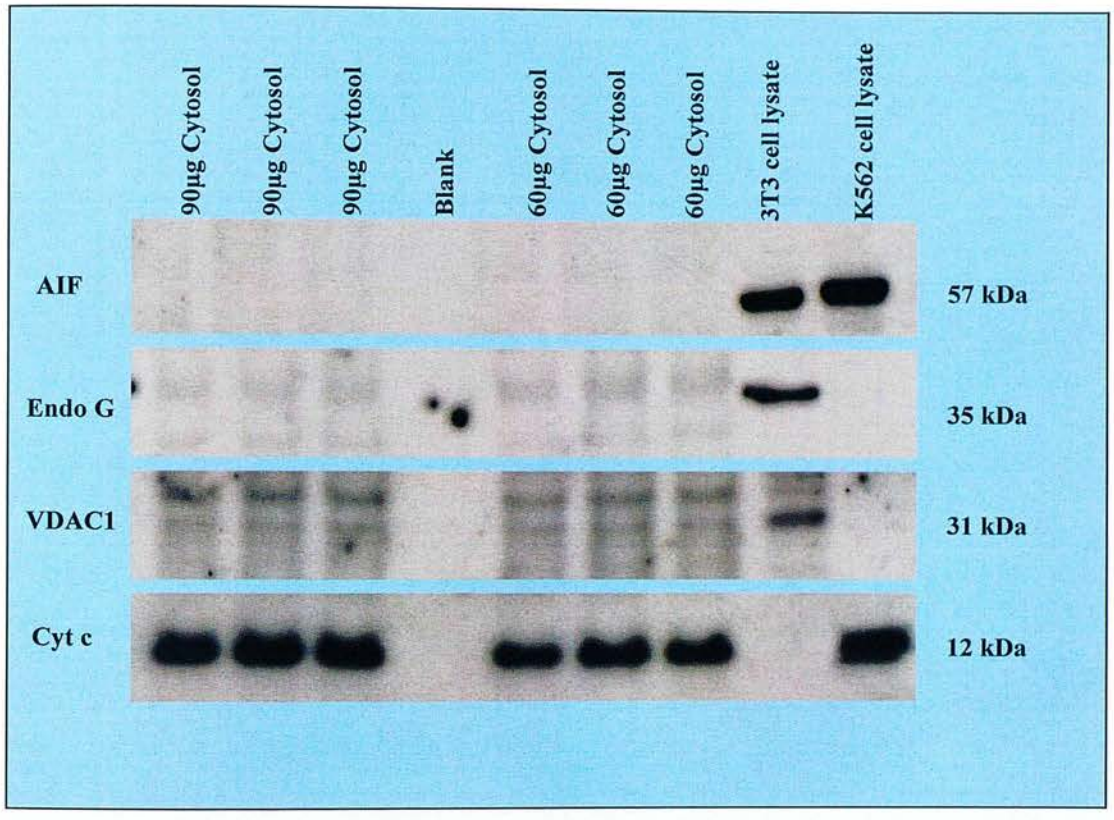

Figure 3.3 **Sub-cellular location of apoptosis-related proteins isolated from whole brain homogenates from normal brain injected terminal stage age-matched CV mice**

AIF, Endo G and VDAC1 are not detected in cytosolic fractions. Cyt c was detected in both 60µg and 90µg cytosolic fractions from the normal CV brains. 60µg and 90µg of each cytosolic fraction from normal CV brains (n=3), and 3µg of K562 and 3T3 positive control cell lysates (Abcam), were loaded to each gel. Samples were prepared and analyzed for VDAC1 as described (Sections 2.3.5., 2.3.6. and 2.3.8.). One blot was used for this analysis, which was stripped and re-probed (Section 2.3.9.) for AIF, Endo G and cyt c respectively. Western blots were exposed for periods of 1, 5 and 10 mins. Blots shown here were obtained following 5 mins exposure. Some unspecific bands are visible following probing with the Endo G and VDAC polyclonal antibodies.

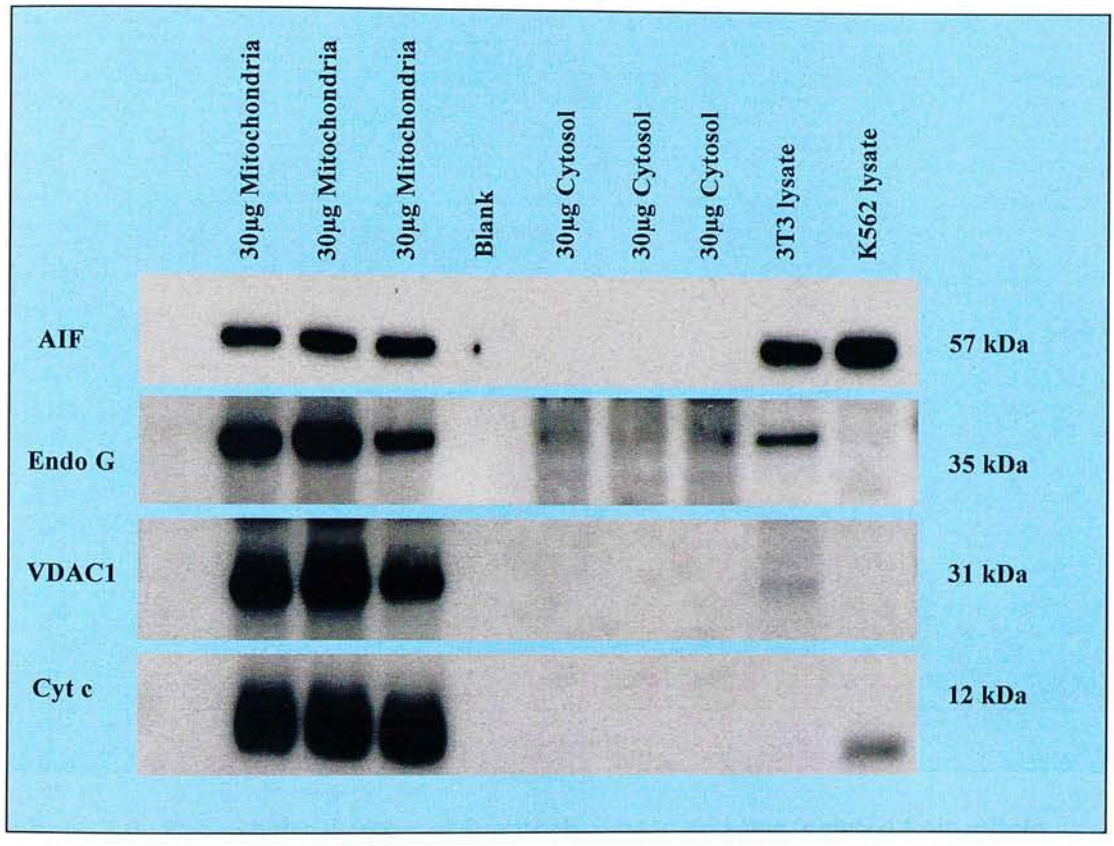

Figure 3.4 **Sub-cellular location of apoptosis-related proteins isolated from whole brain homogenates from ME7 injected terminal stage CV mice**

AIF, Endo G, VDAC1 and cyt c localize to the mitochondria, but are not detected in cytosolic fractions. 30µg of each mitochondrial and cytosolic fraction from ME7/CV brains (n=3), and 3µg of K562 and 3T3 positive control cell lysates (Abcam), were loaded to each gel. Samples were prepared and analyzed for VDAC1 as described (Sections 2.3.5., 2.3.6. and 2.3.8.). One blot was used for this analysis, which was stripped and re-probed (Section 2.3.9.) for AIF, Endo G and cyt c respectively. Western blots were exposed for periods of 1, 5 and 10 mins. Blots shown here were obtained following 5 mins exposure. Some unspecific bands are visible following probing with the Endo G and VDAC polyclonal antibodies.

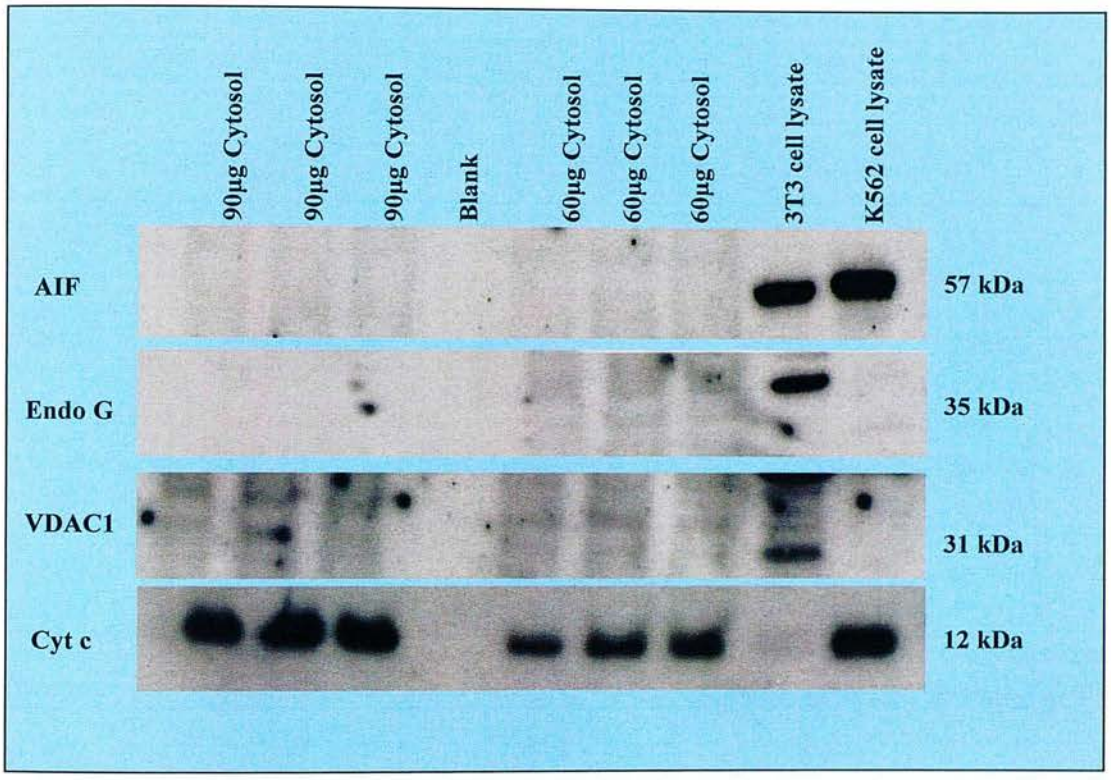

Figure 3.5 **Sub-cellular location of apoptosis-related proteins isolated from whole brain homogenates from ME7 injected terminal stage CV mice**

AIF, Endo G and VDAC1 are not detected in cytosolic fractions. Cyt c was detected in both 60µg and 90µg cytosolic fractions from the ME7/CV brains. 60µg and 90µg of each cytosolic fraction from ME7/CV brains (n=3), and 3µg of K562 and 3T3 positive control cell lysates (Abcam), were loaded to each gel. Samples were prepared and analyzed for VDAC1 as described (Sections 2.3.5., 2.3.6. and 2.3.8.). Two blots were used for analysis, which were then stripped and re-probed (Section 2.3.9.) for AIF, Endo G and cyt c respectively. Western blots were exposed for periods of 1, 5 and 10 mins. Blots shown here were obtained following 5 mins exposure. Some unspecific bands are visible following probing with the Endo G and VDAC polyclonal antibodies.

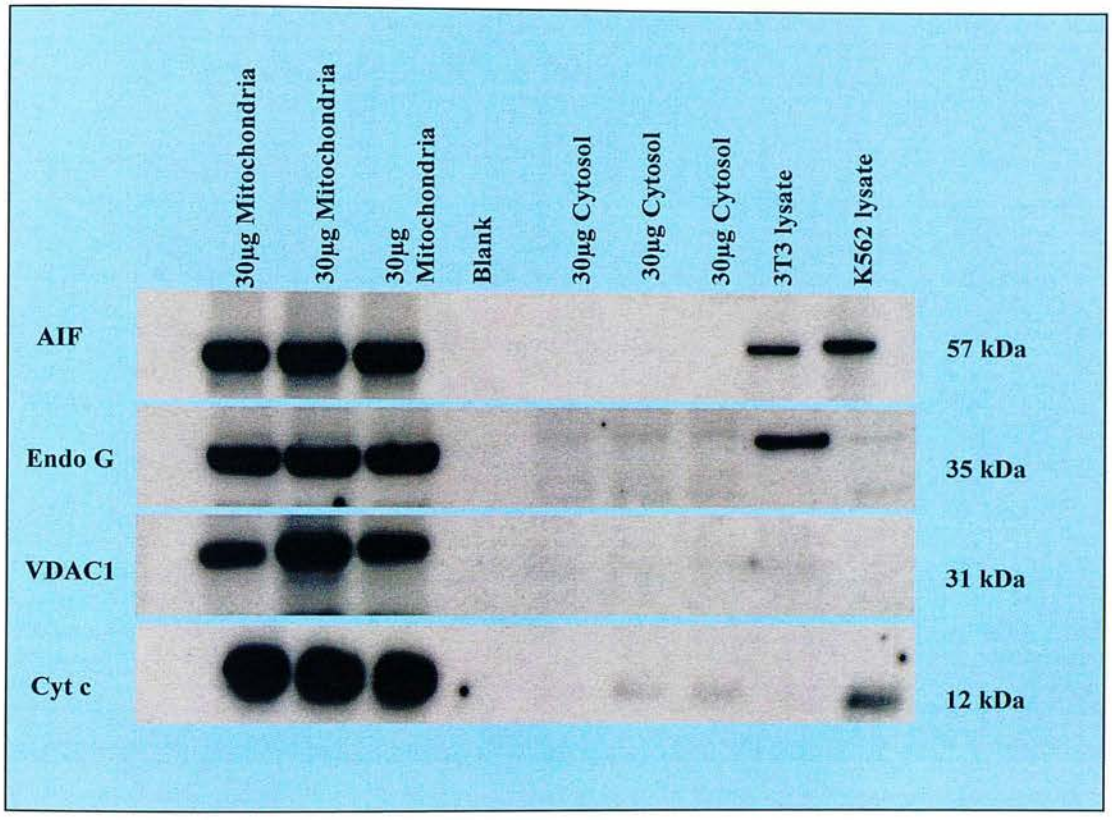

Figure 3.6 **Sub-cellular location of apoptosis-related proteins isolated from whole brain homogenates from normal brain injected terminal stage age-matched VM mice**

AIF, Endo G and VDAC1 localize to the mitochondria, but are not detected in cytosolic fractions. Cyt c is detected in the mitochondrial fractions, and low levels are present in cytosolic fractions. 30µg of each mitochondrial and cytosolic fraction from normal VM brains (n=3), and 3µg of K562 and 3T3 positive control cell lysates (Abcam), were loaded to each gel. Samples were prepared and analyzed for VDAC1 as described (Sections 2.3.5., 2.3.6. and 2.3.8.). Two blots were used for this analysis, which were then stripped and re-probed (Section 2.3.9.) for AIF, Endo G and cyt c respectively. Western blots were exposed for periods of 1, 5 and 10 mins. Blots shown here were obtained following 5 mins exposure.

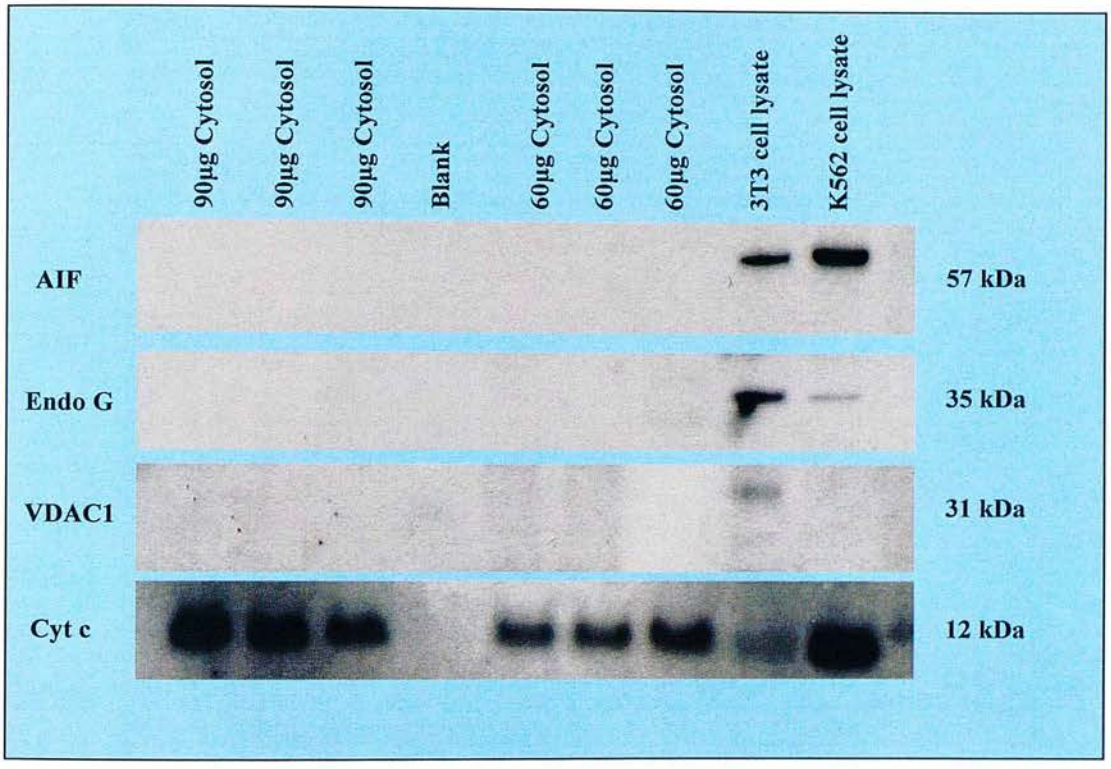

Figure 3.7 **Sub-cellular location of apoptosis-related proteins isolated from whole brain homogenates from normal brain injected terminal stage age-matched VM mice**

AIF, Endo G and VDAC1 are not detected in cytosolic fractions. Cyt c was detected at both 60µg and 90µg cytosolic fractions from the normal VM brains. 60µg and 90µg of each cytosolic fraction from normal VM brains (n=3), and 3µg of K562 and 3T3 positive control cell lysates (Abcam), were loaded to each gel. Samples were prepared and analyzed for VDAC1 as described (Sections 2.3.5., 2.3.6. and 2.3.8.). Western blots were exposed for periods of 1, 5 and 10 mins. One blot was used for this analysis, which was then stripped and re-probed (Section 2.3.9.) for AIF, Endo G and cyt c respectively. Western blots were exposed for periods of 1, 5 and 10 mins. Blots shown here were obtained following 5 mins exposure.

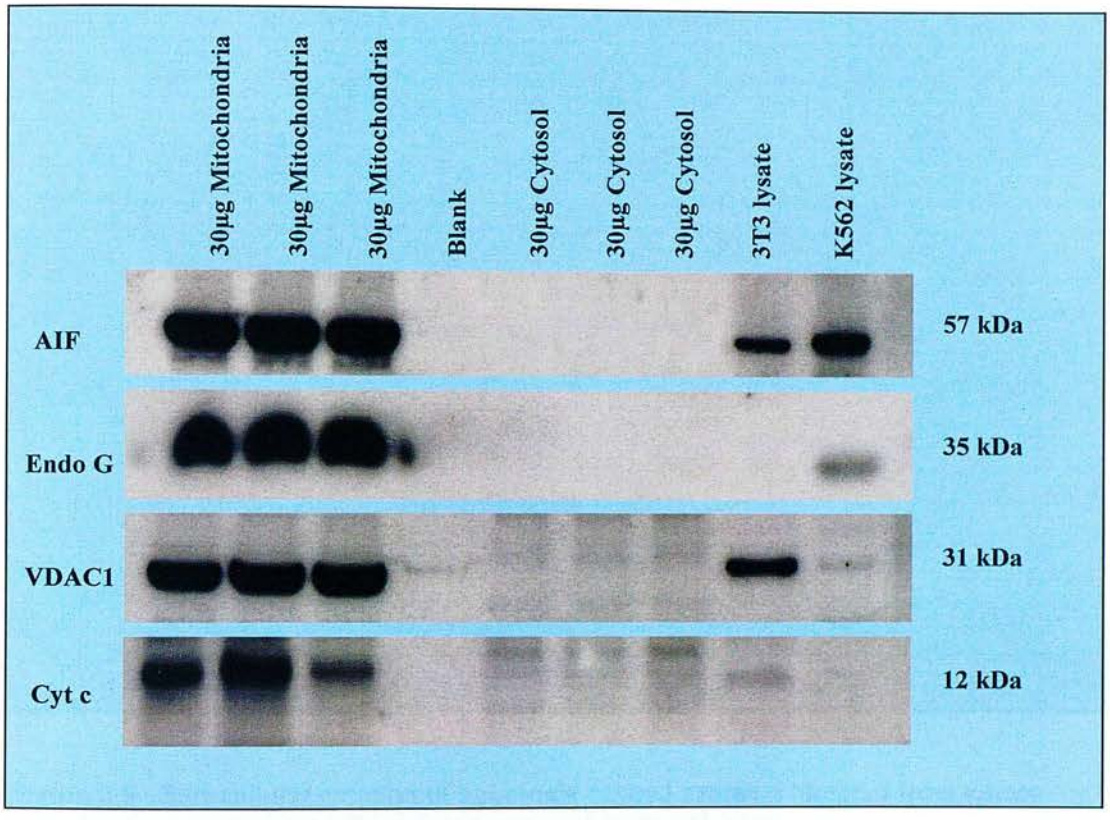

Figure 3.8 **Sub-cellular location of apoptosis-related proteins isolated from whole brain homogenates from 87V injected terminal stage VM mice**

AIF, Endo G, VDAC1 and cyt c localize to the mitochondria, but are not detected in cytosolic fractions. 30µg of each mitochondrial and cytosolic fraction from 87V/VM brains (n=3), and 3µg of K562 and 3T3 positive control cell lysates (Abcam), were loaded to each gel. Samples were prepared and analyzed for VDAC1 as described (Sections 2.3.5., 2.3.6. and 2.3.8.). Two blots were used for this analysis, which were then stripped and re-probed (Section 2.3.9.) for AIF, Endo G and cyt c respectively. Western blots were exposed for periods of 1, 5 and 10 mins. Blots shown here were obtained following 5 mins exposure. Some unspecific bands are visible following probing with the VDAC polyclonal antibody.

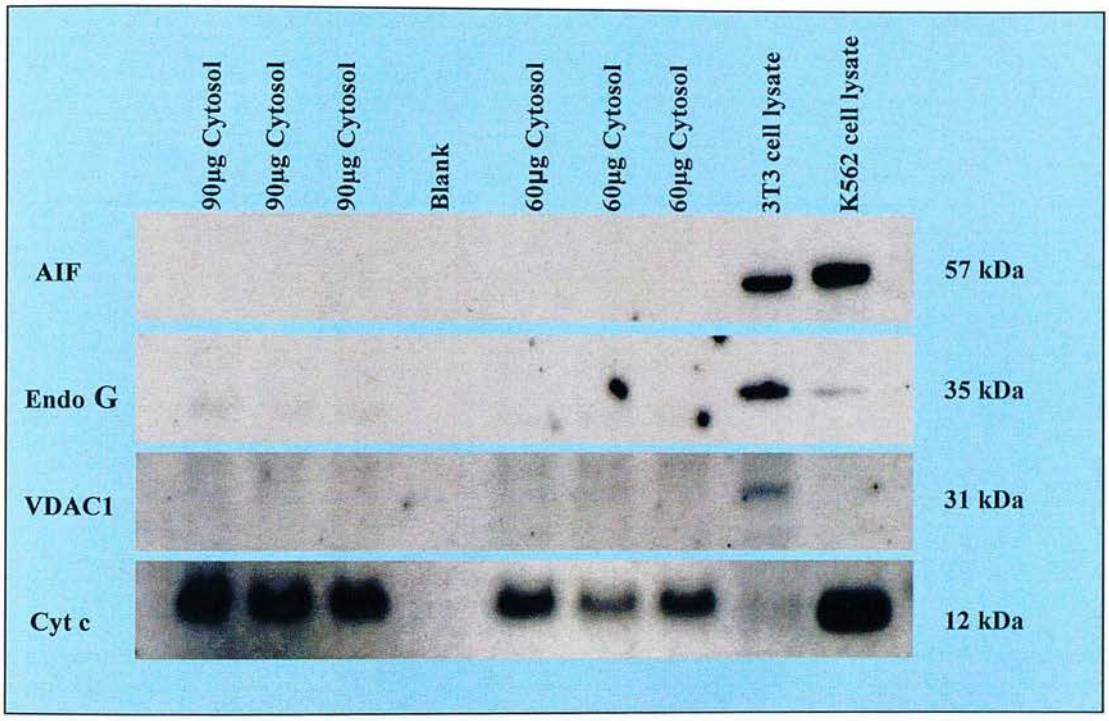

Figure 3.9 **Sub-cellular location of apoptosis-related proteins isolated from whole brain homogenates from 87V injected terminal stage VM mice**

AIF, Endo G and VDAC1 are not detected in cytosolic fractions. Cyt c was detected in both 60µg and 90µg cytosolic fractions from the 87V/VM brains. 60µg and 90µg of each cytosolic fraction from 87V/VM brains (n=3), and 3µg of K562 and 3T3 positive control cell lysates (Abcam), were loaded to each gel. Samples were prepared and analyzed for VDAC1 as described (Sections 2.3.5., 2.3.6. and 2.3.8.). One blot was used for this analysis, which was then stripped and re-probed (Section 2.3.9.) for AIF, Endo G and cyt c respectively. Western blots were exposed for periods of 1, 5 and 10 mins. Blots shown here were obtained following 5 mins exposure.

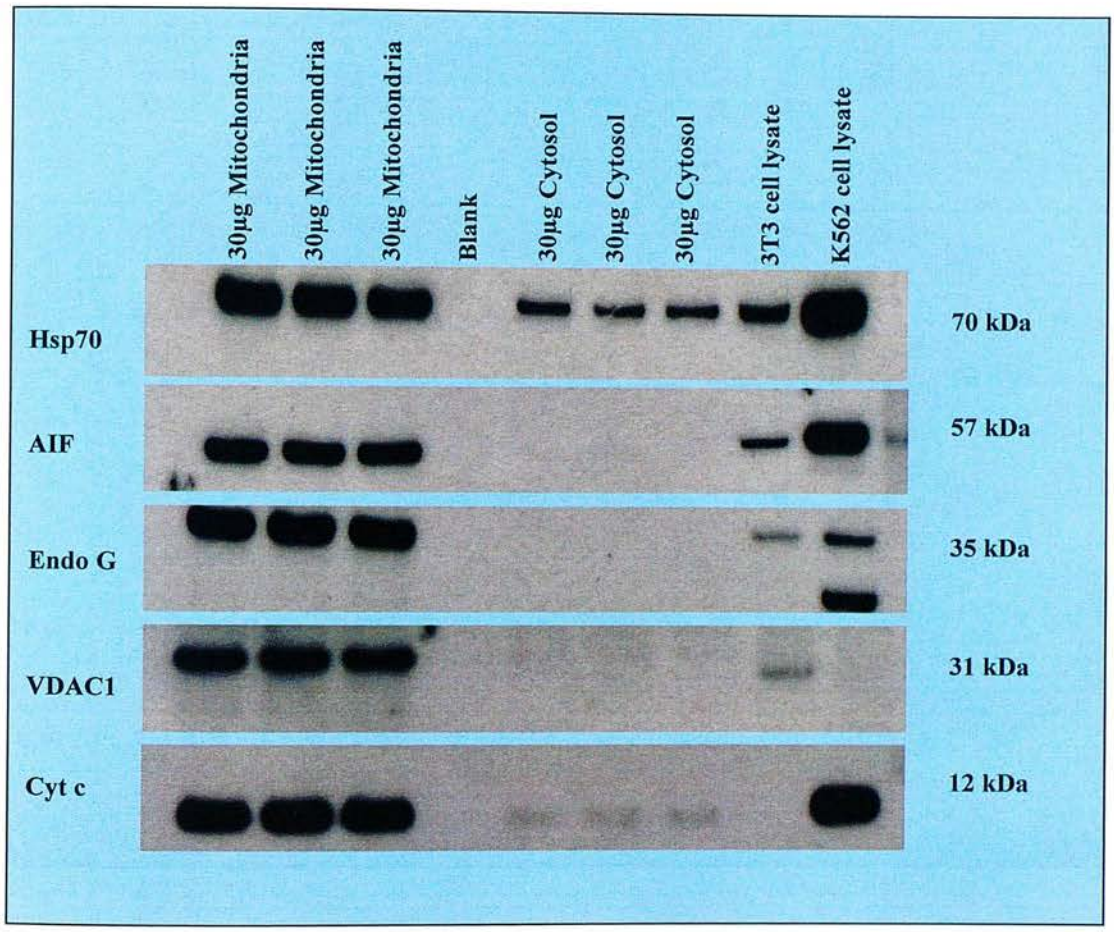

Figure 3.10 **Sub-cellular location of apoptosis-related proteins isolated from the micro-dissected hippocampus and thalamus from normal brain injected terminal stage age-matched CV mice**

AIF, Endo G and VDAC1 localize to the mitochondria, but are not detected in cytosolic fractions. Hsp70 is present in both the mitochondrial and cytosolic fractions. Cyt c localizes to the mitochondria, and low levels are present in cytosolic fractions. 30µg of each mitochondrial and cytosolic fraction from normal CV brains (n=3), and 3µg of K562 and 3T3 positive control cell lysates (Abcam), were loaded to each gel. Samples were prepared and analyzed for VDAC1 as described (Sections 2.3.5., 2.3.6. and 2.3.8.). Two blots were used for this analysis, which were then stripped and re-probed (Section 2.3.9.) for AIF, Endo G, cyt c and Hsp70 respectively. Western blots were exposed for periods of 1, 5 and 10 mins. Blots shown here were obtained following 5 mins exposure.

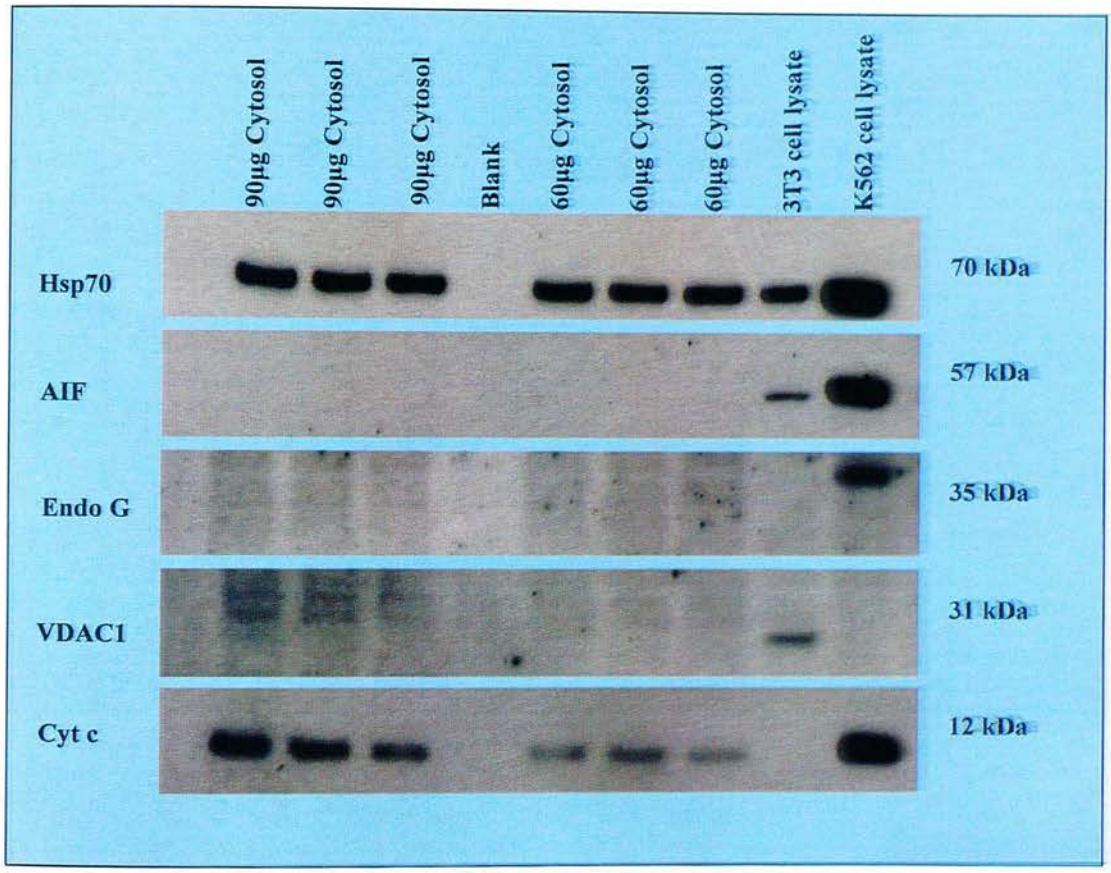

Figure 3.11 **Sub-cellular location of apoptosis-related proteins isolated from the micro-dissected hippocampus and thalamus from normal brain injected terminal stage age-matched CV mice**

AIF, Endo G and VDAC1 are not detected in cytosolic fractions. Hsp70 and cyt c were detected in both 60µg and 90µg cytosolic fractions from the normal CV brains. 60µg and 90µg of each cytosolic fraction from normal CV brains (n=3), and 3µg of K562 and 3T3 positive control cell lysates (Abcam), were loaded to each gel. Samples were prepared and analyzed for VDAC1 as described (Sections 2.3.5., 2.3.6. and 2.3.8.). Two blots were used for this analysis, which were then stripped and re-probed (Section 2.3.9.) for AIF, Endo G, cyt c and Hsp70 respectively. Western blots were exposed for periods of 1, 5 and 10 mins. Blots shown here were obtained following 5 mins exposure. Some unspecific bands are visible following probing with the VDAC and Endo G polyclonal antibodies.

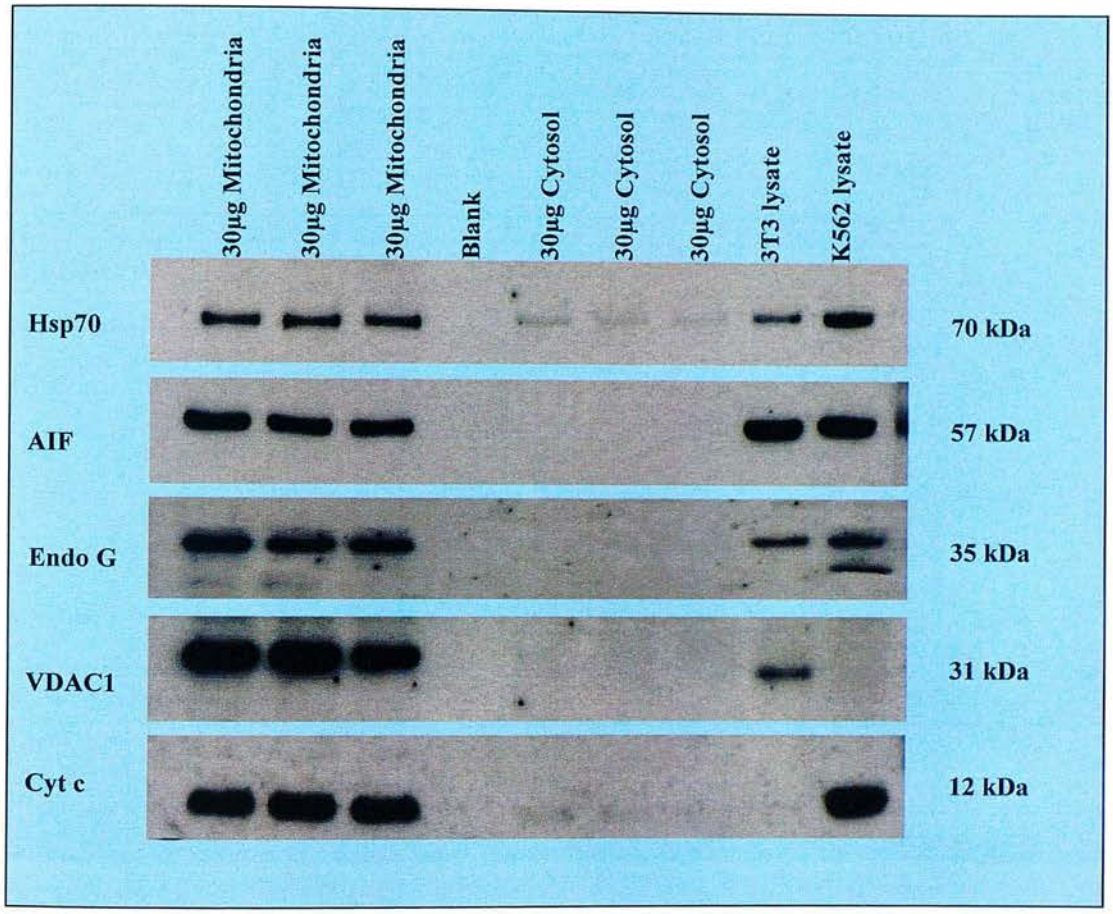

Figure 3.12 **Sub-cellular location of apoptosis-related proteins isolated from the micro-dissected hippocampus and thalamus from ME7 injected terminal stage CV mice**

AIF, Endo G and VDAC1 localize to the mitochondria, but are not detected in cytosolic fractions. Hsp70 is present in both the mitochondrial and cytosolic fractions. Cyt c localizes to the mitochondria, and low levels are present in cytosolic fractions. 30µg of each mitochondrial and cytosolic fraction from ME7/CV brains (n=3), and 3µg of K562 and 3T3 positive control cell lysates (Abcam), were loaded to each gel. Samples were prepared and analyzed for VDAC1 as described (Sections 2.3.5., 2.3.6. and 2.3.8.). Two blots were used for this analysis, which were then stripped and re-probed (Section 2.3.9.) for AIF, Endo G, cyt c and Hsp70 respectively. Western blots were exposed for periods of 1, 5 and 10 mins. Blots shown here were obtained following 5 mins exposure.

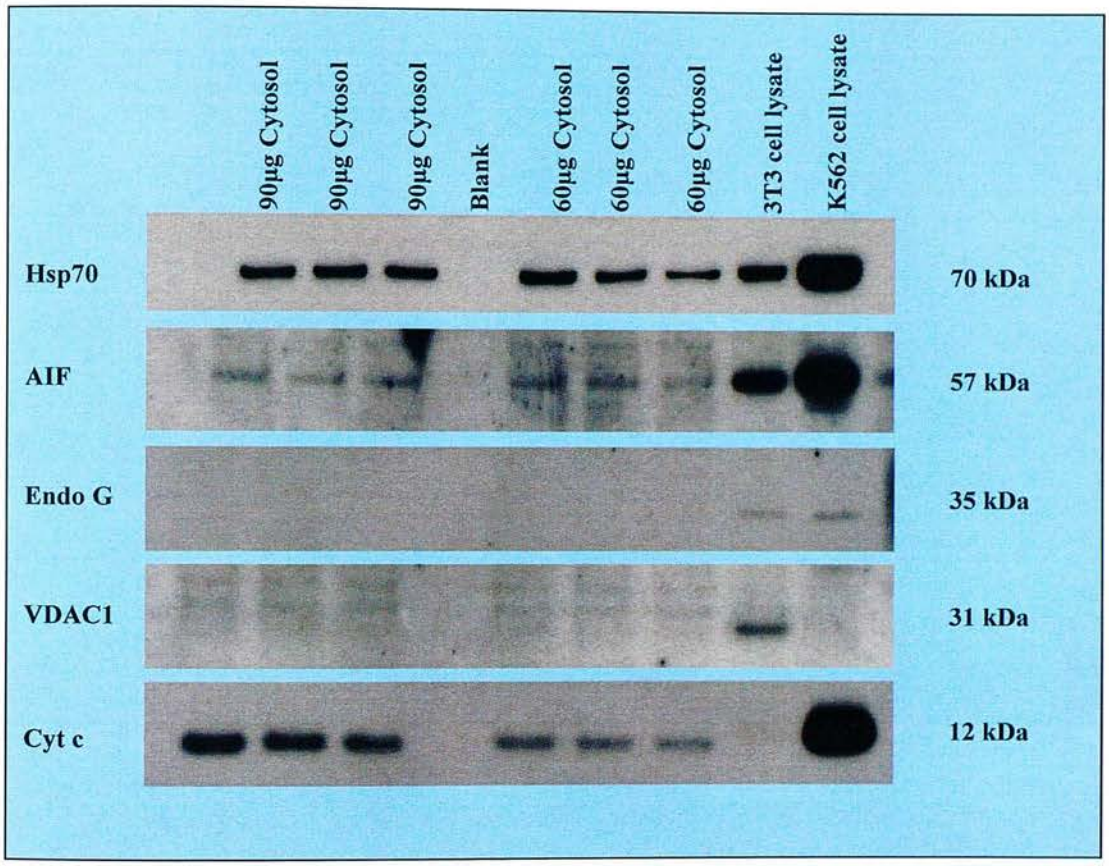

Figure 3.13 **Apoptosis-related AIF and cyt c translocate to the cytosol in samples prepared from the micro-dissected hippocampus and thalamus from ME7 injected terminal stage CV mice**

AIF, Hsp70 and cyt c were detected in both 60µg and 90µg cytosolic fractions from the ME7/CV brains. The presence of AIF and cyt c in the cytosolic fractions represents translocation from the mitochondria as a consequence of mitochondrial malfunction. Endo G and VDAC1 are not detected in cytosolic fractions. 60µg and 90µg of each cytosolic fraction from ME7/CV brains (n=3), and 3µg of K562 and 3T3 positive control cell lysates (Abcam), were loaded to each gel. Samples were prepared and analyzed for VDAC1 as described (Sections 2.3.5., 2.3.6. and 2.3.8.). Two blots were used for this analysis, which were then stripped and re-probed (Section 2.3.9.) for AIF, Endo G, cyt c and Hsp70 respectively. Western blots were exposed for periods of 1, 5 and 10 mins. Blots shown here were obtained following 5 mins exposure, except that for AIF which was exposed for 10 mins. Some unspecific bands are visible following probing with the VDAC polyclonal antibody.

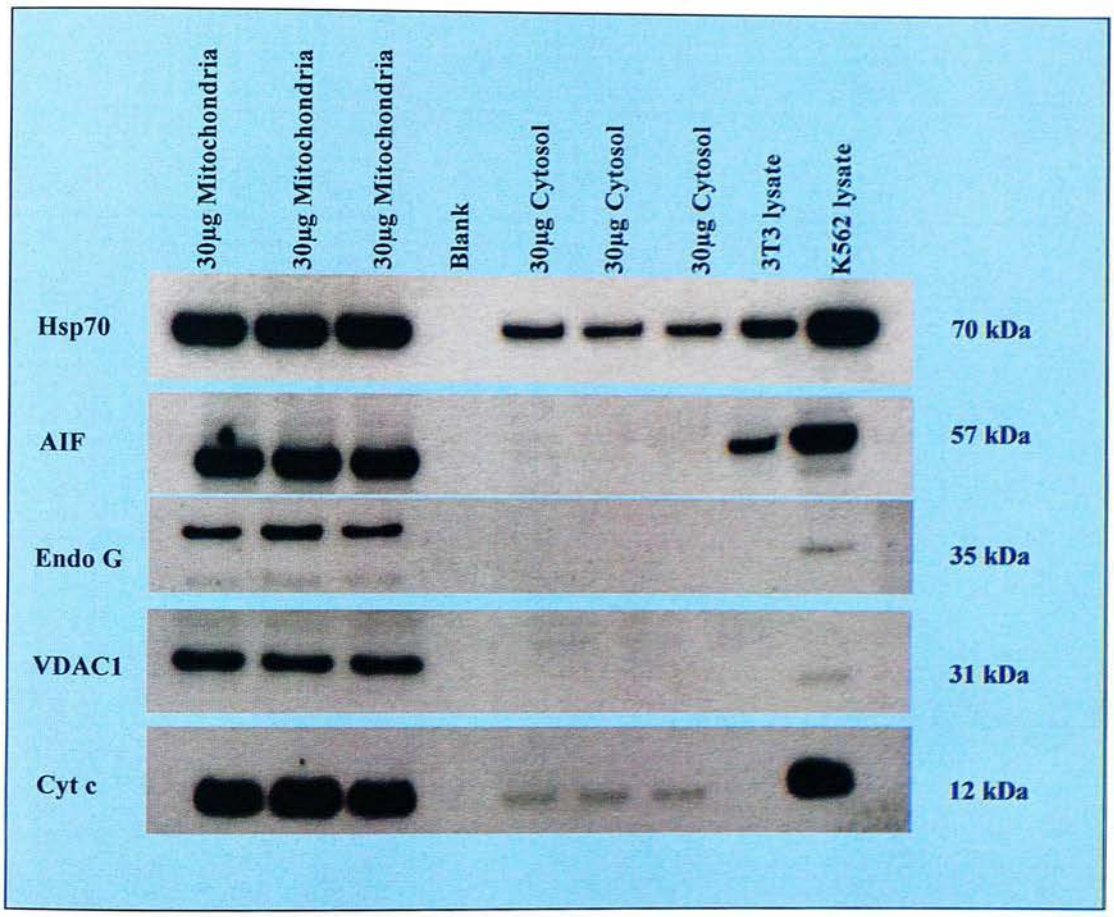

Figure 3.14 **Sub-cellular location of apoptosis-related proteins isolated from the micro-dissected hippocampus and thalamus from normal brain injected terminal stage age-matched VM mice**

AIF, Endo G and VDAC1 localize to the mitochondria, but are not detected in cytosolic fractions. Hsp70 is present in both the mitochondrial and cytosolic fractions. Cyt c localizes to the mitochondria, and low levels are present in cytosolic fractions. 30µg of each mitochondrial and cytosolic fraction from normal VM brains (n=3), and 3µg of K562 and 3T3 positive control cell lysates (Abcam), were loaded to each gel. Samples were prepared and analyzed for VDAC1 as described (Sections 2.3.5., 2.3.6. and 2.3.8.). Two blots were used for this analysis, which were then stripped and re-probed (Section 2.3.9.) for AIF, Endo G, cyt c and Hsp70 respectively. Western blots were exposed for periods of 1, 5 and 10 mins. Blots shown here were obtained following 5 mins exposure.

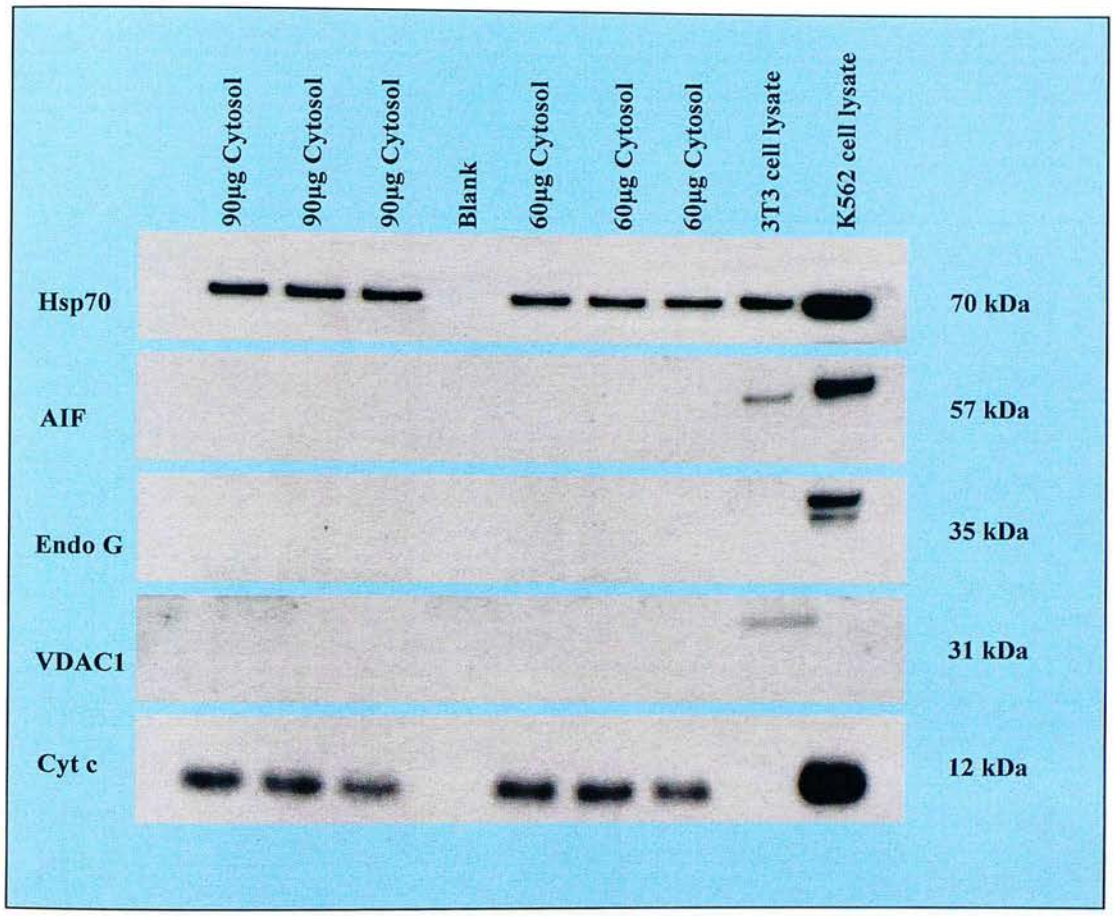

Figure 3.15 **Sub-cellular location of apoptosis-related proteins isolated from the micro-dissected hippocampus and thalamus from normal brain injected terminal stage age-matched VM mice**

AIF, Endo G and VDAC1 are not detected in cytosolic fractions. Hsp70 and cyt c were detected in both 60µg and 90µg cytosolic fractions from the normal VM brains. 60µg and 90µg of each cytosolic fraction from normal VM brains (n=3), and 3µg of K562 and 3T3 positive control cell lysates (Abcam), were loaded to each gel. Samples were prepared and analyzed for VDAC1 as described (Sections 2.3.5., 2.3.6. and 2.3.8.). Two blots were used for this analysis, which were then stripped and re-probed (Section 2.3.9.) for AIF, Endo G, cyt c and Hsp70 respectively. Western blots were exposed for periods of 1, 5 and 10 mins. Blots shown here were obtained following 5 mins exposure.

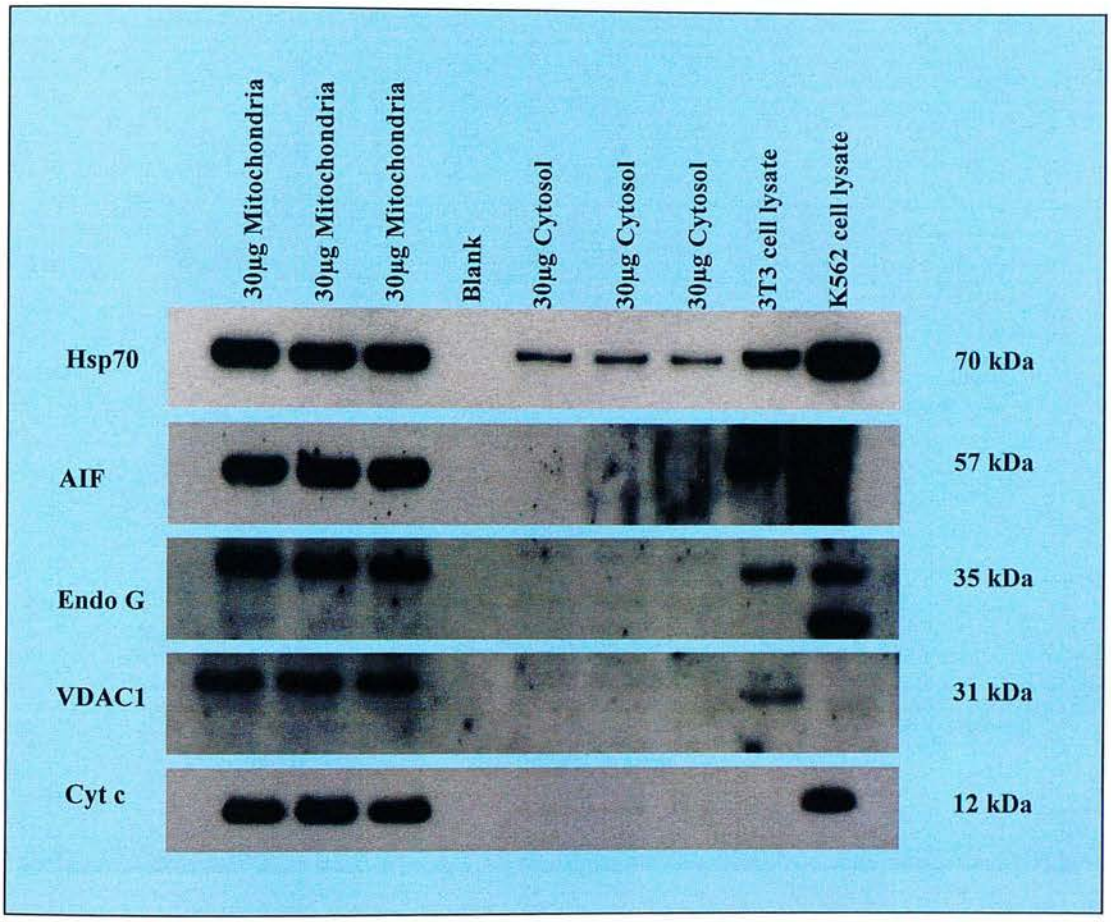

Figure 3.16 **Sub-cellular location of apoptosis-related proteins isolated from the micro-dissected hippocampus and thalamus from 87V injected terminal stage VM mice**

AIF, Endo G and VDAC1 localize to the mitochondria, but are not detected in cytosolic fractions. Hsp70 is present in both the mitochondrial and cytosolic fractions. Cyt c localizes to the mitochondria, and low levels are present in cytosolic fractions. 30µg of each mitochondrial and cytosolic fraction from 87V/VM brains (n=3), and 3µg of K562 and 3T3 positive control cell lysates (Abcam), were loaded to each gel. Samples were prepared and analyzed for VDAC1 as described (Sections 2.3.5., 2.3.6. and 2.3.8.). Two blots were used for this analysis, which were then stripped and re-probed (Section 2.3.9.) for AIF, Endo G, cyt c and Hsp70 respectively. Western blots were exposed for periods of 1, 5 and 10 mins. Blots shown here were obtained following 5 mins exposure. Some unspecific bands are visible following probing with the Endo G polyclonal antibody.

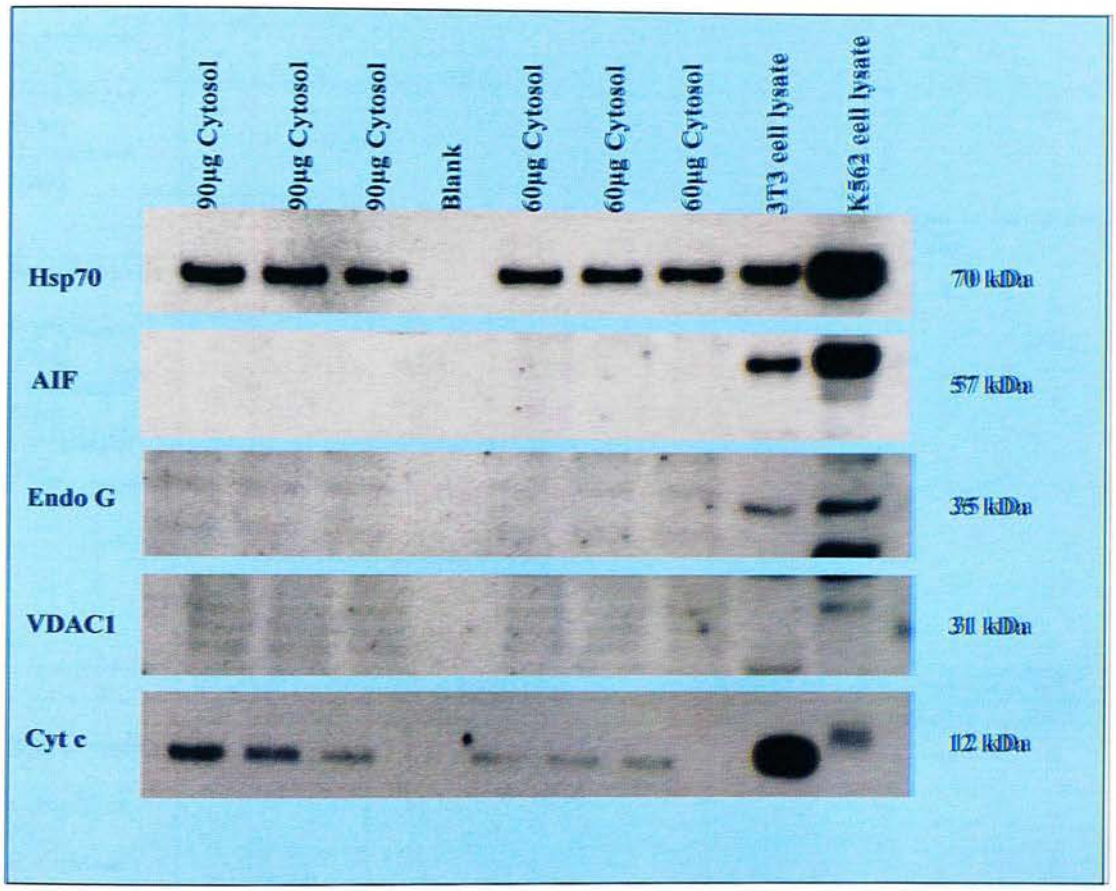

Figure 3.17 **Sub-cellular location of apoptosis-related proteins isolated from the micro-dissected hippocampus and thalamus from 87V injected terminal stage VM mice**

AIF, Endo G and VDAC1 are not detected in cytosolic fractions. Hsp70 and cyt c were detected in both 60µg and 90µg cytosolic fractions from the 87V/VM brains. 60µg and 90µg of each cytosolic fraction from 87V/VM brains (n=3), and 3µg of K562 and 3T3 positive control cell lysates (Abcam), were loaded to each gel. Samples were prepared and analyzed for VDAC1 as described (Sections 2.3.5., 2.3.6. and 2.3.8.). Two blots were used for this analysis, which were then stripped and re-probed (Section 2.3.9.) for AIF, Endo G, cyt c and Hsp70 respectively. Western blots were exposed for periods of 1, 5 and 10 mins. Blots shown here were obtained following 5 mins exposure. Some unspecific bands are visible following probing with the VDAC and Endo G polyclonal antibodies.

A

	ME7/CV (whole brain samples)					NB/CV (whole brain samples)				
	AIF	EndoG	VDAC1	CytC		AIF	EndoG	VDAC1	CytC	
Mitochondria	+	+	+	+		+	+	+	+	
Cytoplasm 30µg	-	-	-	-		-	-	-	-	
Cytoplasm 60µg	-	-	-	+		-	-	-	+	
Cytoplasm 90µg	-	-	-	+		-	-	-	+	
	ME7/CV (subcellular brain samples)					NB/CV (subcellular brain samples)				
	AIF	EndoG	VDAC1	CytC	Hsp70	AIF	EndoG	VDAC1	CytC	Hsp70
Mitochondria	+	+	+	+	+	+	+	+	+	+
Cytoplasm 30µg	-	-	-	-	+/-	-	-	-	+/-	+
Cytoplasm 60µg	+	-	-	+	+	-	-	-	+	+
Cytoplasm 90µg	+	-	-	+	+	-	-	-	+	+

B

	87V/VM (whole brain samples)					NB/VM (whole brain samples)				
	AIF	EndoG	VDAC1	CytC		AIF	EndoG	VDAC1	CytC	
Mitochondria	+	+	+	+		+	+	+	+	
Cytoplasm 30µg	-	-	-	-		-	-	-	-	
Cytoplasm 60µg	-	-	-	+		-	-	-	+	
Cytoplasm 90µg	-	-	-	+		-	-	-	+	
	87V/VM (subcellular brain samples)					NB/VM (subcellular brain samples)				
	AIF	EndoG	VDAC1	CytC	Hsp70	AIF	EndoG	VDAC1	CytC	Hsp70
Mitochondria	+	+	+	+	+	+	+	+	+	+
Cytoplasm 30µg	-	-	-	-	+	-	-	-	+/-	+
Cytoplasm 60µg	-	-	-	+	+	-	-	-	+	+
Cytoplasm 90µg	-	-	-	+	+	-	-	-	+	+

Table 3.1 **Summary of immunoreactivity of samples analysed by Westerb blot from ME7/CV and 87V/VM and age-matched control animals at terminal stages of disease**

Mitochondrial and cytosolic samples prepared from whole brain and subcellularly fractionated brain samples and analysed by Western blot in Figures 3.2 to 3.17 are summarised in the table above. Positive immunoreactivity is denoted with +, whereas those samples with no immunoreactivity are shown with -. Samples which were weakly immunoreactive are illustrated with +/-.

3.2.6 Analysis of uninfected 70dpi animals for cytochrome c

The detection of cyt c in normal and scrapie-infected brain samples, from both the sucrose-gradient and micro-dissected procedures, required clarification. Samples from 70dpi normal-brain injected mice were analysed for cyt c to determine if this detection was as a result of sample preparation or through age-related mechanisms.

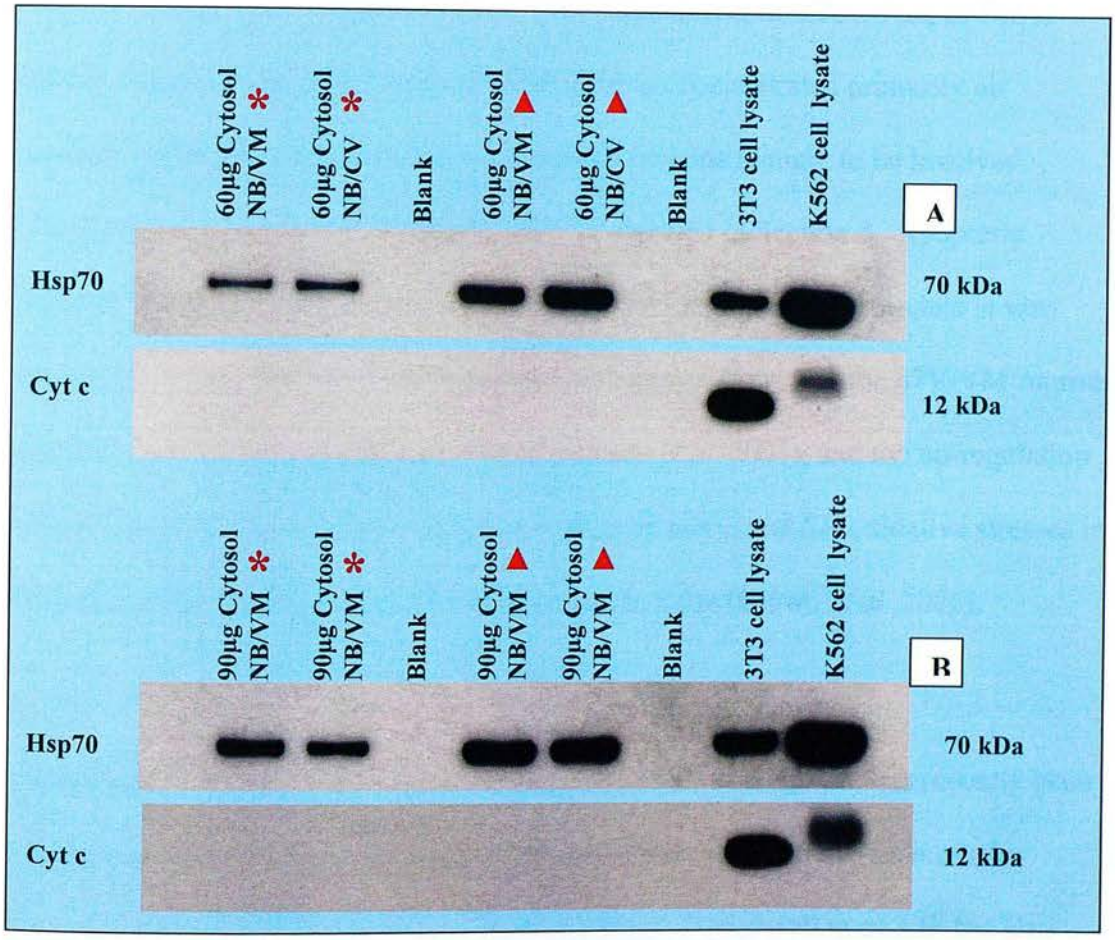

Figure 3.19 **Cytochrome c is not present in the cytosol in young (70dpi) uninfected control mouse brains**

Cyt c was not detected in the cytosol of younger mice, although the presence of Hsp70 verifies that protein was present in each of the tested samples. Cytosolic samples were prepared from 70dpi NB/CV and NB/VM mice (* =sucrose gradient fractionated, ▲=micro-dissected and fractionated). 60µg and 90µg of each cytosolic fraction, and 3µg of K562 and 3T3 positive control cell lysates (Abcam), were loaded to each gel. Samples were prepared and analyzed for cyt c as described (Sections 2.3.5., 2.3.6. and 2.3.8.). One blot was used for this analysis, which was then stripped and re-probed (Section 2.3.9.) for Hsp70 respectively. Western blots were exposed for periods of 1, 5 and 10 mins. Blots shown here were obtained following 10 mins exposure.

3.3 Discussion

Apoptosis is thought to be an important mechanism of neuronal cell death in TSE infections based upon the detection of cellular and nuclear shrinkage, condensation and fragmentation of nuclear chromatin by electron microscopy and biochemically by endonuclease-mediated internucleosomal fragmentation of DNA into multiple oligosomal sub-units of 180 bp (Giese *et al.* 1995; Lucassen *et al.* 1995; Fraser *et al.* 1996; Dorandeu *et al.* 1998; Gray *et al.* 1999; Jamieson *et al.* 2001; Puig & Ferrer 2001). Apoptosis research within the TSE field has concentrated primarily on extrinsic pathways, and the numerous apoptotic proteins thought to be involved following exposure to PrP peptides *in vitro* are detailed in Section 4. Apoptotic proteins documented for the ME7/CV and 87V/VM murine scrapie models *in vivo* include the up-regulation of Fas ligand and activated caspase 3 in the 87V/VM murine scrapie model by ICC and Western blot (Jamieson *et al.* 2001), and the up-regulation of several apoptotic proteins in response to mitochondrial and ER oxidative stresses in the ME7/CV model by Affymetrix micro-array analysis (Brown *et al.* 2005).

Apoptosis mediated by the caspase-independent IMM protein, AIF, has recently been reported in rodent models of transient-global ischemia and hypoxia-ischemia in neonatal animals (Cao *et al.* 2003; Zhu *et al.* 2003). Translocation of AIF has also been detected in rodent models of traumatic brain injury (such as middle cerebral artery occlusion) (Ferrer *et al.* 2003) and in the MPTP model of spontaneous Parkinson's disease (Wang *et al.* 2003). Caspase-independent apoptosis represents a novel research area of the mechanisms of neuronal cell death in these diseases. I therefore concentrated the research of this thesis on intrinsic mitochondrial apoptotic

pathways, in an effort to identify novel apoptotic markers in the ME7/CV and 87V/VM murine scrapie models.

3.3.1 Translocation of apoptosis-related proteins is not evident when analysing whole brain samples

Samples prepared by the whole brain sucrose-gradient fractionation technique were prepared to analyse IMM protein translocation to the cytosol. Three ME7/CV and 87V/VM, and three respective age-match normal brain injected control animals were sacrificed at the terminal stages of disease. Analysis of cytosolic samples containing 30, 60 and 90μg (and mitochondrial samples containing 30μg) total protein were analysed for AIF, Endo G and cyt c by Western blot. Cyt c was detected in all of the cytosolic samples, and this is discussed in Section 3.3.3. However, AIF and Endo G were not detected in any of the cytosolic samples created by the whole brain fractionation procedure (Figures 3.2-3.9). The lack of detection of AIF and Endo G in the cytosolic samples could indicate that these IMM proteins are not involved in apoptosis in these murine scrapie models. However, if infected cell populations do not display relatively large scale synchronous apoptosis it would be extremely difficult to detect single apoptotic cells *in vivo*. Additionally, the rapid clearance of cells with abnormal neuronal functions by apoptosis would further hinder their detection.

Certain neuronal subsets are more sensitive to murine scrapie pathology than others. This is particularly evident in the murine hippocampus, where the CA1 pyramidal neurons are lost during ME7/CV infections (Scott & Fraser 1984) and the CA2

pyramidal cells are damaged during 87V/VM infections (Belichenko *et al.* 2000; Jeffrey *et al.* 2000). Murine scrapie brain samples created by the micro-dissection of such pathologically targeted areas, notably the hippocampus and thalamus for these models, should contain a higher proportion of apoptotic to normal cells in comparison to the samples prepared from whole brain homogenates. The recently published micro-dissection technique, developed by the CNS pathogenesis group at IAH Edinburgh, has proved to be a valuable technique for the detection of PrP^{sc} (Barr *et al.* 2004) and also for the *in vivo* detection of apoptosis in the CA2 neurons of 87V/VM murine scrapie brains (Jamieson *et al.* 2001a; Jamieson *et al.* 2001b). Based on this evidence, micro-dissected areas were created to maximise the likelihood of detecting apoptosis-related proteins in this research. As before three terminal animals from each of the ME7/CV and 87V/VM, and NB inoculated aged-matched control animals were analysed. After failed initial attempts to develop a scaled down version of the whole brain sucrose gradient technique, a commercially available sub-cellular fractionation kit (Calbiochem) was purchased and optimised for the analysis of frozen mouse brain samples. Mitochondria (containing 30μg) and cytosolic fractions containing 30, 60 and 90μg total protein were analysed as before by Western blot (Figures 3.10-3.17). AIF was clearly detected in the cytosolic samples (60 and 90μg total protein) created from the ME7/CV but not NB/CV control animals. The relevance of this translocation to neuronal apoptosis in TSE infections will be discussed in Section 3.3.2. In summary, AIF translocation was detected in the micro-dissected brain samples, but not in the samples prepared from whole brain homogenates. Consequently, the micro-dissection of scrapie-infected brain areas has proven to be a useful research technique for the *in vivo* detection of apoptosis-related proteins in neurodegenerative disease models.

3.3.2 Translocation of apoptosis inducing factor to the cytosol is specific to the ME7/CV murine scrapie model

The analysis of whole brain fractionated and micro-dissected (hippocampal and thalamus) samples revealed that the micro-dissection procedure was much more sensitive for the *in vivo* detection of apoptosis-related proteins (Section 3.3.1). AIF and Endo G translocation from the IMM to the cytosol was never detected in samples prepared by the whole brain sucrose gradient fractionation technique (Figures 3.2-3.9). Furthermore, Endo G was not detected in the micro-dissected cytosolic fractions created from the ME7/CV and 87V/VM scrapie models (Figures 3.10-3.17), implying that this protein is not released into the cytosol in response to these murine scrapie infections. However, low amounts of AIF were detected in the cytosolic samples created from ME7 infected CV animals but not in the NB-inoculated aged matched cohorts (Figures 3.13/3.11). AIF was detected in ME7/CV cytosolic samples containing 60 and 90μg total protein (Figure 3.13), but not in cytosol samples containing 30μg protein (Figure 3.12). AIF was not detected in any of the cytosolic samples prepared from the 87V infected VM animals (Figures 3.16/.17), or in the NB-inoculated aged matched control animals (Figures 3.14/.15). This indicates that the release of AIF into the cytosol is a specific event related to infection with the ME7 murine scrapie isolate.

The translocation of AIF in the ME7/CV but not 87V/VM model further adds to the observed differences in the sequence of neuropathological changes and apparent mechanisms of neuronal cell death in these murine scrapie models (described in detail in Section 1.4.5). In the 87V/VM hippocampus, neuronal damage occurs from 70dpi and PrP^{sc} is detected much later at 200dpi indicating that neuronal damage in this

model is not directly linked to PrP^{sc} deposition (Jamieson *et al.* 2001). Caspase 3 activation and the up-regulation of Fas ligand have been detected in the 87V/VM murine scrapie model (Jamieson *et al.* 2001). Furthermore, terminal deoxynucleotidyl transferase mediated dUTP nick end labelling (TUNEL) analysis confirmed apoptosis in this model by the presence of the characteristic 180-200bp DNA ladder (Jamieson *et al.* 2001(a); Jamieson *et al.* 2001(b)). In the ME7/CV hippocampus, PrP^{sc} deposition is detected at 70dpi, the loss of neuronal axon terminals and synapses is detected from 100dpi, and significant neuronal loss is detected from 170dpi (Jeffrey & Fraser 2001; Jeffrey *et al.* 2001). In contrast to the 87V/VM model, apoptosis involving activated caspase 3 and up-regulation of Fas ligand has not been detected in ME7/CV mice. However, the research of this thesis shows that translocation of AIF is a specific event related to infection with the ME7 scrapie isolate. The detection of AIF and cyt c in the cytosol of terminal stage ME7 infected CV mice indicates that these intrinsic mitochondrial proteins are likely to contribute to apoptotic cell death. However, it is possible that the preparation of these samples may have resulted in the disruption of some cells. A high degree of DNA fragmentation (180-200bp), as detected by the TUNEL assay, is not characteristic of caspase-independent apoptotic cell death pathways. Therefore future work should attempt to detect HMW DNA fragmentation (~50 kB), as this would confirm that caspase-independent apoptosis contributes to the neurodegenerative process in the ME7/CV model. Furthermore, ICC analysis would be beneficial as it would allow quantification (and multiple protein detection) of apoptosis-related proteins at the single cell level. ICC analysis would identify the distribution of AIF and Endo G in these diseases; however it was not possible to establish ICC protocols due to time constraints of other experiments.

Ever-increasing evidence confirms that oxidative stress contributes to neuronal cell death in experimental TSE infections. This includes: lipid peroxidation by reactive oxygen species (ROS) and alterations in mitochondrial Mn SOD enzyme activities in 263K and 87V murine scrapie infected rodents (Choi *et al.* 1998; Lee *et al.* 1999), increased sensitivity of *Prnp*$^{0/0}$ cerebellar neurons to oxidative stresses (Brown *et al.* 1996), increased resistance of PC12 cells over-expressing PrP^{c} to ROS when treated with PrP106-126 (Brown *et al.* 1997), and detection of the oxidative stress marker heme oxygenase-1 in ME7 infected murine scrapie brains (Choi *et al.* 2000). Oxidative stress may also be enhanced by the production of ROS by activated microglia in response to PrP106-126 (Brown *et al.* 1996; Brown *et al.* 1997). Furthermore, it is thought that PrP^{c} protects cells from oxidative stress by incorporating copper atoms into the cytosolic Cu/Zn SOD which is responsible for the dismutation of ROS (Brown *et al.* 1997; Brown & Besinger 1998; Brown *et al.* 1999). It is possible that PrP^{c} conversion to PrP^{sc} during TSE infection may reduce the capabilities of such infected cells to withstand oxidative stress, possibly by a reduced Cu/Zn SOD activity (Brown *et al.* 1999). Structural mitochondrial abnormalities, in correlation with oxidative stress, have been reported in Syrian hamsters infected with the 263K scrapie isolate (Choi *et al.* 1998) and also in the 87V/VM murine scrapie model (Lee *et al.* 1999). Therefore the release of AIF and cyt c from the IMM to the cytosol in the ME7/CV model further indicates mitochondrial dysfunction in the TSE infections. Evidence for oxidative stress and apoptosis in this model has recently been published in pre-clinical animals (~170 dpi) (Brown *et al.* 2005), a critical time-point corresponding to a significant loss (50%) of CA1 hippocampal neurons (Jeffrey *et al.* 2000). Several genes involved in mitochondrial and ER oxidative stress and apoptosis are significantly up-regulated, indicting that oxidative stress and apoptosis

contribute to the neuropathological process in this model (Brown *et al.* 2005). Therefore, the release of IMM apoptosis-related proteins (such as AIF and cyt c) from disrupted mitochondria may be due to elevated levels of oxidative stress in the ME7/CV model. Further work investigating the mechanisms resulting in the translocation of these proteins could include *in situ* hybridisation for mtDNA or ICC analysis for markers of oxidative damage to DNA and RNA, such as 8-hydroxyguanosine/8-hydroxydeoxyguanosine (8-OHG/8-OHdG). 8-OHG/8-OHdG has been found in brain sections taken from individuals diagnosed with sCJD and GSS (Guentchev *et al.* 2002; Petersen *et al.* 2005). 8-OHG/8-OhdG have also been used as reliable oxidative stress markers in neurodegenerative diseases such as Alzheimer's disease and Down's syndrome (Nunomura *et al.* 1999), and Parkinson's disease (Kikuchi *et al.* 2002).

The release of AIF to the cytosol in the ME7/CV model represents a relatively downstream event in the apoptosis cascade. Therefore, future research should concentrate not only on mechanisms resulting in the release of IMM proteins (e.g. oxidative stress) but also on discovering other apoptosis-related proteins involved in this process. As described the release of IMM proteins is carefully controlled by pro- and anti-apoptotic members of the Bcl-2 family, and have been reported in human neuronal cells treated with the neurotoxic PrP106-126 peptide (O'Donovan *et al.* 2001). Furthermore, other IMM apoptosis-related proteins which may contribute to neuronal cell death are the secondary mitochondrial activator of caspases/direct IAP-binding protein of low isoelectric point (Smac/Diablo) (Du *et al.* 2000) and HtrA2/Omi proteins (Suzuki *et al.* 2001). Following apoptotic stimuli, these proteins are also released into the cytosol and either bind to (Smac/Diablo) or cleave (HtrA2)

with inhibitor of apoptosis proteins (IAPs). Inactivation of IAP proteins enhances caspase-9 activation, and therefore downstream caspases through the enhanced formation of the apoptosome. Neurodegeneration involving Smac/Diablo and HtrA2 has recently been reported in a model of Huntington's disease (Goffredo *et al.* 2005), and the up-regulation of HtrA2 (which cleaves IAPs) has recently been published in the ME7/CV murine scrapie model (Brown *et al.* 2005). In order to understand the role of the mitochondria in mediating intrinsic apoptotic pathways in protein misfolding neurodegenerative diseases, future research should include these IMM proteins. Research for the TSE field could include; investigations at various time points of the incubation period in experimental TSE models and also the neurodegenerative model established and described in Section 4 using the neurotoxic MoPrP105-125 peptide. This analysis may therefore result in the development of intervention strategies which could limit or inhibit these neurodegenerative mechanisms.

3.3.3 Cytochrome c detection in the cytosol of terminal murine scrapie infected and normal aged-matched control animals may represent mitochondrial dysfunction with age

Mitochondria are involved in adenosine triphosphate (ATP) and phospholipid synthesis, calcium homeostasis, generation of ROS, and induction of apoptosis. Mitochondrial dysfunction, following homeostatic/oxidative stresses and apoptotic stimuli, can result in the translocation of IMM proteins (such as AIF, Endo G and cyt c) to the cytosol. The apoptotic research for this thesis was conceived to investigate the translocation of such IMM proteins to the cytosol in two murine scrapie models. IMM protein release can be instigated by the PTP, most likely

through balanced interactions with pro- and anti-apoptotic members of the Bcl-2 protein family (Kluck *et al.* 1997; Yang *et al.* 1997). Although there is strong evidence for the roles of cyt c in mediating apoptotic cell death (Liu *et al.* 1996; Zou *et al.* 1999), cyt c has received little attention with respect to TSE disease models. However, cytosolic translocation has been reported in human neuronal SH-SY5Y cells treated with PrP106-126 (O'Donovan *et al.* 2001). Also, the mitochondrial chloride channel mtCLIC4, capable of inducing cyt c release and activation of apoptosis (Fernandez-Salas *et al.* 2002), has recently been found to be up-regulated in the ME7/CV murine scrapie model (Brown *et al.* 2005).

My initial hypothesis was that if cyt c was involved in apoptosis, then cyt c would be detected only in the cytosolic extracts prepared from murine scrapie infected brain homogenates, and not in the normal brain-injected control samples. Western blot analysis revealed that cyt c was present in all of the cytosolic samples (60 and 90μg protein) created from ME7/CV and 87V/VM mice, and also in NB control samples, created by both the micro-dissection (Figures 3.11/.13/.15/.17) and whole brain fractionation (Figures 3.3/.5/.7/.9) techniques. The detection of cyt c in the cytosolic fractions from the NB control animals was an unexpected finding as the purity of these cytosolic fractions had been confirmed by the absence of the abundant mitochondrial membrane protein, VDAC1. To assess whether the detection of cyt c was as a result of age-related mechanisms or experimental procedures, both fractionation procedures were repeated on NB animals sacrificed at ~70 days dpi (the ages of the normal-injected aged matched controls from the original experiments were approximately 250 dpi for the NB/CV and 320 dpi for the NB/VM animals). Cytosolic samples containing 60μg total protein from both NB/CV and NB/VM,

prepared by both fractionation procedures, were analysed on a single SDS gel (Figure 3.19A). Similarly, samples containing 90μg total protein from the same samples were also analysed on a separate gel (Figure 3.19B). This ensured that samples containing the same total protein content, but prepared by different techniques, would be comparable to each other by removing possible variations between Western blots. Immunoreactivity with the anti-cyt c antibody was confirmed by inclusion of the 3T3 positive control cell lysate; however, cyt c was not detected in any of the cytosolic samples at this time point. Protein content within these samples on the PVDF membranes was confirmed by stripping and re-probing the membranes with the anti-Hsp70 primary antibody (Tables 3.1A & B). The presence of cyt c in the terminal murine scrapie cytosolic samples may therefore be due to age-related mitochondrial damage or cell death, and not the sub-cellular fractionation procedures.

Disruptions to the mitochondrial membrane potential, such as elevated concentrations of cytosolic Ca^{2+}, are responsible for cyt c release and induction of apoptosis in Alzheimer's disease thus further indicating oxidative stress in the activation of apoptosis (Schild *et al.* 2001). In age-related protein misfolding diseases, it is unclear whether apoptosis is due to the accumulation of misfolded proteins or due to the accumulation of ROS. Oxidative stress caused by fluctuations in cytosolic Ca^{2+} levels have been reported following exposure of neuronal cells to the PrP106-126 peptide (Thellung *et al.* 2000; Taylor *et al.* 2001), however, this has not been observed *in vivo*. The biological mechanisms of ageing are poorly understood, however, ROS generation is thought to contribute to mitochondrial dysfunction as an organism ages (Harman 1973). ATP generation, by electron transfer along the respiratory complex, generates excess superoxide anions which are normally dismutated to hydrogen

peroxide by SOD enzymes and free radical scavengers. The mechanisms resulting in disruptions to the homeostatic controls, which normally prevent the accumulation of excess ROS as an organism ages, are unknown. It is thought that the constant exposure of mtDNA to ROS results in the accumulation of mutations and therefore mitochondrial dysfunction with age. Oxidative stress is one of the key apoptosis-inducing stimuli, and may connect ageing CNS mitochondria and apoptosis in age-related neurodegenerative diseases such as Alzheimer's disease, Parkinson's disease and amyotrophic lateral sclerosis. There is also strong evidence indicating that oxidative stress may be involved in neuronal cell death in the TSE infections, as discussed in Section 3.3.2, and therefore may be responsible for the release of both AIF and cyt c in these models. Since the loss of mitochondrial cristae has been observed in some experimental murine scrapie models (Choi *et al.* 1998; Lee *et al.* 1999), it is possible that higher levels of cyt c may be present in the cytosols of scrapie infected mice. Future work would have to quantitatively determine (e.g. using an Enzyme Linked ImmunoSorbent assay-ELISA) cytosolic cyt c to determine if concentrations are higher in murine scrapie-infected animals in comparison to the age-matched control mice.

For the work of this thesis; the presence of cytosolic cyt c in infected and uninfected animals, but absence in younger animals (~70 dpi), implies its release is influenced by age related mechanisms. The effects of the ageing process on CNS mitochondrial protein expression have just been published in normal mice (C57Bl6; 2 and 12 months) (Manczak *et al.* 2005), of similar age to those chosen for the research in this thesis. ICC analysis revealed an increase in cyt c release in 12 month old mice when compared to 2 month old mice, particularly within the pyramidal neurons (CA1-CA3)

of the hippocampus. Mitochondrial dysfunction is thought to be responsible for this release due to increased detection of 8-OHG. Therefore, these results are complementary to the observations of cytosolic cyt c release in older mice in the research presented in this thesis. However, the release of cytosolic cyt c may not necessarily stimulate apoptosis, as it is believed a threshold concentration must be exceeded prior to the initiation of apoptosis. It was recently reported that cyt c release is proportional to the degree of CNS mitochondrial dysfunction in a rat model of Parkinson's disease (Clayton *et al.* 2005). This study also demonstrated sub-threshold levels of cytosolic cyt c release, which were not sufficient to induce apoptosis in cortical neurons. The presence of cyt c in the cytosolic fractions analysed in this thesis research does therefore not necessarily mean that apoptosis will be activated in all samples. *In vitro* research has shown that physiological cytosolic concentrations of K^+ (the most abundant cytosolic ion) prevent the activation of apoptosis (Bortner *et al.* 1997; Hughes *et al.* 1997), and inhibit cyt c formation of the apoptosome (Cain *et al.* 2001). Decreases in cytosolic K^+ concentrations occur prior to the induction of apoptosis, and are sufficient to allow the activation of apoptotic mechanisms of cell death (Hughes *et al.* 1997). Abnormalities in Ca^{2+}–activated K^+ currents have been reported in the ME7/CV murine scrapie model (in which both AIF and cyt c were detected in this thesis) (Johnston *et al.* 1998), in PC12 cells treated with the neurotoxic PrP106-126 peptide (Taylor *et al.* 2001), and also in *Prnp*$^{0/0}$ cerebellar Purkinje cells (Herms *et al.* 2001). Interruptions to these Ca^{2+}–dependent K^+ currents in experimental TSE models may be sufficient to abolish the control of K^+ in inhibiting activation of apoptosis. Reduced concentrations of intracellular K^+ in scrapie-infected neurons may therefore allow activation of cyt c-mediated apoptosis, which may not occur in non-infected cells if K^+ concentrations are at physiological

concentrations. More research is therefore required to determine the effects of infection with TSE agents in combination with enhanced cytosolic cyt c concentrations in aged mice. Future work should quantitatively monitor cyt c and K^+ levels at various stages of the incubation period of murine scrapie infected mice, in addition to the other IMM apoptosis-related proteins discussed in Section 3.3.2. These factors could also be monitored by immunofluorescence and FACS analysis using *in vitro* models, such as the PrP105-125 model established in Section 4. Future research will therefore have to determine the potential contributions of mitochondrial dysfunction, age and misfolded PrP^{sc} in contributing to neuronal cell death in the TSE diseases.

Chapter 4: Synthetic PrP peptides

4.1 GSS and synthetic PrP peptides

TSE amyloid peptides were first successfully isolated from cases of the GSS Indiana kindred (carrying a phenylalanine to serine substitution at 198) (Ghetti *et al.* 1989), identifying a large proportion of 11 kDa peptide fragments within the amyloid plaque deposits (Tagliavini *et al.* 1991). Also present were polymers of the 11 kDa peptides, and a number of larger PrP fragments with intact N-termini of smaller molecular mass. Subsequent analysis of amyloid proteins from GSS patients with different mutated alleles (alanine to valine substitution at 117) identified 7 kDa peptide subunits (Tagliavini *et al.* 2001). These smaller peptides spanned amino acids 81-150, and were truncated at both the C- and N-termini. Sequencing of the 11kDa (amino acids 58-150) and 7 kDa peptides (amino acids 81-150) revealed that these peptides correspond to the N-terminal region of PrP^{res} (PrP^{27-30}) (Prusiner *et al.* 1983). This is an essential region of the PrP molecule, as deletions within this region inhibit the generation of PrP^{sc} molecules (Muramoto *et al.* 1996). This sequence represents the most conserved region of the PrP protein across all tested species, and contains the hydrophobic palindrome amino acid sequence AGAAAAGA (found within the PrP106-126 peptide). This amino acid sequence is thought to be important in mediating the transmission of TSE disease through hypothesised interactions of PrP^{c} with PrP^{sc} (Muramoto *et al.* 1996; Supattapone *et al.* 1999; Norstrom & Mastrianni 2005). Ablation of this palindromic sequence has also been shown to affect the fibrillogenic and neurotoxic properties of synthetic peptides *in vitro* (Jobling *et al.* 1999). The primary and secondary structures of synthetic peptides containing this sequence therefore represent *in vitro* models relevant to the study of the neurodegenerative processes associated with TSE infections.

These findings were in agreement with synthetic Syrian hamster PrP peptide studies identifying the high propensity of this region to form stable β-sheet, and the It is thought that limited *in vivo* proteolytic cleavage of PrP molecules results in the formation of these amyloidogenic peptides, capable of polymerising into insoluble fibrillar structures. The synthesis of numerous peptides based upon the 7 kDa amyloid fragments (amino acids 81-150), revealed that these peptides harboured fibrillogenic and neurotoxic properties (Forloni *et al.* 1993; Tagliavini *et al.* 1993). The sequence representing amino acids 106-147 was found to be central to the fibrillogenic properties of this sequence and that several peptide sequences within this region formed distinct fibrillar structures (PrP106-126, PrP106-114, and PrP124-147) (Tagliavini *et al.* 1993). PrP106-126, was found to be neurotoxic to rat hippocampal cultures, and will be discussed in Section 4.2.

4.2 PrP106-126

4.2.1 PrP106-126 primary structure

PrP106-126 (Appendix I) consists of an N-terminal hydrophilic head (KTNMKHM-) followed by a hydrophobic tail (-AGAAAAGAVVGGLC), containing the previously mentioned palindrome sequence (AGAAAAGA) important for the conversion of PrP^{c} to PrP^{sc}. PrP106-126 conformation is influenced by a number of factors including solvent composition, ionic strength, pH, the presence of membranes and mutations to specific amino acids. Structural analysis by circular dichroism revealed that PrP106-126 forms a high proportion of stable β–sheet in ionic acid environments (pH 5), and also in the presence of liposomes (De Gioia *et al.* 1994). However, when dissolved in non-ionic or neutral pH environments, the peptide adopts more random coil and less β–sheet structures. The structural plasticity of the peptide in different environments is

thought to be influenced significantly by protonation of the Histidine (His111), located between the hydrophilic head and hydrophobic tail segments. Unlike the other amino acid residues in the sequence, the ionisation of His111 is enhanced in acidic, but not neutral, pH conditions (De Gioia *et al.* 1994; Ragg *et al.* 1999). The substitution of $_{L}$-His111 with $_{D}$-His111 reduces the formation of β–sheet structure and eliminates the influence of pH on the peptide structure, thought to be due to the steric hindrance of $_{D}$-His111 with the neighbouring residues (Salmona *et al.* 1999). Substituting His111 with a non-ionisable hydrophobic amino acid such as alanine, reduces the solubility of the peptide. Therefore, the ionisable side chain of His111 is thought to be extremely important in mediating the structural conformations of PrP106-126. However, a PrP106-126 peptide homologue containing methylated His111 has comparable neurotoxicity to the normal sequence indicating that His111 does not influence the toxicity of the peptide to murine cerebellar cultures (Brown 2000). The conformation and accessibility of the PrP106-126 sequence *in vivo* is potentially important for the generation of PrP^{res} molecules, as normal physiological processes cleave PrP^{c} but not PrP^{res} molecules between Lysine110 and His111 (Chen *et al.* 1995). The sequence spanning PrP106-126 contains two pathogenic point mutations responsible for GSS disease. These point mutations represent an alanine to valine substitution at 117 (Wu *et al.* 1987), and the more recently discovered glycine to valine substitution at 114 in members of a Uruguayan family (Rodriguez *et al.* 2005). A synthetic PrP106-126 peptide homologue containing the A117V mutation has an enhanced β–sheet content and neurotoxicity compared to the normal peptide, however, this change to the primary sequence abolishes the requirement for PrP^{c} expression for toxicity (Brown 2000). The primary structure of PrP106-126 is clearly

important in modulating the secondary structure, and consequentially, the toxicity of this sequence *in vitro*.

4.2.2 PrP106-126 secondary structure and biochemical properties

PrP106-126 is sparingly soluble in distilled water, aggregating to produce straight fibrils 0.1-1μm in length and with a diameter range of 4-8 nm (similar to those identified in GSS amyloid plaques) (Forloni *et al.* 1993). Peptide aggregates present the characteristic birefringence of amyloid deposits, and the peptide is neurotoxic in a dose-dependent manner to rat hippocampal cultures (Forloni *et al.* 1993). PrP106-126 shows partial resistance to proteinase-K digestion (Selvaggini *et al.* 1993), requires the neuronal expression of PrP^c for neurotoxicity (Brown *et al.* 1994; Brown *et al.* 1996), has a high β–sheet content (Selvaggini *et al.* 1993; De Gioia *et al.* 1994), and stimulates astrocytes and microglial cells (Forloni *et al.* 1994; Brown *et al.* 1996). PrP106-126 therefore shares many of the biochemical properties of PrP^{sc} (Table 1.2.), further reflecting the relevance of this peptide for the *in vitro* modelling of the proposed conversion of PrP^c to PrP^{sc}, and also for the *in vitro* modelling of TSE related neurodegeneration.

The fibrillogenic properties of PrP106-126 aggregates appear to result from the primary structure, as a random scrambled sequence of the same amino acids fails to form fibrillar structures and also lacks the neurotoxic properties of the normal sequence. However, the toxicity of PrP106-126 is not due solely to the formation of amyloid fibrils, as other fibrillogenic peptide sequences (PrP106-114, PrP127-147) fail to exhibit neurotoxic effects when added to rat hippocampal cells (Forloni *et al.* 1993). Furthermore, amidation of the C-terminus of PrP106-126 with NH_2 results in a

non-fibrillar random-coil structure with toxicity comparable to that of the normal peptide sequence (Salmona *et al.* 1999). However, amidation of PrP106-126 abolishes astrocyte proliferation in comparison to the normal peptide. Consequently, astrocyte proliferation by PrP106-126 appears to be due to the indirect effect of the presence of fibrillar amyloidogenic peptide deposits, and not due to direct effects of the peptide. Therefore the primary structure appears to be important in mediating both the formation of amyloid fibrils and the toxicity of the normal PrP106-126 peptide, but this toxicity is not due solely to the formation of these amyloid fibrils. A recent study revealed that PrP106-126 peptides containing G114A and G119A substitutions form protofibrillar structures (but not mature fibrils), are more soluble, and are more neurotoxic than the normal sequence to human neuroblastoma cells (Florio *et al.* 2003). The mechanisms by which the mutated and normal PrP106-126 peptides elicited their neurotoxic responses were identical, indicating that these substitutions did not alter the mechanisms by which the peptides interacted with the cells. Therefore, the neurotoxic properties of PrP106-126 may be controlled by a fine balance between the solubility/insolubility and structural properties. Protofibrillar or pre-amyloid forms of PrP have in some cases been associated with selective damage to axon terminals and dendritic spines in the 87V/VM murine scrapie model (Jeffrey *et al.* 1997). Therefore, the formation of soluble protofibrillar structures prior to the appearance of mature fibrils, may contribute to the neurotoxicity of PrP106-126. This thesis aims to further clarify such structure/toxicity relationships using the PrP106-126 murine homologous peptide, PrP105-125.

4.2.3 PrP106-126 neurotoxicity

The first report of the neurotoxic properties of PrP106-126 identified apoptosis as the mechanism of cell death following chronic exposures of the peptide to rat hippocampal cultures (Forloni *et al.* 1993). This was based upon the typical cell morphology and condensation of nuclear chromatin, and also the detection of the characteristic DNA ladder (180-200bp) (Section 3). Subsequent neurotoxicity studies revealed that PrP106-126 was responsible for apoptotic cell death when added to mouse cerebellar neurons (Brown *et al.* 1996), rat pituitary cells (Florio *et al.* 1998), and human neuroblastoma cells (O'Donovan *et al.* 2001; Florio *et al.* 2003). Apoptotic cell death has also been confirmed *in vivo*, following intraocular inoculations of PrP106-126 into rat retinal cells (Ettaiche *et al.* 2000; Bergstrom *et al.* 2005). In addition to the morphological changes and fragmentation of DNA, numerous biochemical markers of apoptosis and membrane dysfunction have been detected *in vitro* following exposure to PrP106-126. Enhanced Annexin V binding and activation of caspases-3, -6, and -8 have been reported following the exposure of PrP106-126 to mouse cortical neurons (White *et al.* 2001). Pre-treating cells with the pan-caspase inhibitor (Z-VAD-FMK) marginally reduced the peptide's toxicity, whereas a caspase-3-specific inhibitor (Z-DEVD-FMK) did not, suggesting the involvement of further cell death mechanisms. Similarly, these caspase inhibitors also failed to protect human neuroblastoma cells following the detection of activated caspase-3 as a consequence of chronic exposures to PrP106-126 (Thellung *et al.* 2002). These authors reported the activation of p38 MAP kinases, which may be activated as a consequence of mitochondrial depolarisation. The p38 MAP kinase pathway has been reported by other researchers (Florio *et al.* 2003), as has

mitochondrial membrane potential disruption of human neuroblastoma cells (O'Donovan *et al.* 2001).

The upstream events responsible for the induction of apoptosis, following exposure to PrP106-126, are thought to include disruptions to intracellular calcium levels and oxidative stress. Intracellular accumulations of calcium are capable of inducing apoptosis (Section 3.1.3.), and disruptions to calcium homeostasis have been reported (Florio *et al.* 1996; Florio *et al.* 1998; O'Donovan *et al.* 2001). The neurotoxic effects of PrP106-126 are enhanced in conditions with decreased anti-oxidant enzymes such as Cu/Zn SOD (Brown *et al.* 1997; Brown *et al.* 1997) and also by the production of ROS from activated microglia (Brown *et al.* 1996). One postulated role of PrP^{c} is that of an anti-oxidant similar to a SOD, as $Prnp^{0/0}$ mouse cerebellar cells are more sensitive to oxidative stress from ROS than wild-type cells (Brown *et al.* 1996). These authors believe that indirect interactions of PrP106-126 with Cu/Zn SOD enzymes result in the decreased dismutation of ROS, and therefore decreased protection from oxidative stresses. If PrP^{c} does possess SOD activities, these may be compromised by interactions with PrP106-126.

However, there is conflicting evidence as to the role, if any, of microglia in mediating the toxicity of PrP106-126. The co-culture of PC12 cells with microglia has been reported to be vital for the toxicity of PrP106-126 (Brown *et al.* 1997), however, the dependence of microglia for toxic effects have been disputed by other researchers using the PC12 cell culture system (Hope *et al.* 1996). Microglial stimulation to release ROS may contribute to the neurotoxicity, but does not appear to be essential. The research detailed in this thesis does not include a co-culture of microglia and

PC12 cells however, the effects of the naive and neuronal phenotypes of PC12 cells were tested with different morphologies of PrP105-125 peptides (Section 4.2.4.).

4.2.4 Murine PrP105-125

The murine PrP105-125 peptide, homologous to the human PrP106-126 peptide sequence, was synthesised for the research described in this thesis. The murine PrP105-125 peptide differs by two amino acids from the homologous region within the human genome (Appendix I) and is identical in sequence to the same region within the rat genome. This peptide sequence therefore removes potential species barrier effects, in comparison to previous studies using the human PrP106-126 peptide for the purposes of correlating the structure/toxicity effects of this peptide in a rat PC12 cell culture system. The MoPrP105-125 peptide represents a novel feature of the work of this thesis for this purpose.

4.3 Results

4.3.1 Electron microscopic analysis of MoPrP105-125 and scrambled MoPrP105-125 at various aggregation times and buffer conditions

The ability of the MoPrP105-125 and scrambled MoPrP105-125 peptides to form fibrillar structures was checked by negatively staining peptide solutions with sodium phosphotungstate, and analysing by transmission electron microscopy (Section 2.4.5.). For the normal peptides, EM photomicrographs are representative of the fibrils present within that grid. For the scrambled peptide samples, the photomicrographs show what was actually present on the grids. These samples contained sparse amorphous aggregated material. Initial studies using 200mM citrate (pH7), distilled water (GibcoBRL) and 10mM MES (pH7) buffers with incubation at room temperature for 48 hours revealed that all buffers permitted the MoPrP105-125 peptides to form fibrillar structures. Although fibrillar-like structures were found in the scrambled equivalents, these structures were distinctly different to those formed by the normal peptides. MoPrP105-125 dissolved in 200mM citrate (pH7) buffer (Figure 4.1.A.) formed frequent long straight fibrils. In the same conditions, the scrambled peptide formed smaller straight fibril-like structures (Figure 4.1.B.). The normal peptide dissolved in distilled water formed highly branched straight fibrils (Figure 4.1.C.), whereas the scrambled equivalent (Figure 4.1.D.) formed occasionally small fibril-like structures which were also highly branched. The normal peptide formed very frequent long straight fibrillar structures, which were often branched, when dissolved in 10mM MES (Figure 4.1.E.). However, the scrambled peptide (Figure 4.1.F.) formed infrequent fibril-like structures which were also distinctly different from those formed by the normal peptide.

Based on the observations of the incompatibility of the 200mM citrate buffer for FTIR analysis (Section 4.3.3.) and the poor amyloidogenic properties of the peptides when dissolved in distilled water (Section 4.3.2.), a series of factors were manipulated to alter the amyloidogenic and secondary structural properties of the peptides when dissolved in the remaining buffer (10mM MES). These changes involved altering the NaCl concentration (0, 50, 200mM), analysing the buffers at two different pH values (pH 5 and 7), performing this analysis over a longer time scale of up to 14 days, and increasing the incubation temperature to 37°C. The EM photomicrographs in Figure 4.2 (10mM MES, pH 7) and Figure 4.3 (10mM MES, pH 5) were taken following incubations at 37°C for 5 and 14 days respectively. These time points were chosen based upon the amyloidogenic properties of these peptides as monitored by the Thioflavin-T binding assay, as it was apparent that maximum aggregation had occurred at these time points in these buffers (Section 4.3.2.).

MoPrP105-125 dissolved in 10mM MES pH7 (Figure 4.2.) formed frequent straight fibrils in this buffer. The morphology of these fibrils altered with NaCl concentration; fibrils formed in the absence of NaCl formed a dense mat of fibrils, these fibrils were distinctly longer and straight in the presence of 50mM NaCl. Fibrils formed in the presence of 200mM were found in dense bundles of straight fibrils; although these were less compact than at lower NaCl concentrations. The scrambled peptides dissolved in these buffers did not form any fibrillar structures. MoPrP105-125 dissolved in 10mM MES pH5 (Figure 4.3.) formed dense networks of straight fibrils. The fibrils became slightly larger with increasing concentrations of NaCl, and were also less compact at 200mM NaCl. The grid containing fibrils created in 50mM NaCl was a dense mass of fibrils, which were frequently overlapping. In the presence of

200mM NaCl the quality of the staining was poorer in comparison to the other samples, but these fibrils were long and overlapping. The fibrils formed in the presence of 50mM and 200mM NaCl had slight bending in comparison to the much straighter fibrils within those networks. In the samples containing the scrambled equivalents fibrillar structures were absent in the samples with 0mM and 50mM NaCl. However; fibrillar structures were present in the 200mM NaCl samples, although these were distinctly different from the normal peptide as these were extremely short and infrequently observed.

4.3.2 Amyloidogenic properties of MoPrP105-125 and scrambled MoPrP105-125 measured by Thioflavin-T binding assay

The amyloidogenic/aggregation properties of the MoPrP105-125 and scrambled MoPrP105-125 peptides were monitored by incubating aliquots of these peptides with molar excesses of Thioflavin-T (Section 2.4.3.). Initial studies tested the effects of 10mM MES (pH7), distilled water and 200mM citrate buffer (pH7) on the amyloidogenicity (tendency to form fibrils) of the normal and scrambled peptides following incubation at room temperature for 48 hours. Thioflavin-T binding is a specific assay for the formation of fibrils, where binding alters the excitation maxima to ~480nm. Figure 4.4 shows the Thioflavin-T binding profiles of the buffers described above for the normal and scrambled peptide sequences. Scrambled peptides in these tested conditions never bound to Thioflavin-T, indicating that the scrambled sequences do not possess amyloidogenic properties. The normal peptide dissolved in 200mM citrate buffer (pH7) had the highest propensity to form amyloid fibrils, whereas the normal peptide in 10mM MES had relatively low Thioflavin-T binding in comparison. Furthermore, the normal peptide dissolved in distilled water had

negligible fibril forming properties. Although the normal peptide dissolved in 200mM citrate buffer was the favoured choice for future studies at this stage, it was found that this buffer was incompatible with FTIR analysis (Section 4.3.3.). Therefore, the compatibility of the MES buffer with all tested techniques concentrated the following studies on variations of the MES buffer (described in Section 4.3.1.) in efforts to enhance the fibril forming properties. Furthermore, the fluorimeter slit width for emitting fluorescent light was found to be optimal at 4nm for Thioflavin-T binding in comparison to the 2nm slit width used in the above mentioned research.

Figure 4.5. shows the Thioflavin-T binding of normal and scrambled MoPrP105-125 peptides (10mM MES, pH7) at serial time points at increasing concentration of NaCl (0, 50 or 200mM) (immediately dissolved t=0, 0.5, 1, 24 and 120 hours). Scrambled peptides never bound to Thioflavin-T, demonstrating the lack of fibril forming abilities of these samples. Fibril formation was highest in normal peptides created in the 50mM NaCl buffer, although fibril formation was only marginally higher than those samples prepared in the presence of 200mM NaCl. The buffer lacking NaCl had even lower amyloidogenic properties than the other tested NaCl concentrations. However, maximum formation of fibrils had occurred by 24 hours incubation as Thioflavin-T binding was relatively unchanged following 120 hours (5 days) aggregation. Figure 4.6. shows the Thioflavin-T binding of normal and scrambled MoPrP105-125 peptides (10mM MES, pH5) at serial time points at increasing concentration of NaCl (0, 50 or 200mM) (immediately dissolved t=0, 0.5, 1, 24,120, 168, 240 and 336 hours). Correlating with the scrambled sequences from MES pH7, scrambled peptides in these buffer conditions never bound to Thioflavin-T and therefore were also non-amyloidogenic. Normal peptide samples created in the

presence of 200mM NaCl had an extremely low tendency to form fibrils, and samples without NaCl were only slightly more amyloidogenic. However, 50mM NaCl buffers had a high tendency to form amyloid fibres and a plateau for Thioflavin-T binding was achieved following 240-336 hours (10-14 days) incubation. Therefore, normal peptide sequences created in MES buffers at pH5 had a lower propensity to form fibrils than samples created at pH7. Also, the highest Thioflavin-T binding was reached following incubations of 240-336 hours (10-14 days) in comparison to the rapid binding of 24-120 hours (1-5 days) observed at pH 7.

4.3.3 Secondary structure analysis of MoPrP105-125 and scrambled MoPrP105-125 by Fourier transform infrared spectroscopy

FT-IR was used to analyse the effects of the vehicle buffers on the secondary structure of the MoPrP105-125 and scrambled MoPrP105-125 peptides (Section 2.4.4.). Secondary structure analysis by FTIR concentrated primarily on the amide I region (1600-1700cm^{-1}), although the amide II region was also analysed as this can provide additional information on the aggregation state of tested samples. Initial studies using 200mM citrate (pH 7) revealed that this buffer formed highly aggregated fibrillar structures when analysed by EM and Thioflavin-T binding (Sections 4.3.1. and 4.3.2.), although the strong carbonyl bonds in the citrate buffer prevented secondary structure analysis by FTIR within the amide I region. Coupled with the poor amyloidogenic properties of the normal peptide in distilled water (Section 4.3.2.), it was decided to discontinue studies using these buffers. Since the normal peptide in MES was amyloidogenic and formed dense fibrillar networks (Section 4.3.1. and 4.3.2.), it was decided to continue further studies with this buffer as it was also compatible with FTIR.

The FTIR spectra displayed in Figure 4.7. (MES pH 7, 50mM NaCl) and Figure 4.8. (MES pH 5, 50mM NaCl) were from aliquots of peptide samples incubated at 37°C for 5 and 14 days respectively . Secondary structure analysis of these samples was coupled with the amyloidogenic properties (Section 4.3.2.) and the fibrillar structures following EM analysis (Section 4.3.1) at these time points. Based upon the fibrillar and amyloidogenic profiles of the normal peptide samples supplemented with 50mM NaCl (Figures 4.2.C. & 4.5. for pH 7, and Figures 4.3.C. & 4.6. for pH 5), these peptide solutions were analysed by FTIR and their cytotoxicities measured using the alamarblue reduction assay (Section 2.5.11.2.). Although FTIR analysis concentrates primarily on the amide I (1600-1700cm^{-1}) region, in the absence of aggregated structures, complete hydrogen/deuterium exchange occurs and the amide II peak appears as amide II′. However, amide II peaks remain for both the MoPrP105-125, but not scrambled, peptide conformations (Figures 4.7. and 4.8.). This is indicative of highly aggregated structures in the normal peptide solutions which prevent complete deuterium exchange. Highly aggregated fibrillar structures are present in both normal peptides as detected by EM (Section 4.3.1.) and Thioflavin-T analysis (Section 4.3.2.). Although I performed the sample preparation, acquisition and majority of the analysis; secondary structural curve fitting using the Grams software (Thermo Corporation, California) was performed by Dr. Matt Hicks (University of Warwick). Using this information, I was then able to assign secondary structures to each of the normal and scrambled peptide solutions. Secondary structure assignments for the normal and scrambled peptides (10mM MES+50mM NaCl pH7) are described in Tables 4.1 and 4.2 respectively. The normal peptide sequence has a high proportion of β-sheet (69.21%) in comparison to the scrambled peptide (32.61%). The normal peptide also consists of 11.05% α-helix and 19.74% β-turn; whereas the scrambled

peptide contains 21.94% α-helix and a large proportion (45.45%) β-turn. The secondary structure assignments for the normal and scrambled peptides (10mM MES+50mM NaCl pH5) are described in Tables 4.3 and 4.4 respectively. The normal peptide sequence also has a high proportion of β-sheet (61.11%) in comparison to the scrambled peptide (combined β-sheet = 42.08%). The normal peptide also consists of 17.51% α-helix and 21.38% β-turn; whereas the scrambled peptide contains 19.12% α-helix, 16.71% β-turn and 22.09% random coil.

4.3.4 Secondary structure overview of the MoPrP105-125 and scrambled peptides chosen for cytotoxicity analysis

Peptide solutions chosen for the cytotoxicity analysis were derived from the accumulation of information relative to the secondary structure properties of these peptide solutions under different conditions. Two peptide solutions were chosen for this analysis, in addition to their non-aggregating scrambled control sequences. The first peptides (normal and scrambled) chosen were those created in 10mM MES+50mM NaCl (pH 7) pre-incubated for 5 days at 37°C. Under these conditions the normal peptide formed distinctly long straight fibrils which were located frequently on the EM grid (Figure 4.2.C.). This peptide also had the highest propensity to form amyloid fibrils of all of the tested buffers in this research, as measured by Thioflavin-T binding (Figure 4.5.). The secondary structure as analysed within the amide I (1600-1700cm^{-1}) region; consisted of 19.74% β-turn, 11.05% α-helix, and 69.21% β-sheet (Figures 4.7. & Table 4.1.). In comparison, the scrambled peptide did not form any fibrillar structures (Figure 4.2.D.), and was non-amyloidogenic (Figure 4.5.). The secondary structure of the scrambled peptide

consisted of 45.45% β-turn, 21.94% α-helix, and 32.61% β-sheet (Figures 4.7. & Table 4.2.).

The second set of peptides (normal and scrambled) chosen for cytotoxicity analysis were those created in 10mM MES+50mM NaCl (pH 5) pre-incubated for 14 days at 37°C. Under these conditions the normal peptide formed an extremely dense network of fibrils which were shorter than those created at pH 7. These fibrils were so frequent that they often over-lapped and some fibrils appeared to slightly bend (Figure 4.3.C.). This normal peptide also had a high propensity to form amyloid fibrils, although this was slightly lower than that of the other normal peptide described above (Figure 4.6.). The secondary structure, as analysed within the amide I region (1600-1700cm^{-1}), comprised 21.38% β-turn, 17.51% α-helix, and 61.11% β-sheet (Figures 4.8. and Table 4.3.). In comparison the scrambled peptide control did not form fibrillar structures (Figure 4.3.D.), and was non-amyloidogenic (Figure 4.6.). The scrambled peptide had a secondary structure consisting of 16.71% β-turn, 19.12% α-helix, 22.09% random coil, and 42.08% combined β-sheet (Figures 4.8. and Table 4.4.).

4.3.5 Treatment of PC12 cells with nerve growth factor differentiates cells to the neuronal phenotype

The PC12 cell line can be reversibly differentiated into a neuronal phenotype when cultured on collagen IV coated surfaces in the presence of NGF (Section 1.5.3.). PC12 cells were cultured with 100ng/ml NGF and analysed following exposure for 7 and 14 days in comparison to untreated (naive) cell cultures. Phase contrast microscopic analysis shows that naive PC12 cells (Figure 4.9.A.) are round with a

tendency to grow in small clumps. PC12 cells exposed to NGF for 7 days (Figure 4.9.B.) are more isolated from each other, and dendritic processes start to develop and extend to neighbouring cells. 14 day NGF-differentiated PC12 cells (Figure 4.9.C.) have enlarged cell bodies and extended mature neuritic processes in comparison to naive and 7 day NGF-differentiated PC12 cells. Neuronal differentiation of the PC12 cell cultures was confirmed by FACS analysis (Section 2.5.10.2.) using the anti-neurofilament protein primary antibody (Table 2.1.). Figures 4.10-4.13 are concearned with the expression of PrP^c by PC12 morphologies and are discussed in Section 4.3.6. Neurofilament proteins, the major structural subunits of mammalian neurons, exist in three subunits; NF-L (~68kDa), NF-M (~145kDa) and NF-H (~200kDa) where NF-L forms heterodimers with either NF-M or NF-H (Lee & Cleveland 1996). PC12 cell NF-L mRNA increases significantly following differentiation with NGF (Lindenbaum *et al.* 1998), and has been shown to be reliable in quantitatively determining PC12 cell differentiation to the neuronal phenotype (Schimmelpfeng *et al.* 2004). FACS analysis with the anti-NF-L primary antibody confirmed that naive cells express negligible amounts of the NF-L subunit (1.61%) (n=4, SEM=0.2) (Figures 4.14.A. and 4.14.B.). In contrast, 16.05% (n=4, SEM=0.76) of cells expressed NF-L following exposure to NGF for 7 days (Figures 4.14.C & D). This increase in NF-L protein expression was highly significant ($p<0.005$) in comparison to the naive cell cultures. Furthermore, 14 day differentiated PC12 cells were much larger and more complex than the naive and 7 day differentiated counterparts, as confirmed by forward and side scatter analysis. NF-L expression by 14 day differentiated cell cultures increased by almost 20–fold in comparison to naive cells, with 31.04% (n=4, SEM=0.33) of cells expressing the neuron-specific protein (Figures 4.14.E. and 4.14.F.). This increase in NF-L expression was also highly

significant ($p<0.005$) in comparison to 7 day differentiated cultures. PC12 cells differentiated for 14 days were deemed to be neuronal, and were used for the cytotoxicity analysis of conformational phenotypes of the MoPrP105-125 peptide. The cytotoxicity analysis further confirmed the neuronal phenotype, as these differentiated PC12 cells were much more sensitive to the TMT compound than naive non-NF-L expressing cultures. TMT, a neurotoxic compound, was chosen as a positive control for the Alamarblue cytotoxicity assay (Section 2.5.11.2.). Although hippocampal pyramidal and dentate gyrus cells are particularly sensitive to TMT; the compound is also toxic to glial cells. The mechanisms of TMT toxicity are unclear, but are thought to be influenced by the expression of stannin and are thought to be mediated by apoptosis. Naive and neuronal PC12 cells were both sensitive to the neurotoxicity of TMT, but neuronal PC12 cells were more susceptible. The mean viability of naive PC12 cells, as measured by Alamarblue reduction, was 65.45% of the positive untreated growth control (i.e. TMT inhibited viability by 34.55%) after 24 hours exposure (Figure 4.15.). Naive PC12 cells which were chronically exposed for 7 days (Figure 4.15.) had a mean viability of 39.68% (or inhibited by 60.32%). In contrast, the mean viability of neuronal PC12 cells exposed to TMT for 24 hours was 45.53% (or inhibited by 54.47%) when compared to the positive growth control (Figure 4.17.). This mean viability was decreased further to 10.68% (or inhibited by 89.32%) following chronic exposure for 7 days (Figure 4.17.). Therefore 14 day NGF-differentiated PC12 cells not only express neuronal-specific proteins (i.e. NF-L), morphologically resemble neurons, but they also respond like neurons in the presence of neurotoxic TMT. Naive and neuronal (14 day NGF-differentiated) PC12 cells were used for monitoring the structure/toxicity relationships of MoPrP105-125 in this thesis.

4.3.6 PrP^c expression by PC12 cells increases following differentiation with nerve growth factor

To analyse the possible effects of PrP^c upon the toxicity of MoPrP105-125, the expression of PrP^c was analysed in naive, 7- and 14 day-NGF differentiated PC12 cell cultures. Preliminary immunofluorescence and FACS analysis revealed that the anti-PrP 8H4 monoclonal primary antibody (Table 2.1.) was superior in recognizing rat PrP^c, in comparison to the anti-PrP 6H4 (Table 2.1.) monoclonal and 1B3 (Farquhar *et al.* 1989) (kindly donated by K. Brown and C. Farquhar) polyclonal antibodies. 8H4 was therefore used for the immunofluorescence and FACS studies detailed in this thesis. The PrP^c expression by naive and neuronal PC12 cells was attempted using the Western blot techniques described using these anti-PrP antibodies (Section 2.5.9.); however, these studies were unsuccessful and are not discussed further. It is possible that the Western Blot techniques were not sensitive enough for detecting the low levels PrP^c expressed in naive PC12 cultures or that the methods for removing the naive PC12 cells damaged the cell surface PrP^c. Immunofluorescence analysis revealed that PrP^c expression was increased according to the differentiation status of the PC12 cells. Naive PC12 cells expressed low levels of PrP^c (Figures 4.10.A. and 4.10.C.), which was restricted to the cytosol and cell membrane. PrP^c expression increased following differentiation for 7 days (Figures 4.11.A. and 4.11.C.); expression levels were higher again in PC12 cells fully differentiated after 14 days (Figures 4.12.A. and 4.12.C.).

FACS analysis corroborates the immunofluorescence results, as 9.02% of naive PC12 cells express PrP^c when labelled with the 8H4 monoclonal antibody (n=4, SEM=0.27) (Figures 4.13.A. and 4.13.B.). After 7 days of NGF-differentiation, 30.18% of cells

express PrP^c (n=4, SEM=0.59) (Figures 4.13.C. and 4.13.D.), representing a highly significant increase in PrP^c expression ($P<0.005$). The number of cells expressing PrP^c is increased further to 42.22% (n=4, SEM=0.7) following differentiation for 14 days (Figures 4.13.E. and 4.13.F.), representing over a 4-fold increase in PrP^c expression in comparison to naive cells which is also highly significant in comparison to 7 day differentiated cultures ($p<0.005$). The apparent higher detection of PrP^c in the immunofluorescence images in comparison to the FACS data could be due to inadequate permeabilisation of the PC12 cells during FACS analysis, or possible damage to cell surface PrP^c during procedures to harvest the cells for analysis.

4.3.7 MoPrP105-125 toxicity

MoPrP105-125 peptide conformations (Section 4.3.4.) were added at concentrations of 50, 80, 100 or 150μM to naive or neuronal PC12 cells. Neither of the MoPrP105-125 peptides, nor their scrambled counterparts (Section 4.3.8.), were toxic to naive PC12 cell cultures (Figures 4.15.-4.16. and 4.19.-.4.20.). However, both of the MoPrP105-125 conformations were toxic to neuronal PC12 cell cultures (Figures 4.17.-4.18. and 4.21.-4.22.). Balanced two-way ANOVA analysis showed that toxicity on neuronal cells was highly significant in comparison to the naive cell cultures ($p<0.005$), and also that this toxicity was dependent on the normal and not scrambled peptide ($p<0.005$). There is therefore a highly significant relationship that requires the neuronal phenotype for the peptide conformations to be toxic.

To analyse the effects of short and longer exposure times of MoPrP105-125 peptides on neuronal PC12 cells, alamarblue cytotoxicity assays were performed at exposures of 24, 48, and 72 hours and also 5 and 7 days (Section 2.5.11.2.). Exposure time for

both peptides was statistically highly significant ($p<0.005$), and there was a highly significant two-way relationship between exposure time and cell type. This indicates that the presence of neuronal PC12 cells and the duration of peptide exposure are extremely important variables, as such toxicity is not observed for the naive cell cultures. Analysis of the alamarblue reduction values across all concentrations shows that the maximum toxicity of both normal peptides is observed following exposure for 5 days. It is likely that toxicity would increase even further with increased peptide exposure times, although this was not analysed for the research of this thesis. Analysis of the secondary structure of these normal peptides shows that the β–sheet content is similar (Tables 4.1. and 4.3.), although the fibrillar structures are very different (Figures 4.2. and 4.3.). The β–sheet content of the normal peptide created at pH 7 is 69.21%, and analysis of fibrillar morphology shows that these fibrils are very straight along in comparison to all other peptide solutions. At pH 5 the β–sheet content is 61.11%, and EM analysis revealed a dense mass of fibrils, which were small, occasionally bent and frequently overlapping. It was hypothesised that the toxicities of morphologically distinct fibrillar structures would not have such comparable neurotoxic properties. Possible reasons for such similar toxicities are discussed in Section 4.4.

4.3.8 Scrambled MoPrP105-125 is non-toxic to naive PC12 cells, but moderately toxic to neuronal PC12 cells following chronic exposure

A randomly generated scrambled sequence of the human PrP106-126 synthetic peptide has been widely demonstrated to be non-neurotoxic in comparison to the normal peptide sequence (Forloni *et al.* 1993). A scrambled version of MoPrP105-125 was synthesised and analysed as a non-aggregating (Section 4.3.2.) control which had the same amino acid composition as the normal peptide sequence (Appendix I). Cytotoxicity of the scrambled peptide was monitored by alamarblue reduction in contrast to non-treated positive growth controls, and compared to cultures treated with equivalent volumes of vehicle buffer lacking peptide. The scrambled peptide sequence, of the two tested peptide conformations, was non-toxic to naive PC12 cultures at all of the tested time points (Figures 4.16. and 4.20.). However; when neuronal cells were treated for 5/7 days (Figures 4.18. and 4.22.), viability was slightly decreased in comparison to the vehicle treated control cells. The toxicity of these two scrambled peptides is therefore comparable after 7 days exposure to neuronal PC12 cells, but not as remarkable as that observed in the normal peptide experiments. Therefore, the MoPrP105-125 peptides tested in this thesis are much more toxic than their scrambled counterparts.

4.3.9 Analysis of apoptosis in MoPrP105-125 treated neuronal PC12 cells

Two approaches were chosen in an attempt to identify apoptosis in the normal peptide-treated neuronal PC12 cells. Annexin V and anti-active caspase-3 antibodies were used to search for apoptotic markers. Analysis included replicates of cells treated with; the two normal peptide conformations, TMT, and untreated controls. Staining with Annexin V proved problematic as it stained non-specifically in all of the cell replicates. It is thought that the procedures used to remove adherent cell cultures may damage the neuritic processes, which may therefore account for the non-specific binding of annexin V (Schutte *et al.* 1998). Further work would have to optimise the cell harvesting procedures and/or techniques to block non-specific binding. Therefore, annexin V binding as a marker of early apoptosis could not be used to obtain results for this thesis. The *in vitro* and *in vivo* detection of active caspase 3, following exposure of neuronal cells to PrP106-126 and in the 87V/VM murine scrapie model, represented a downstream marker of apoptosis which should be analysed in this thesis. However, reactivity of the anti-caspase 3 antibody could also not be confirmed in any of the cell cultures. These studies were the final experiments of the research of this thesis, and due to considerable time constraints could not be optimised or studied further.

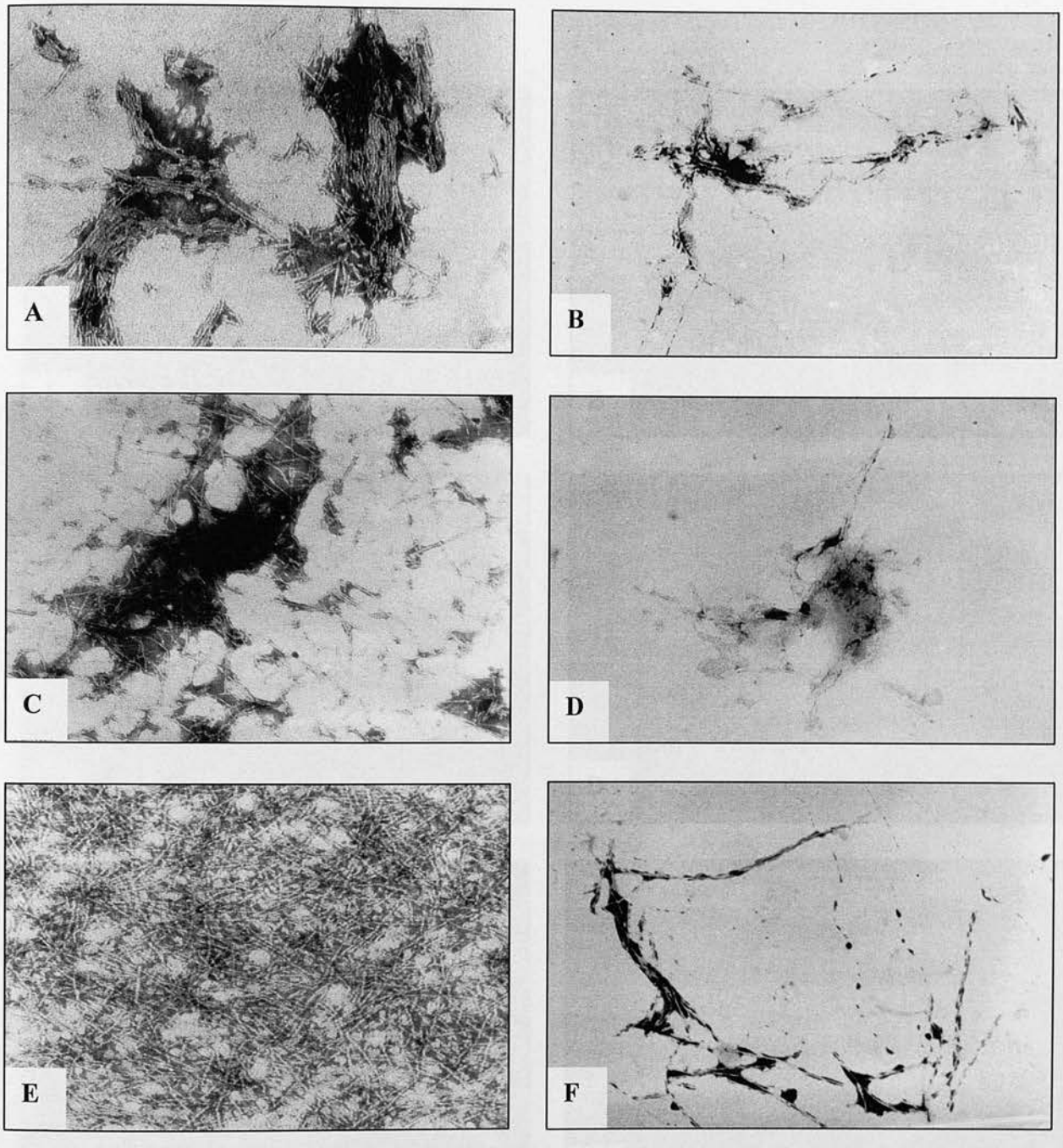

Figure 4.1 **Electron micrographs of MoPrP105-125 and scrambled MoPrP105-125 prepared in 200mM citrate buffer (pH7), distilled water, and 10mM MES buffer (pH7) after 48 hours incubation at room temperature**

MoPrP105-125 and scrambled MoPrP105-125 samples (5µl) were dried onto carbon/formvar 200 mesh grids and negatively stained with 2% sodium phosphotungstate (Section 2.4.5). (A) normal peptide in 200mM citrate pH 7 (B) scrambled peptide in 200mM citrate pH 7 (C) normal peptide in distilled water (D) scrambled peptide in distilled water (E) normal peptide in 10mM MES pH 7 (F) scrambled peptide in 10mM MES pH 7. Magnifications: x45,000 (A, C, E) and x15,000 (B, D, F).

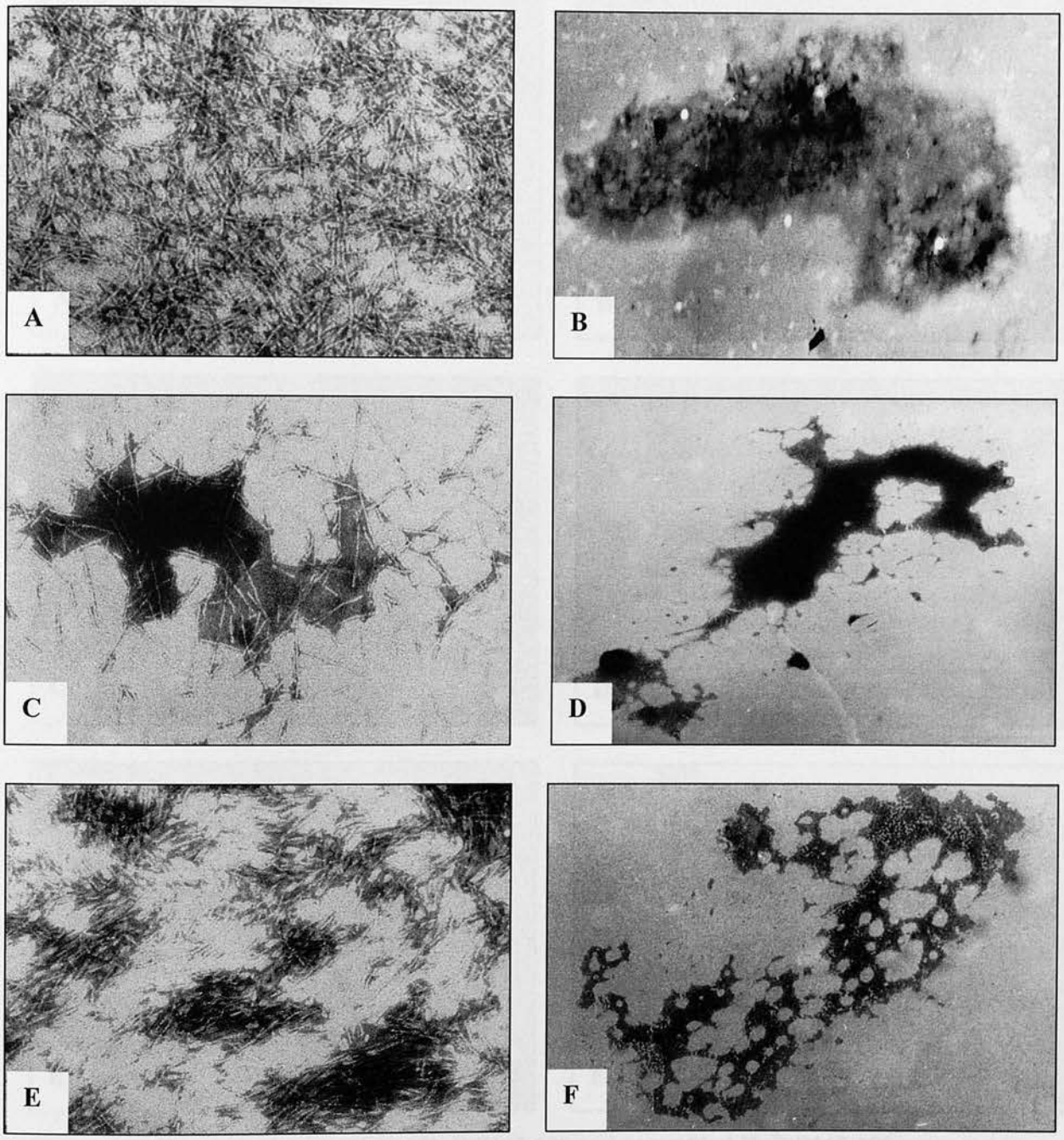

Figure 4.2 **Electron micrographs of MoPrP105-125 and scrambled MoPrP105-125 prepared in 10mM MES buffer (pH 7) at increasing NaCl concentrations after 5 days incubation at 37°C**
MoPrP105-125 and scrambled MoPrP105-125 samples (5µl) were dried onto carbon/formvar 200 mesh grids and negatively stained with 2% sodium phosphotungstate (Section 2.4.5). (A) normal peptide and (B) scrambled peptide with 0mM NaCl, (C) normal peptide and (D) scrambled peptide with 50mM NaCl, (E) normal peptide and (F) scrambled peptide with 200mM NaCl. Magnifications: x45,000 (A, C, E) and x15,000 (B, D, F).

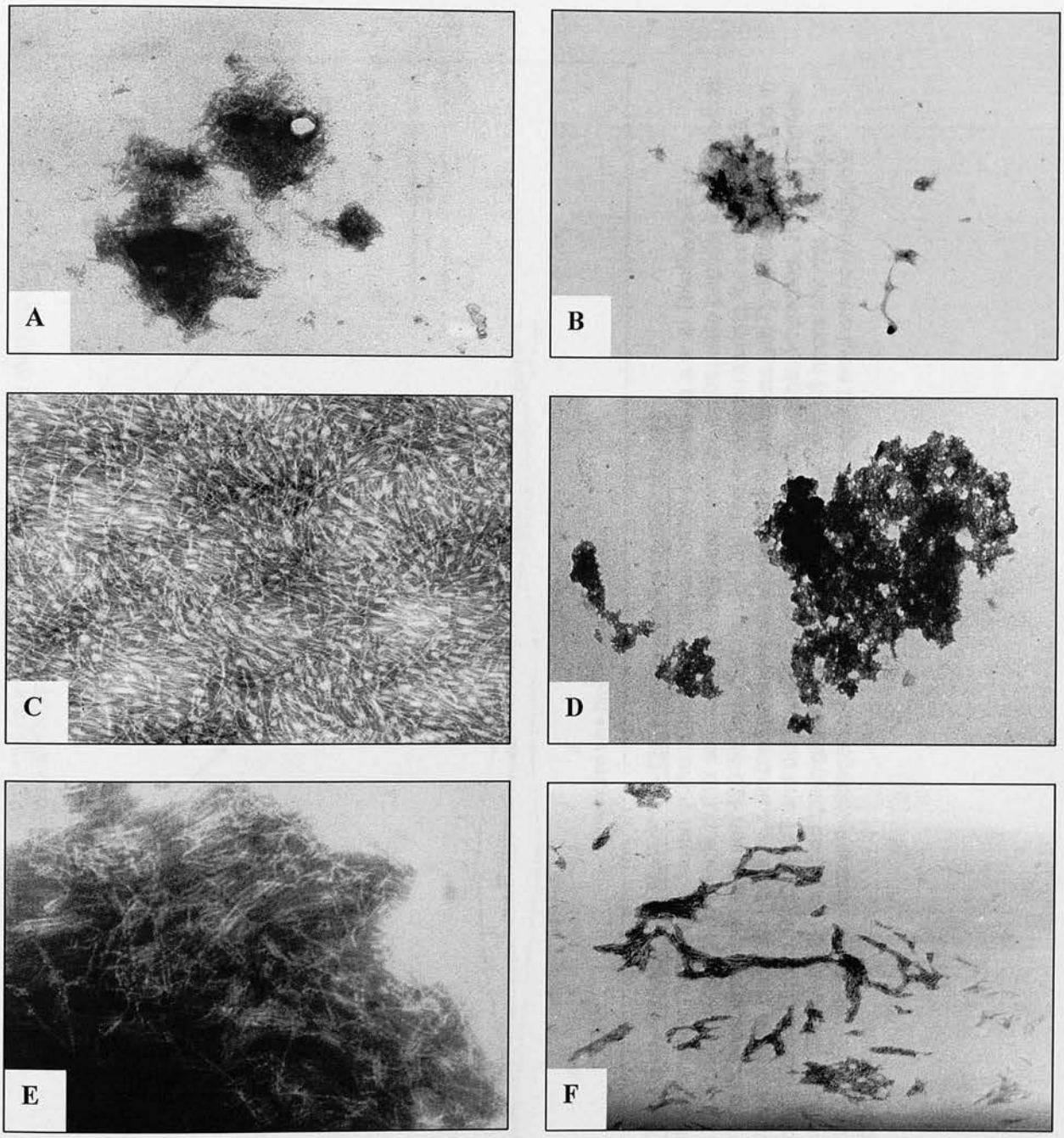

Figure 4.3 **Electron micrographs of MoPrP105-125 and scrambled MoPrP105-125 prepared in 10mM MES buffer (pH 5) at increasing NaCl concentrations after 14 days incubation at 37°C**
MoPrP105-125 and scrambled MoPrP105-125 samples (5µl) were dried onto carbon/formvar 200 mesh grids and negatively stained with 2% sodium phosphotungstate (Section 2.4.5). (A) normal peptide and (B) scrambled peptide with 0mM NaCl, (C) normal peptide and (D) scrambled peptide with 50mM NaCl, (E) normal peptide and (F) scrambled peptide with 200mM NaCl. Magnifications: x45,000 (A, C, E) and x15,000 (B, D, F).

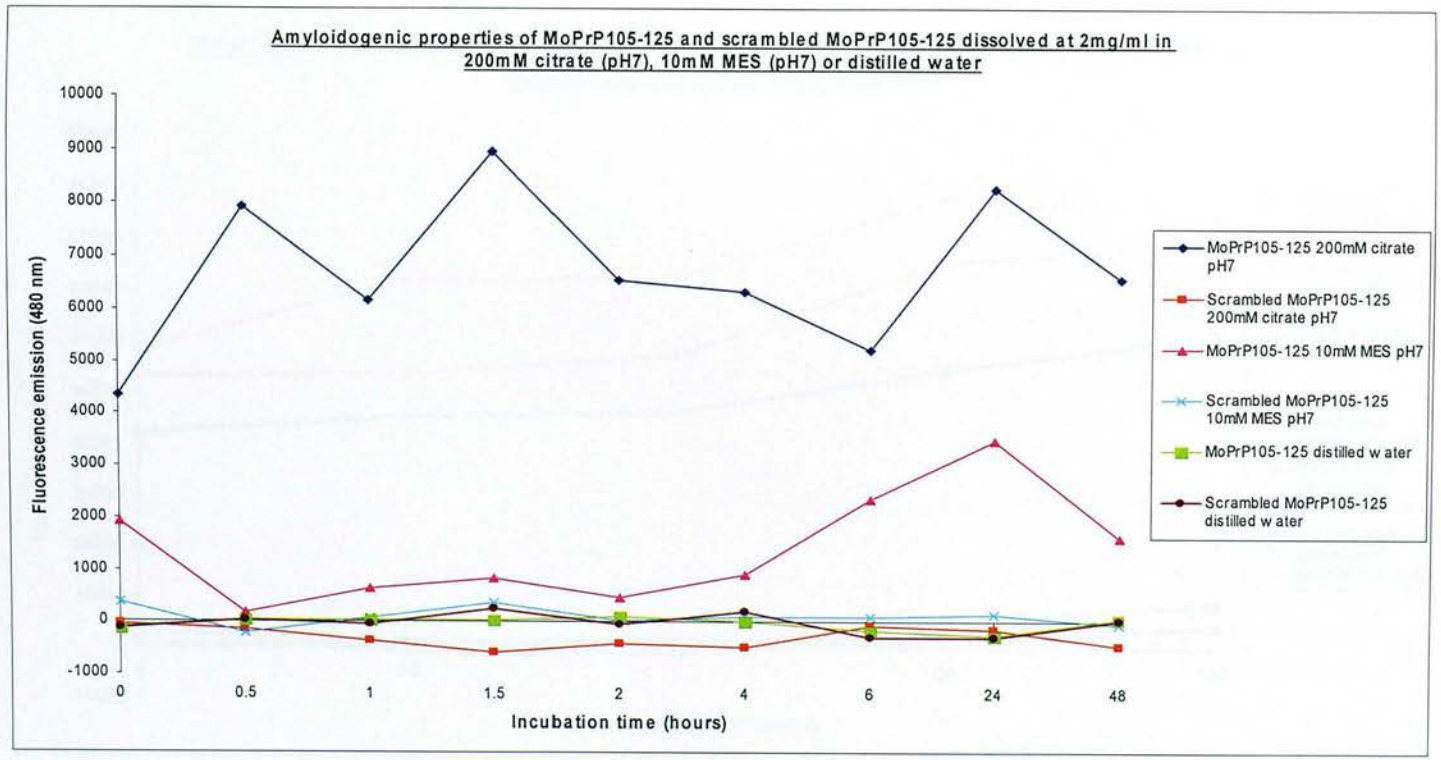

Figure 4.4 **Thioflavin-T binding of MoPrP105-125 and scrambled MoPrP105-125**

Thioflavin-T stock in water (2mM) was diluted in the appropriate vehicle buffer to achieve a final Thioflavin-T concentration of 20μM. Thioflavin-T/vehicle buffer solutions were incubated with the appropriate peptide solution in that vehicle buffer and fluorescence read between 450-550nm (Section 2.4.3). The emission maxima for amyloid-bound Thioflavin T was monitored over 48 hours. Scrambled peptides dissolved in 200mM citrate (pH7), distilled water, and in 10mM MES (pH7) did not bind to Thioflavin-T and did therefore not possess amyloidogenic properties. Normal peptide samples prepared in 200mM MES (pH7) had the highest propensity to form fibrils over 48 hours. Normal peptides dissolved in 10mM MES (pH7) were less amyloidogenic and the distilled water-dissolved solutions had negligible amyloidogenic properties.

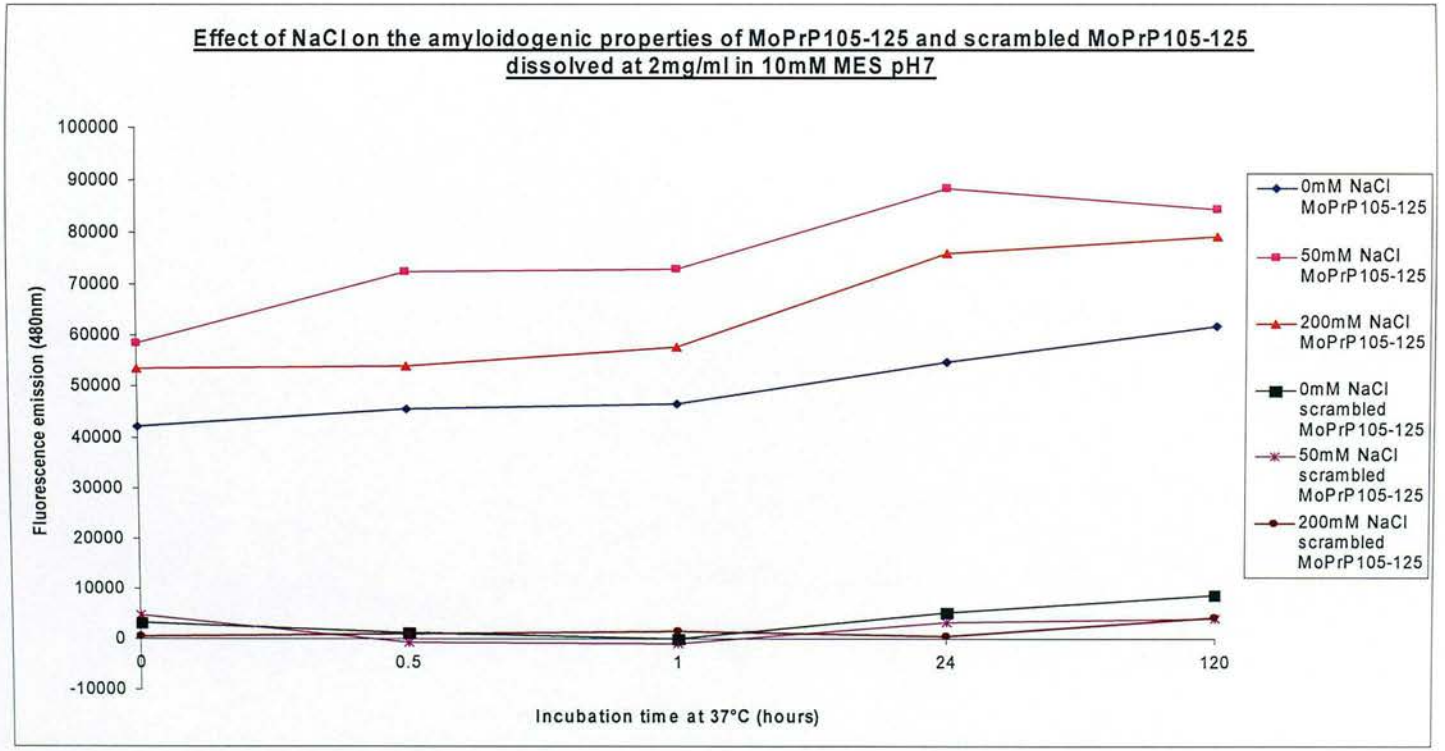

Figure 4.5 **Thioflavin-T binding of MoPrP105-125 and scrambled MoPrP105-125**

Thioflavin-T stock in water (2mM) was diluted in the appropriate vehicle buffer to achieve a final Thioflavin-T concentration of 20μM. Thioflavin-T/vehicle buffer solutions were incubated with the appropriate peptide solution in that vehicle buffer and fluorescence read between 450-550nm (Section 2.4.3). The emission maxima for amyloid-bound Thioflavin T was monitored over 5 days (120 hours). Scrambled peptides dissolved in 10mM MES (pH7) at all tested NaCl concentrations did not bind to Thioflavin-T and did therefore not possess amyloidogenic properties. MoPrP105-125 amyloidogenicity is maximum at 50mM NaCl between 24-120 hours (1-5 days). 200mM NaCl solutions were only slightly less amyloidogenic . Peptide solutions containing 0mM NaCl had the lowest propensity for fibril formation at pH7. Amyloidogenicity was relatively static after 24 hours incubation in relation to 120 hour incubated samples, indicating that maximum aggregation was likely to have occurred.

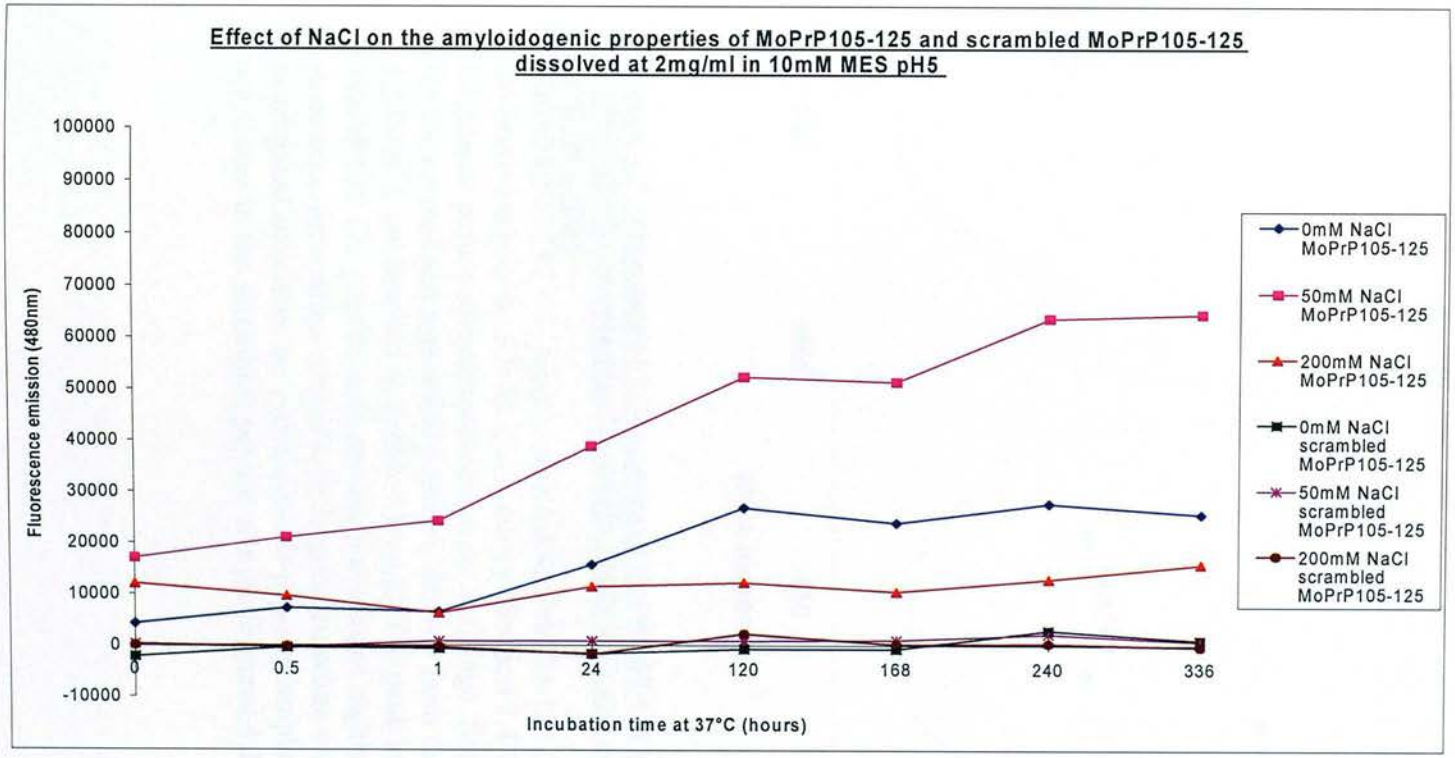

Figure 4.6 **Thioflavin-T binding of MoPrP105-125 and scrambled MoPrP105-125**

Thioflavin-T stock in water (2mM) was diluted in the appropriate vehicle buffer to achieve a final Thioflavin-T concentration of 20μM. Thioflavin-T/vehicle buffer solutions were incubated with the appropriate peptide solution in that vehicle buffer and fluorescence read between 450-550nm (Section 2.4.3). The emission maxima for amyloid-bound Thioflavin T was monitored over 14 days (336 hours). Scrambled peptides dissolved in 10mM MES (pH5) at all tested NaCl concentrations did not bind to Thioflavin-T and did therefore not possess amyloidogenic properties. MoPrP105-125 amyloidogenicity is maximum at 50mM NaCl between 240-366 hours (10-14 days). 200mM NaCl solutions have an extremely low propensity to form amyloid fibrils, and solutions containing 0mM NaCl are only slightly more amyloidogenic. The propensity for fibril formation at pH5 is lower than at pH7, this process also trequires longer incubation periods than at pH7 (Figure 4.5). There was little change in amyloidogenicity between 240-336 hours (10-14 days) and it was assumed that maximum aggregation had occurred at this stage.

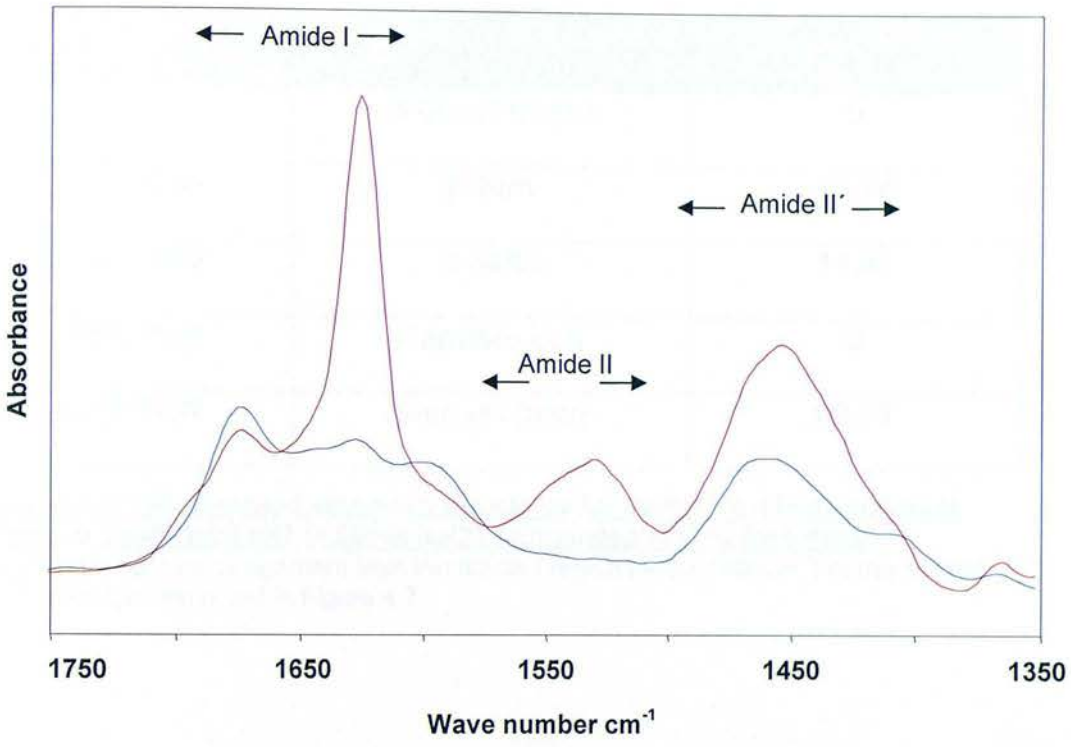

Figure 4.7 **Attenuated FT-IR spectra of MoPrP105-125 and scrambled MoPrP105-125 dissolved at 2mg/ml in 10mM MES pH7 (+ 50mM NaCl), aggregated at 37°C for 5 days**

MoPrP105-125 (—) and scrambled MoPrP105-125 (—) peptide secondary structure analysis by FT-IR spectroscopy (Section 2.4.4) were collected following a 20 minute period of hydrogen/deuterium exchange. Secondary structure assignments for the normal and scrambled peptides, derived from the amide I region (1600-1700cm^{-1}), are detailed in Tables 4.1 - 4.2. The peak in the Amide II region in the MoPrP105-125 peptide indicates the presence of highly aggregated fibrillar structures, preventing complete hydrogen/deuterium exchange (Amide II´). Such aggregated structures are present in this peptide sample (Figures 4.2.C and 4.5), and are absent in the scrambled peptide sample (Figures 4.2.D and 4.5)

Wave number cm^{-1}	Secondary structure	% secondary structure
1689-1682	β-sheet (high)	0
1662-1682	β-turn	19.74
1645-1662	α-helix	11.05
1637-1645	Random coil	0
1613-1637	β-sheet (low)	69.21

Table 4.1 **FT-IR assigned secondary structures for MoPrP105-125 dissolved at 2mg/ml in 10mM MES pH7 (+ 50mM NaCl), aggregated at 37°C for 5 days**
Secondary structure assignment from the amide I region (1600-1700cm^{-1}) of the normal MoPrP105-125 displayed in Figure 4.7

Wave number cm^{-1}	Secondary structure	% secondary structure
1689-1682	β-sheet (high)	0
1662-1682	β-turn	45.45
1645-1662	α-helix	21.94
1637-1645	Random coil	0
1613-1637	β-sheet (low)	32.61

Table 4.2 **FT-IR assigned secondary structures for scrambled MoPrP105-125 dissolved at 2mg/ml in 10mM MES pH7 (+ 50mM NaCl), aggregated at 37°C for 5 days**
Secondary structure assignment from the amide I region (1600-1700cm^{-1}) of the scrambled MoPrP105-125 displayed in Figure 4.7

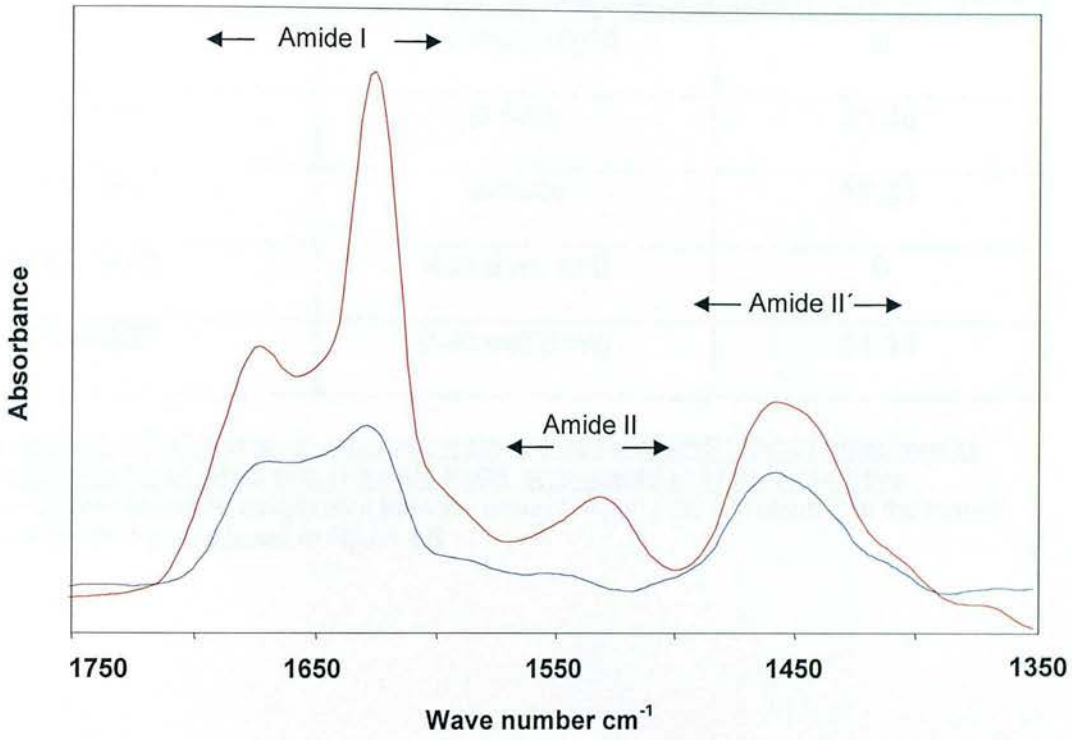

Figure 4.8 **Attenuated FT-IR spectra of MoPrP105-125 and scrambled MoPrP105-125 dissolved at 2mg/ml in 10mM MES pH5 (+ 50mM NaCl), aggregated at 37°C for 14 days**

MoPrP105-125 (——) and scrambled MoPrP105-125 (——) peptide secondary structure analysis by FT-IR spectroscopy (Section 2.4.4) were collected following a 20 minute period of hydrogen/deuterium exchange. Secondary structure assignments for the normal and scrambled peptides, derived from the amide I region (1600-1700cm^{-1}), are detailed in Tables 4.3 - 4.4. The peak in the Amide II region in the MoPrP105-125 peptide indicates the presence of highly aggregated fibrillar structures, preventing complete hydrogen/deuterium exchange (Amide II´). Such aggregated structures are present in this peptide sample (Figures 4.3.C and 4.6), and are absent in the scrambled peptide sample (Figures 4.3.D and 4.6)

Wave number cm^{-1}	Secondary structure	% secondary structure
1689-1682	β-sheet (high)	0
1662-1682	β-turn	21.38
1645-1662	α-helix	17.51
1637-1645	Random coil	0
1613-1637	β-sheet (low)	61.11

Table 4.3 **FT-IR assigned secondary structures for MoPrP105-125 dissolved at 2mg/ml in 10mM MES pH5 (+ 50mM NaCl), aggregated at 37°C for 14 days**
Secondary structure assignment from the amide I region (1600-1700cm^{-1}) of the normal MoPrP105-125 displayed in Figure 4.8

Wave number cm^{-1}	Secondary structure	% secondary structure
1689-1682	β-sheet (high)	10.96
1662-1682	β-turn	16.71
1645-1662	α-helix	19.12
1637-1645	Random coil	22.09
1613-1637	β-sheet (low)	31.12

Table 4.4 **FT-IR assigned secondary structures for scrambled MoPrP105-125 dissolved at 2mg/ml in 10mM MES pH5 (+ 50mM NaCl), aggregated at 37°C for 14 days**
Secondary structure assignment from the amide I region (1600-1700cm^{-1}) of the scrambled MoPrP105-125 displayed in Figure 4.8

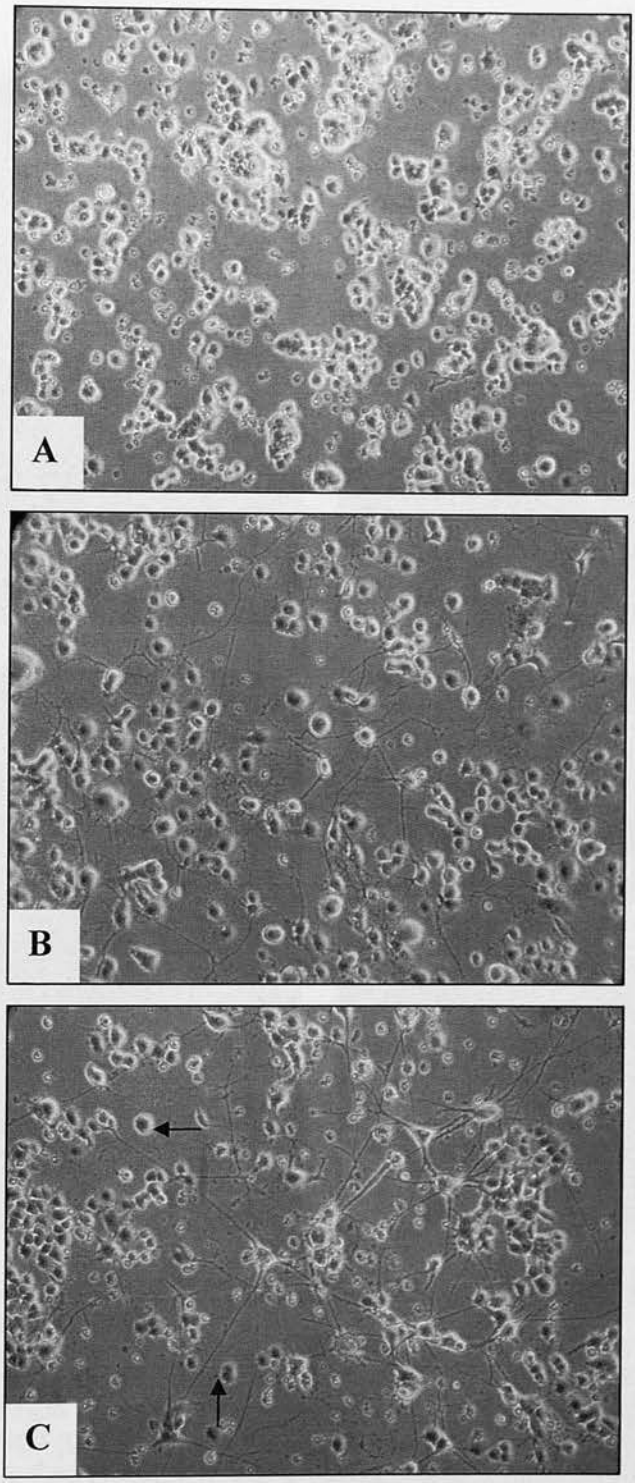

Figure 4.9 **Inverted microscopic analysis of rat pheochromocytoma PC12 cells at various stages of differentiation with nerve-growth factor**

Naive PC12 cells were grown on collagen IV coated T-25cm^2 flasks and treated with 100ng/ml of murine NGF (Section 2.5). Morphological analysis using an inverted microscope (Zeiss) was performed daily, and images of cells at various stages of differentiation were captured using a digital camera (Nikon). (A) Naive PC12 cell cultures prior to NGF treatment. Cells are round/oval in shape and tend to grow in dense clusters. (B) PC12 cells following 7 days differentiation with NGF have some dendritic processes, grow more distant from neighbouring cells and some cells have slightly larger cell bodies. (C) 14 day differentiated cells have a dense network of dendritic processes, grow more independently from clusters, and have enlarged cell bodies. The majority of cells are fully differentiated, however, some cells (⟶) do not morphologically resemble neurons

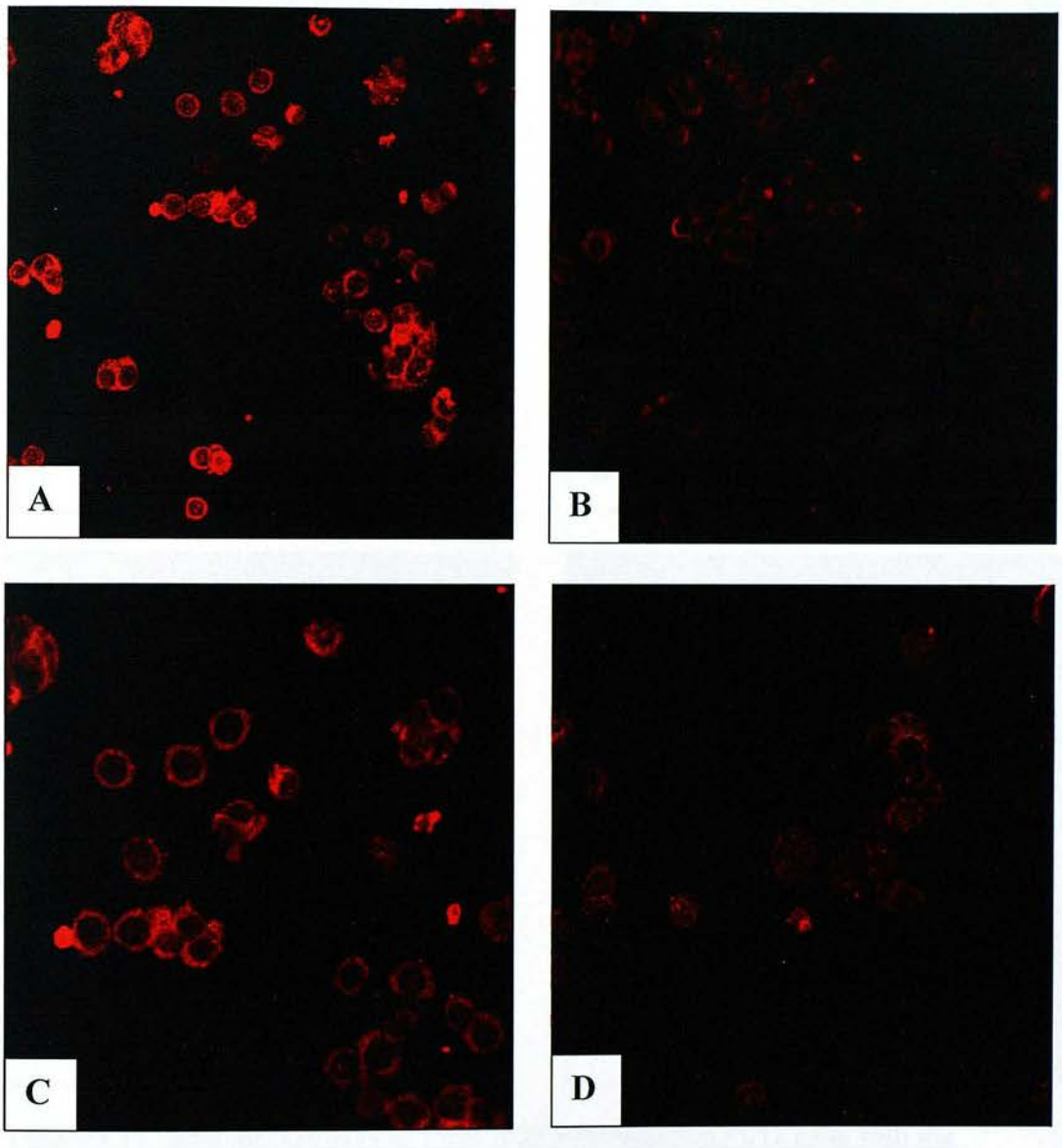

Figure 4.10 **Immunoreactivity of naive PC12 cells with the anti-PrP 8H4 monoclonal primary antibody**

Naive PC12 cells were grown on collagen IV coated coverslips (Section 2.5.2) and stained according to the described protocol (Section 2.5.8). Images were captured using the confocal microscope (Zeiss) and the Axioskop 2 camera software at magnifications of x40 (A & B) and x63 (C & D). Naive PC12 cells express PrP at low levels (A & C), which is restricted to the cytosol. B and D show the negative control samples, where 8H4 was replaced with normal mouse serum to demonstrate the specificity of the 8H4 immunoreactivity.

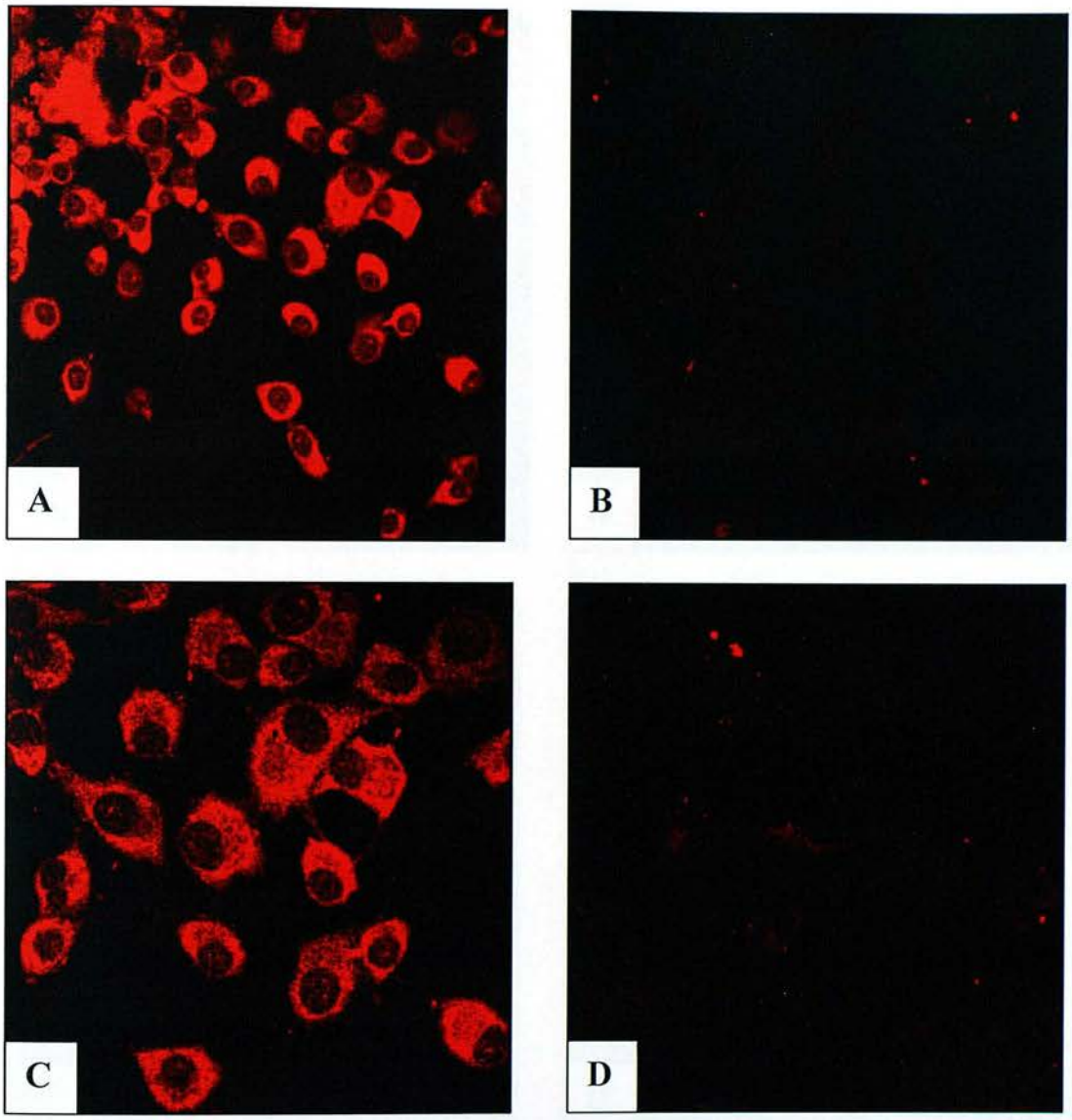

Figure 4.11 **Immunoreactivity of 7 day NGF-differentiated PC12 cells with the anti-8H4 monoclonal primary antibody**

Naive PC12 cells were grown on collagen IV coated coverslips (Section 2.5.2), cultured for 7 days (Section 2.5), and stained according to the described protocol (Section 2.5.8). Images were captured using the confocal microscope (Zeiss) and Axioskop 2 camera software at magnifications of x40 (A & B) and x63 (C & D). 7 day differentiated PC12 cells express PrP at higher levels (A & C), which is restricted to the cell body. Cell bodies of 7 day NGF-differentiated cells are larger than those of the naive cultures (Figure 4.10) and dendritic processes begin to form. B and D show the negative control samples, where 8H4 was replaced with normal mouse serum to demonstrate the specificity of the 8H4 immunoreactivity.

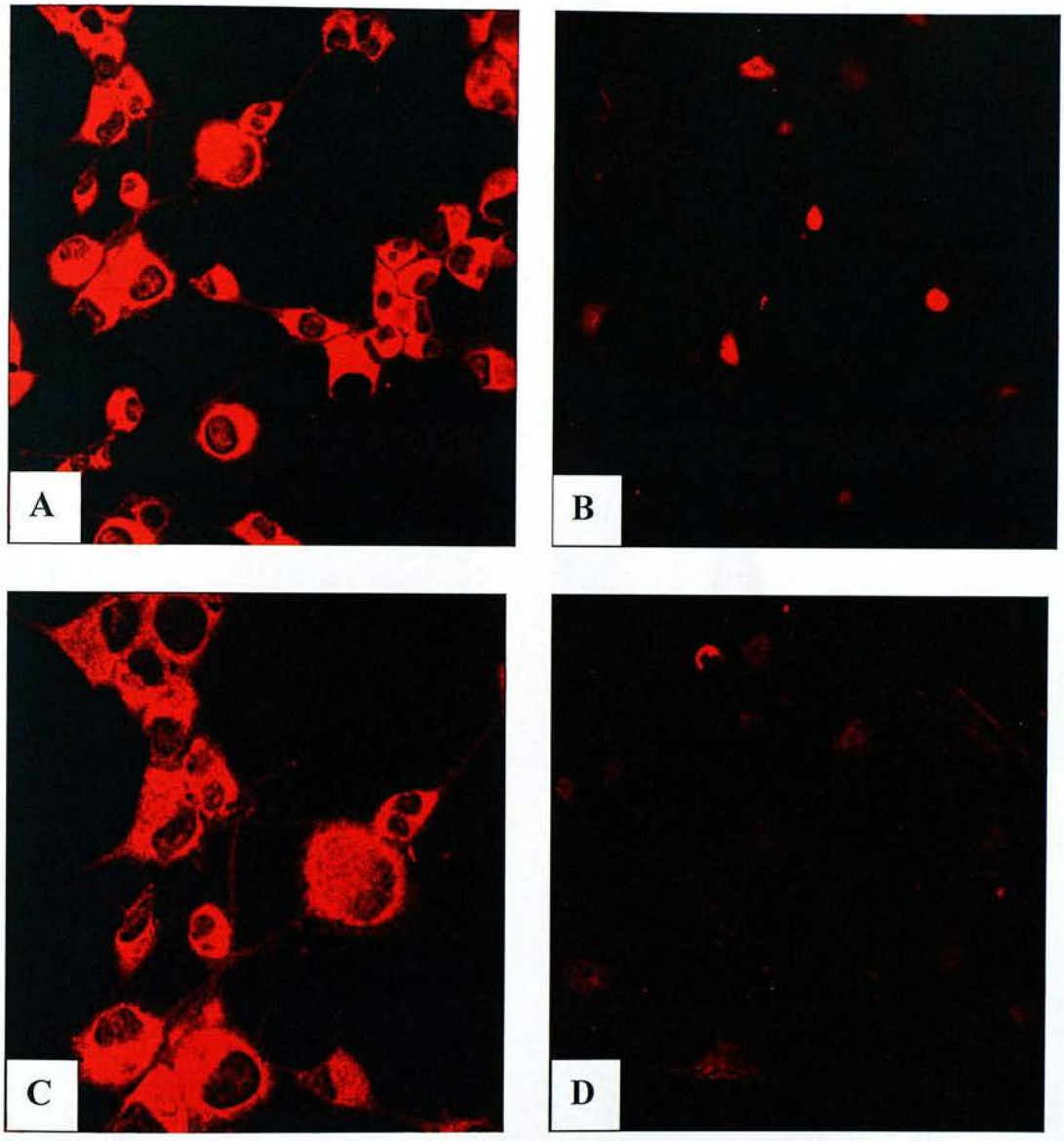

Figure 4.12 **Immunoreactivity of 14 day NGF-differentiated PC12 cells with the anti-8H4 monoclonal primary antibody**

Naive PC12 cells were grown on collagen IV coated coverslips (Section 2.5.2), cultured for 14 days (Section 2.5), and stained according to the described protocol (Section 2.5.8). Images were captured using the confocal microscope (Zeiss) and Axioskop 2 camera software at magnifications of x40 (A & B) and x63 (C & D). 14 day differentiated PC12 cells express PrP at very high levels (A & C), which is restricted to the cell body. Cell bodies of 14 day NGF-differentiated cells are even larger than those of the 7 day differentiated cultures (Figure 4.11) and have extensive dendritic processes. B and D show the negative control samples, where 8H4 was replaced with normal mouse serum to demonstrate the specificity of the 8H4 immunoreactivity.

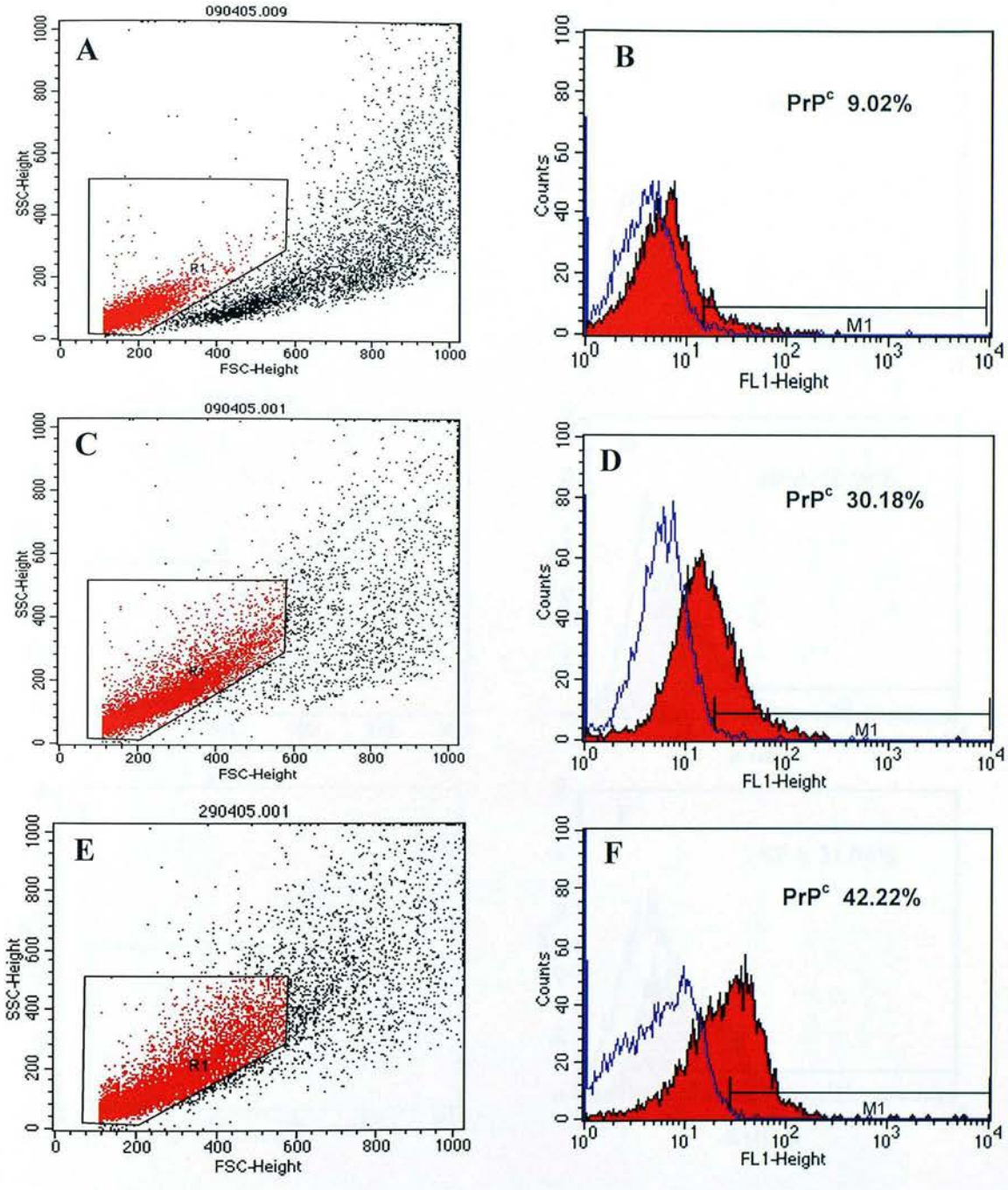

Figure 4.13 **FACS analysis for the expression of PrP^c by differentiating PC12 cells**
Naive, 7 day and 14 day differentiated PC12 cells were analysed for PrP^c expression with the 8H4 monoclonal antibody (Figure 2.1) by FACS analysis (Section 2.5.9). Cells were analysed (in quadruplicate, n=4) at the naive (A & B), 7 day NGF-differentiated (C & D), and 14 day NGF-differentiated phenotypes (E & F). Cells were gated as shown (A, C, E). Histograms for control cells, treated with secondary but no primary antibodies, are shown by an unfilled purple histogram. Cells staining positively for PrP^c are represented by the solid red coloured histograms. The mean PrP^c expression significantly increases from naive 9.02% (SEM= 0.27), 7 day 30.18% (SEM= 0.59) to 14 day 42.22% (SEM= 0.7) treated PC12 cells.

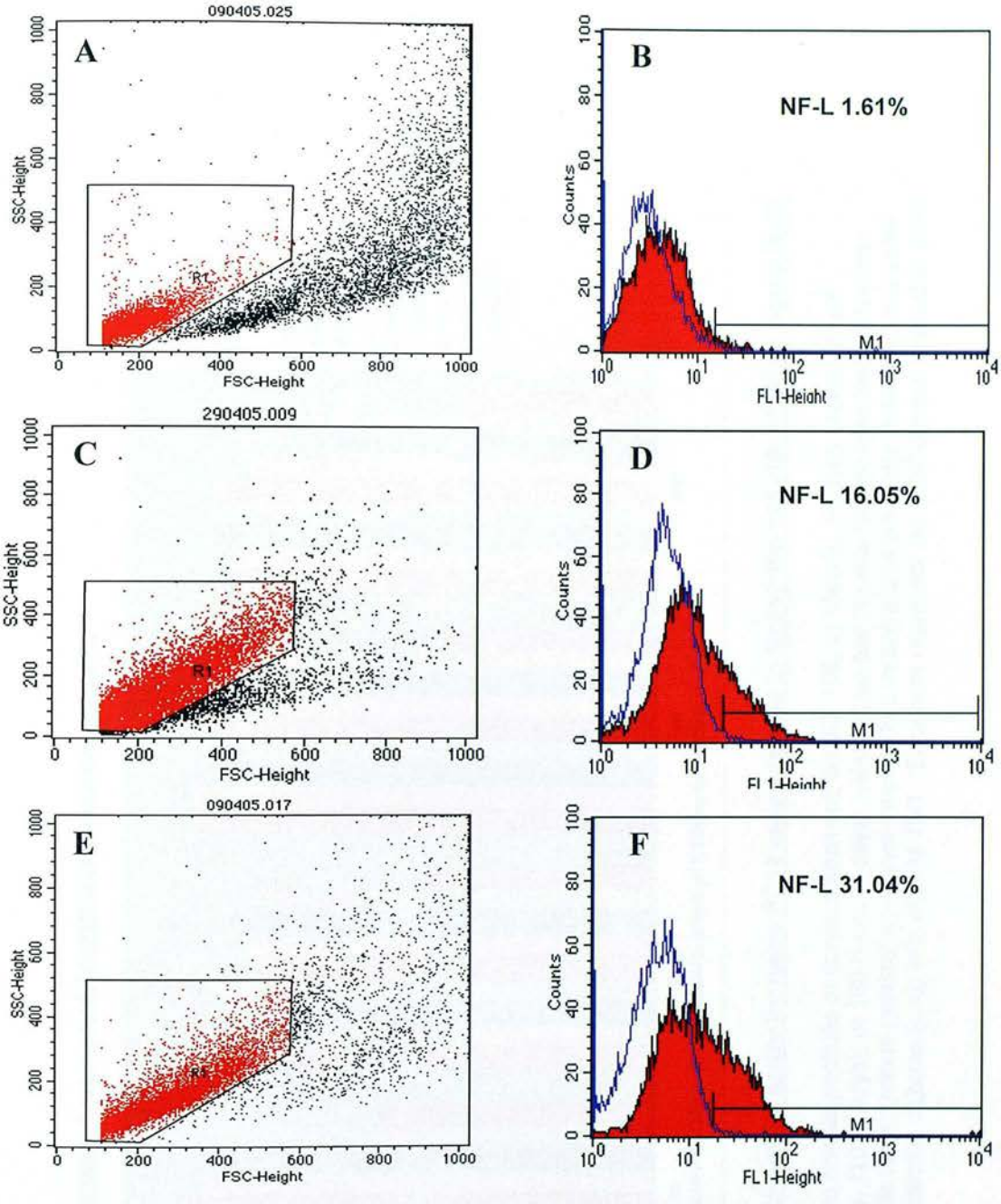

Figure 4.14 **FACS analysis for the expression of neurofilament protein by differentiating PC12 cells**

Naive, 7 day and 14 day differentiated PC12 cells were analysed for NF-L expression with the neurofilament (light sub-unit) monoclonal antibody (Figure 2.1) by FACS analysis (Section 2.5.9). Cells were analysed (in quadruplicate, n=4) at the naive (A & B), 7 day NGF-differentiated (C & D), and 14 day NGF-differentiated phenotypes (E & F). Cells were gated as shown (A, C, E). Histograms for control cells, treated with secondary but no primary antibodies, are shown by an unfilled purple histogram. Cells staining positively for NF-L are represented by the solid red coloured histograms. The mean NF-L expression significantly increases from naive 1.61% (SEM= 0.2), 7 day 16.05% (SEM= 0.76) to 14 day 31.04% (SEM= 0.33) treated PC12 cells.

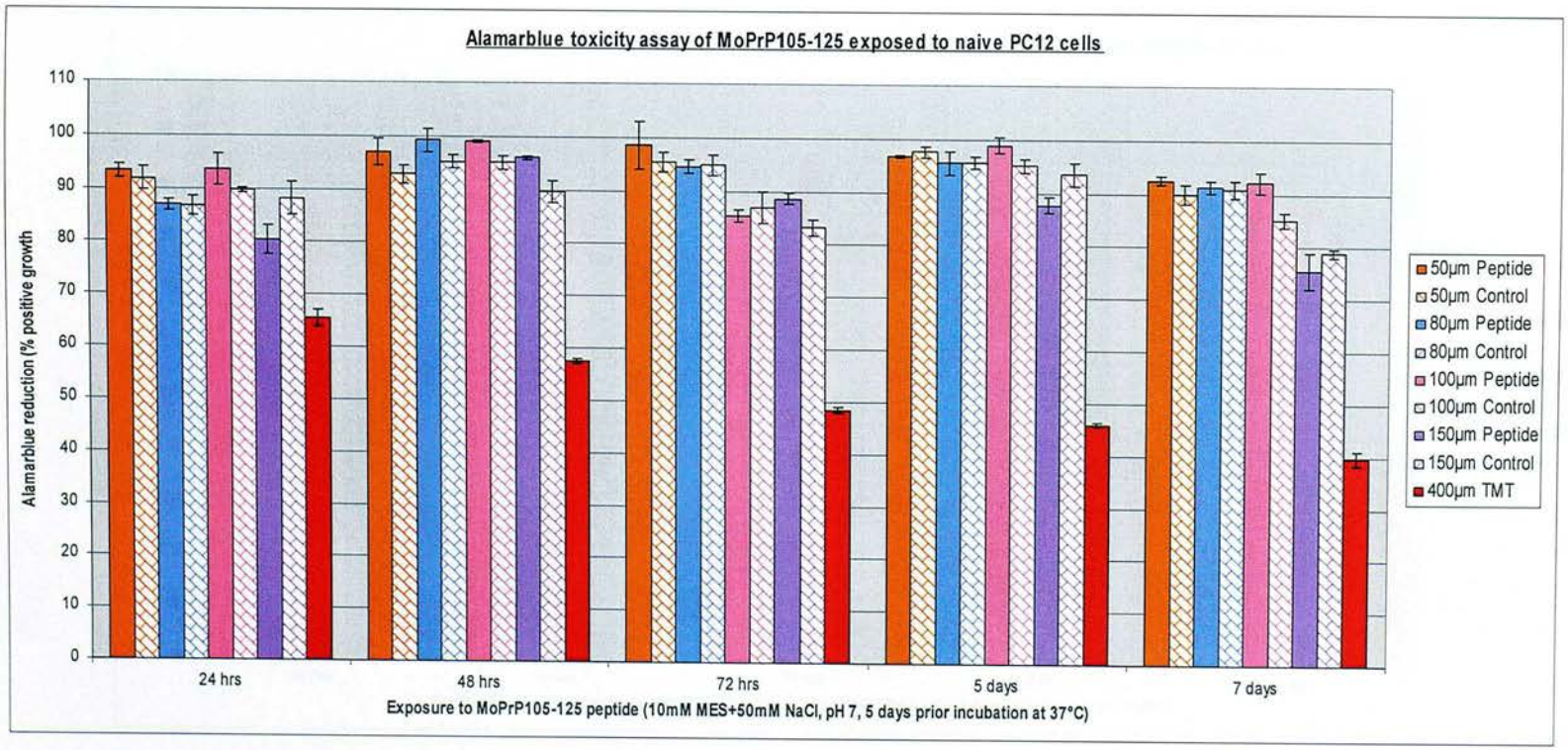

Figure 4.15 **Alamarblue reduction cytotoxicity assay for naive PC12 cells exposed to MoPrP105-125 (10mM MES+ 50mM NaCl, pH 7, 5 days prior incubation at 37°C)**

PC12 cells (800cells/well) were exposed to normal peptides at concentrations of; 50, 80, 100, or 150µM. Peptide exposure was maintained for periods of 24, 48, 72 hours, 120 (5 days), or 168 hours (7 days). Alamarblue toxicity was related to untreated control PC12 cultures (n=3). The effects of vehicle buffer (minus peptide) at equivalent peptide concentrations were also monitored and assay reproducibility was confirmed by treating parallel cultures (n=3) with 400µM TMT. Error bars represent the SEM of each population (n=3)

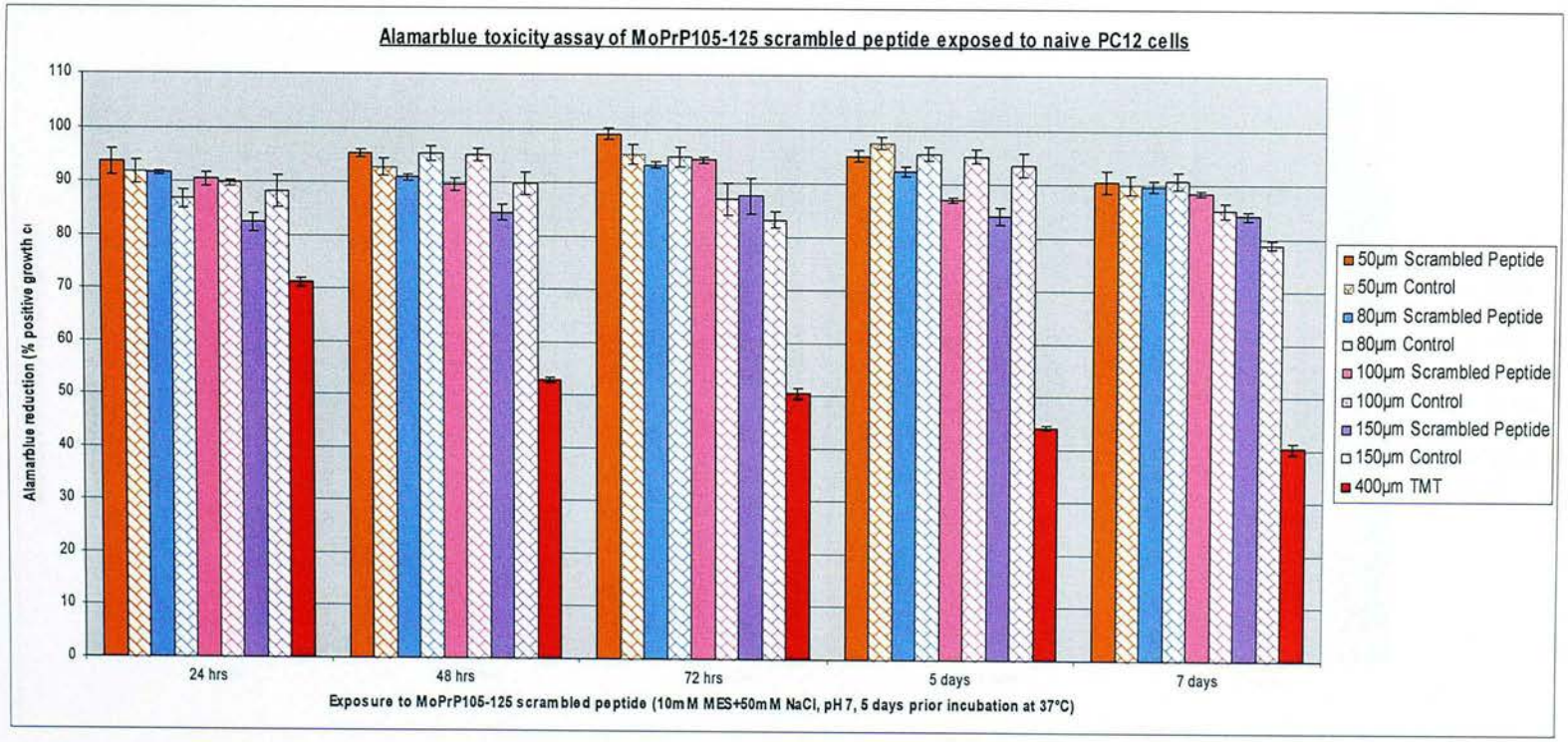

Figure 4.16 **Alamarblue reduction cytotoxicity assay for naive PC12 cells exposed to scrambled MoPrP105-125 (10mM MES+ 50mM NaCl, pH 7, 5 days prior incubation at 37°C)**

PC12 cells (800cells/well) were exposed to scrambled peptides at concentrations of; 50, 80, 100, or 150µM. Peptide exposure was maintained for periods of 24, 48, 72 hours, 120 (5 days), or 168 hours (7 days). Alamarblue toxicity was related to untreated control PC12 cultures (n=3). The effects of vehicle buffer (minus peptide) at equivalent peptide concentrations were also monitored and assay reproducibility was confirmed by treating parallel cultures (n=3) with 400µM TMT. Error bars represent the SEM of each population (n=3)

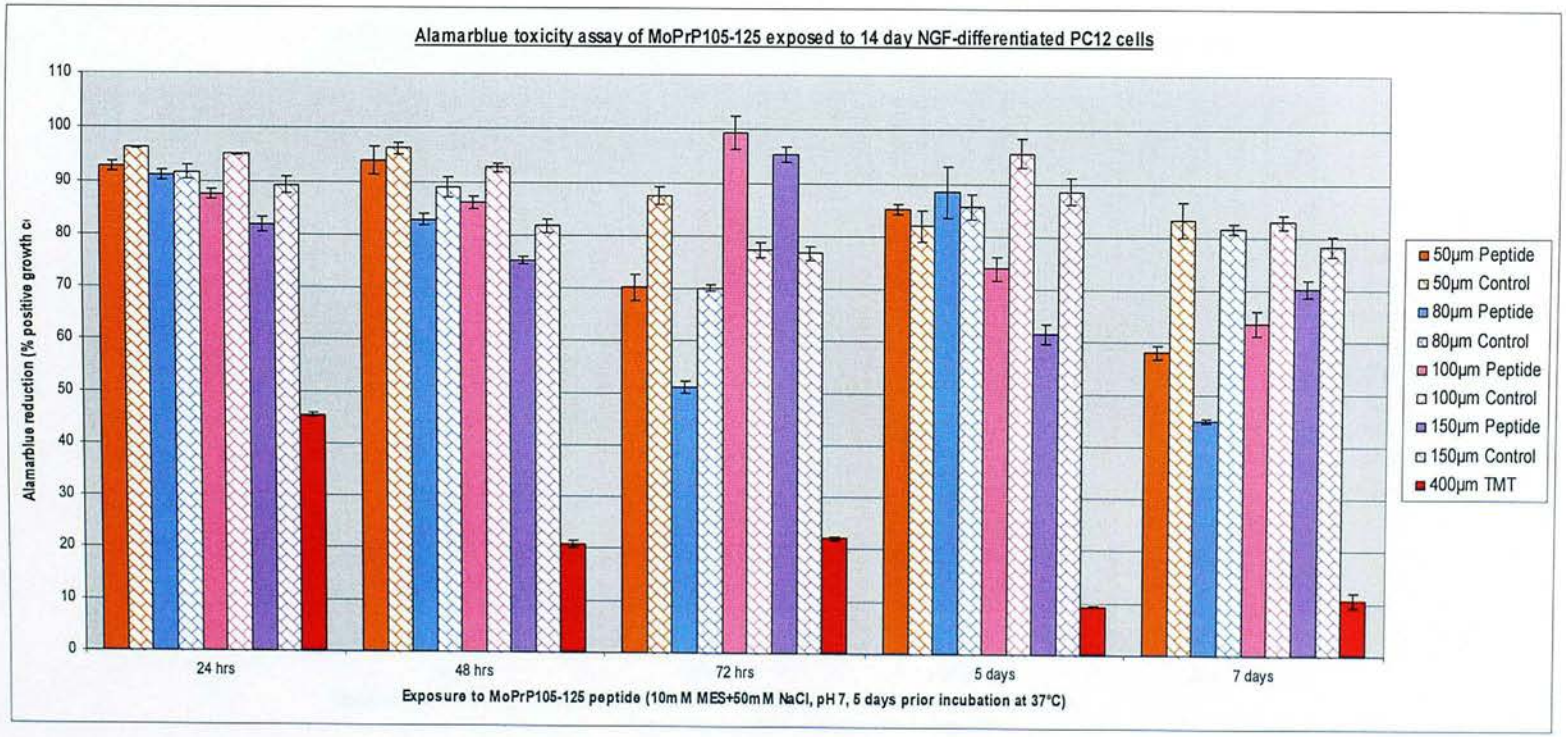

Figure 4.17 **Alamarblue reduction cytotoxicity assay for neuronal PC12 cells exposed to MoPrP105-125 (10mM MES+ 50mM NaCl, pH 7, 5 days prior incubation at 37°C)**

Peptide samples were pre-incubated at 37°C for 5 days to obtain maximal aggregation properties. 14 day NGF-differentiated PC12 cells (800cells/well) were exposed to normal peptides at concentrations of; 50, 80, 100, or 150µM. Peptide exposure was maintained for periods of 24, 48, 72 hours, 120 (5 days), or 168 hours (7 days). Alamarblue toxicity was related to untreated control PC12 cultures (n=3). The effects of vehicle buffer (minus peptide) at equivalent peptide concentrations were also monitored and assay reproducibility was confirmed by treating parallel cultures (n=3) with 400µM TMT. Error bars represent the SEM of each population (n=3)

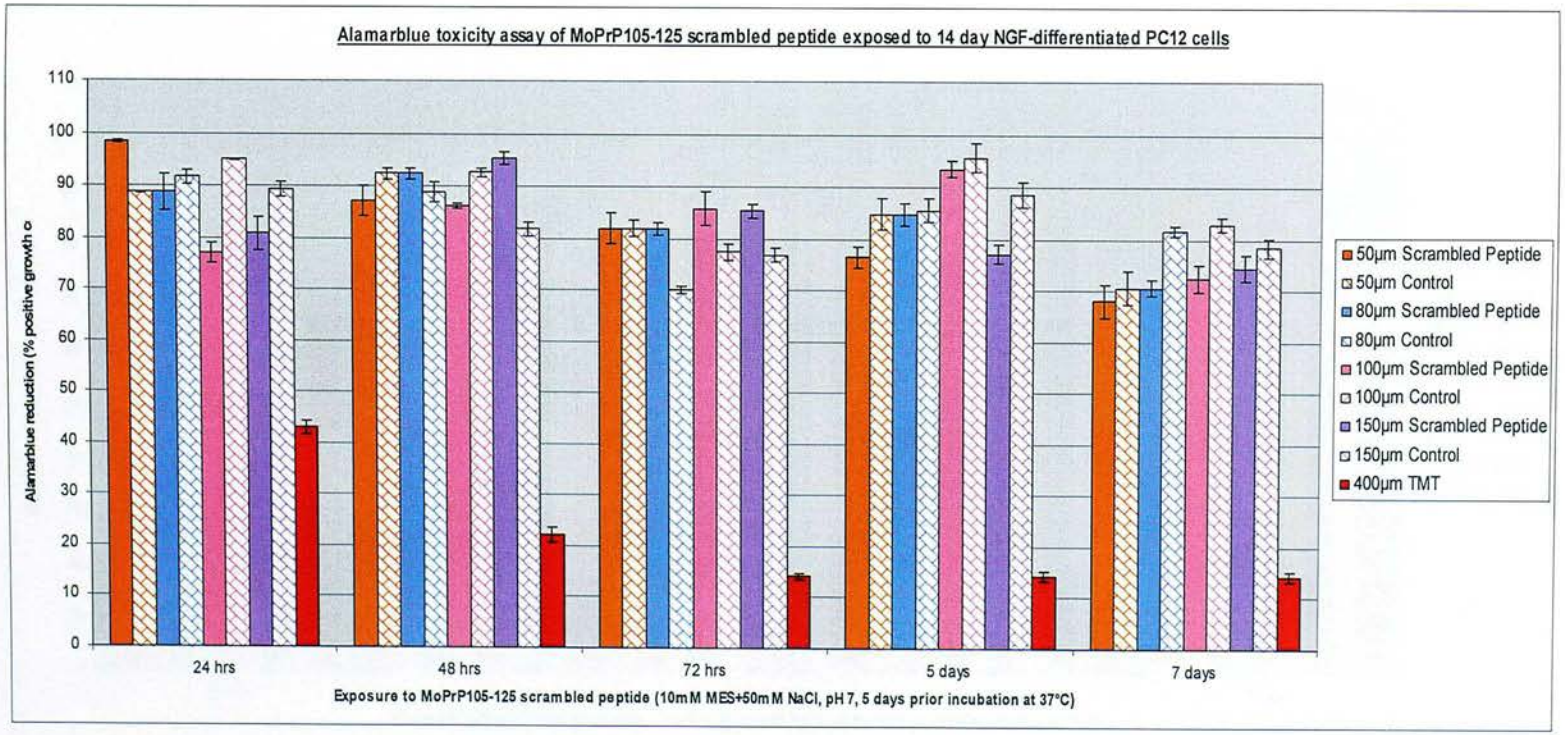

Figure 4.18 **Alamarblue reduction cytotoxicity assay for neuronal PC12 cells exposed to scrambled MoPrP105-125 (10mM MES+ 50mM NaCl, pH 7, 5 days prior incubation at 37°C)**

Peptide samples were pre-incubated at 37°C for 5 days to obtain maximal aggregation properties. 14 day NGF-differentiated PC12 cells (800cells/well) were exposed to scrambled peptides at concentrations of; 50, 80, 100, or 150µM. Peptide exposure was maintained for periods of 24, 48, 72 hours, 120 (5 days), or 168 hours (7 days). Alamarblue toxicity was related to untreated control PC12 cultures (n=3). The effects of vehicle buffer (minus peptide) at equivalent peptide concentrations were also monitored and assay reproducibility was confirmed by treating parallel cultures (n=3) with 400µM TMT. Error bars represent the SEM of each population (n=3)

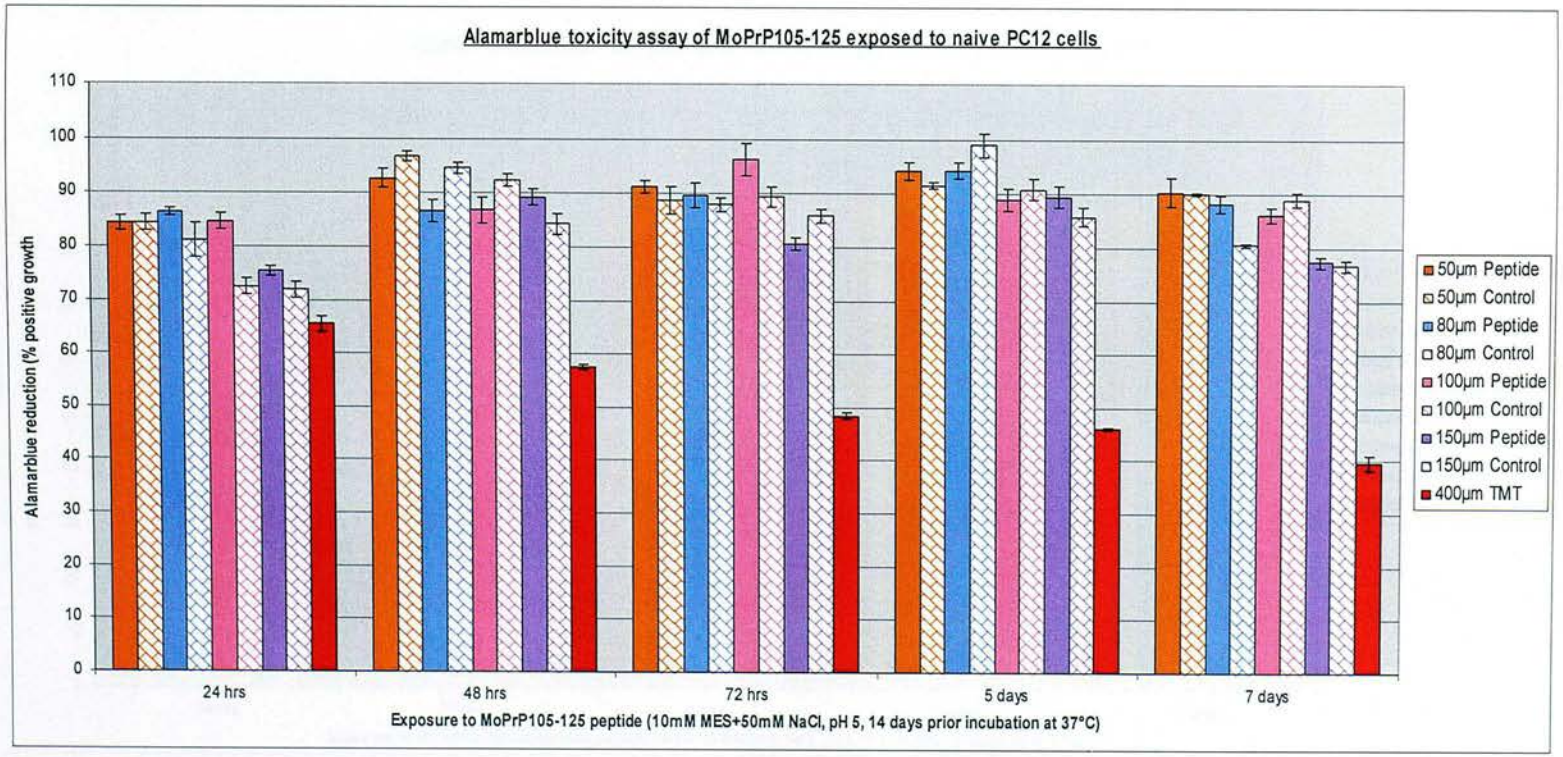

Figure 4.19 **Alamarblue reduction cytotoxicity assay for naive PC12 cells exposed to MoPrP105-125 (10mM MES+ 50mM NaCl, pH 5, 14 days prior incubation at 37°C)**

Peptide samples were pre-incubated at 37°C for 14 days to obtain maximal aggregation properties. PC12 cells (800cells/well) were exposed to normal peptides at concentrations of; 50, 80, 100, or 150µM. Peptide exposure was maintained for periods of 24, 48, 72 hours, 120 (5 days), or 168 hours (7 days). Alamarblue toxicity was related to untreated control PC12 cultures (n=3). The effects of vehicle buffer (minus peptide) at equivalent peptide concentrations were also monitored and assay reproducibility was confirmed by treating parallel cultures (n=3) with 400µM TMT. Error bars represent the SEM of each population (n=3)

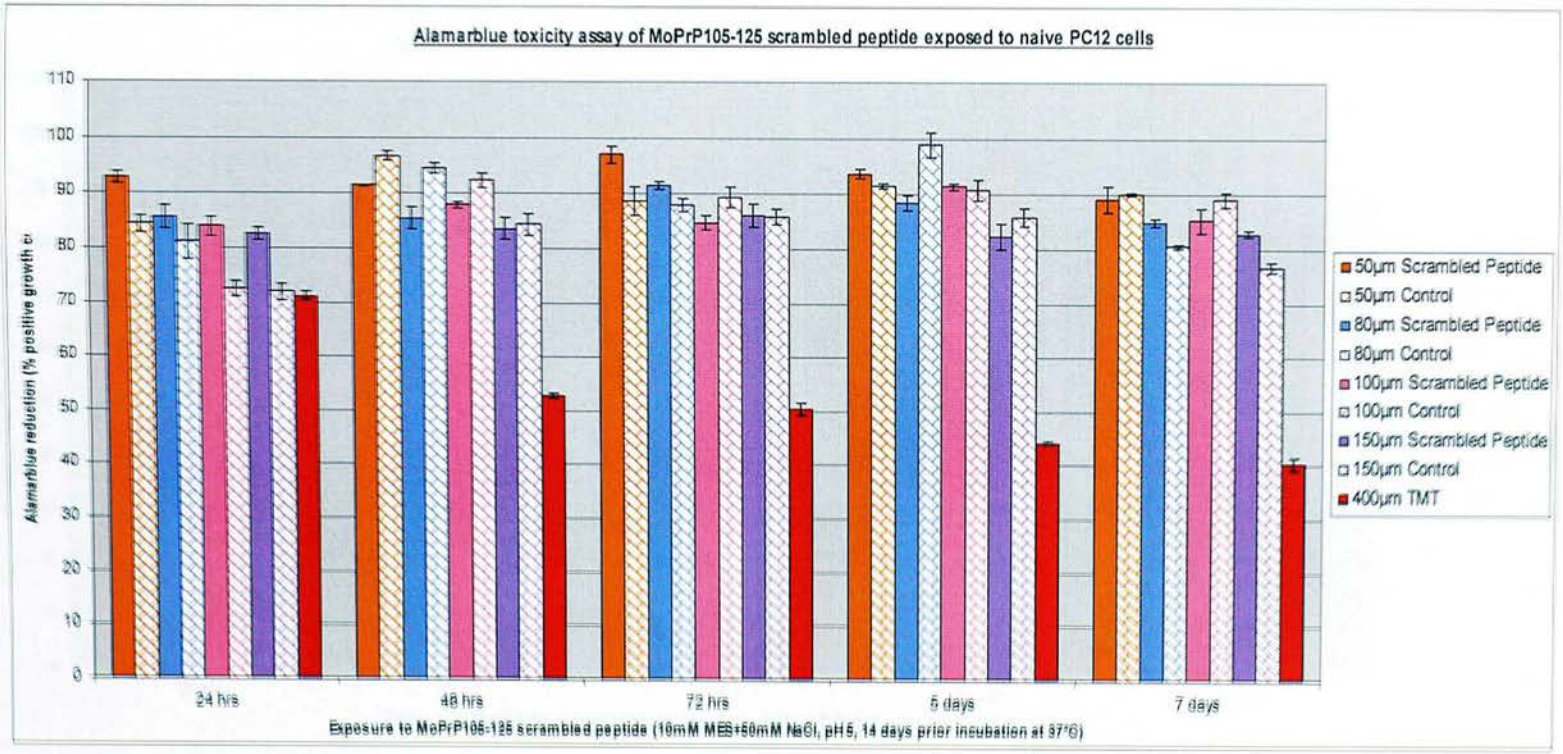

Figure 4.20 **Alamarblue reduction cytotoxicity assay for naive PC12 cells exposed to scrambled MoPrP105-125 (10mM MES+ 50mM NaCl, pH 5, 14 days prior incubation at 37°C)**

Peptide samples were pre-incubated at 37°C for 14 days to obtain maximal aggregation properties. PC12 cells (800cells/well) were exposed to scrambled peptides at concentrations of; 50, 80, 100, or 150µM. Peptide exposure was maintained for periods of 24, 48, 72 hours, 120 (5 days), or 168 hours (7 days). Alamarblue toxicity was related to untreated control PC12 cultures (n=3). The effects of vehicle buffer (minus peptide) at equivalent peptide concentrations were also monitored and assay reproducibility was confirmed by treating parallel cultures (n=3) with 400µM TMT. Error bars represent the SEM of each population (n=3)

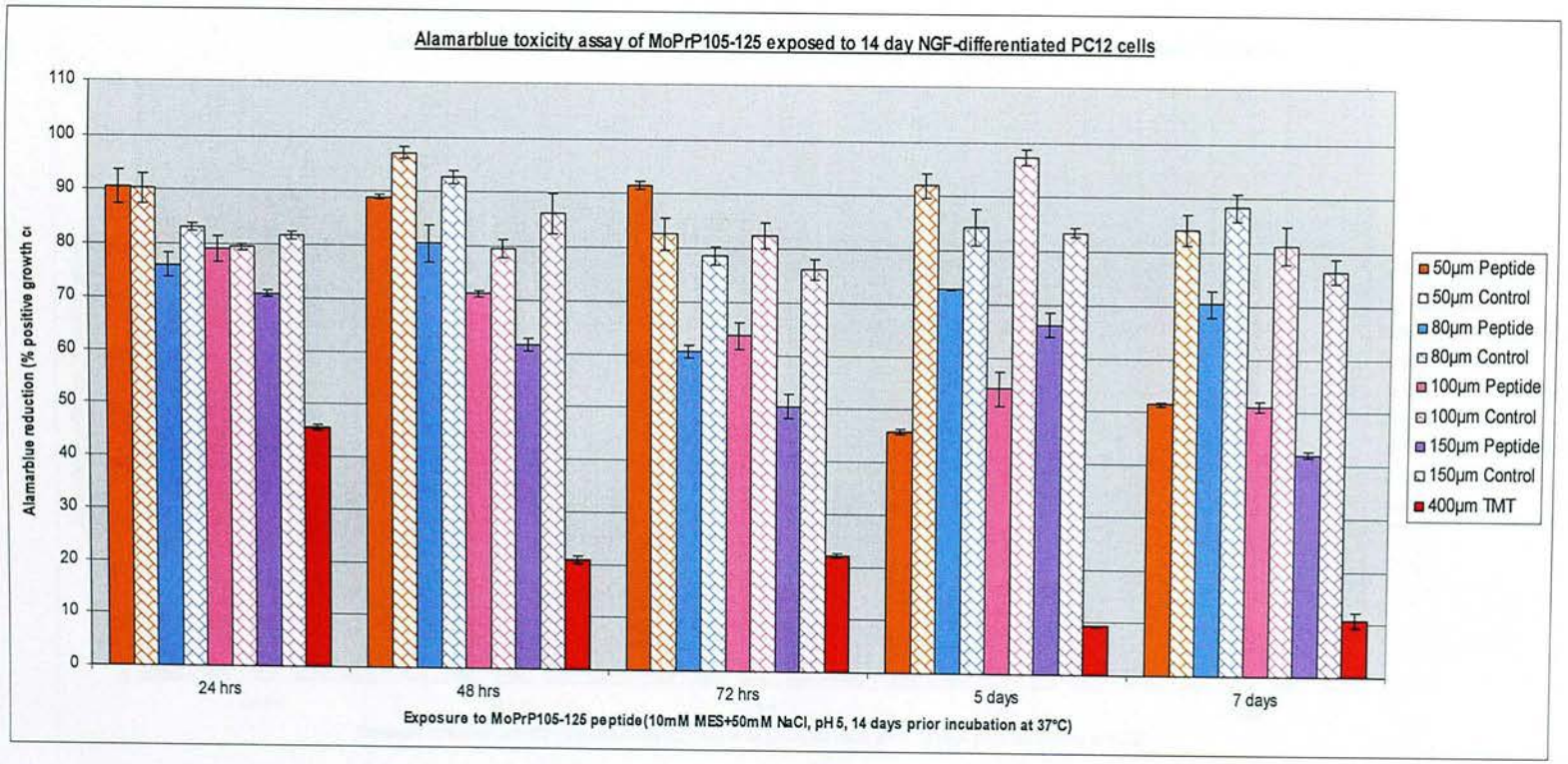

Figure 4.21 **Alamarblue reduction cytotoxicity assay for neuronal PC12 cells exposed to MoPrP105-125 (10mM MES+ 50mM NaCl, pH 5, 14 days prior incubation at 37°C)**

Peptide samples were pre-incubated at 37°C for 14 days to obtain maximal aggregation properties. 14 day NGF-differentiated PC12 cells (800cells/well) were exposed to normal peptides at concentrations of; 50, 80, 100, or 150µM. Peptide exposure was maintained for periods of 24, 48, 72 hours, 120 (5 days), or 168 hours (7 days). Alamarblue toxicity was related to untreated control PC12 cultures (n=3). The effects of vehicle buffer (minus peptide) at equivalent peptide concentrations were also monitored and assay reproducibility was confirmed by treating parallel cultures (n=3) with 400µM TMT. Error bars represent the SEM of each population (n=3)

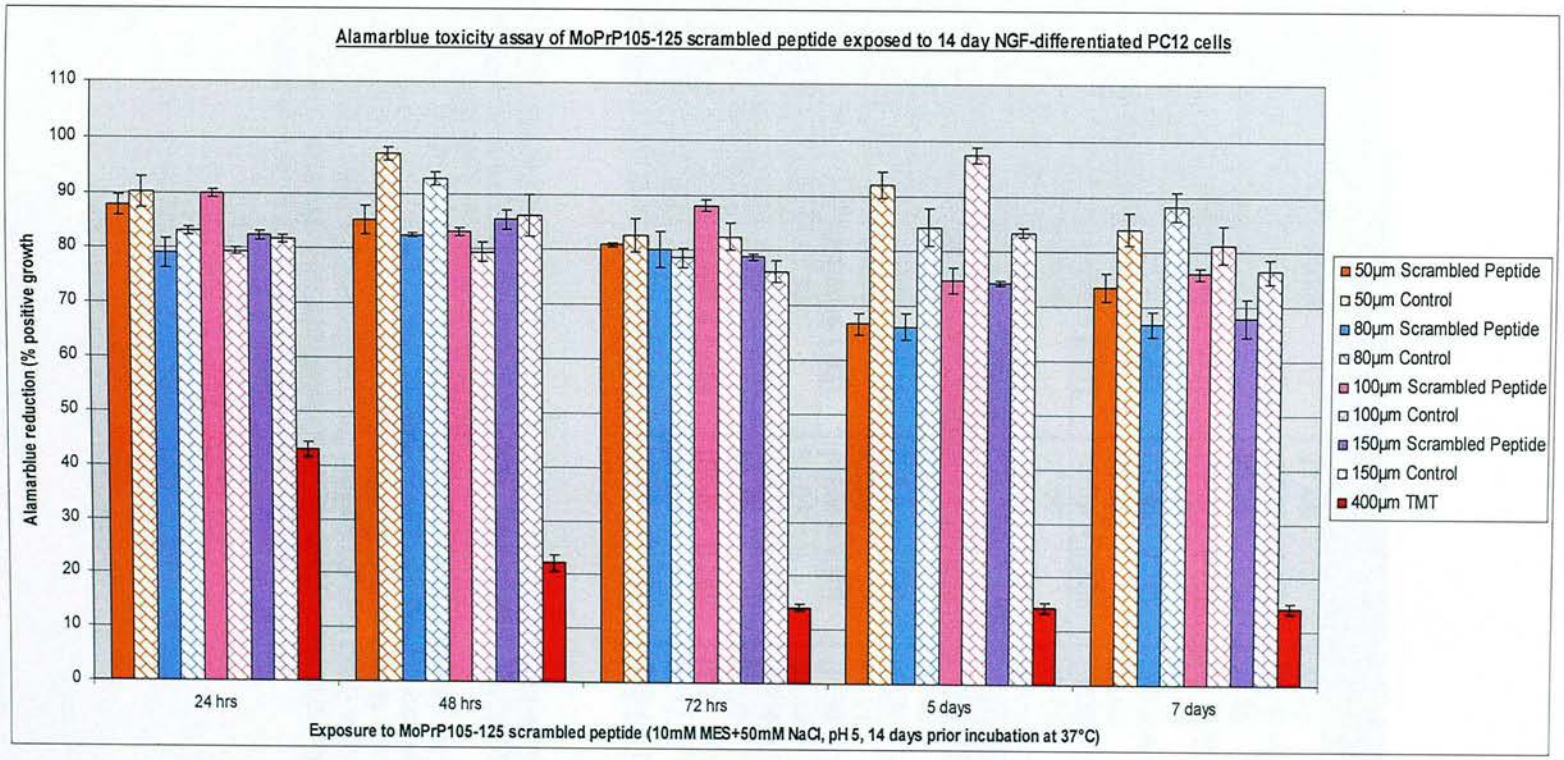

Figure 4.22 **Alamarblue reduction cytotoxicity assay for neuronal PC12 cells exposed to scrambled MoPrP105-125 (10mM MES+ 50mM NaCl, pH 5, 14 days prior incubation at 37°C)**

Peptide samples were pre-incubated at 37°C for 14 days to obtain maximal aggregation properties. 14 day NGF-differentiated PC12 cells (800cells/well) were exposed to scrambled peptides at concentrations of; 50, 80, 100, or 150µM. Peptide exposure was maintained for periods of 24, 48, 72 hours, 120 (5 days), or 168 hours (7 days). Alamarblue toxicity was related to untreated control PC12 cultures (n=3). The effects of vehicle buffer (minus peptide) at equivalent peptide concentrations were also monitored and assay reproducibility was confirmed by treating parallel cultures (n=3) with 400µM TMT. Error bars represent the SEM of each

Naive PC12 cells	% Reduction 24 hours	% Reduction 48 hours	% Reduction 72 hours	% Reduction 5 days	% Reduction 7 days
50µM MoPrP105-125	93.26 (SEM = 1.27)	97.00 (SEM = 2.47)	98.48 (SEM = 4.40)	96.84 (SEM = 0.25)	92.53 (SEM = 0.85)
80µM MoPrP105-125	86.93 (SEM = 1.01)	99.21 (SEM = 2.15)	94.59 (SEM = 1.16)	95.59 (SEM = 2.16)	91.32 (SEM = 1.22)
100µM MoPrP105-125	93.64 (SEM = 2.95)	98.97 (SEM = 0.20)	85.44 (SEM = 1.14)	98.93 (SEM = 1.44)	92.13 (SEM = 1.95)
150µM MoPrP105-125	80.38 (SEM = 2.71)	95.97 (SEM = 0.38)	88.60 (SEM = 1.01)	87.73 (SEM = 1.45)	75.46 (SEM = 3.40)
400µM TMT	64.45 (SEM = 1.58)	57.50 (SEM = 0.46)	48.46 (SEM = 0.61)	45.98 (SEM = 0.25)	39.68 (SEM = 1.43)
Differentiated PC12 cells	% Reduction 24 hours	% Reduction 48 hours	% Reduction 72 hours	% Reduction 5 days	% Reduction 7 days
50µM MoPrP105-125	92.69 (SEM = 0.91)	93.91 (SEM = 2.56)	70.16 (SEM = 2.45)	85.09 (SEM = 0.90)	58.15 (SEM = 1.32)
80µM MoPrP105-125	91.11 (SEM = 1.02)	82.84 (SEM = 1.10)	51.11 (SEM = 1.19)	88.39 (SEM = 4.82)	44.92 (SEM = 0.39)
100µM MoPrP105-125	87.53 (SEM = 0.84)	86.01 (SEM = 1.18)	99.43 (SEM = 3.10)	74.01 (SEM = 2.23)	63.67 (SEM = 2.32)
150µM MoPrP105-125	81.78 (SEM = 1.45)	75.17 (SEM = 0.75)	95.37 (SEM = 1.49)	61.51 (SEM = 1.95)	70.25 (SEM = 1.59)
400µM TMT	45.53 (SEM = 0.41)	20.87 (SEM = 0.69)	22.16 (SEM = 0.42)	9.34 (SEM = 0.12)	10.68 (SEM = 1.44)

Table 4.5 **Summary of mean % Alamarblue reduction compared to positive growth controls for naive and 14 day differentiated PC12 cells, treated with MoPrP105-125 (10mM MES+ 50mM NaCl, pH 7, 5 days prior incubation at 37°C)**

PC12 cells (800cells/well) (n=3), naive or differentiated with NGF for 14 days, were exposed to normal peptides at concentrations of; 50, 80, 100, or 150µM. Peptide exposure was maintained for periods of 24, 48, 72 hours, 5 or 7 days. Alamarblue toxicity was related to untreated control PC12 cultures (n=3). Reproducibility was confirmed by treating parallel cultures (n=3) with 400µM TMT. The reduction of Alamarblue is expressed as a percentage of the growth control (untreated, n=3) PC12 cells to monitor the toxixtiy of normal peptides to tested cell cultures.

Naive PC12 cells	% Reduction 24 hours	% Reduction 48 hours	% Reduction 72 hours	% Reduction 5 days	% Reduction 7 days
50µM MoPrP105-125	84.42 (SEM = 1.36)	92.69 (SEM = 1.71)	91.31 (SEM = 1.14)	94.19 (SEM = 1.60)	90.34 (SEM = 2.62)
80µM MoPrP105-125	86.40 (SEM = 1.27)	86.61 (SEM = 2.03)	89.59 (SEM = 2.33)	94.30 (SEM = 1.49)	88.28 (SEM = 1.61)
100µM MoPrP105-125	84.65 (SEM = 1.46)	86.81 (SEM = 2.40)	96.27 (SEM = 2.96)	88.92 (SEM = 1.98)	86.15 (SEM = 1.31)
150µM MoPrP105-125	75.35 (SEM = 0.89)	89.22 (SEM = 1.55)	80.68 (SEM = 1.14)	89.44 (SEM = 1.99)	77.39 (SEM = 1.09)
400µM TMT	64.45 (SEM = 1.58)	57.50 (SEM = 0.46)	48.46 (SEM = 0.61)	45.98 (SEM = 0.25)	39.68 (SEM = 1.43)
Differentiated PC12 cells	% Reduction 24 hours	% Reduction 48 hours	% Reduction 72 hours	% Reduction 5 days	% Reduction 7 days
50µM MoPrP105-125	90.54 (SEM = 3.14)	88.99 (SEM = 0.42)	91.47 (SEM = 0.70)	45.84 (SEM = 0.46)	51.47 (SEM = 0.34)
80µM MoPrP105-125	76.07 (SEM = 2.20)	80.41 (SEM = 3.44)	60.65 (SEM = 1.24)	72.76 (SEM = 0.21)	70.42 (SEM = 2.51)
100µM MoPrP105-125	79.11 (SEM = 2.40)	71.07 (SEM = 0.64)	63.67 (SEM = 2.54)	54.05 (SEM = 3.19)	51.03 (SEM = 0.95)
150µM MoPrP105-125	70.73 (SEM = 0.60)	61.56 (SEM = 1.15)	50.37 (SEM = 2.30)	66.21 (SEM = 2.28)	42.02 (SEM = 0.54)
400µM TMT	45.53 (SEM = 0.41)	20.87 (SEM = 0.69)	22.16 (SEM = 0.42)	9.34 (SEM = 0.12)	10.68 (SEM = 1.44)

Table 4.6 **Summary of mean % Alamarblue reduction compared to positive growth controls for naive and 14 day differentiated PC12 cells, treated with MoPrP105-125 (10mM MES+ 50mM NaCl, pH 5, 14 days prior incubation at 37°C)**

PC12 cells (800cells/well) (n=3), naive or differentiated with NGF for 14 days, were exposed to normal peptides at concentrations of; 50, 80, 100, or 150µM. Peptide exposure was maintained for periods of 24, 48, 72 hours, 5 or 7 days. Alamarblue toxicity was related to untreated control PC12 cultures (n=3). Reproducibility was confirmed by treating parallel cultures (n=3) with 400µM TMT. The reduction of Alamarblue is expressed as a percentage of the growth control (untreated, n=3) PC12 cells to monitor the toxixtiy of normal peptides to tested cell cultures.

4.4. Discussion

The misfolding of proteins into insoluble aggregates is associated with a number of neurodegenerative diseases, including TSEs, Alzheimer's, Huntington's, and Parkinson's diseases. These insoluble aggregates are formed from disruptions to the normal tertiary structure, resulting in the exposure of normally buried hydrophobic regions of the protein and a toxic gain of function of the misfolded proteins (Muchowski 2002). These hydrophobic regions (such as the AGAAAAGA palindrome sequence found within the PrP106-126 peptide) then interact with similar hydrophobic regions to form fibrillar structures. These fibrillar structures range from short protofibrillar structures, to mature amyloid plaques observed in Alzheimer's disease and some of the TSE infections. Misfolded aggregates are characterised by a high content of β–sheet structure, and the binding to histopathologic dyes such as Thioflavin-T and Congo red.

Neuronal cultures exposed to synthetic PrP peptides have been developed to model, *in vitro*, TSE-mediated neurodegeneration. Of particular interest is the PrP106-126 peptide, corresponding to the most highly conserved portion of the PrP protein, found within the 7 kDa peptides (amino acids 81-150) isolated *in vivo* from GSS amyloid plaques (Tagliavini *et al.* 2001). The PrP106-126 peptide contains the hydrophobic palindrome sequence (AGAAAAGA) thought to be important not only for the conversion of PrP^{c} to PrP^{sc} (Muramoto *et al.* 1996; Norstrom & Mastrianni 2005), but also for conferring the toxic properties of the synthetic peptide (Jobling *et al.* 1999). The synthetic peptide was found to be neurotoxic following exposures to rat hippocampal cultures (Forloni *et al.* 1993). Furthermore, the peptide shares many of the biochemical and physical properties of PrP^{sc}. Peptide aggregates exhibit the

birefringence of amyloid deposits when bound to Thioflavin-T or Congo red, have partial resistance to proteinase-K digestion (Selvaggini *et al.* 1993), require the neuronal expression of PrP^c for neurotoxicity (Brown *et al.* 1994; Brown *et al.* 1996), have a high β–sheet content (Selvaggini *et al.* 1993; De Gioia *et al.* 1994), and stimulate astrocytes and microglial cells (Forloni *et al.* 1994; Brown *et al.* 1996). The PrP106-126 peptide represents the minimal amino acid sequence capable of replicating the properties of PrP^{sc} *in vitro,* and is also more practical for research purposes due to the insoluble nature of PrP^{sc} isolated *in vivo*. The homologous sequence of this peptide in mice, PrP105-125, was synthesised to establish a model of neurodegeneration and also to remove potential species barrier effects in this model. This is because this sequence is identical between MoPrP105-125 and rat PC12 cells, whereas the human PrP106-126 differs by two amino acids (Appendix I). As it is well known that even a single amino acid difference can dramatically alter the susceptibility to infection with TSEs *in vivo* (Hsiao *et al.* 1990; Manson *et al.* 1999), this peptide sequence represents a better *in vitro* model of neurodegeneration. The long incubation periods of the TSE diseases, and the difficulties in identifying apoptosis *in vivo* (as discussed in Section 3), reiterate the importance of establishing such an *in vitro* model to clarify the as yet unknown mechanisms of neuronal loss in these fatal diseases.

4.4.1 Secondary structure of MoPrP105-125 is influenced by pH, NaCl concentration and aggregation time

The secondary structural properties, including β–sheet content, of HuPrP106-126 are hugely influenced by a number of factors including solvent composition, ionic strength, pH, the presence of membranes and mutations to specific amino acids (Section 4.2.1.). The mouse sequence differs by two amino acids to the homologous sequence of the human PrP106-126 peptide (Appendix I). These amino acids differences (in place of methionine in the human sequence) are leucine and valine at positions 108 and 111 respectively. These amino acids only moderately increase the hydrophobicity of the mouse peptide (hydroplot analysis; http://www.innovagen.se/custom-peptide-synthesis/peptide-property-calculator/peptide-property-calculator.asp) in comparison to the human sequence, as these amino acids are also non-polar and non-charged like methionine. Therefore, the factors which influence the human peptide were expected to similarly affect the secondary structure of the homologous MoPrP105-125 peptide. Prior to testing the neurotoxic properties of the MoPrP105-125 in the PC12 cell culture system, I felt that the detailed analysis of the secondary structures in each buffer must be performed. The main objective was to create peptide solutions containing a large proportion of β–sheet and with altered fibrillar morphologies. This was because the secondary structure of PrP^{sc} consists of a large proportion of β–sheet (43%), in comparison to PrP^{c} which has a low proportion of β–sheet (3%) (Caughey *et al.* 1991; Safar *et al.* 1993). Also, *in vitro* studies had previously correlated the toxicity of PrP106-126 with β–sheet content (Forloni *et al.* 1993; Brown *et al.* 1998) and the morphologies of fibrillar structures may alter the toxicity of these peptide solutions.

Initial experiments analysed the propensity of the MoPrP105-125 and scrambled equivalents to form fibrils in the presence of different buffers. This amyloidogenicity was monitored by binding to Thioflavin-T and morphologically by EM analysis. Amyloid fibrils bind to Thioflavin-T (and Congo red) in a mechanism that is specific, but poorly understood. It has recently been proposed that Thioflavin-T binding occurs along alternate residues on the alternate sides of the β-sheet (i.e. channels) of amyloid fibrils (Krebs *et al.* 2005). This binding is thought to maintain Thioflavin-T in a short flat structure when in close proximity to such tightly packed β–sheet structures present within amyloid fibrils. The EM images of the scrambled peptide samples represent the small amounts of amorphous aggregates that were actually present on the EM grids (Figures 4.2/4.3). Thioflavin-T analysis (Figures 4.4-4.6) revealed that these structures formed from the scrambled peptide were non-fibrillar and are not discussed further in this section.

The ability of the normal peptide to form amyloid fibrils was in the order: 200mM citrate pH 7 < 10mM MES pH 7 < distilled water, as analysed by Thioflavin-T binding. EM analysis revealed that the normal peptides formed distinctly different fibrillar structures in all buffers. FTIR was the only technology available for the secondary structure analysis; however, it was apparent that the citrate buffer was incompatible with the FTIR due to the presence of strong carbonyl bonds. Further research concentrated on the 10mM MES buffer, altering the secondary structures by changing the pH (5 & 7), NaCl and incubation time. Initial studies using the citrate, MES buffers and distilled water were analysed over a 48 hour period. Aggregation periods for this additional research were extended for periods up to 14 days. Additionally; salt concentration is known to affect the morphology of PrP fibrils

(Apetri & Surewicz 2003), therefore a range of NaCl concentrations was applied to each of the murine peptide samples. In summary, the MoPrP105-125 peptide was dissolved in 10mM MES at pH7 or pH5 (containing 0, 50, or 200mM NaCl) and incubated at 37°C.

Thioflavin-T binding revealed that regardless of the NaCl concentration, the samples dissolved at pH 7 were much more aggregated than equivalent samples dissolved at pH 5. Maximum aggregation occurred much more quickly at pH 7 (5 days, Figure 4.5) than at pH 5 (14 days, Figure 4.6). At pH 7, salt concentrations of 0mM had the lowest propensity to form fibrils but these levels were similar to the maximum aggregation which was obtained at pH 5 when supplemented with 50mM NaCl. Salt concentrations of 50mM NaCl were found to maximise the formation of fibrils in both of the tested pH environments, therefore highlighting the importance of ionic strength in influencing the aggregation state. The slow aggregation of the peptide dissolved at pH 5 therefore represents an opportunity for future research to isolate soluble protofibrils, which are now believed to be more toxic than mature insoluble aggregated fibrils (discussed in Section 4.4.4.). This research therefore shows that the ability of the murine PrP105-125 peptide sequence is greatly influenced by differences of pH within the same buffer conditions. The differences attributed to these differences in pH can be modified further by altering the salt concentration and aggregation period. These factors were also found to modify the morphology of the mature aggregated fibrils. Generally, fibrils formed in the presence of increasing NaCl concentration (in both tested pH environments) were found to be less dense and less compact than samples lacking NaCl. These findings are in strong agreement with a recent report which noted similar morphologies of recPrP in MES buffer when

incubated with increasing NaCl concentrations (Kazlauskaite *et al.* 2005). For the research of this thesis; fibrils formed at pH 7 were all found to be straight, although fibril morphology was altered with different NaCl concentrations. At 0mM NaCl; fibrils were long, straight and present in dense layers. Fibrils formed at 50mM NaCl were distinctly longer, although appeared shorter when incubated with 200mM NaCl. Fibrils formed from incubating the peptide at pH 5 were straight, however, slight curving of fibrils was observed at concentrations of 50mM and 200mM NaCl and fibrils appeared to slightly increase in length with increasing NaCl concentration. Based on the highest levels of aggregation in the tested buffers, samples chosen for toxicity analysis were the 10mM MES buffers at pH 5 and pH 7 supplemented with 50mM NaCl. The mature fibrils were distinctly different in the two samples, as the fibres were very long and straight at pH 7 but were much shorter with slight bending of some fibrils in the extremely dense network of fibrils observed at pH 5.

The FTIR analysis presented was from the two samples described above which were chosen for the neurotoxicity analysis. The β–sheet content of the normal peptides was 69.21% at pH 7, and 61.11% at pH 5. Previous studies using the HuPrP106-125 peptide have shown that a larger proportion of β–sheet is obtained at pH 5 in 200mM phosphate buffer (Selvaggini *et al.* 1993). This research has found that the β–sheet content was slightly higher at pH 5 in the MES buffer, however this may be due to the two amino acid differences in the mouse peptide (in comparison to the human peptide). This suggestion is based on the observation that amino acid substitutions, representative of the A117V GSS mutation in the HuPrP106-126, have comparable quantities of β–sheet at both pH 5 and pH 7 (Salmona *et al.* 1999). There are therefore highly complex interactions between the pH, salt concentration in

influencing the development and morphology of aggregated amyloid fibrils of MoPrP105-125. More detailed secondary structure analysis could be performed to help understand the relationships of these variables with the amino acid composition and primary structure of the MoPrP105-125. These factors will influence the secondary structure of dissolved peptides and may therefore influence the toxicity of tested peptides. This knowledge will enable the effects of secondary structure (including protofibrillar and mature fibrillar morphologies) to be correlated with toxicity, and therefore lead to a better understanding of the neurodegeneration associated with these diseases.

4.4.2 PC12 cells cultured with NGF adopt a neuronal phenotype

The rat pheochromocytoma cells were used to model the neurodegenerative potential of the MoPrP105-125 peptides, following the unsuccessful attempts to establish murine organotypic hippocampal slice cultures for this thesis (Section 1.5.1.). However, the PC12 cells represent a good model for such research as they are believed to be early progenitor cells of neural cleft origin which differentiate to the neuronal phenotype *in vitro* in the presence of NGF (Greene & Tischler 1976). NGF *in vivo* is believed to cause the neuronal differentiation of stem cells migrating from the neural cleft (Bjerre & Bjorklund 1973). Differentiation of PC12 cells to the neuronal phenotype depends on the presence of a collagen IV coated matrix, NGF concentration, differentiation time, and also the initial density of plated cells (Greene & Tischler 1976). The morphology of differentiating cells was monitored daily up to 14 days by inverted microscopic analysis. The expression of NF-L mRNA increases significantly in NGF-differentiated cells and has been proven to be reliable as a quantitative measure of differentiation in PC12 cells (Lindenbaum *et al.* 1998;

Schimmelpfeng *et al.* 2004). Although PrP^c is expressed by a number of cells (Section 1.2.2.), the highest levels of PrP^c are expressed by neurons of the CNS (Manson *et al.* 1992). PrP^c expression by PC12 cells has been shown to increase following differentiation with NGF (Wion *et al.* 1988; Lazarini *et al.* 1994), and was therefore examined by immunofluorescence and FACS analysis.

Microscopic analysis showed that naive PC12 cultures were rounded and grew optimally when in close contact with other cells (Figure 4.9.A.). FACS analysis for NF-L protein showed that the mean expression of naive cells was 1.61%, confirming that these cells were not neuronal (Figures 4.14.A.-.B.). Immunofluorescence analysis confirmed low level expression of PrP^c restricted to the cell membrane and cytosol (Figures 4.10.A. & .C.). Quantitative analysis by FACS analysis showed that 9.02% of cells express PrP^c (Figures 4.13.A.-.B.). Following 7 days NGF-exposure; the cell bodies of some cells were extended, cells were present in much lower proximities to each other and neuritic processes extended between some cells (Figure 4.9.B.). The cells were morphologically immature in their neuronal status, but FACS analysis showed that the mean increase in NF-L expression was highly significantly at 16.05% in comparison to naive cell cultures (Figures 4.14.C.-.D.). Immunofluorescence analysis showed that PrP^c expression was increased greatly following 7 days NGF treatment (Figures 4.11.A. & .C.). FACS analysis confirmed this, as 30.18% of these cells expressed PrP^c (Figures 4.13.C.-.D.) 14 day differentiated cells had larger cell bodies and mature neuritic processes extending to neighbouring neuronal cells (Figure 4.9.C.). Forward and side scatter analysis revealed that these cells were larger and more complex than the naive cells (Figures 4.13. and 4.14.). These cells resembled mature neurons and the mean NF-L protein

expression was 31.04% (Figures 4.14.E.-.F.); this increase was highly significant and represented a 20-fold increase in comparison to the non-neuronal naive cultures. PrP^c expression in these cultures was higher again as confirmed by immunofluorescence (Figures 4.12.A. & .C.) and FACS analysis (42.22%) (Figures 4.13.E.-.F.). FACS dot plots for naive, 7 day and 14 day differentiated cultures showed that the two populations observed in the naive PC12 cell analysis had virtually disappeared following exposure to NGF for 14 days (Figures 4.13. and 4.14.). The full differentiation by NGF correlates with the cessation of mitosis in neuronal cells (Greene & Tischler 1976), therefore the combined evidence of this research classified these cells as neuronal. Furthermore, the research of this thesis is strengthened since the relative increases in PrP^c and NF-L protein expression are in line with previous reports using neuronal PC12 cells (Wion *et al.* 1988; Lindenbaum *et al.* 1998).

In addition to the observations that 14 day NGF-differentiated PC12 cells were morphologically neuronal and expressed neuron specific proteins, these cells also responded like neurons to the neurotoxic TMT (as measured by alamarblue cytotoxicity assay). TMT was included as a positive control of cell death and also to monitor the reproducibility of the alamarblue assays, as these assays were performed over a four week period. Although TMT treatments induced cell death in the naive PC12 cultures, toxicity was significantly enhanced in the neuronally differentiated cells. These results further confirmed that the 14 day NGF-differentiated PC12 cells developed for this thesis were neuronal. This is extremely important as the establishment of a reproducible *in vitro* neuronal model was a central aim of the work described in this thesis. Therefore, the neuronal PC12 cells established here morphologically resemble and express neuronal specific proteins, in addition to

responding like neurons when exposed to neurotoxic substances (i.e. TMT). These neuronal cells therefore represent a very suitable *in vitro* model for studying the neurodegenerative mechanisms associated with the TSE diseases.

4.4.3 Neuronal, but not naive, PC12 cell cultures are sensitive to toxic conformations of MoPrP105-125

The research of this thesis concentrated on establishing an *in vitro* model for the neurodegenerative mechanisms associated with the TSE diseases. Initial research plans of this thesis included the HuPrP106-126 peptide (and its scrambled equivalent), as the novelty of using the mouse peptide sequence represented an uncertainty in terms of whether it too would be neurotoxic. However, secondary structural analysis of the normal and scrambled mouse peptides became so extensive that the human peptides had to be removed from the research plan.

Neurotoxicity of MoPrP105-125 was confirmed by alamarblue reduction assay (Section 2.5.11.2.); however, toxicity was restricted to PC12 cells exhibiting the neuronal phenotype. In the work presented in this thesis, normal mouse peptides had negligible effects on naive PC12 cells (Figure 4.15.), whereas neuronal cells were highly susceptible to the toxicity of the normal mouse peptides (Figures 4.18). Both MoPrP105-125 peptide preparations were toxic to neuronal PC12 cells in comparison to scrambled peptides, and also their vehicle buffer control equivalents. There was a highly significant relationship between exposure time and the neuronal cell status (i.e. neuronal morphology, $p<0.005$, two-way ANOVA) (Tables 4.5 & 4.6), and also between the cell status (i.e. neuronal morphology) and normal peptides ($p<0.005$, two-way ANOVA). Therefore, the susceptibility of neuronal PC12 cells could be due

to mechanisms specific to the neuronal phenotype. One such observation of the neuronal phenotype is the significant enhanced expression of PrP^c in comparison to 7 day differentiated ($p<0.005$) or naive ($p<0.005$) cultures (Section 4.3.6.). It is well known that PrP^c expression is essential for toxicity of PrP106-126 and also for the development of TSE disease *in vivo*. PrP^c expression levels have previously been shown to affect the susceptibility of cell cultures to the human PrP106-126 peptide (Hope *et al.* 1996). Neuronally differentiated PC12 cells were not included in this study by Hope *et al.*, however; naive PC12 cells, which express low levels of PrP^c, were relatively unaffected by PrP106-126 peptides and therefore this is in agreement with the results of this thesis. However, these observations disagree with a recent paper analysing PrP106-126 (Fioriti *et al.* 2005), which found PrP106-126 was comparably toxic to naive and neuronal PC12 cells. In contrast, it has also been reported that naive and neuronal PC12 cells are resistant to PrP106-126 unless co-cultured with microglial cells (Brown *et al.* 1997). It is likely that neuron-specific factors in partially differentiated cells in these two studies, such as PrP^c expression levels, would be different to the neuronal PC12 cell cultures investigated in this thesis. Furthermore, secondary structure analysis of the peptide solutions in these studies was not tested. This is an extremely important variable as; (1) β–sheet content has been shown to correlate with infectivity *in vivo* (Wille *et al.* 2000), and (2) PrP106-126 solutions containing high quantities of β–sheet have been shown to be more toxic *in vitro* (Brown *et al.* 1998). Therefore, the β–sheet content and fibrillogenic properties of the peptides in these studies were unknown, which would account for differences in toxicity. Therefore the results of this thesis, demonstrating the vulnerability of neuronal PC12 cells to the toxic effects of fibrillogenic peptides (Figures 4.17. and 4.21.) containing a large proportion of β-sheet (Figures 4.7.- Table

4.4.), represents positive progress in developing an *in vitro* model for analysing the mechanisms of cell death which *in vivo* is also restricted to neuronal populations.

Future work arising from this thesis could determine if the observed differences in the susceptibility of neuronal and naive PC12 cells was due to differences in PrP^c expression levels, or due to other neuron specific traits. The creation of PrP^c knockout and PrP^c over-expressing PC12 cells, would allow for such analysis in naive and neuronal PC12 cells. Brown *et al.* have already shown increased neurotoxic effects of PrP106-126 in cultured cerebellar neurons over-expressing PrP^c; however, microglial cells were thought to be important in assisting this toxicity (Brown 1998). Even though the cell culture system established in this thesis does not require microglia for PrP105-125 toxicity, future research could establish a co-culture system with PC12 cells to see if toxicity is indirectly enhanced by the presence of microglial cells. Since microglial activation occurs prior to neuronal loss in murine scrapie models and that PrP^{sc} toxicity is enhanced by microglial cells (Giese *et al.* 1998; Bate *et al.* 2001), the development of such a model would better replicate the *in vivo* neurodegenerative process. The release of ROS by activated microglia, in response to PrP peptides, would allow further analysis for the role of oxidative stress in mediating neurodegeneration (as discussed in Chapter 3). Furthermore; this research had originally planned to include the human PrP106-126 peptide, created in the conditions tested for the mouse peptides, to analyse toxicity on rat PC12 cells in relation to the mouse peptide containing the identical sequence to that in the rat genome. Future research could include the human peptide to test its toxicity in relation to the mouse peptide on rat PC12 cells. In summary; the observations that neuronal and not naive PC12 cells are susceptible to the *in vitro* neurotoxicity of MoPrP105-125 peptides is

therefore an illustration of the selective vulnerability of neurons *in vivo*, when exposed to TSE agents. The complete development of an *in vitro* neurodegeneration model could therefore lead to strategies to interrupt the mechanisms of neuronal cell loss in these diseases, which would be beneficial due to the prolonged incubation periods required when performing such analysis using animal TSE models.

4.4.4 Neurotoxicity of MoPrP105-125 in relation to secondary structural properties

Toxicity analysis in this thesis concentrated on the creation of highly aggregated mature fibrils containing a large proportion of β–sheet (>60%), as HuPrP106-126 peptides containing a large proportion of β–sheet are more toxic to neuronal cell cultures (Forloni *et al.* 1993; Tagliavini *et al.* 1993). The mature fibrils formed by MoPrP105-125 were very toxic and this was highly statistically significant with respect to the independent variables of; the normal peptide ($p<0.005$), concentration ($p<0.005$), time ($p<0.005$) and the presence PC12 cells with the neuronal morphology ($p<0.005$). There were significant two-way relationships between the presence of neuronal cells and the normal peptide ($p<0.05$), and also the presence of neuronal cells and the exposure time ($p<0.05$). The β–sheet contents of the two normal peptides were relatively similar (Tables 4.1. and 4.3.) however the fibrils were morphologically different (Figures 4.2.-4.3.). Fibrils formed in 10mM MES pH 7 (+50mM NaCl) were very long and straight, whereas fibrils formed in the 10mM MES pH 5 (+50mM NaCl) buffer were much shorter, over-lapping and some fibrils had slight bending. Interestingly, increasing evidence suggests that soluble intermediates, even in non-disease associated proteins, are more toxic than mature fibrils (Bucciantini *et al.* 2002). Mature fibrils created from PrP peptides are toxic *in*

vitro however the toxicity of mature fibrillar plaques (containing PrP^{sc}) is less clear *in vivo*, for a number of reasons including; (1) amyloid plaques are characteristic of some but not all TSE infections, (2) infectivity does not appear to correlate with PrP^{sc} (Telling *et al.* 1995; Dorandeu *et al.* 1998; Foster *et al.* 2001), (3) diseases such as Alzheimer's disease, which also contains brain amyloid deposits, are not transmissible.

Future work should try to identify soluble intermediates formed during the growth of murine PrP peptides into mature fibrils. Such soluble intermediates have been described in the 87V/VM murine scrapie model *in vivo*; Jeffrey *et al.* described the presence of accumulated pre-amyloidogenic PrP in association with selective damage to axon terminals and dendritic spines (Jeffrey *et al.* 1997). Investigations by Brown *et al.* showed that maximum toxicity of the HuPrP106-126 peptide was obtained in the presence of both highly aggregated and soluble conformations of the peptide (Brown *et al.* 1998). Highly toxic protofibrillar structures were obtained following G114A and G119A mutations in HuPrP106-126 which reduced the ability of the peptide to aggregate (Florio *et al.* 2003). Soluble intermediate protofibrillar structures which are rich in β-turn structure have recently been created *in vitro*, from recPrP molecules in lipid raft membranes, and have been shown to be more toxic than more mature insoluble aggregated fibrils (Kazlauskaite *et al.* 2005). Therefore, future research could attempt to identify protofibrillar conformations of MoPrP105-125, and analyse the neurotoxic mechanisms of these structures on neuronal PC12 cells. Protofibrillar conformations are more likely to be obtained using the 10mM MES pH 5 (+50mM NaCl) buffer, as fibril formation is a much slower process in this reaction as observed by Thioflavin-T binding (Figure 4.6.), than at pH 7 (Figure 4.5.) which

aggregates immediately upon being dissolved. The formation of mature fibrillar structures appears to be a much slower process at pH 5, and I believe this would allow for the identification of soluble intermediate protofibrillar structures. Therefore the observations that the amyloid formation in 10mM MES pH 5 may prove to be very important for future analysis to identify protofibrillar intermediated in the reaction leading to mature amyloid fibrils. Due to constraints of not having our own EM facilities, EM analysis in this research could only be performed at critical points as determined by Thioflavin-T analysis. Analysis of peptide conformations at much earlier time points would have to be performed in order to identify protofibrillar structures in this system. The identification of soluble toxic PrP species may help in identifying the infectious agent and explain the transmissibility of these diseases. Therapeutic strategies to interrupt the neuronal loss can only be developed by these studies which increase our knowledge of the neurodegenerative process by different fibrillar forms of PrP. The findings of this thesis that mature amyloid fibrils have comparable toxicities even though they are structurally very distinct, therefore contributes to the theory that soluble intermediates (such as in the conversion reaction of PrP^{c} to PrP^{sc}) may be more neurotoxic and may even represent the infectious agent (Caughey & Lansbury 2003).

4.4.5 Scrambled MoPrP105-125 peptides are moderately toxic following prolonged exposures

As discussed in Section 4.3.3., the toxicity of normal peptides was restricted to the neuronal phenotype. The differences in toxicity between the scrambled and normal peptides (highly toxic) were highly significant ($p<0.005$), as was the presence of PC12 cells with the neuronal morphology in comparison to naive cultures when treated with normal peptides ($p<0.005$), as analysed by two-way ANOVA analysis. These alamarblue reduction assays confirmed that the scrambled peptide conformations had negligible effects on naive PC12 cells (Figures 4.16. and 4.20.). However; when added to the neuronal PC12 cells for periods of 5 or 7 days, scrambled peptide treated cells had slightly reduced mean reduction values in comparison to buffer equivalent treated cells (Figures 4.18. and 4.22.). However, the differences between the mean reduction values for buffer and scrambled peptide treated neuronal cells, was much less remarkable than that observed for the normal peptide experiments (Figures 4.17. and 4.21.). Analysis of the tested concentrations shows that mean alamarblue reduction values for pH 7 created scrambled peptides fell from 88.28% after 24 hours to 71.38% after exposure for 7 days (Figure 4.18.). In comparison, the mean alamarblue reduction values for pH 5 created scrambled peptides fell from 84.79% after 24 hours to 71.08% after 7 days exposure (Figure 4.22.). The observed reduction in viability was due to the presence of the scrambled peptides, as the mean alamarblue reduction values for vehicle buffer treated cells were fairly constant and unaffected by exposure time (Figures 4.18. and 4.22.). The toxicity of the scrambled peptides after 7 days exposure is much less than that observed for the normal peptides (Figures 4.17. and 4.18. compared to Figures 4.21 and 4.22.). The scrambled peptide conformations have different secondary structure

compositions (Tables 4.2 & 4.4), but similar mean alamarblue reduction values as described above. The observed toxicities of scrambled peptides may be; (1) due to the similar quantities of β–sheet (32.61% and 31.12% in pH 7 and pH 5 respectively) as recorded by FTIR spectroscopy, or (2) non-specific due to prolonged exposures of the neuronal PC12 cells to misfolded, but non-fibrillar (Figures 4.2.-4.3.), scrambled peptides. Larger quantities of β–sheet have been shown to increase the toxicity of the normal PrP106-126 peptide (Brown *et al.* 1998), and also has become widely accepted that the misfolding of proteins, even from non-disease related proteins, can result in the formation of toxic species (Bucciantini *et al.* 2002). Therefore the evidence I have gathered indicates that the actual presence of these misfolded insoluble aggregates, containing a relatively large proportion of β–sheet, could account for the small toxicities observed with these scrambled peptides. The neuronal phenotype contributes to the mechanisms of this toxicity, as naive PC12 cultures are resistant to the mildly toxic effects of these scrambled peptides. The mechanisms for the increased sensitivity of neuronal, in comparison to naive, PC12 cells are unclear. However, to analyse the relationship between toxicity and the proportion of β–sheet in the scrambled peptides, these peptide solutions could be incubated with β–strand breakers (Soto *et al.* 2000). Toxicity could then be analysed by alamarblue reduction over the same time scale in comparison to untreated scrambled peptide solutions. Therefore the slight neurotoxicity of the misfolded scrambled peptides in this thesis correlate with observations that the misfolding of any protein into soluble non-fibrillar aggregates will be cytotoxic (Bucciantini *et al.* 2002).

4.4.6 Mechanisms of neuronal cell death following MoPrP105-125 exposure have yet to be clarified

Neuronal PC12 cells cultured in the presence of MoPrP105-125 peptides were analysed biochemically for the presence of apoptosis-related markers. Annexin V staining was attempted to identify early signs of apoptosis such as changes to the plasma membrane, and activation of caspase 3 was analysed to monitor more downstream events. FACS analysis using Annexin V staining could not be monitored, as annexin V was found to bind non-specifically to all cells (Section 4.3.9). Damage to neuritic processes, whilst harvesting adherent neuronal cells for FACS analysis, is the most likely explanation for the non-specific binding of annexin V (Schutte *et al.* 1998). Therefore, further research is required to optimise annexin V staining protocols for the identification of early-stage apoptosis. The activation of caspase 3 *in vitro* (with PrP106-126) and caspase 3 and Fas ligand *in vivo* (87V/VM model) represented obvious starting points for the identification of biochemical markers of apoptosis (Jamieson *et al.* 2001a; White *et al.* 2001). Unfortunately, an antibody recognising the Fas ligand in rats (for FACS analysis) arrived after this research ended and could not be included in this analysis. Furthermore, the antibody chosen for the FACS analysis failed to recognise activated caspase 3 in any of the peptide or TMT treated samples. These experiments represented the final research area of this thesis, and unfortunately further attempts at identifying neurodegenerative mechanisms could not be performed. The required differentiation period of PC12 cells for 14 days, then treatment durations of up to 7 days, meant that considerable time constraints were fixed into such analysis.

The time consuming process of completing the secondary structure analysis of MoPrP105-125 and the long cell culture conditions required, was disappointing as planned work to investigate apoptosis-related proteins *in vitro* could not be performed. Future research should analyse mechanisms of neurodegeneration, following treatments of PC12 cells with protofibrillar conformations of human and mouse normal peptides (Section 4.4.4.). The optimisation of active caspase 3 and Fas ligand protocols for FACS analysis would not prove to be time consuming, as FACS protocols for PC12 cells have now been established. Furthermore, the co-culture of cells with specific or pan caspase inhibitors, in addition to toxic normal peptide species, would have provided detailed analysis of the roles of these proteases in the mechanisms of neuronal cell death in this model. The cytosolic translocation of AIF in the ME7/CV murine scrapie model (Chapter 3), and cyt c in fractions from scrapie-infected and normal brain, represented an opportunity to investigate mitochondrial dysfunction in this *in vitro* system. The sub-cellular fractionation kit (Calbiochem) used for separating brain homogenates (Section 3), was purchased as it was also compatible with adherent cell cultures. Western blot analysis of the separated fractions would allow similar analysis to be investigated in this model. Furthermore, the roles of the Bcl-2 family proteins in controlling the release of the IMM proteins (Section 3) could also be investigated. This analysis could also include FACS, immunofluorescence, and an ELISA (e.g. for cyt c) which would allow much more detailed analysis of the role of apoptotic proteins in mediating neuronal cell death in the TSEs and other neurodegenerative diseases. With increasing publications investigating mechanisms of cell death, it is becoming clearer that the classifications of apoptosis, autophagy and necrosis are not as distinct as was previously thought. With respect to the caspase-independent pathways included in this thesis; AIF has

also been shown to interact with PARP (Yu *et al.* 2003), which had historically been considered to be specific to necrotic cell death. Furthermore; although the release of IMM proteins (such as AIF and Endo G) is caspase-independent, it is thought that once released these proteins may also interact with proteins which influence the activation of the caspase cascade (e.g. by interrupting Hsp70/Apaf-1 binding) (Ravagnan *et al.* 2001). These are only two examples of apparent cross-talk between the different "classes" of neuronal cell death. Furthermore evidence of cell death displaying characteristic features of apoptosis and necrosis, termed aponecrosis, has been described (Formigli *et al.* 2000). Therefore the complexity and apparent cross-talk between apoptosis and necrosis, and evidence that inhibition of one can lead to domination of the other (Pohl *et al.* 1999), means that approaches to modulate cell death in the TSE diseases should be taken with extreme caution. Further research may reveal the precise mechanisms of neuronal cell death in TSE diseases, and lead to the development of therapeutic treatments to inhibit the neurodegenerative process or to delay/prolong the process to a period beyond the natural lifespan of the infected host. The investigations of these pathogenic mechanisms of neuronal cell death in this thesis are therefore of direct relevance to the development of future intervention and therapeutic strategies to combat the fatal neurodegenerative processes in the TSEs.

Chapter 5: Final conclusions and future work

The research described in this thesis was designed to obtain a better understanding of the mechanisms leading to and resulting in the characteristic neurodegeneration of the TSE diseases. Infection with TSEs results in a number of pathological changes in the brain, including the deposition of PrP^{sc} and, in several cases, the presence of dense amyloid plaques composed of accumulated PrP^{sc} molecules. These diseases occur following the misfolding of normal host encoded PrP^{c}, via intermediate conformations, and result in the deposition of PrP^{sc}. PrP^{sc} remains the most reliable biomarker in verifying TSE infection; however, confirmation that PrP^{sc} represents the infectious agent has yet to be obtained. Therefore, research is required to show which conformation of PrP is the most neurotoxic and also verify if this conformation represents the infectious agent, and not just a pathological by-product of the disease process. The mechanisms resulting in TSE neurodegeneration must be identified if successful therapeutic strategies are to be developed.

The occurrence and sequence of pathological changes following infection with TSE agents are strongly influenced by the infecting agent and the host genotype combination (Bruce *et al.* 1976). TSE agents also selectively target neuronal populations; however, the mechanisms resulting in such targeting are unknown. Therefore, the mechanisms associated with the pathological changes which occur during the course of infection with TSE agents are poorly understood and the mechanisms of cell death may also differ in accordance with the infecting TSE agent and the genotype of the infected host. This research was designed to address the mechanisms leading to the activation and also subsequent execution of neuronal cell

death pathways. This research was accomplished using (1) an *in vitro* model to analyse the structure/toxicity relationships of a PrP peptide which stimulates neuronal cell death and (2) analyse the precise mechanisms of neuronal cell death *in vivo* using two well characterised murine scrapie models.

The synthetic murine PrP105-125 peptide, homologous to the neurotoxic human PrP106-126 peptide, was developed to model the activation of TSE related neurodegeneration *in vitro*. This region represents the most highly conserved region of the PrP protein in all tested species, and peptides isolated from amyloid deposits of GSS patients also contain this neurotoxic sequence (Tagliavini *et al.* 2001). This sequence is also believed to be essential for the conversion of PrP^{c} to PrP^{sc}, and *in vitro* shares many of the biochemical properties of PrP^{sc} (as discussed in Section 4). These factors therefore verify its suitability as an *in vitro* model of TSE neurodegeneration. Conformations of this peptide containing different secondary structures were created and were found to be toxic specifically to neuronal cell cultures. The primary amino acid sequence of MoPrP105-125 peptides was essential for this toxicity, as a scrambled version of this peptide was not toxic. Peptide samples containing mature amyloidogenic fibrils, but with distinct conformations, were analysed to assess secondary structure/toxicity relationships. This research revealed that differences in the structure of mature amyloid fibrils had no discernable effects on toxicities. Studies by other researchers, published during the course of the work described in this thesis (and also described in Section 4), reported that protofibrillar structures caused by the misfolding of even non-disease associated proteins can be toxic (Bucciantini *et al.* 2002). Protofibrillar structures have been reported using synthetic PrP peptides, including HuPrP106-126 and recPrP (Florio *et al.* 2003;

Kazlauskaite *et al.* 2005), and Jeffrey *et al.* described the association of pre-amyloidogenic PrP with selective damage to axon terminals and dendritic spines *in vivo* in the 87V/VM murine scrapie model (Jeffrey *et al.* 1997). The research of my collaborators on the peptide work of this thesis found that the protofibrillar intermediates of recPrP were more toxic than more mature insoluble aggregated fibrils (Kazlauskaite *et al.* 2005). Therefore, protofibrillar conformations of the MoPrP105-125 peptides may also prove to be the more toxic species, and the mature amyloid fibrils may be a by-product of the misfolding reaction. The poor correlation of PrP^{sc} and infectivity in some TSE disease models (Dorandeu *et al.* 1998; Foster *et al.* 2001) further strengthens the hypothesis that another fibrillar form of PrP may represent the infectious agent, and also that PrP^{sc} may correspond to a pathological disease by-product. Future research should prepare protofibrillar structures of MoPrP105-125 peptides and analyse toxicity in relation to the mature amyloid fibrils in the PC12 neuronal cell culture model. These protofibrillar structures may well more accurately represent the infectious disease process during the conversion of PrP^{c} to PrP^{sc}; therefore, future work should monitor both *in vivo* and *in vitro* the stimulation and downstream pathways of neuronal cell death. This research will be important in assessing the effects of protofibrillar PrP in the neuropathological changes which occur in the TSEs, in the identification of the infectious agent, and explain the transmissibility of these diseases. Therapeutic strategies to interrupt the neuronal loss may be developed by studies which increase our knowledge of the neurodegenerative process by different fibrillar forms of PrP, or better still prevent the misfolding of such disease-related proteins.

To understand the mechanisms which result in neuronal cell death in response to misfolded PrP, two well characterised murine scrapie models (ME7/CV & 87V/VM) were analysed at the terminal stages of disease. The targeting and sequence of pathological changes differs between these two models; this is particularly evident in the murine hippocampus, where the CA1 pyramidal neurons are lost during ME7/CV infections (Scott & Fraser 1984) and the CA2 pyramidal cells are damaged during 87V/VM infections (Belichenko *et al.* 2000; Jeffrey *et al.* 2000). Whole brains infected with either scrapie agent, and age-matched controls, were separated into mitochondrial and cytosolic fractions. Additionally, neuropathologically restricted areas of the brain, such as the hippocampus and thalamus, were micro-dissected and subcellularly fractionated into mitochondrial and cytosolic samples. This proved to be a more suitable technique for the *in vivo* analysis of apoptosis, as these samples contained a higher proportion of apoptotic to normal cells in comparison to the samples prepared from the whole brains. AIF was released from the IMM to the cytosol in the ME7/CV scrapie model, but not in 87V/VM or normal age-matched control animals. The release of AIF is therefore specific to infection with the ME7 murine scrapie strain, confirming that the mechanisms of neurodegeneration differ in these two models. The stimulation of different mechanisms of cell death may be due to the targeting of these scrapie agents to distinct neuronal populations, which may therefore activate different cellular receptors. Future work is required to identify the upstream events which result in the release of AIF in the ME7/CV model; the mechanisms of neurodegeneration in the ME7/CV clearly involve caspase-independent proteins, however, it is highly likely that caspase-mediated apoptosis will also be involved. Future research should therefore concentrate on identifying proteins which activate neuronal apoptosis both prior to and following the release of AIF. The

identification of these pathways will aid in the identification of mechanisms of neurodegeneration in other TSEs.

This research inadvertently revealed mitochondrial damage in animals at the terminal stages of the incubation period, which was absent in young mice, and which was also independent of infection with murine scrapie strains. The release of cyt c from the IMM indicates increased mitochondrial permeability in aged animals, correlating with evidence reporting mitochondrial dysfunction in other rodent TSE disease models (Choi *et al.* 1998; Lee *et al.* 1999). The effects of this age-related deterioration on the progression of TSE disease are unclear and future research should analyse the effects of cyt c release on the activation and/or release of downstream caspase dependent and independent proteins. As discussed in Section 3, the release of cyt c may not be sufficient to stimulate apoptosis due to physiological interactions with K^+ ions. However, if a threshold is exceeded (e.g. due to elevated cyt c release or fluctuations in K^+ ion concentrations) apoptosis can be activated (Bortner *et al.* 1997; Hughes *et al.* 1997). Such fluctuations in K^+ ions have been observed in various *in vitro* and *in vivo* TSE models, including the ME7/CV murine scrapie model described here. Therefore, reduced physiological concentrations of K^+ in scrapie-infected neurons may therefore allow activation of cyt c-mediated apoptosis. The incorporation of ICC analysis into future research will allow the detection of apoptotic proteins at the single cell level.

The *in vitro* model of neurodegeneration established in this thesis would provide a population of apoptotic cells which could be analysed following treatments with neurotoxic conformations of PrP peptides. As previously discussed the protofibrillar conformations of these peptides may prove to be the more toxic species, and the mature amyloid deposits may be a by-product of the protein misfolding reaction. The mechanisms of cell death induced by these protofibrillar conformations could be analysed for apoptotic proteins such as AIF. The use of this *in vitro* model would enhance the detection of apoptotic cells and will therefore aid in the understanding of neuronal cell death pathways. Such analysis had been planned for this thesis, but due to time constraints these studies could not be performed. A wide range of techniques could be used to analyse neurodegenerative mechanisms in the *in vitro* system; the identification of apoptosis-related proteins could then be analysed complementary in the *in vivo* models. FACS and immunofluorescence analysis of neuronal PC12 cells could be used to analyse the translocation of ions such as K^+ and Ca^{2+}, which are known to control the activation of apoptotic pathways (as discussed in Section 3). Furthermore, sub-cellular fractionation of neuronal PC12 cells could also be performed to analyse the roles of other IMM proteins, such as Smac/Diablo and HtrA2 which have been reported respectively in a model of Huntington's disease and ME7/CV murine scrapie (Brown *et al.* 2005; Goffredo *et al.* 2005). The complexity and cross-talk between neuronal cell death pathways in these diseases could also be investigated using caspase-inhibitor proteins to identify potential roles of specific caspases in mediating cell death. Future research will also have to determine the roles of mitochondrial dysfunction, age and misfolded PrP in contributing to neuronal cell death in these fatal infectious neurodegenerative diseases.

The identification of the precise mechanisms of neuronal cell death in TSE diseases may lead to the development of therapeutic treatments to inhibit the neurodegenerative process or to delay/prolong the process to a period beyond the natural lifespan of the infected host. These therapeutic strategies could include; (1) preventing TSE-specific cell death activation by the successful identification of the neurotoxic/infectious agent, or (2) blocking the activated pathways using specific inhibitory molecules. The research of this thesis is therefore of direct relevance to the future development of potential therapeutic strategies for TSEs, and may also have wider implications for the treatment of other amyloidogenic neurodegenerative diseases.

Bibliography

Alper, T., Cramp, W. A., Haig, D. A. and Clarke, M. C. (1967). Does the agent of scrapie replicate without nucleic acid? *Nature* **214**:764-766.

Alper, T., Haig, D. A. and Clarke, M. C. (1966). The exceptionally small size of the scrapie agent. *Biochemical and Biophysical Research Communications* **22**:278-284.

Anglade, P., Vyas, S., Javoy-Agid, F., Herrero, M. T., Michel, P. P., Marquez, J., Mouatt-Prigent, A., Ruberg, M., Hirsch, E. C. and Agid, Y. (1997). Apoptosis and autophagy in nigral neurons of patients with Parkinson's disease. *Histology and Histopathology* **12**:25-31.

Apetri, A. C. and Surewicz, W. K. (2003). A typical effect of salts on the thermodynamic stability of human prion protein. *Journal of Biological Chemistry* **25**:22187-22192.

Barr, J. B., Somerville, R. A., Chung, Y.-L. and Fraser, J. R. (2004). Microdissection: A method developed to investigate mechanisms involved in transmissible spongiform encephalopathy pathogenesis. *BMC Infectious Diseases* **4**.

Basler, K., Oesch, B., Scott, M., Westaway, D., Walchli, M., Groth, D. F., McKinley, M. P., Prusiner, S. B. and Weissmann, C. (1986). Scrapie and cellular PrP isoforms are encoded by the same chromosomal gene. *Cell* **46**:417-428.

Bate, C., Reid, S. and Williams, A. (2001). Killing of prion-damaged neurones by microglia. *Neuroreport* **12**:1-6.

Beaudry, P., Cohen, P., Brandel, J. P., DelasnerieLaupretre, N., Richard, S., Launay, J. M. and Laplanche, J. L. (1999). 14-3-3 protein, neuron-specific enolase, and S-100 protein in cerebrospinal fluid of patients with Creutzfeldt-Jakob disease. *Dementia and Geriatric Cognitive Disorders* **10**:40-46.

Beekes, M., McBride, P. A. and Baldauf, E. (1998). Cerebral targeting indicates vagal spread of infection in hamsters fed with scrapie. *Journal Of General Virology* **79**:601-607.

Beere, H. M., Wolf, B. B., Cain, K., Mosser, D. D., Mahboubi, A., Kuwana, T., Tailor, P., Morimoto, R. I., Cohen, G. M. and Green, D. R. (2000). Heat-shock protein 70 inhibits apoptosis by preventing recruitment of procaspase-9 to the Apaf-1 apoptosome. *Nature Cell Biology* **2**:469-475.

Belichenko, P. V., Brown, D., Jeffrey, M. and Fraser, J. R. (2000). Dendritic and synaptic alterations of hippocampal pyramidal neurones in scrapie-infected mice. *Neuropathology and Applied Neurobiology* **26**:143-149.

Bergstrom, A.-L., Cordes, H., Zsurger, N., Heegaard, P. M. H., Laursen, H. and Chabry, J. (2005). Amidation and structure relaxation abolish the neurotoxicity of the prion peptide PrP106-126 in vivo and in vitro. *The Journal of Biological Chemistry* **280**:23114-23121.

Bessen, R. A., Kocisko, D. A., Raymond, G. J., Nandan, S., Lansbury, P. T. and Caughey, B. (1995). Non-genetic propagation of strain-specific properties of scrapie prion protein. *Nature* **375**:698-700.

Birkett, C. R., Hennion, R. M., Bembridge, D. A., Clarke, M. C., Chree, A., Bruce, M. E. and Bostock, C. J. (2001). Scrapie strains maintain biological phenotypes on propagation in a cell line in culture. *Embo Journal* **20**:3351-3358.

Bjerre, B. and Bjorklund, A. (1973). The production of catecholamine-containing cells in vitro by young chick embryos: effects of "nerve growth factor" (NGF) and its antiserum. *Neurobiology* **3**:140-161.

Boellaard, J. W., Kao, M., Schlote, W. and Diringer, H. (1991). Neuronal autophagy in experimental scrapie. *Acta Neuropathologica* **82**:225-228.

Boellaard, J. W., Schlote, W. and Tateishi, J. (1989). Neuronal autophagy in experimental Creutzfeldt-Jakob's disease. *Acta Neuropathologica* **78**:410-418.

Bolton, D. C., McKinley, M. P. and Prusiner, S. B. (1982). Identification of a protein that purifies with the scrapie prion. *Science* **218**:1309-1311.

Bolton, D. C., Meyer, R. K. and Prusiner, S. B. (1985). Scrapie PrP27-30 is a sialoglycoprotein. *Journal of Virology* **53**:596-606.

Bolton, D. C., Rudelli, R. D., Currie, J. R. and Bendheim, P. E. (1991). Copurification of Sp33-37 and scrapie agent from hamster brain prior to detectable histopathology and clinical disease. *Journal of General Virology* **72**:2905-2913.

Bortner, C. D., Hughes, F. M. and Cidlowski, J. A. (1997). A primary role for K^+ and Na^+ efflux in the activation of apoptosis. *The Journal of Biological Chemistry* **272**:32436-32442.

Bosma, G. C., Custer, R. P. and Bosma, M. J. (1983). A severe combined immunodeficiency mutation in the mouse. *Nature* **301**:527-530.

Bosque, P. J. and Prusiner, S. B. (2000). Cultured cell sublines highly susceptible to prion infection. *Journal of Virology* **74**:4377-4386.

Brown, A. R., Rebus, S., McKimmie, C. S., Robertson, K., Williams, A. and Fazakerley, J. K. (2005). Gene expression profiling of the preclinical scrapie-infected hippocampus. *Biochemical and Biophysical Research Communications* **334**:86-95.

Brown, D. R. (2000). Atered toxicity of the prion protein peptide PrP106-126 carrying the Ala^{117} to Val mutation. *Biochemical Journal* **346**:785-791.

Brown, D. R. (1998). Prion protein-overexpressing cells show altered response to a neurotoxic prion protein peptide. *Journal of Neuroscience Research* **54**:331- 340.

Brown, D. R. (2000). Prion protein peptides: optimal toxicity and peptide blockade of toxicity. *Molecular and Cellular Neuroscience* **15**:66-78.

Brown, D. R., Belichenko, P. V., Sales, J., Jeffrey, M. and Fraser, J. R. (2001). Early loss of dendritic spines in murine scrapie revealed by confocal analysis. *Neuroreport* **12**.

Brown, D. R. and Besinger, A. (1998). Prion protein expression and superoxide dismutase activity. *Biochemical Journal* **334**:423-429.

Brown, D. R., Herms, J. and Kretzchmar, H. A. (1994). Mouse cortical cells lacking cellular PrP survive in culture with a neurotoxic PrP fragment. *Neuroreport* **5**:2057-2060.

Brown, D. R., Pitschke, M., Riesner, D. and Kretzschmar, H. A. (1998). Cellular effects of a neurotoxic prion protein peptide are related to its beta-sheet content. *Neuroscience Research Communications* **23**:119-128.

Brown, D. R., Qin, K. F., Herms, J. W., Madlung, A., Manson, J., Strome, R., Fraser, P. E., Kruck, T., vonBohlen, A., SchulzSchaeffer, W., Giese, A., Westaway, D. and Kretzschmar, H. (1997). The cellular prion protein binds copper *in vivo*. *Nature* **390**:684-687.

Brown, D. R., Schmidt, B. and Kretzschmar, H. A. (1996). A neurotoxic prion protein fragment enhances proliferation of microglia but not astrocytes in culture. *Glia* **18**:59-67.

Brown, D. R., Schmidt, B. and Kretzschmar, H. A. (1996). Role of microglia and host prion protein in neurotoxicity of a prion protein fragment. *Nature* **380**:345-347.

Brown, D. R., Schmidt, B. and Kretzschmar, H. A. (1997). Effects of oxidative stress on prion protein expression in PC12 cells. *International Journal of Developmental Neuroscience* **15**:961-972.

Brown, D. R., SchulzSchaeffer, W. J., Schmidt, B. and Kretzschmar, H. A. (1997). Prion protein-deficient cells show altered response to oxidative stress due to decreased SOD-1 activity. *Experimental Neurology* **146**:104-112.

Brown, D. R., Wong, B.-S., Hafiz, F., Clive, C., Haswell, S. J. and Jones, I. M. (1999). Normal prion protein has an activity like that of superoxide dismutase. *Biochemical Journal* **344**:1-5.

Brown, K., Stewart.K., Bruce, M. and Fraser, H. (1996) in *Transmissible Spongiform Encephalopathies: Prion Diseases*, eds. Court, L. & Dodet, B. (Elsevier, Paris), pp. 159-166.

Bruce, M. E. (1985). Agent replication dynamics in a long incubation period model of mouse scrapie. *Journal of General Virology* **66**:2517-2522.

Bruce, M. E. and Dickinson, A. G. (1987). Biological evidence that scrapie agent has an independent genome. *Journal of General Virology* **68**:79-89.

Bruce, M. E., Dickinson, A. G. and Fraser, H. (1976). Cerebral amyloidosis in scrapie in the mouse: effect of agent strain and mouse genotype. *Neuropathology and Appied Neurobiology* **2**:471-478.

Bruce, M. E. and Fraser, H. (1975). Amyloid plaques in the brains of mice infected with scrapie: morphological variation and staining properties. *Neuropathology and Applied Neurobiology* **1**:189-202.

Bruce, M. E., Fraser, H., McBride, P. A., Scott, J. R. and Dickinson, A. G. (1992) in *Prion diseases of humans and animals*, eds. Prusiner, S. B.,Collinge, J.,Powell, J. & Anderton, B. (Ellis Horwood, New York), pp. 497-508.

Bruce, M. E., McBride, P. A. and Farquhar, C. F. (1989). Precise targeting of the pathology of the sialoglycoprotein, PrP, and vacuolar degeneration in mouse scrapie. *Neuroscience Letters* **102**:1-6.

Bruce, M. E., McBride, P. A., Jeffrey, K., Rozemuller, J. M. and Eikelenboom, P. (1993). PrP in scrapie and B/A4 in Alzheimer's disease show similar patterns of deposition in the brain. *Alzheimer's Disease: Advences in Clinical and Basic Research* 481-487.

Bruce, M. E., McConnell, I., Fraser, H. and Dickinson, A. G. (1991). The disease characteristics of different strains of scrapie in Sinc congenic mouse lines: implications for the nature of the agent and host control of pathogenesis. *Journal of General Virology* **72**:595-603.

Bruce, M. E., Will, R. G., Ironside, J. W., McConnell, I., Drummond, D., Suttie, A., McCardle, L., Chree, A., Hope, J., Birkett, C., Cousens, S., Fraser, H. and Bostock, C. J. (1997). Transmissions to mice indicate that 'new variant' CJD is caused by the BSE agent. *Nature* **389**:498-501.

Bucciantini, M., Giannioni, E., Chiti, F., Baroni, F., Formigli, L., Zurdo, J., Taddel, N., Ramponi, G., Dobson, C. M. and Stefani, M. (2002). Inherent toxicity of aggregates implies a common mechanism for protein misfolding diseases. *Nature* **416**:507-511.

Bueler, H., Aguzzi, A., Sailer, A., Greiner, R. A., Autenried, P., Aguet, M. and Weissmann, C. (1993). Mice devoid of PrP are resistant to scrapie. *Cell* **73**:1339-1347.

Bueler, H., Fischer, M., Lang, Y., Bluethmann, H., Lipp, H. P., Dearmond, S. J., Prusiner, S. B., Aguet, M. and Weissmann, C. (1992). Normal development and behaviour of mice lacking the neuronal cell-surface PrP protein. *Nature* **356**:577-582.

Butler, D. A., Scott, M. R., Bockman, J. M., Borchelt, D. R., Taraboulos, A., Hsiao, K. K., Kingsbury, D. T. and Prusiner, S. B. (1988). Scrapie-infected murine neuroblastoma cells produce protease-resistant prion proteins. *Journal of Virology* **62**:1558-1564.

Cain, K., Langlais, C., Sun, X.-M., Brown, D. G. and Cohen, G. M. (2001). Physiological concentrations of K^+ inhibit cytochrome c-dependent formation of the apoptosome. *The Journal of Biological Chemistry* **276**:41985-41990.

Cao, G., Clark, R. S., Pei, W., Yin, W., Zhang, F., Sun, F. Y., Graham, S. H. and Chen, J. (2003). Translocation of apoptosis-inducing factor in vulnerable neurons after transient cerebral ischemia and in neuronal cultures after oxygen-glucose deprivation. *Journal of Cereb Blood Flow Metab* **23**:1137-1150.

Carlson, G. A., Goodman, P. A., Lovett, M., Taylor, B. A., Marshall, S. T., Petersontorchia, M., Westaway, D. and Prusiner, S. B. (1988). Genetics and polymorphism of the mouse prion gene complex - control of scrapie incubation time. *Molecular and Cellular Biology* **8**:5528-5540.

Carlson, G. A., Kingsbury, D. T., Goodman, P. A., Coleman, S., Marshall, S. T., DeArmond, S., Westaway, D. and Prusiner, S. B. (1986). Linkage of prion protein and scrapie incubation time genes. *Cell* **46**:503-511.

Cashman, N. R., Loertscher, R., Nalbantoglu, J., Shaw, I., Kascsak, R. J., Bolton, D. C. and Bendheim, P. E. (1990). Cellular isoform of the scrapie agent protein participates in lymphocyte activation. *Cell* **61**:185-192.

Castilla, J., Saa, P., Hetz, C. and Soto, C. (2005). *In vitro* generation of infectious scrapie prions. *Cell* **121**:195-206.

Cataldo, A. M., Barnett, J. L., Berman, S. A., Li, J., Quarless, S., Bursztajn, S., Lippa, C. and Nixon, R. A. (1995). Gene expression and cellular content of cathepsin D in Alzheimer's disease brain: evidence for early up-regulation of the endosomal-lysosomal system. *Neuron* **14**:671-680.

Cataldo, A. M., Hamilton, D. J., Barnett, J. L., Paskevich, P. A. and Nixon, R. A. (1996). Properties of the endosomal-lysosomal system in the human central nervous system: disturbances mark most neurons in populations at risk to degenerate in Alzheimer's disease. *Journal of Neuroscience* **16**:186-199.

Cataldo, A. M., Hamilton, D. J. and Nixon, R. A. (1994). Lysosomal abnormalities in degenerating neurons link neuronal compromise to senile plaque development in Alzheimer disease. *Brain Research* **640**:68-80.

Caughey, B. and Lansbury, P. T. (2003). Protofibrils, pores, fibrils, and neurodegeneration: Separating the responsible protein aggregates from the innocent bystanders. *Annual Reviews of Neuroscience* **26**:267-298.

Caughey, B., Race, R. E. and Chesebro, B. (1988). Detection of prion protein mRNA in normal and scrapie-infected tissues and cell lines. *Journal of General Virology* **69**:711-716.

Caughey, B. and Raymond, G. J. (1991). The scrapie-associated form of PrP is made from a cell-surface precursor that is both protease-sensitive and phospholipase-sensitive. *Journal of Biological Chemistry* **266**:18217-18223.

Caughey, B., Raymond, G. J., Ernst, D. and Race, R. E. (1991). N-terminal truncation of the scrapie-associated form of PrP by lysosomal protease(s) - implications regarding the site of conversion of PrP to the protease-resistant state. *Journal of Virology* **65**:6597-6603.

Caughey, B. W., Dong, A., Bhat, K. S., Ernst, D., Hayes, S. F. and Caughey, W. S. (1991). Secondary structure-analysis of the scrapie-associated protein prp 27-30 in water by infrared-spectroscopy. *Biochemistry* **30**:7672-7680.

Chandler, R. L. (1961). Encephalopathy in mice produced with scrapie brain material. *Lancet* **i**:1378-1379.

Chen, S. G., Teplow, D. B., Parchi, P., Teller, J. K., Gambetti, P. and Autiliogambetti, L. (1995). Truncated forms of the human prion protein in normal brain and in prion diseases. *Journal of Biological Chemistry* **270**:19173-19180.

Chesebro, B., Trifilo, M., Race, R. E., Meade-White, K., Teng, C., LaCasse, R., Raymond, L., Favara, C., Baron, G., Priola, S. A., Caughey, B., Masliah, E. and Oldstone, M. (2005). Anchorless prion protein results in infectious amyloid disease without clinical scrapie. *Science* **308**:1435-1439.

Choi, S. I., Ju, W. K., Choi, E. K., Kim, J., Lea, H. Z., Carp, R. I., Wisniewski, H. M. and Kim, Y. S. (1998). Mitochondrial dysfunction induced by oxidative stress in the brains of hamsters infected with the 263 K scrapie agent. *Acta Neuropathologica* **96**:279-286.

Choi, Y. G., Kim, J. I., Lee, H. P., Jin, J. K., Choi, E. K., Carp, R. I. and Kim, Y. S. (2000). Induction of heme oxygenase-1 in the brains of scrapie infected mice. *Neuroscience Letters* **289**:173-176.

Clarke, M. C. and Haig, D. A. (1970). Evidence for the multiplication of scrapie agent in cell culture. *Nature* **225**:100-101.

Clarke, M. C. and Haig, D. A. (1970). Multiplication of scrapie agent in cell culture. *Res. vet. Sci.* **11**:500-501.

Clarke, M. C. and Millson, G. C. (1976). Infection of a cell line of mouse L fibroblasts with scrapie agent. *Nature* **261**:144-145.

Clayton, R., Clark, J. B. and Sharpe, M. (2005). Cytochrome c release from rat brain mitochondria is proportional to the mitochondrial functional deficit: implications for apoptosis and neurodegenerative disease. *Journal of Neurochemistry* **92**:840-849.

Collinge, J., Whittington, M. A., Sidle, K. C. L., Smith, C. J., Palmer, M. S., Clarke, A. R. and Jefferys, J. G. R. (1994). Prion protein is necessary for normal synaptic function. *Nature* **370**:295-297.

Cote, J. and Ruiz-Carrillo, A. (1993). Primers for mitochondrial DNA replication generated by endonuclease G. *Science* **261**:765-769.

Cuille, J. and Chelle, P.-L. (1936). La maladie dite "tremblante" du mouton; est-elle inoculable? *Compte Rend Acad Sci* **203**:1552.

Daude, N., Lehmann, S. and Harris, D. A. (1997). Identification of intermediate steps in the conversion of a mutant prion protein to a scrapie-like form in cultured cells. *Journal Of Biological Chemistry* **272**:11604-11612.

Daugas, E., Susin, S. A., Zamzami, N., Ferri, K. F., Irinopoulou, T., Larochette, N., Prevost, M. C., Leber, B., Andrews, D., Penninger, J. and Kroemer, G. (2000). Mitochondrio-nuclear translocation of AIF in apoptosis and necrosis. *Faseb Journal* **14**:729-739.

David-Ferreira, J. F., David-Ferreira, K. L., Gibbs, C. J., Jr. and Morris, J. A. (1968). Scrapie in mice: ultrastructural observations in the cerebral cortex. *Proceedings soc exp med* **127**:313-320.

De Gioia, L., Selvaggini, C., Ghibaudi, E., Diomede, L., Bugiani, O., Forloni, G., Tagliavini, F. and Salmona, M. (1994). Conformational polymorphism of the amyloidogenic and neurotoxic peptide homologous to residues 106-126 of the prion protein. *The Journal of Biological Chemistry* **269**:7859-7862.

Deleault, N. R., Lucassen, R. W. and Supattapone, S. (2003). RNA molecules stimulate prion protein conversion. *Nature* **425**:673-674.

Dickinson, A. G. (1975). Host-pathogen interactions in scrapie. *Genetics* **79**:387-395.
Dickinson, A. G. and Meikle, V. M. H. (1971). Host-Genotype and agent effects in Scrapie induction: change in allelic interaction with different strains of agent. *Molec. Gen. Genetics* **112**:73-79.

Dickinson, A. G., Meikle, V. M. H. and Fraser, H. (1968). Identification of a gene which controls the incubation period of some strains of scrapie agent in mice. *Journal of Comparative Pathology* **78**:239-299.

Dickinson, A. G., Stamp, J. T. and Renwick, C. C. (1974). Maternal and lateral transmission of scrapie in sheep. *Journal of Comparative Pathology* **84**:19-25.

Dickinson, A. G. and Taylor, D. M. (1978). Resistance of scrapie agent to decontamination. *New England Journal of Medecine* **299**:1413-1414.

Diener, T. O. (1971). Potato spindle tuber "virus": a plant virus with properties of a free nucleic acid. III. Subcellular location of PSTV-RNA and the question of whether virions exist in extracts or *in situ*. *Virology* **43**:75-89.

Doerr-Schott, J., Kitamoto, T., Tateishi, J., Boellaard, J. W., Heldt, N. and Lichte, C. (1990). Immunogold light and electron microscopic detection of amyloid plaques in transmissible spongiform encephalopathies. *Neuropathology and Applied Neurobiology* **16**:85-89.

Dorandeu, A., Wingertsmann, L., Chretien, F., Delisle, M. B., Vital, C., Parchi, P., Montagna, P., Lugaresi, E., Ironside, J. W., Budka, H., Gambetti, P. and Gray, F. (1998). Neuronal apoptosis in fatal familial insomnia. *Brain Pathology* **8**:531-537.

Du, C., Fang, M., Li, Y. and Wang, X. (2000). Smac, a mitochondrial protein that promotes cytochrome c-dependent caspase activation by eliminating IAP inhibition. *Cell* **102**:33-42.

Eckland, C. M., Kennedy, R. C. and Hadlow, W. J. (1967). Pathogenesis of scrapie virus infection in the mouse. *Journal of Infectious Diseases* **117**:15-22.

Ettaiche, M., Pichot, R., Vincent, J.-P. and Chabry, J. (2000). *In vivo* cytotoxicity of the prion protein fragment 106-126. *The Journal of Biological Chemistry* **275**:36487-36490.

Farquhar, C. F., Somerville, R. A. and Ritchie, L. A. (1989). Post-mortem immunodiagnosis of scrapie and bovine spongiform encephalopathy. *Journal of Virological Methods* **24**:215-221.

Fernandez-Salas, E., Suh, K. S., Speransky, V. V., Bowers, W. L., Levy, J. M., Adams, T., Pathak, K. R., Edwards, L. E., Hayes, D. D., Cheng, C., Steven, A. C., Weinberg, W. C. and Yuspa, S. H. (2002). mtCLIC/CLIC4, an organellular chloride channel protein, is increased by DNA damage and participates in the apoptotic response to p53. *Molecular and Cellular Biology* **22**:3610-3620.

Ferrer, I., Friguls, B., Dalfo, E., Justicia, C. and Planas, A. M. (2003). Caspase-dependent and caspase-independent signalling of apoptosis in the penumbra following middle cerebral artery occlusion in the adult rat. *Neuropathol Applied Neurobiology* **29**:472-481.

Fioriti, L., Quaglio, E., Massignan, T., Colombo, L., Stewart, R. S., Salmona, M., Harris, D. A., Forloni, G. and Chiesa, R. (2005). The neurotoxicity of prion protein (PrP) peptide 106-126 is independent of the expression level of PrP and is not mediated by abnormal PrP species. *Molecular and Cellular Neuroscience* **28**:165-176.

Fleetwood, A. J. and Furley, C. W. (1990). Spongiform encephalopathy in an eland [letter]. *Veterinary Record* **126**:408-409.

Florio, T., Grimaldi, M., Scorziello, A., Salmona, M., Bugiani, O., Tagliavini, F., Forloni, G. and Schettini, G. (1996). Intracellular calcium rise through L-type calcium channels, as molecular mechanism for prion protein-fragment 106-126-induced astroglial proliferation. *Biochemical and Biophysical Research Communications* **228**:397-405.

Florio, T., Paludi, D., Villa, V., Principe, D.-R., Corsaro, A., Millo, E., Damonte, G., D'Arrigo, C., Russo, C., Schettini, G. and Aceto, A. (2003). Contribution of two conserved glycine residues to fibrillogenesis of the 106-126 prion protein fragment. Evidence that a soluble variant of the 106-126 peptide is neurotoxic. *Journal of Neurochemistry* **85**:62-72.

Florio, T., Thellung, S., Amico, C., Robello, M., Salmona, M., Bugiani, O., Tagliavini, F., Forloni, G. and Schettini, G. (1998). Prion protein fragment 106-126 induces apoptotic cell death and impairment of L-type voltage-sensitive calcium channel activity in the GH3 cell line. *Journal of Neuroscience Research* **54**:341-352.

Forloni, G., Angeretti, N., Chiesa, R., Monzani, E., Salmona, M., Bugiani, O. and Tagliavini, F. (1993). Neurotoxicity of a prion protein-fragment. *Nature* **362**:543-546.

Forloni, G., Delbo, R., Angeretti, N., Chiesa, R., Smiroldo, S., Doni, R., Ghibaudi, E., Salmona, M., Porro, M., Verga, L., Giaccone, G., Bugiani, O. and Tagliavini, F. (1994). A neurotoxic prion protein fragment induces rat astroglial proliferation and hypertrophy. *European Journal of Neuroscience* **6**:1415-1422.

Formigli, L., Papucci, L., Tani, A., Schiavone, N., Tempestini, A., Orlandini, G. E., Capaccioli, S. and Orlandini, S. Z. (2000). Aponecrosis: Morphological and biochemical exploration of a syncretic process of cell death sharing apoptosis and necrosis. *Journal of Cellular Physiology* **182**:41-49.

Foster, J. D., Parnham, D. W., Chong, A., Goldmann, W. and Hunter, N. (2001). Clinical signs, histopathology and genetics of experimental transmission of BSE and natural scrapie to sheep and goats. *Veterinary Record* **148**:165-171.

Fraser, H. (1979). Scrapie: A transmissible degenerative CNS disease. *Progress in Neurological Research* 194-210.

Fraser, H. (1982). Neuronal spread of scrapie agent and targeting of lesions within the retino-tectal pathway. *Nature* **295**:149-150.

Fraser, H., Brown, K. L., Stewart, K., McConnell, I., McBride, P. and Williams, A. (1996). Replication Of Scrapie In Spleens Of Scid Mice Follows Reconstitution With Wild-Type Mouse Bone-Marrow. *Journal Of General Virology* **77**:1935-1940.

Fraser, H. and Bruce, M. E. (1983). Experimental control of cerebral amyloid in scrapie in mice. *Progress in Brain Research* **59**:281-290.

Fraser, H., Bruce, M. E., Davies, D., Farquhar, C. F. and McBride, P. A. (1992) in *Prion diseases of Humans and Animals*, eds. Prusiner, S. B.,Collinge, J.,Powell, J. & Anderton, B. (Ellis Horwood, Chichester), pp. 308-317.

Fraser, H. and Dickinson, A. G. (1968). The sequential development of the brain lesion of scrapie in three strains of mice. *Journal of Comparative Pathology* **78**:301-311.

Fraser, H. and Dickinson, A. G. (1970). Pathogenesis of scrapie in the mouse: the role of the spleen. *Nature* **226**:462-463.

Fraser, H. and Dickinson, A. G. (1973). Scrapie in mice. Agent-strain differences in the distribution and intensity of grey matter vacuolation. *Journal of Comparative Pathology* **83**:29-40.

Fraser, H. and Farquhar, C. F. (1987). Ionising radiation has no influence on scrapie incubation period in mice. *Veterinary Microbiology* **13**:211-223.

Fraser, J., Halliday, W., Brown, D., Belichenko , P. and Jeffrey, M. (1996). Mechanisms of scrapie-induced neuronal cell death. *Transmissible Spongiform Encephalopathies:Prion Diseases* 107-112.

Gahwiler, B. H. (1984). Slice cultures of cerebellar, hippocampal and hypothalamic tissue. *Experientia* **40**:235-308.

Gahwiler, B. H. (1988). Organotypic cultures of neural tissue. *Trends in Neuroscience* **11**:484-489.

Gahwiler, B. H., Capogna, M., Debanne, D., McKinney, R. A. and Thompson, S. M. (1997). Organotypic slice cultures: a technique has come of age. *Trends in Neuroscience* **20**:471-477.

Gajdusek, D. C., Gibbs, C. J. and Alpers, M. (1966). Experimental transmission of a Kuru-like syndrome to chimpanzees. *Nature* **209**:794-796.

Gajdusek, D. C. and Zigas, V. (1957). Degenerative disease of the central nervous system in New Guinea; the endemic occurrence of kuru in the normal population. *New England Journal of Medicine* **257**:974-978.

Gasset, M., Baldwin, M. A., Lloyd, D. H., Gabriel, J. M., Holtzman, D. M., Cohen, F., Fletterick, R. and Prusiner, S. B. (1992). Predicted alpha-helical regions of the prion protein when synthesized as peptides form amyloid. *Proceedings Of the National Academy Of Sciences Of the United States Of America* **89**:10940-10944.

Ghetti, B., Tagliavini, F., Masters, C. L., Beyreuther, K., Giaccone, G., Verga, L., Farlow, M. R., Conneally, P. M., Dlouhy, S. R., Azzarelli, B. and Bugiani, O. (1989). Gerstmann-Straussler-Scheinker disease II. Neurofibrillary tangles and plaques with PrP-amyloid coexist in an affected family. *Neurology* **39**:1453-1461.

Gibbs, C. J., Gajdusek, D. C., Asher, D. M., Alpers, M. P. and Beck, E. (1969). Creutzfeldt-Jakob disease (spongiform encephalopathy): transmission to the chimpanzee. *Science* **161**:388-389.

Giese, A., Brown, D. R., Groschup, M. H., Feldmann, C., Haist, I. and Kretzschmar, H. A. (1998). Role of microglia in neuronal cell death in prion disease. *Brain Pathology* **8**:449-457.

Giese, A., Groschup, M. H., Hess, B. and Kretzschmar, H. A. (1995). Neuronal cell death in scrapie-infected mice is due to apoptosis. *Brain Pathology* **5**:213-221.

Glatzel, M. and Aguzzi, A. (2000). PrPc expression in the peripheral nervous system is a determinant of prion neuroinvasion. *Journal of General Virology* **81**:2813-2821.

Glatzel, M., Heppner, F. L., Albers, K. M. and Aguzzi, A. (2001). Sympathetic innervation of lymphoreticular organs is rate limiting for prion neuroinvasion. *Neuron* **31**:25-34.

Goffredo, D., Rigamonti, D., Zuccato, C., Tartari, M., Valenza, M. and Cattaneo, E. (2005). Prevention of cytosolic IAPs degradation: a potential pharmacological target in Huntington's Disease. *Pharmacological Research* **52**:140-150.

Graner, E., Mercandante, A. F. and Zanata, S. (2000). Cellular prion protein binds laminin and mediates neuritogenesis. *Brain Research Molecular Brain Research* **76**:85-92.

Gray, F., Chretien, F., Adle-Biassette, H., Dorandeu, A., Ereau, T., Delisle, M. B., Kopp, N., Ironside, J. W. and Vital, C. (1999). Neuronal apoptosis in Creutzfeldt-Jakob disease. *Journal Neuropathol Exp Neurol* **58**:321-328.

Greene, L. A. and Tischler, A. S. (1976). Establishment of a noradrenergic clonal line of rat adrenal pheochromocytoma cells which respond to nerve growth factor. *Proceedings of the National Academy Of Sciences Of the United States Of America* **73**:2424-2428.

Gross, A., Yin, X. M., Wang, K., Wei, M. C., Jockel, J., Milliman, C., Erdjument-Bromage, H., Tempst, P. and Korsmeyer, S. J. (1999). Caspase cleaved BID targets mitochondria and is required for cytochrome c release, while Bcl-xL prevents this release but not tumor necrosis factor-R1/Fas death. *Journal of Biological Chemistry* **274**:1156-1163.

Guentchev, M., Siedlak, S. L., Jarius, C., Tagliavini, F., Castellani, R. J., Perry, G., Smith, M. A. and Budka, H. (2002). Oxidative damage to nucleic acids in human prion disease. *Neurobiology of Disease* **9**:275-281.

Hadlow, W. J. (1959). Scrapie and Kuru. *The Lancet* 289-290.

Hampton, M. B., Zhivotovsky, B., Slater, A. F. G., Burgess, D., H. and Orrenius, S. (1998). Importance of the redox state of cytochrome c during caspase activation in cytosolic extracts. *Biochemical Journal* **329**:95-99.

Haraguchi, T., Fisher, S., Olofsson, S., Endo, T., Groth, D., Tarentino, A., Borchelt, D. R., Teplow, D., Hood, L., Burlingame, A., Lycke, E., Kobata, A. and Prusiner, S. B. (1989). Asparagine-linked glycosylation of the scrapie and cellular prion proteins. *Archives of Biochemistry and Biophysics* **274**:1-13.

Harman, D. (1973). Free radical theory of aging. *Triangle* **12**:153-158.

Harris, D. A. (1999). Cellular biology of prion diseases. *Clinical Microbiology Reviews* **12**:429-447.

Head, M. W., Bunn, T. J., Bishop, M. T., McLoughlin, V., Lowrie, S., McKimmie, C. S., Williams, M. C., McCardle, L., MacKenzie, J., Knight, R., Will, R. G. and Ironside, J. W. (2004). Prion protein heterogeneity in sporadic but not variant Creutzfeldt-Jakob disease: UK cases 1991-2002. *Annals of Neurology* **55**:851-859.

Head, M. W., Tissingh, G., Uitdehaag, B. M., Barkhof, F., Bunn, T. J., Ironside, J. W., Kamphorst, W. and Scheltens, P. (2001). Sporadic Creutzfeldt-Jakob disease in a young Dutch valine homozygote: atypical molecular phenotype. *Annals of Neurology* **50**:258-261.

Hecker, R., Taraboulos, A., Scott, M., Pan, K. M., Yang, S. L., Torchia, M., Jendroska, K., DeArmond, S. J. and Prusiner, S. B. (1992). Replication of distinct scrapie prion isolates is region specific in brains of transgenic mice and hamsters. *Genes & Development* **6**:1213-1228.

Heegaard, P. M., Pedersen, H. G., Flink, J. and Boas, U. (2004). Amyloid aggregates of the prion peptide PrP106-126 are destabilised by oxidation and by the action of dendrimers. *FEBS Letters* **577**:127-133.

Heibein, J. A., Barry, M., Motyka, B. and Bleackley, R. C. (1999). Granzyme B-induced loss of mitochondrial inner membrane potential ({Delta}{Psi}m) and cytochrome c release are caspase-independent. *Journal of Immunology* **163**:4683-4693.

Herms, J. W., Tings, T., Dunker, S. and Kretzschmar, H. A. (2001). Prion protein affects Ca^{2+}-activated K^{+} currents in cerebellar Purkinje cells. *Neurobiology of Disease* **8**:324-330.

Hill, A. F., Butterworth, R. J., Joiner, S., Jackson, G., Rossor, M. N., Thomas, D. J., Frosh, A., Tolley, N., Bell, J. E., Spencer, M., King, A., Al-Sarraj, S., Ironside, J. W., Lantos, P. L. and Collinge, J. (1999). Investigation of variant Creutzfeldt-Jakob disease and other human prion diseases with tonsil biopsy samples. *Lancet* **353**:183-189.

Hill, A. F., Desbruslais, M., Joiner, S., Sidle, K. C. L., Gowland, I., Collinge, J., Doey, L. J. and Lantos, P. (1997). The same prion strain causes vCJD and BSE. *Nature* **389**:448-450.

Hope, J., Shearman, M. S., Baxter, H. C., Chong, A., Kelly, S. M. and Price, N. C. (1996). Cytotoxicity of prion protein peptide (PrP106-126) differs in mechanism from the cytotoxic activity of the Alzheimers disease amyloid peptide, a-Beta-25-35. *Neurodegeneration* **5**:1-11.

Hourigan, J., Kingspan, A., Clark, W. and de Camp, M. (1979) in *Transmissible diseases of the nervous system*, eds. Prusiner, S. B. & Hadlow, W. J. (Academy Press, New York), Vol. 1, pp. 339-343.

Hsiao, K. K., Groth, D., Scott, M., Yang, S. L., Serban, H., Raff, D., Foster, D., Torchia, M., Dearmond, S. J. and Prusiner, S. B. (1994). Serial transmission in rodents of neurodegeneration from transgenic mice expressing mutant prion protein. *Proceedings Of the National Academy Of Sciences Of the United States Of America* **91**:9126-9130.

Hsiao, K. K., Scott, M., Foster, D., Groth, D. F., DeArmond, S. J. and Prusiner, S. B. (1990). Spontaneous neurodegeneration in transgenic mice with mutant prion protein. *Science* **250**:1587-1590.

Hsich, G., Kinney, K., Gibbs, C. J., Lee, K. H. and Harrington, M. G. (1996). The 14-3-3-Brain-Protein In Cerebrospinal-Fluid As a Marker For Transmissible Spongiform Encephalopathies. *New England Journal Of Medicine* **335**:924- 930.

Hughes, F. M., Bortner, C. D., Purdy, G. D. and Cidlowski, J. A. (1997). Intracellular K^+ suppresses the activation of apoptosis in lymphocytes. *The Journal of Biological Chemistry* **272**:30567-30576.

Hunter, G. D. and Millson, G. C. (1964). Studies on the heat stability and chromatographic behaviour of the scrapie agent. *Journal of General Microbiology* **37**:251-258.

Jamieson, E., Jeffrey, M., Ironside, J. W. and Fraser, J. R. (2001) (a). Activation of Fas and caspase 3 precedes PrP accumulation in 87V scrapie. *Neurochemistry* **12**:3567-3572

Jamieson, E., Jeffrey, M., Ironside, J. W. and Fraser, J. R. (2001) (b). Apoptosis and dendritic dysfunction precede prion protein accumulation in 87V scrapie. *Neuroreport* **12**:2147-2153.

Jeffrey, M. and Fraser, J. R. (2000). Tubulovesicular particles are present early in the incubation period of scrapie infected mice. *Acta Neuropathol.* **99**:525-528.

Jeffrey, M. and Fraser, J. R. (2001) in *Molecular pathology of the prions*, ed. Baker, H. F. (Humana Press Inc., Totowa, NJ), Vol. Methods in Molecular Medicine vol.59, pp. 199-221.

Jeffrey, M., Goodsir, C. M., Bruce, M., McBride, P. A., Scott, J. R. and Halliday, W. G. (1994). Correlative light and electron-microscopy studies of PrP localization in 87V scrapie. *Brain Research* **656**:329-343.

Jeffrey, M., Goodsir, C. M., Bruce, M. E., McBride, P. A. and Farquhar, C. (1994). Morphogenesis of amyloid plaques in 87V murine scrapie. *Neuropathology and Applied Neurobiology* **20**:535-542.

Jeffrey, M., Goodsir, C. M., Bruce, M. E., McBride, P. A., Fowler, N. and Scott, J. R. (1994). Murine scrapie-infected neurons in-vivo release excess prion protein into the extracellular-space. *Neuroscience Letters* **174**:39-42.

Jeffrey, M., Goodsir, C. M., Bruce, M. E., McBride, P. A. and Fraser, J. R. (1997). *In vivo* toxicity of prion protein in murine scrapie: ultrastructural and immunogold studies. *Neuropathology and Applied Neurobiology* **23**:93-101.

Jeffrey, M., Halliday, W. G., Bell, J., Johnson, A. R., MacLeod, N. K., Ingham, C., Sayers, A. R., Brown, K. L. and Fraser, J. R. (2000). Synapse loss associated with abnormal PrP precedes neuronal degeneration in the scrapie-infected murine hippocampus. *Neuropathology and Applied Neurobiology* **26**:41-56.

Jeffrey, M., Martin, S., Barr, J., Chong, A. and Fraser, J. R. (2001). Onset and accumulation PrPres in murine ME7 scrapie in relation to pathological and PrP immunohistochemical changes. *Journal of Comparative Pathology* **124**:20-28.

Jeffrey, M., Scott, J. R., Williams, A. and Fraser, H. (1992). Ultrastructural features of spongiform encephalopathy transmitted to mice from three species of bovidae. *Acta Neuropathologica* **84**:559-569.

Jeffrey, M. and Wells, G. A. H. (1988). Spongiform encephalopathy in a nyala (tragelaphus-angasi). *Veterinary Pathology* **25**:398-399.

Jesionek-Kupnicka, D., Buczynski, J., Kordek, R., Sobow, T., Kloszewska, I., Papierz, W. and Liberski, P. P. (1997). Programmed cell death (apoptosis) in Alzheimer's disease and Creutzfeldt-Jakob disease. *Folia Neuropathologica* **35**:233-235.

Jia, L., Dourmashkin, R. R., Allen, P. D., Gray, A. B., Newland, A. C. and Kelsey, S. M. (1997). Inhibition of autophagy abrogates tumor necrosis factor alpha induced apoptosis in human T-lymphoblastic leukaemic cells. *British Journal of Histopathology* **98**:673-685.

Jobling, M. F., Stewart, L. R., White, A. R., McLean, C., Friedhuber, A., Maher, F., Beyreuther, K., Masters, C. L., Barrow, C. J., Collins, S. J. and Cappai, R. (1999). The hydrophobic core sequence modulates the neurotoxic and secondary structure properties of the prion peptide 106-126. *Journal of Neurochemistry* **73**:1557-1565.

Johnston, A. R., Black, C., Fraser, J. and MacLeod, N. (1997). Scrapie infection alters the membrane and synaptic properties of mouse hippocampal CA1 pyramidal neurones. *Journal Of Physiology* **500**:1-15.

Johnston, A. R., Fraser, J. R., Jeffrey, M. and MacLeod, N. (1998). Alterations in potassium currents may trigger neurodegeneration in murine scrapie. *Experimental Neurology* **151**:326-333.

Joza, N., Susin, S. A., Daugas, E., Stanford, W. L., Cho, S. K., Li, C. Y., Sasaki, T., Elia, A. J., Cheng, H. Y., Ravagnan, L., Ferri, K. F., Zamzami, N., Wakeham, A., Hakem, R., Yoshida, H., Kong, Y. Y., Mak, T. W., Zuniga-Pflucker, J. C., Kroemer, G. and Penninger, J. M. (2001). Essential role of the mitochondrial apoptosis-inducing factor in programmed cell death. *Nature* **410**:549-554.

Kascsak, R. J., Rubenstein, R., Merz, P. A., Carp, R. I., Robakis, N. K., Wisniewski, H. M. and Diringer, H. (1986). Immunological comparison of scrapie-associated fibrils isolated from animals infected with 4 different scrapie strains. *Journal of Virology* **59**:676-683.

Kaneko, K., Zulianello, L., Scott, M., Pilkuhn, S., Cohen, F. E. and Prusiner, S. B. (1997). Evidence for protein X binding to a discontinuous epitope on the cellular prion protein during scrapie prion propagation. *Proceedings of the National Academy of Sciences of the United States of America* **94**:10069-10074.

Kazlauskaite, J., Young, A., Gardner, C. E., Macpherson, J. V., Venien-Bryan, C. and Pinheiro, T. J. T. (2005). An unusual soluble β-turn-rich conformation of prion is involved in fibril formation and toxic to neuronal cells. *Biochemical and Biophysical Research Communications* **328**:292-305.

Kegel, K. B., Kim, M., Sapp, E., McIntyre, C., Castano, J. G. and Aronin, N. (2000). Huntingtin expression stimulates endosomal-lysosomal activity, endosome tubulation, and autophagy. *Journal of Neuroscience* **20**:7268-7278.

Kerr, J. F., Wyllie, A. H. and Currie, A. R. (1972). Apoptosis: a basic biological phenomenon with wide-ranging implications in tissue kinetics. *Br J Cancer* **26**:239-257.

Kikuchi, A., Takeda, A., Onodera, H., Kimpara, T., Hisanaga, K., Sato, N., Nunomura, A., Castellani, R. J., Perry, G., Smith, M. A. and Itoyama, Y. (2002). Systemic increase of oxidative nucleic acid damage in Parkinson's disease and multiple system atrophy. *Neurobiology of Disease* **9**:244-248.

Kimberlin, R. H., Hall, S. M. and Walker, C. A. (1983). Pathogenesis of mouse scrapie - Evidence for direct neural spread of infection to the CNS after injection of sciatic nerve. *Journal of the Neurological Sciences* **61**:315-325.

Kimberlin, R. H. and Walker, C. A. (1979). Pathogenesis of mouse scrapie: dynamics of agent replication in spleen, spinal cord and brain after infection by different routes. *Journal of Comparative Pathology* **89**:551-562.

Kimberlin, R. H. and Walker, C. A. (1980). Pathogenesis of mouse scrapie: evidence for neural spread of infection to the CNS. *Journal of General Virology* **51**:183-187.

Kimberlin, R. H. and Walker, C. A. (1989). The role of the spleen in the neuroinvasion of scrapie in mice. *Virus Research* **12**:201-211.

Kirkwood, J. K. and Cunningham, A. A. (1999) in *26th World Veterinary Congress*, Lyon).

Kirkwood, J. K., Wells, G. A. H., Wilesmith, J. W., Cunningham, A. A. and Jackson, S. I. (1990). Spongiform encephalopathy in an arabian oryx and a greater kudu. *The Vet Record* 418-420.

Klatzo, Gajdusek, D. C. and Zigas, V. (1959). Pathology of Kuru. *Lab Investig* **8**:799-847.

Klebe, R. J. and Ruddle, F. H. (1969). Neuroblastoma: cell culture analysis of a differentiating stem cell system. *Journal of Cell Biology* **43**:69.

Klein, J. A., Longo-Guess, C. M., Rossmann, M. P., Seburn, K. L., Hurd, R. E., Frankel, W. N., Bronson, R. T. and Ackerman, S. L. (2002). The harlequin mouse mutation downregulates apoptosis-inducing factor. *Nature* **419**:367-374.

Klein, M. A., Frigg, R., Flechsig, E., Raeber, A. J., Kalinke, U., Bluethmann, H., Bootz, F., Suter, M., Zinkernagel, R. M. and Aguzzi, A. (1997). A crucial role for B cells in neuroinvasive scrapie. *Nature* **390**:687-690.

Kluck, R. M., Bossy-Wetzel, E., Green, D. R. and Newmeyer, D. D. (1997). The release of cytochrome c from mitochondria: a primary site for Bcl-2 regulation of apoptosis. *Science* **275**:1132-1136.

Kocisko, D. A., Come, J. H., Priola, S. A., Chesebro, B., Raymond, G. J., Lansbury, P. T. and Caughey, B. (1994). Cell-free formation of protease-resistant prion protein. *Nature* **370**:471-474.

Korth, C., Stierli, B., Streit, P., Moser, M., Schaller, O., Fischer, R., SchulzSchaeffer, W., Kretzschmar, H., Raeber, A., Braun, U., Ehrensperger, F., Hornemann, S., Glockshuber, R., Riek, R., Billeter, M., Wuthrich, K. and Oesch, B. (1997). Prion (PrP^{Sc})-specific epitope defined by a monoclonal antibody. *Nature* **390**:74-77.

Kocisko, D. A., Come, J. H., Priola, S. A., Chesbro, B., Raymond, G. J., Lansbury, P. T. and Caughey, B. (1994). Cell-free formation of protease-resistant prion protein. *Nature* **370**:471-474

Kocisko, D. A., Priola, S. A., Raymond, G. J., Chesbro, B., Lansbury, P. T. and Caughey, B. (1995). Species specificity in the cell-free conversion of prion protein to protease-resistant forms: a model for the scrapie species barrier. *Proceedings of the National Academy of Sciences of the United States of America* **92**:3923-3927

Krebs, M. R. H., Bromley, E. H. C. and Donald, A. M. (2005). The binding of thioflavin-T to amyloid fibrils: localisation and implications. *Journal of Structural Biology* **149**:30-37.

Laemmli, U. K. (1970). Cleavage of structural proteins during the assembly of the head of bacteriophage T4. *Nature* **277**:680-685.

Larsen, K. E. and Sulzer, D. (2002). Autophagy in neurons: a review. *Histology and Histopathology* **17**:897-908.

Lasmezas, C. I., Cesbron, J. Y., Deslys, J. P., Demaimay, R., Anjou, K. T., Rioux, R., Lemaire, C., Locht, C. and Dormont, D. (1996). Immune System-Dependent and System-Independent Replication Of the Scrapie Agent. *Journal Of Virology* **70**:1292-1295.

Latarjet, R. and Muel, B. (1970). Inactivation of the Scrapie Agent by near Monochromatic Ultra Violet Light. *Nature* **227**:1341-1343.

Lazarini, F., Castelnau, P., Chermann, J. F., Deslys, J. P. and Dormont, D. (1994). Modulation of prion protein gene expression by growth factors in cultured mouse astrocytes and PC12 cells. *Molecular Brain Research* **22**:268-274.

Lee, D. W., Sohn, H. O., Lim, H. B., Lee, Y. G., Kim, Y. S., Carp, R. I. and Wisniewski, H. M. (1999). Alteration of free radical metabolism in the brain of mice infected with scrapie agent. *Free Radical Research* **30**:499-507.

Lee, M. K. and Cleveland, D. W. (1996). Neuronal intermediate filaments. *Annual Reviews of Neuroscience* **19**:187-217.

Legname, G., Baskakov, I. V., Nguyen, H.-O. B., Riesner, D., Cohen, F. E., DeArmond, S. J. and Prusiner, S. B. (2004). Synthetic mammalian prions. *Science* **305**:673-676.

Legname, G., Hoang-Oanh, B. N., Baskakov, I. V., Cohen, F. E., DeArmond, S. J. and Prusiner, S. B. (2005). Strain-specified characteristics of mouse synthetic prions. *Proceedings of the National Academy of Sciences of the United States of America* **102**:2168-2173.

Lemasters, J. J., Nieminen, A. L., Qian, T., Trost, L. C., Elmore, S. P., Nishimura, Y., Crowe, R. A., Cascio, W. E., Bradham, C. A., Brenner, D. A. and Herman, B. (1998). The mitochondrial permeability transition in cell death: a common mechanism in necrosis, apoptosis and autophagy *Biochimica and biophysica Acta* **1366**:177-196.

Li, H., Zhu, H., Xu, C. J. and Yuan, J. (1998). Cleavage of BID by caspase 8 mediates the mitochondrial damage in the Fas pathway of apoptosis. *Cell* **94**:491-501.

Li, L. Y., Luo, X. and Wang, X. (2001). Endonuclease G is an apoptotic DNase when released from mitochondria. *Nature* **412**:95-99.

Liao, Y. C. J., Lebo, R. V., Clawson, G. A. and Smuckler, E. A. (1986). Human prion protein cDNA- molecular-cloning, chromosomal mapping, and biological implications. *Science* **233**:364-367.

Liberski, P. P., Budka, H., Yanagihara, R., Gibbs, C. J. and Gajdusek, D. C. (1993) in *Light and Electron Microscopic Neuropathology of Slow Virus Disorders*, ed. Liberski, P. P. (CRC, Boca Raton, pp. 373-392.

Liberski, P. P., Jeffrey, M. and Goodsir, C. (1997). Tubulovesicular structures are not labeled using antibodies to prion protein (PrP) with the immunogold electron microscopy techniques. *Acta Neuropathologica* **93**:260-264.

Liberski, P. P., Yanagihara, R., Gibbs, C. J. and Gajdusek, D. C. (1992). Neuronal autophagic vacuoles in experimental scrapie and Creutzfeldt-Jakob disease. *Acta Neuropathologica* **83**:134-139.

Lindenbaum, M. H., Carbonetto, S., Grosveld, F., Flavell, D. and Mushynski, W. E. (1998). Transcriptional and post-transcriptional effects of nerve growth factor on the expression of three neurofilament subunits in PC-12 cells. *The Journal of Biological Chemistry* **263**:5662-5667.

Liu, X., Kim, C. N., Yang, J., Jemmerson, R. and Wang, X. (1996). Induction of apoptotic program in cell-free extracts: requirement for dATP and cytochrome c. *Cell* **86**:147-57.

Lloyd, S. E., Thompson, S. R., Beck, J. A., Linehan, J. M., Wadsworth, J. D., Brandner, S., Collinge, J. and Fisher, E. M. (2004). Identification and characterization of a novel mouse prion gene allele. *Mammalian Genome* **15**:383-9.

Lucassen, P. J., Williams, A., Chung, W. C. J. and Fraser, H. (1995). Detection of apoptosis in murine scrapie. *Neuroscience Letters* **198**:185-188.

Luo, X., Budihardjo, I., Zou, H., Slaughter, C. and Wang, X. (1998). Bid, a Bcl2 interacting protein, mediates cytochrome c release from mitochondria in response to activation of cell surface death receptors. *Cell* **94**:481-490.

Ma, J. and Lindquist, S. (1999). *De novo* generation of a PrP^{sc}-like conformation in living cells. *Nature Cell Biology* **1**:358-361.

Mabbott, N. A., Brown, K. L., Manson, J. and Bruce, M. E. (1997). T-lymphocyte activation and the cellular form of the prion protein. *Immunology* **92**:161-165.

Mabbott, N. A. and Bruce, M. E. (2002). Follicular dendritic cells as targets for intervention in transmissible spongiform encephalopathies. *Semin Immunol* **14**:285-293.

Manczak, M., Jung, Y., Park, B. S., Partovi, D. and Reddy, P. H. (2005). Time-course of mitochondrial gene expressions in mice brains: implications for mitochondrial dysfunction, oxidative damage, and cytochrome c in aging. *Journal of Neurochemistry* **92**:494-504.

Manson, J., Jamieson, E., Baybutt, H., Tuzi, N., Barron, R., McConnell, I., Somerville, R. A., Ironside, J. W., Will, R. G., Sy, M.-S., Melton, D. W., Hope, J. and Bostock, C. J. (1999). A single amino acid alteration (101L) introduced into murine PrP dramatically alters incubation time of transmissible spongiform encephalopathy. *Embo Journal* **18**:101-110.

Manson, J., McBride, P. and Hope, J. (1992). Expression of the PrP gene in the brain of *Sinc* congenic mice and its relationship to the development of scrapie. *Neurodegeneration* **1**:45-52.

Martinou, J. C. (1994). Overexpression of Bcl-2 in transgenic mice protects neurons from naturally occuring cell death and experimental ischemia. *Neuron* **13**:1017-1030.

Masters, C. L., Gajdusek, D. C. and Gibbs, C. J. (1981). Creutzfeld-Jakob disease virus isolations from the Gerstmann-Straussler syndrome with the analysis of the various forms of amyloid plaque deposition in the virus-induced spongiform encephalopathies. *Brain* **104**:559-588.

Mate, M. J., Ortiz-Lombardia, M., Boitel, B., Haouz, A., Tello, D., Susin, S. A., Penninger, J., Kroemer, G. and Alzari, P. M. (2002). The crystal structure of the mouse apoptosis-inducing factor AIF. *Nature Structural Biology* **9**:442-446.

McBride, P. A. and Beekes, M. (1999). Pathological PrP is abundant in sympathetic and sensory ganglia of hamsters fed with scrapie. *Neuroscience Letters* **265**:135-138.

McBride, P. A., Eikelenboom, P., Kraal, G., Fraser, H. and Bruce, M. E. (1992). PrP protein is associated with follicular dendritic cells of spleens and lymph nodes in uninfected and scrapie-infected mice. *Journal of Pathology* **168**:413-418.

McBride, P. A., Schulz-Schaeffer, W. J., Donaldson, M., Bruce, M., Diringer, H., Kretzschmar, H. A. and Beekes, M. (2001). Early spread of scrapie from the gastrointestinal tract to the central nervous system involves autonomic fibres of the splanchnic and vagus nerves. *Journal of Virology* **75**:9320-9327.

McBride, P. A., Wilson, M. I., Eikelenboom, P., Tunstall, A. and Bruce, M. E. (1998). Heparan sulfate proteoglycan is associated with amyloid plaques and neuroanatomically targeted PrP pathology throughout the incubation period of scrapie-infected mice. *Experimental Neurology* **149**:447-454.

McKinley, M. P., Bolton, D. C. and Prusiner, S. B. (1983). A protease-resistant protein is a structural component of the scrapie prion. *Cell* **35**:57-62.

Mellon, P. L., Windle, J. J., Goldsmith, P. C., Padula, C. A., Roberts, J. L. and Weiner, R. I. (1990). Immortalization of a hypothalamic GnRH neurons by genetically targeted tumorigenesis. *Neuron* **5**:1-10.

Merz, P. A., Somerville, R. A., Wisniewski, H. M. and Iqbal, K. (1981). Abnormal fibrils from scrapie-infected brain. *Acta Neuropathol.* **54**:63-74.

Merz, P. A., Wisniewski, H. M., Somerville, R. A., Bobin, S. A., Masters, C. L. and Iqbal, K. (1983). Ultrastructural morphology of amyloid fibrils from neuritic and amyloid plaques. *Acta Neuropathologica* **60**:113-124.

Meyer, R. K., McKinley, M. P., Bowman, K. A., Braunfeld, M. B., Barry, R. A. and Prusiner, S. B. (1986). Separation and properties of cellular and scrapie prion proteins. *Proceedings of the National Academy of Sciences of the United States of America* **83**:2310-2314.

Millson, G. C., Hunter, G. D. and Kimberlin, R. H. (1976) in *Slow virus diseases of animals and man*, ed. Kimberlin, R. H. (North-Holland, pp. 243-266.

Millson, G. C., Kimberlin, R. H., Manning, E. J. and Collis, S. C. (1979). Early distribution of radioactive liposomes and scrapie infectivity in mouse tissues following administration by different routes. *Veterinary Microbiology* **4**:89-99.

Miramar, M. D., Costantini, P., Ravagnan, L., Saraiva, L. M., Haouzi, D., Brothers, G., Penninger, J. M., Peleato, M. L., Kroemer, G. and Susin, S. A. (2001). NADH oxidase activity of mitochondrial apoptosis-inducing factor. *Journal of Biological Chemistry* **276**:16391-8.

Mohan, J., Brown, K. L., Farquhar, C. F., Bruce, M. E. and Mabbott, N. A. (2004). Scrapie transmission following exposure through the skin is dependent on follicular dendritic cells in lymphoid tissues. *Journal of Dermatological Science* **35**:101-111.

Mohan, J., Bruce, M. E. and Mabbott, N. A. (2005). Follicular dendritic cell dedifferentiation reduces scrapie susceptibility following inoculation via the skin. *Immunology* **114**:225-234.

Moore, R. C., Hope, J., McBride, P. A., McConnell, I., Selfridge, J., Melton, D. W. and Manson, J. C. (1998). Mice with gene targetted prion protein alterations show that Prnp, Sinc and Prni are congruent. *Nature Genetics* **18**:118-125.

Moore, R. C., Lee, I. Y., Silverman, G. L., Harrison, P. M., Strome, R., Heinrich, C., Karunaratne, A., Pasternak, S. H., Chishti, M. A., Liang, Y., Mastrangelo, P., Wang, K., Smit, A. F., Katamine, S., Carlson, G. A., Cohen, F. E., Prusiner, S. B., Melton, D. W., Tremblay, P., Hood, L. E. and Westaway, D. (1999). Ataxia in prion protein (PrP)-deficient mice is associated with upregulation of the novel PrP-like protein doppel. *Journal of Molecular Biology* **292**:797-817.

Moser, M., Colello, R. J., Pott, U. and Oesch, B. (1995). Developmental expression of the prion protein gene in glial-cells. *Neuron* **14**:509-517.

Muchowski, P. J. (2002). Protein misfolding, amyloid formation, and neurodegeneration: A critical role for molecular chaperones? *Neuron* **35**:9-12.

Muramoto, T., Scott, M., Cohen, F. E. and Prusiner, S. B. (1996). Recombinant scrapie-like prion protein of 106 amino acids is soluble. *Proceedings of the National Academy of Sciences Of the United States Of America* **93**:15457-15462.

Narang, H. K., Asher, D. M. and Gajdusek, D. C. (1987). Tubulofilaments in negatively stained scrapie-infected brains: relationship to scrapie-associated fibrils. *Proceedings of the National Academy Of Sciences Of the United States Of America* **84**:7730-7734.

Norstrom, E. M. and Mastrianni, J. A. (2005). The AGAAAAGA palindrome in PrP is required to generate a productive PrP^{Sc}-PrP^{C} complex that leads to prion propagation. *The Journal of Biological Chemistry* **280**:27236-27243.

Nunomura, A., Perry, G., Hirai, K., Aliev, G., Takeda, A., Chiba, S. and Smith, M. A. (1999). Neuronal RNA oxidation in Alzheimer's disease and Down's syndrome. *Annals of the New York Academy of Sciences* **893**:362-364.

O'Donovan, C., Tobin, D. and Cotter, T. G. (2001). Prion protein fragment PrP106-126 induces apoptosis via mitochondrial disruption in human neuronal SH-SY5Y cells. *The Journal of Biological Chemistry* **276**:43516-43523.

Oesch, B., Westaway, D., Walchli, M., McKinley, M. P., Kent, S. B., Aebersold, R., Barry, R. A., Tempst, P., Teplow, D. B. and Hood, L. E. (1985). A cellular gene encodes scrapie PrP 27-30 protein. *Cell* **40**:735-746.

Pan, K. M., Baldwin, M., Nguyen, J., Gasset, M., Serban, A., Groth, D., Mehlhorn, I., Huang, Z., Fletterick, R. J. and Cohen, F. E. (1993). Conversion of alpha-helices into beta-sheets features in the formation of the scrapie prion proteins. *Proceedings of the National Academy of Sciences of the United States of America* **90**:10962-10966.

Pan, K. M., Stahl, N. and Prusiner, S. B. (1992). Purification and properties of the cellular prion protein from Syrian hamster brain. *Protein Science* **1**:1343-1352

Parchi, P., Zou, W., Wang, W., Brown, P., Capellari, S., Ghetti, B., Kopp, N., Schulz-Schaeffer, W. J., Kretzschmar, H. A., Head, M. W., Ironside, J. W., Gambetti, P. and Chen, S.G. (2000). Genetic influence on the structural variations of the abnormal prion protein. *Proceedings of the National Academy Of Sciences Of the United States Of America* **97**:10168-10172.

Pattison, I. (1965) in *Slow latent and temperate virus infections, NINDB Monograph 2*, eds. Gajdusek, D. C.,Gibbs, C. J. & Alpers, M. P. (US Government printing, Washington DC), Vol. 249-257.

Pattison, I. and Milson, G. (1961). Experimental transmission of scrapie to goats and sheep by the oral route. *Journal of Comparative Pathology* **71**:171-176.

Pattison, I. H. (1965). Resistance of the Scrapie agent to Formalin. *Journal of Comparative Pathology* **75**:159-164.

Pauly, P. C. and Harris, D. A. (1998). Copper stimulates endocytosis of the prion protein. *Journal of Biological Chemistry* **273**:107-133.

Peet, R. L. and Curran, J. M. (1992). Spongiform encephalopathy in an imported cheetah (acinonyx-jubatus). *Australian Veterinary Journal* **69**:171.

Petersen, R. B., Parchi, P., Richardson, S. L., Urig, C. B. and Gambetti, P. (1996). Effect of the D178N mutation and the codon 129 polymorphism on the metabolism of the prion protein. *Journal of Biological Chemistry* **271**:12661-12668.

Petersen, A., Larsen, K. E., Behr, G. G., Romero, N., Przedborski, S., Brundin, P. and Sulzer, D. (2001). Effect of the D178N mutation and the codon 129 polymorphism on the metabolism of the prion protein. *Human Molecular Genetics* **10**:1243-1254.

Petersen, R. B., Siedlak, S. L., Lee, H. G., Kim, Y. S., Nunomura, A., Tagliavini, F., Ghetti, B., Cras, P., Moreira, P. I., Castellani, R. J., Guentchev, M., Budka, H., Ironside, J. W., Gambetti, P., Smith, M. A. and Perry, G. (2005). Redox metals and oxidative abnormalities in human prion diseases. *Acta Neuropathologica* **110**:232-238.

Pohl, D., Bittigau, P., Ishimaru, M. J., Stadthaus, D., Hubner, C. and Olney, J. W. (1999). N-methyl-D-aspartate antagonists and apoptotic cell death triggered by head trauma in developing rat brain. *Proceedings of the National Academy Of Sciences Of the United States Of America* **96**:2508-2513.

Priola, S. A. and Chesebro, B. (1995). A single hamster PrP amino acid blocks conversion to protease-resistant PrP in scrapie-infected mouse neuroblastoma cells. *Journal of Virology* **69**:7754-7758.

Priola, S. A. and Chesebro, B. (1998). Abnormal properties of prion protein with insertional mutations in different cell types. *Journal of Biological Chemistry* **273**:11980-11985.

Prusiner, S. B. (1982). Novel proteinaceous infections particles cause scrapie. *Science* **216**:136-144.

Prusiner, S. B. (1998). Prions. *Proceedings of the National Academy of Sciences of the United States of America* **95**:13363-13383.

Prusiner, S. B., Groth, D. F., McKinley, M. P., Cochran, S. P., Bowman, K. A. and Masiarz, F. R. (1982). Scrapie agent is a novel proteinaceous infectious particle. *Federation Proceedings* **41**:695.

Prusiner, S. B., McKinley, M. P., Bowman, K. A., Bolton, D. C., Bendheim, P. E., Groth, D. F. and Glenner, G. G. (1983). Scrapie prions aggregate to form amyloid-like birefringent rods. *Cell* **35**:349-358.

Prusiner, S. B., Groath, D. F., Bolton, D. C., Kent, S. B. and Hood, L. E. (1984). Purification and structural properties of a major scrapie prion protein. *Cell* **38**:127-134.

Puig, B. and Ferrer, I. (2001). Cell death signaling in the cerebellum in Creutzfeldt-Jakob disease. *Acta Neuropathologica* **102**:207-215.

Quaglio, E., Chiesa, R. and Harris, D. A. (2001). Copper converts the cellular prion protein into a protease-resistant species that is distinct from the scrapie isoform. *The Journal of Biological Chemistry* **276**:11432-11438.

Race, R. E., Caughey, B., Graham, K., Ernst, D. and Chesebro, B. (1988). Analyses of frequency of infection, specific infectivity, and prion protein biosynthesis in scrapie-infected neuroblastoma cell clones. *Journal of Virology* **62**:2845-2849.

Race, R. E., Fadness, L. H. and Chesebro, B. (1987). Characterization of scrapie infection in mouse neuroblastoma cells. *Journal of General Virology* **68**:1391-1399.

Raeber, A. J., Race, R. E., Brandner, S., Priola, S. A., Sailer, A., Bessen, R. A., Mucke, L., Manson, J., Aguzzi, A., Oldstone, M. B. A., Weissmann, C. and Chesebro, B. (1997). Astrocyte-specific expression of hamster prion protein (PrP) renders PrP knockout mice susceptible to hamster scrapie. *Embo Journal* **16**:6057-6065.

Ragg, E., Tagliavini, F., Malesani, P., Monticelli, L., Bugiani, O., Forloni, G. and Salmona, M. (1999). Determination of solution conformations of PrP106-126, a neurotoxic fragment of prion protein, by ^{1}H NMR and restrained molecular dynamics. *European Journal of Biochemistry* **266**:1192-1201.

Ravagnan, L., Gurbuxani, S., Susin, S. A., Maisse, C., Daugas, E., Zamzami, N., Mak, T., Jaattela, M., Penninger, J. M., Garrido, C. and Kroemer, G. (2001). Heat-shock protein 70 antagonizes apoptosis-inducing factor. *Nature Cell Biology* **3**:839-843.

Rieger, R., Edenhofer, F., Lasmezas, C. I. and Weiss, S. (1997). The human 37-kDa laminin receptor precursor interacts with the prion protein in eukaryotic cells. *Nature Medicine* **3**:1383-1388.

Rodriguez, M., M., Peoc'h, K., Haik, S., Bouchet, C., Verengo, L., Manana, G., Salamano, R., Carrasco, L., Lenne, M., Beaudry, P., Launay, J. M. and Laplanche, J. L. (2005). A novel mutation (G114V) in the prion protein gene in a family with inherited prion disease. *Neurology* **64**:1455-1457.

Roizon, L., Stellar, S. and Liu, J. C. (1974). Electron microscope and enzyme studies in cerebral biopsies of Huntington's chorea. *Transcripts of the American Neurological Association* **99**:240-243.

Roizon, L., Stellar, S. and Liu, J. C. (1979). Neuronal nuclear-cytoplasmic changes in Huntington's chorea: electron microscope investigations. *Advanced Neurology* **23**:93-122.

Rubenstein, R., Carp, R. I. and Callahan, S. M. (1984). *In vitro* replication of scrapie agent in a neuronal model: Infection of PC12 cells. *Journal of General Virology* **65**:2191-2198.

Rubenstein, R., Deng, H., Race, R. E., Ju, W., Scalici, C. L., Papini, M. C., Kascsak, R. J. and Carp, R. I. (1992). Demonstration of scrapie strain diversity in infected PC12 cells. *Journal of General Virology* **73**:3027-3031.

Rubenstein, R., Deng, H., Race, R. E., Ju, W., Scalici, C. L., Papini, M. C., Rubenstein, A., Kascsak, R. J. and Carp, R. I. (1994). Scrapie strain infection *in vitro* induces changes in neuronal cells. *Molecular Neurobiology* **8**:129-138.

Rubenstein, R., Scalici, C. L., Papini, M. C., Callahan, S. M. and Carp, R. I. (1990). Further characterization of scrapie replication in PC12 cells. *Journal of General Virology* **71**:825-831.

Saborio, G. P., Permanne, B. and Soto, C. (2001). Sensitive detection of pathological prion protein by cyclic amplification of protein misfolding. *Nature* **411**:810-813.

Safar, J., Roller, P. P., Gajdusek, D. C. and Gibbs, C. J. (1993). Conformational transitions, dissociation, and unfolding of scrapie amyloid (prion) protein. *Journal of Biological Chemistry* **268**:20276-20284.

Sakaguchi, S., Katamine, S., Nishida, N., Moriuchi, R., Shigematsu, K., Sugimoto, T., Nakatani, A., Kataoka, Y., Houtani, T., Shirabe, S., Okada, H., Hasegawa, S., Miyamoto, T. and Noda, T. (1996). Loss of Cerebellar Purkinje-Cells In Aged Mice Homozygous For a Disrupted Prp Gene. *Nature* **380**:528-531.

Saleh, A., Srinivasula, S. M., Balkir, L., Robbins, P. D. and Alnemri, E. S. (2000). Negative regulation of the Apaf-1 apoptosome by Hsp70. *Nature Cell Biology* **2**:476-483.

Salmona, M., Malesani, P., DeGioia, L., Gorla, S., Bruschi, M., Molinari, A., DellaVedova, F., Pedrotti, B., Marrari, M. A., Awan, T., Bugiani, O., Forloni, G. and Tagliavini, F. (1999). Molecular determinants of the physicochemical properties of a critical prion protein region comprising residues 106-126. *Biochemical Journal* **342**:207-214.

Scaffidi, C., Fulda, S., Srinivasan, A., Friesen, C., Li, F., Tomaselli, K. J., Debatin, K.-M., Krammer, P. H. and Peter, M. E. (1998). Two CD95 (APO-1/Fas) signaling pathways. *Journal of Biological Chemistry* **17**:1675-1687.

Schätzl, H. M., Laszlo, L., Holtzman, D. M., Tatzelt, J., Dearmond, S. J., Weiner, R. I., Mobley, W. C. and Prusiner, S. B. (1997). A hypothalamic neuronal cell line persistently infected with scrapie prions exhibits apoptosis. *Journal of Virology* **71**:8821-8831.

Schild, L., Keilhoff, G., Augustin, W., Resiser, G. and Striggow, F. (2001). Distinct Ca^{2+} thresholds determine cytochrome c release or permeability transition pore opening in brain mitochondria. *Faseb Journal* **15**:565-567.

Schimmelpfeng, J., Weibezahn, K.-F. and Dertinger, H. (2004). Quantification of NGF-dependent neuronal differentiation of PC-12 cells by means of neurofilament-L mRNA expression and neuronal outgrowth. *Journal of Neuroscience Methods* **139**:299-306.

Schutte, B., Nuydens, R., Geerts, H. and Ramaekers, F. (1998). Annexin V binding assay as a tool to measure apoptosis in differentiated neuronal cells. *Journal of Neuroscience Methods* **86**:63-69.

Scott, J. R. and Fraser, H. (1984). Degenerative hippocampal pathology in mice infected with scrapie. *Acta Neuropathologica* **65**:62-68.

Scott, M. R., Safar, J., Telling, G., Nguyen, O., Groth, D., Torchia, M., Koehler, R., Tremblay, P., Walther, D., Cohen, F. E., DeArmond, S. J. and Prusiner, S. B. (1997). Identification of a prion protein epitope modulating transmission of bovine spongiform encephalopathy prions to transgenic mice. *Proceedings of the National Academy Of Sciences Of the United States Of America* **94**:14279-14284.

Scott, M. R., Will, R. G., Ironside, J. W., Nguyen, H.-O. B., Tremblay, P., Dearmond, S. J. and Prusiner, S. B. (1999). Compelling transgenic evidence for transmission of bovine spongiform encephalopathy prions to humans. *Proceedings of the National Academy Of Sciences Of the United States Of America* **96**:15137-15142.

Selvaggini, C., Degioia, L., Cantu, L., Ghibaudi, E., Diomede, L., Passerini, F., Forloni, G., Bugiani, O., Tagliavini, F. and Salmona, M. (1993). Molecular characteristics of a protease-resistant, amyloidogenic and neurotoxic peptide homologous to residues-106-126 of the prion protein. *Biochemical and Biophysical Research Communications* **194**:1380-1386.

Shearman, M. S., Ragan, C. I. and Iversen, L. L. (1994). Inhibition of PC12 cell redox activity is a specific, early indicator of the mechanism of ß-amyloid-mediated cell death. *Proceedings of the National Academy Of Sciences Of the United States Of America* **91**:1470-1474.

Shimizu, S., Narita, M. and Tsujimoto, Y. (1999). Bcl-2 family proteins regulate the release of apoptogenic cytochrome c by the mitochondrial channel VDAC. *Nature* **399**:483-487.

Shyng, S. L., Heuser, J. E. and Harris, D. A. (1994). A glycolipid-anchored prion protein is endocytosed via clathrin-coated pits. *Journal of Cell Biology* **125**:1239-1250.

Shyng, S. L., Huber, M. T. and Harris, D. A. (1993). A prion protein cycles between the cell-surface and an endocytic compartment in cultured neuroblastoma-cells. *Journal of Biological Chemistry* **268**:15922-15928.

Somerville, R. A. (1999). Host and transmissible spongiform encephalopathy agent strain control glycosylation of PrP. *Journal of General Virology* **80**:1865-1872.

Somerville, R. A., Chong, A., Mulqueen, O. U., Birkett, C. R., Wood, S. C. E. R. and Hope, J. (1997). Biochemical typing of scrapie strains. *Nature* **386**:564.
Somerville, R. A. and Ritchie, L. A. (1990). Differential glycosylation of the protein (prp) forming scrapie-associated fibrils. *Journal of General Virology* **71**:833-839.

Soto, C., Anderes, L., Suardi, S., Cardone, F., Castilla, J., Frossard, M.-J., Peano, S., Saa, P., Limido, L., Carbonatto, M., Ironside, J. W., Torres, J.-M., Pocchiari, M. and Tagliavini, F. (2005). Pre-symptomatic detection of prions by cyclic amplification of protein misfolding. *FEBS Letters* **579**.

Soto, C., Kascsak, R. J., Saborio, G. P., Aucouturier, P., Wisniewski, T., Prelli, F., Kascsak, R., Mendez, E., Harris, D. A., Ironside, J. W., Tagliavini, F., Carp, R. I. and Frangione, B. (2000). Reversion of prion protein conformational changes by synthetic β-sheet breaker peptides. *The Lancet* **355**:192-197.

Sparkes, R. S., Simon, M., Cohn, V. H., Fournier, R. E. K., Lem, J., Klisak, I., Heinzmann, C., Blatt, C., Lucero, M., Mohandas, T., Dearmond, S. J., Westaway, D., Prusiner, S. B. and Weiner, L. P. (1986). Assignment of the human and mouse prion protein genes to homologous chromosomes. *Proceedings of the National Academy Of Sciences Of the United States Of America* **83**:7358-7362.

Stadelmann, C., Deckwerth, T. L., Srinivasan, A., Bancher, C., Bruck, W., Jellinger, K. and Lassmann, H. (1999). Activation of caspase-3 in single neurons and autophagic granules of granulovacuolar degeneration in Alzheimer's disease. Evidence for apoptotic cell death. *American Journal of Pathology* **155**:1459-1466.

Stahl, N., Borchelt, D. R., Hsiao, K. and Prusiner, S. B. (1987). Scrapie prion protein contains a phosphatidylinositol glycolipid. *Cell* **51**:229-240.

Stamp, J., Brotherston, J., Zlotnik, I., Mackay, J. and Smith, W. (1959). Further studies on scrapie. *Journal of Comparative Pathology* **69**:268-280.

Stoka, V., Turk, B., Schendel, S. L., Kim, T. H., Cirman, T., Snipas, S. J., Ellerby, L. M., Bredesen, D., Freeze, H., Abrahamson, M., Bromme, D., Krajewski, S., Reed, J. C., Yin, X. M., Turk, V. and Salvesen, G. S. (2001). Lysosomal protease pathways to apoptosis. Cleavage of bid, not pro-caspases, is the most likely route. *Journal of Biological Chemistry* **276**:3149-3157.

Supattapone, S., Bosque, P., Muramoto, T., Wille, H., Aagaard, C., Peretz, D., Nguyen, H. O. B., Heinrich, C., Torchia, M., Safar, J., Cohen, F. E., DeArmond, S. J., Prusiner, S. B. and Scott, M. (1999). Prion protein of 106 residues creates an artificial transmission barrier for prion replication in transgenic mice. *Cell* **96**:869-878.

Susin, S. A., Lorenzo, H. K., Zamzami, N., Marzo, I., Snow, B. E., Brothers, G. M., Mangion, J., Jacotot, E., Costantini, P., Loeffler, M., Larochette, N., Goodlett, D. R., Aebersold, R., Siderovski, D. P., Penninger, J. M. and Kroemer, G. (1999). Molecular characterization of mitochondrial apoptosis-inducing factor. *Nature* **397**:441-446.

Susin, S. A., Zamzami, N., Castedo, M., Daugas, E., Wang, H. G., Geley, S., Fassy, F., Reed, J. C. and Kroemer, G. (1997). The central executioner of apoptosis: multiple connections between protease activation and mitochondria in Fas/APO-1/CD95- and ceramide-induced apoptosis. *Journal of Experimental Medicine* **186**:25-37.

Suzuki, Y., Imai, Y., Nakayama, H., Takahashi, K., Takio, K. and Takahashi, R. (2001). A serine protease, HtrA2, is released from the mitochondria and interacts with XIAP, inducing cell death. *Molecular Cell* **8**:613-621

Tagliavini, F., Lievens, P. M.-J., Tranchant, C., Warter, J.-M., Mohr, M., Giaccone, G., Perini, F., Rossi, G., Salmona, M., Piccardo, P., Ghetti, B., Beavis, R. C., Bugiani, O., Frangione, B. and Prelli, F. (2001). A 7-kDa prion protein (PrP) fragment, an integral component of the PrP region required for infectivity, is the major amyloid protein in Gerstmann-Straussler-Scheinker disease A117V. *The Journal of Biological Chemistry* **276**:6009-6015.

Tagliavini, F., Prelli, F., Ghiso, J., Bugiani, O., Serban, D., Prusiner, S. B., Farlow, M. R., Ghetti, B. and Frangione, B. (1991). Amyloid protein of Gerstmann-Straussler-Scheinker disease (Indiana kindred) is an 11 kd fragment of prion protein with an N-terminal glycine at codon 58. *Embo Journal* **10**:513-519.

Tagliavini, F., Prelli, F., Verga, L., Giaccone, G., Sarma, R., Gorevic, P., Ghetti, B., Passerini, F., Ghibaudi, E., Forloni, G., Salmona, M., Bugiani, O. and Frangione, B. (1993). Synthetic peptides homologous to prion protein residues 106-147 form amyloid-like fibrils in-vitro. *Proceedings of the National Academy of Sciences Of the United States Of America* **90**:9678-9682.

Tanaka, M., Chien, P., Naber, N., Cooke, R. and Weissman, J. S. (2004). Conformational variations in an infectious protein determine prion strain differences. *Nature* **428**:323-328.

Taraboulos, A., Raeber, A. J., Borchelt, D. R., Serban, D. and Prusiner, S. B. (1992). Synthesis and trafficking of prion proteins in cultured cells. *Molecular Biology of the Cell* **3**:851-863.

Taraboulos, A., Serban, D. and Prusiner, S. B. (1990). Scrapie prion proteins accumulate in the cytoplasm of persistently infected cultured cells. *Journal of Cell Biology* **110**:2117-2132.

Taylor, D. M., McConnell, I. and Fraser, H. (1996). Scrapie infection can be established readily through skin scarification in immunocompetent but not immunodeficient mice. *Journal of General Virology* **77**:1595-1599.

Taylor, S. C., Green, K. N., Smith, I. F. and Peers, C. (2001). Prion protein fragment 106-126 potentiates catecholamine secretion from PC12 cells. *American Journal of Physiological Cell Physiology* **281**:1850-1857.

Telling, G. C., Parchi, P., Dearmond, S. J., Cortelli, P., Montagna, P., Gabizon, R., Mastrianni, J., Lugaresi, E., Gambetti, P. and Prusiner, S. B. (1996). Evidence for the conformation of the pathologic isoform of the prion protein enciphering and propagating prion diversity. *Science* **274**:2079-2082.

Telling, G. C., Scott, M., Mastrianni, J., Gabizon, R., Torchia, M., Cohen, F. E., Dearmond, S. J. and Prusiner, S. B. (1995). Prion propagation in mice expressing human and chimeric PrP transgenes implicates the interaction of cellular PrP with another protein. *Cell* **83**:79-90.

Thellung, S., Florio, T., Villa, V., Corsaro, A., Arena, S., Amico, C., Robello, M., Salmona, M., Forloni, G., Bugiani, O., Tagliavini, F. and Schettini, G. (2000). Apoptotic cell death and impairment of L-type voltage-sensitive calcium channel activity in rat cerebellar granule cells treated with the prion protein fragment PrP106-126. *Neurobiology of Disease* **7**:299-309.

Thellung, S., Villa, V., Corsaro, A., Arena, S., Millo, E., Damonte, G., Benatti, U., Tagliavini, F., Florio, T. and Schettini, G. (2002). p38 MAP kinase mediates the cell death induced by PrP106-126 in the SH-SY5Y neuroblastoma cells. *Neurobiology of Disease* **9**:69-81.

Tobler, I., Deboer, T. and Fischer, M. (1997). Sleep and sleep regulation in normal and prion protein- deficient mice. *Journal of Neuroscience* **17**:1869-1879.

Tobler, I., Gaus, S. E., Deboer, T., Achermann, P., Fischer, M., Rulicke, T., Moser, M., Oesch, B., McBride, P. A. and Manson, J. C. (1996). Altered Circadian Activity Rhythms and Sleep In Mice Devoid Of Prion Protein. *Nature* **380**:639-642.

Turk, E., Teplow, D. B., Hood, L. E. and Prusiner, S. B. (1988). Purification and properties of the cellular and scrapie hamster prion proteins. *European Journal of Biochemistry* **176**:21-30.

Tuzi, N. L., Gall, E., Melton, D. and Manson, J. C. (2002). Expression of doppel in the CNS of mice does not modulate transmissible spongiform encephalopathy disease. *Journal of General Virology* **83**:705-711.

van Loo, G., Schotte, P., van Gurp, M., Demol, H., Hoorelbeke, B., Gevaert, K., Rodriguez, I., Ruiz-Carrillo, A., Vandekerckhove, J., Declercq, W., Beyaert, R. and Vandenabeele, P. (2001). Endonuclease G: a mitochondrial protein released in apoptosis and involved in caspase-independent DNA degradation. *Cell Death Differentiation* **8**:1136-1142.

Vey, M., Pilkuhn, S., Wille, H., Nixon, R., Dearmond, S. J., Smart, E. J., Anderson, R. G. W., Taraboulos, A. and Prusiner, S. B. (1996). Subcellular Colocalization Of the Cellular and Scrapie Prion Proteins In Caveolae-Like Membranous Domains. *Proceedings of the National Academy Of Sciences Of the United States Of America* **93**:14945-14949.

Wang, H., Shimoji, M., Yu, S. W., Dawson, T. M. and Dawson, V. L. (2003). Apoptosis inducing factor and PARP-mediated injury in the MPTP mouse model of Parkinson's disease. *Annals of the New York Academy of Sciences* **991**:132-139.

Wang, X. (2001). The expanding role of mitochondria in apoptosis. *Genes Dev* **15**:2922-2933.

Wang, X., Yang, C., Chai, J., Shi, Y. and Xue, D. (2002). Mechanisms of AIF-mediated apoptotic DNA degradation in *Caenorhabditis elegans*. *Science* **298**:1587-1592.

Weissmann, C., Bueler, H., Fischer, M. and Aguet, M. (1993). Role of the prp gene in transmissible spongiform encephalopathies. *Intervirology* **35**:164-175.

Wells, G. A. H., Scott, A. C., Johnson, C. T., Gunning, R. F., Hancock, R. D., Jeffrey, M., Dawson, M. and Bradley, R. (1987). A novel progressive spongiform encephalopathy in cattle. *Veterinary Record* **121**:419-420.

Westaway, D., DeArmond, S. J., Cayetano-Canlas, J., Groth, D., Foster, D., Yang, S. L., Torchia, M., Carlson, G. A. and Prusiner, S. B. (1994). Degeneration of skeletal muscle, peripheral nerves, and the central nervous system in transgenic mice overexpressing wild-type prion proteins. *Cell* **76**:117-129.

Westaway, D., Goodman, P. A., Mirenda, C. A., McKinley, M. P., Carlson, G. A. and Prusiner, S. B. (1987). Distinct prion proteins in short and long scrapie incubation period mice. *Cell* **51**:651-662.

White, A. R., Guirguis, R., Brazier, M. W., Jobling, M. F., Hill, A. F., Beyreuther, K., Barrow, C. J., Masters, C. L., Collins, S. J. and Cappai, R. (2001). Sublethal concentrations of prion peptide PrP106-126 or the amyloid beta peptide of Alzheimer's disease activates expression of proapoptotic markers in primary cortical neurons. *Neurobiology of Disease* **8**:299-316.

Widlak, P., Li, L. Y., Wang, X. and Garrard, W. T. (2001). Action of recombinant human apoptotic endonuclease G on naked DNA and chromatin substrates: cooperation with exonuclease and DNase I. *Journal of Biological Chemistry* **276**:48404-48409.

Wilesmith, J. W., Wells, G. A. H., Cranwell, M. P. and Ryan, J. B. M. (1988). Bovine spongiform encephalopathy - epidemiological-studies. *Veterinary Record* **123**:638-644.

Will, R. G., Ironside, J. W., Zeidler, M., Cousens, S. N., Estibeiro, K., Alperovitch, A., Poser, S., Pocchiari, M., Hofman, A. and Smith, P. G. (1996). A New Variant Of Creutzfeldt-Jakob-Disease In the UK. *Lancet* **347**:921-925.

Wille, H., Prusiner, S. B. and Cohen, F. E. (2000). Scrapie infectivity is independent of amyloid staining properties of the N-terminally truncated prion protein. *Journal of Structural Biology* **130**:323-338.

Willoughby, K., Kelly, D. F., Lyon, D. G. and Wells, G. A. H. (1992). Spongiform encephalopathy in a captive puma (felis-concolor). *Veterinary Record* **131**:431-434.

Wion, D., Lebert, M. and Brachet, P. (1988). Messenger RNAs of beta-amyloid precursor protein and prion protein are regulated by nerve growth factor in PC12 cells. *International Journal of Developmental Neuroscience* **6**:387-393.

Wong, C., Xiong, L.-W., Horiuchi, M., Raymond, L., Wehrly, K., Chesebro, B. and Caughey, B. (2001). Sulfated glycans and elevated temperature stimulate PrP^{Sc}-dependent cell-free formation of protease-resistant prion protein. *EMBO Journal* **20**:377-386.

Wooten, M. W., Seibenhener, M. L., Neidigh, B. W. and Vandenplas, M. L. (2000). Mapping of atypical protein kinase C within the nerve growth factor signaling cascade: relationship to differentiation and survival of PC12 cells. *Molecular and Cellular Biology* **20**:4494-4504.

Wu, Y., Brown, W. T., Robakis, N. K., Dobkin, C., Devine-Gage, E., Merz, P. and Wisniewski, H. M. (1987). A PvuII RFLP detected in the human prion protein (PrP) gene. *Nucleic Acids Research* **15**:3191.

Wyatt, J. M., Pearson, G. R., Smerdon, T., Gruffyddjones, T. J. and Wells, G. A. H. (1990). Spongiform encephalopathy in a cat. *Veterinary Record* **126**:513.

Yang, J., Liu, X., Bhalla, K., Kim, C. N., Ibrado, A. M., Cai, J., Peng, T. I., Jones, D. P. and Wang, X. (1997). Prevention of apoptosis by Bcl-2: release of cytochrome c from mitochondria is blocked. *Science* **275**:1129-1132.

Ye, H., Cande, C., Stephanou, N. C., Jiang, S., Gurbuxani, S., Larochette, N., Daugas, E., Garrido, C., Kroemer, G. and Wu, H. (2002). DNA binding is required for the apoptogenic action of apoptosis inducing factor. *Nature Structural Biology* **9**:680-684.

Yu, S. W., Wang, H., Dawson, T. M. and Dawson, V. L. (2003). Poly(APD-ribose) polymerase-1 and apoptosis inducing factor in neurotoxicity. *Neurobiology of Disease* **14**:303-317.

Zahn, R., Liu, A., Luhrs, T., Riek, R., von Schroetter, C., Lopez, F., Billeter, M., Calzolai, L., Wider, G. and Wuthrich, K. (2000). NMR solution structure of the human prion protein. *Proceedings of the National Academy Of Sciences Of the United States Of America* **97**:8812-8816.

Zhang, X., Chen, J., Graham, S. H., Du, L., Kochanek, P. M., Draviam, R., Guo, F., Nathaniel, P. D., Szabo, C., Watkins, S. C. and Clark, R. S. (2002). Intranuclear localization of apoptosis-inducing factor (AIF) and large scale DNA fragmentation after traumatic brain injury in rats and in neuronal cultures exposed to peroxynitrite. *Journal of Neurochemistry* **82**:181-191.

Zhu, C., Qiu, L., Wang, X., Hallin, U., Cande, C., Kroemer, G., Hagberg, H. and Blomgren, K. (2003). Involvement of apoptosis-inducing factor in neuronal death after hypoxia-ischemia in the neonatal rat brain. *Journal of Neurochemistry* **86**:306-317.

Zlotnik, I. and Rennie, J. C. (1962). The pathology of the brain of mice inoculated with tissues from scrapie sheep. *Journal of Comparative Pathology* **72**:360-365.

Zlotnik, I. and Rennie, J. C. (1963). Further observations on the experimental transmission of scrapie from sheep and goats to laboratory mice. *Journal of Comparative Pathology* **73**:150-162.

Zou, H., Li, Y., Liu, X. and Wang, X. (1999). An APAF-1.cytochrome c multimeric complex is a functional apoptosome that activates procaspase-9. *Journal of Biological Chemistry* **274**:11549-56.